University of Nottingham

UK | CHINA | MALAYSIA


UNIVERSITY OF BIRMINGHAM

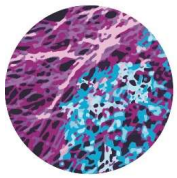

COMPARE

CENTRE OF MEMBRANE PROTEINS AND RECEPTORS

# Cardiovascular Responses Induced by Selective Adenosine $A_{2A}$ and $A_{2B}$ Receptor Agonists

**Edward S. Wragg**

**BSc (Hons), MSc**

A Thesis Submitted to the University of Nottingham for the Degree of Doctor of Philosophy

September 2022

# i. Declaration

This thesis is entirely the candidates' work. The experiments described in this thesis were performed between October 2018 and September 2021 in the Cell Signalling research group at the Centre of Membrane Proteins and Receptors (COMPARE), University of Nottingham, UK. All *in vitro* experiments were completed solely by the author. All *in vivo* work was performed as part of a collaborative research team comprising of Edward Wragg (The Author: Experimenter and Surgical Assistant), Julie March (Surgeon and Senior Lab Technician), Sam Cooper (Experimenter and Surgeon), Jeanette Woolard (Principle Investigator, Project Licence Holder and Surgical Assistant), Patrizia Pannucci (Experimenter and Surgical Assistant) and Marleen Groenen (Surgical Assistant).

Additionally, to complete the scientific story of the thesis, four previously published *in vivo* experiments have been included where a different researcher completed the experiments before or after the authors' time in the lab; the raw data for these experiments was analysed for publication in both research papers and this thesis by the author of this thesis. Where this is the case, express permission was obtained to present these experiments in this thesis, and full credit was given to the experimenter in the appropriate chapters' methodology section.

No part of this material has been previously submitted for a degree or any other qualification at any university.

**Funding:** This work was supported financially by the Centre of Membrane Proteins and Receptors (COMPARE), a collaboration between the Universities of Nottingham and Birmingham.

**Conflicts of Interest:** The author declares no conflicts of interest.

# ii. Abstract

Adenosine is an important modulator of the cardiovascular system, acting at four GPCRs, known as the adenosine receptors. A crucial role of two of those receptors, adenosine $A_{2A}$ and $A_{2B}$ receptors, is the induction of vasodilation in resistance arteries that comprise vascular beds across the body, leading to an increase in the ease with which blood flows, known as vascular conductance, in these beds. As a result of these properties, both $A_2$ receptors have been suggested to have therapeutic potential in treating hypertension and other diseases associated with reductions in blood flow to various regions of the body. However, adenosine receptor expression across the different vasculature beds that make up the circulatory system is neither universal nor ubiquitous, and neither are the physiological changes induced by activation of these receptors; different regions of the body have different sensitivities and responses to adenosine through differences in adenosine receptor expression and function across the body. To gain a greater understanding of how $A_{2A}$ and $A_{2B}$ receptors influence the cardiovascular system, this project aimed to investigate the physiological consequences and potential uses of adenosine $A_{2A}$ and $A_{2B}$ receptor activation on the regional flow of blood in the renal, mesenteric and hindquarter vascular circulations, in conscious, freely moving rats, using Doppler flowmetry.

**First**, functional responses in conscious rats to adenosine, the $A_{2A}$ receptor agonist CGS 21680, and the $A_{2B}$ receptor agonist BAY 60-6583 were investigated in the presence or absence of adenosine $A_{2A}$ and $A_{2B}$ receptor antagonists, SCH 58261 and PSB 1115, respectively. Adenosine was shown to cause increases in the vascular conductance of all three vascular beds studied. It was discovered that $A_{2A}$ receptor activation increased vascular conductance in the hindquarters vascular beds, but had limited effects on vascular conductance in the renal and mesenteric vascular beds. The opposite was the case with the $A_{2B}$ receptor, which caused increases in the vascular conductance in the renal and mesenteric vascular beds, but not the hindquarters. Both $A_{2A}$ and $A_{2B}$ receptor activation induced tachycardia, but only agonism of the $A_{2A}$ receptor caused a decrease in mean arterial blood pressure.

**Second**, experiments were undertaken to ascertain if the physiological responses observed due to CGS 21680 ($A_{2A}$ receptor) and BAY 60-6583 ($A_{2B}$ receptor) treatment were in part caused by a secondary reflex-driven increase in sympathetic nervous system activity resulting in catecholamine stimulation of the heart and vasculature, causing the activation of adrenergic $\beta_1$ and $\beta_2$ receptors, respectively. Haemodynamic experiments involving the pretreatment of the $\beta_1$ selective antagonist CGP 20712A, the $\beta_2$ selective antagonist ICI 118,551 and the non-selective β antagonist propranolol showed that the increase in heart rate caused by both $A_2$ receptor agonists was primarily caused by secondary activation of $\beta_1$ receptors in the heart. Additionally, it was demonstrated that the vasodilatory effects of $A_{2A}$ receptor activation on the hindquarters were not caused by, or enhanced by secondary stimulation of β receptors. Of interest, $\beta_2$ receptor antagonism appeared to enhance the haemodynamic response to $A_{2B}$ receptor activation, including increases in heart rate and increases in regional vascular conductances.

**Third**, *in vivo* experiments were undertaken with sunitinib, a chemotherapeutic receptor tyrosine kinases inhibitor (RTKI) known to inhibit vascular endothelial growth factor receptor 2 (VEGFR2) signalling, which over a three-day protocol caused hypertension associated with reductions in vascular conductance in the vascular beds that make up the renal, mesenteric and hindquarters. Experiments demonstrated that the hypertension and reductions in vascular conductance could be temporarily reversed by CGS 21680 administration via $A_{2A}$ receptor activation.

**Finally**, to explore the link between VEGFR2 and adenosine $A_2$ receptor signalling, explorative *in vitro* studies were conducted. Cyclic adenosine monophosphate (cAMP) accumulation assays found that vascular endothelial growth factor $A_{165}$a (VEGF-$A_{165}$a) acting at VEGFR2 enhanced an $A_{2A}$ receptor-induced cAMP response, with this enhancement able to be blocked by sunitinib. Additionally, bioluminescence resonance energy transfer (BRET) based proximity assays were undertaken to explore receptor-receptor colocalisation; no evidence was found that VEGFR2 and $A_{2A}$ or $A_{2B}$ receptors colocalise on the plasma membrane.

Results from this thesis suggest that $A_{2A}$ receptor activation could help treat hypertension associated with vasoconstriction, such as RTKI-induced hypertension. Furthermore, the ability of $A_{2B}$ receptor activation to selectively cause vasodilations in the renal and mesenteric vascular beds demonstrate that the selective targeting of $A_{2B}$ receptors could be beneficial in conditions associated with deleterious vasoconstrictions in the renal and mesenteric vasculatures, such as acute kidney injury or mesenteric ischemia.

# iii. Publications

## Research Papers

- Wragg, E. S., Pannucci, P., Hill, S. J., Woolard, J. & Cooper, S. L. 2022. Involvement of β-adrenoceptors in the cardiovascular responses induced by selective adenosine $A_{2A}$ and $A_{2B}$ receptor agonists. *Pharmacology Research & Perspectives*, 10, e00975.

- Cooper, S. L., Wragg, E. S., Pannucci, P., Soave, M., Hill, S. J. & Woolard, J. 2022. Regionally selective cardiovascular responses to adenosine $A_{2A}$ and $A_{2B}$ receptor activation. *FASEB J*, 36, e22214.

## Review Articles

- Van Daele, M., Cooper, S. L., Pannucci, P., Wragg, E. S., March, J., De Jong, I. & Woolard, J. 2022. Monitoring haemodynamic changes in rodent models to better inform safety pharmacology: Novel insights from *in vivo* studies and waveform analysis. *JRSM Cardiovascular Disease*, 11, 20480040221092893.

## Conference Proceedings

- Wragg ES, Cooper SL, Hill SJ, Kalia N, March J, Soave M & Woolard J. (2019). Exploring the Haemodynamic Effects of Adenosine $A_{2B}$ Receptor Agonists in Conscious, Freely Moving Rats (poster presentation at COMPARE Research Symposium, 2019, Nottingham, UK).

- Wragg ES, Cooper SL, March J, Kalia N, Hill SJ & Woolard J. (2019). Exploring the Haemodynamic Effects of Adenosine $A_{2B}$ Receptor Ligands in Conscious, Freely Moving Rats (poster presentation at ELRIG Drug Discovery, 2019, Liverpool, UK).

- Wragg ES, Cooper SL, March J, Hill SJ & Woolard J (2019). Exploring the Haemodynamic Effects of Adenosine $A_{2B}$ Receptor Ligands in Conscious, Freely Moving Rats (oral communication at BPS Pharmacology 2019, Edinburgh, UK).

- Wragg ES, Cooper SL, March J, Hill SJ & Woolard J. (2020). Exploring the Haemodynamic Effects of BAY 60-6583, in Conscious, Freely-Moving Rats. *FASEB J*, 34(S1), 1-1. (poster presentation accepted and abstract published for Experimental Biology 2020, San Diego, USA – Conference Cancelled due to COVID-19 pandemic).

- Wragg ES, Cooper SL, March J, Kalia N, Hill SJ & Woolard J. (2020). Exploring the Haemodynamic Effects of BAY 60-6583, in Conscious, Freely-Moving Rats (narrated poster presentation at University of Nottingham PGR Symposium, 2020, online event).

- Wragg ES, Cooper SL, March J, Kalia N, Hill SJ & Woolard J. (2020). Exploring the Haemodynamic Effects of BAY 60-6583, in Conscious, Freely-Moving Rats (oral communication at University of Nottingham PGR Symposium, 2021, online event).

# iv. Acknowledgements

First, I would like to thank my primary supervisor, Jeanette Woolard. Jeanette is a role model, demonstrating that being exceptionally professional and having a good laugh at work are not mutually exclusive. Jeanette has been a fantastic supervisor, helping me through countless difficult situations.

I want to thank my second supervisor, Steve Hill, for being kind and warm on a personal level, but rigorous regarding the science. Additionally, I would like to thank Neena Kalia from the University of Birmingham for her support throughout the project. It was frustrating not to be able to travel to Birmingham to join Neena's lab due to complications arising from the COVID-19 pandemic, but it was still a pleasure to meet Neena and her team.

The *in vivo* experiments that our lab conducts are complicated and challenging. Without the resolute determination of the F-floor team, none of my *in vivo* work would have been possible. First, I want to thank Julie March, from whom I have learned a lot. I want to thank Marleen Groenen for her hard work assisting the experiments on F-floor and for her personal support in helping get me through my research. Finally, I would like to thank Sam Cooper, who taught me how to run the *in vivo* experiments and helped me with them throughout.

I am indebted to a fantastic post-doc team who supported my *in vitro* experiments: Laura Kilpatrick, Mark Soave and Sam Cooper.

The Institute of Cellular Signalling (ICS) is an extraordinary place to work, full of positivity, selflessness, and kindness. It has truly been a joy to work there. The ICS work environment is how science should be done, both for the quality of the science and for the people conducting it. The fantastic people at ICS allowed me to be my eccentric self at work, and for that, I thank you all.

Finally, I wish to thank my parents, Kathryn and Mike, and my wife, Hannah. My family's optimism has got me through this PhD, and their support has made this endeavour possible.

I hope you enjoy reading my thesis!

**All the best**,

Eddy

# v. Acronyms & Abbreviations

| Acronym | In Full |
|---|---|
| **5-HT** | 5-hydroxytryptamine |
| **5-HT3A** | Serotonin 5-hydroxytryptamine 3A |
| **AC** | Adenylyl cyclase |
| **ACEI** | Angiotensin-converting enzyme inhibitor |
| **ACh** | Acetylcholine |
| **ANOVA** | Analysis of variance |
| **ARRIVE** | Animal research: reporting of in vivo experiments |
| **ATCC** | American type culture collection |
| **ATIII** | Antithrombin III |
| **ATP** | Adenosine triphosphate |
| **AV** | Atrioventricular |
| **BiFC** | Bimolecular fluorescence complementation |
| **BRET** | Bioluminescent resonance energy transfer |
| **BSA** | Bovine serum albumin |
| **CAD** | Coronary artery disease |
| **cAMP** | Cyclic adenosine monophosphate |
| **cDNA** | Complementary deoxyribonucleic acid |
| **cGMP** | Cyclic guanosine monophosphate |
| **CMV** | Cytomegalovirus |
| **CNBD** | Cyclic nucleotide-binding domain |
| **COVID-19** | Coronavirus disease 2019 |
| **COX** | Cyclooxygenase |
| **COX-1** | Cyclooxygenase-1 |
| **COX-2** | Cyclooxygenase-2 |
| **CREB** | Cyclic adenosine monophosphate response element-binding protein |
| **CVLM** | Caudal ventrolateral medulla |
| **DAG** | Diacyl glycerol |
| **DMEM** | Dulbecco's modified eagle's medium |
| **DMSO** | Dimethylsulfoxide |
| **DNA** | Deoxyribonucleic acid |
| **E. coli** | *Escherichia coli* |
| **ECG** | Electrocardiogram |
| **ECL2** | Extracellular loop 2 |
| **EDTA** | Ethylenediaminetetraacetic acid |
| **eNOS** | Endothelial nitric oxide synthase |
| **ERK1** | Extracellular signal-regulated kinase 1 |
| **ERK2** | Extracellular signal-regulated kinase 2 |
| **ET-1** | Endothelin-1 |
| **FBS** | Fetal bovine serum |
| **FLT3** | Fms-related tyrosine kinase 3 |

| | |
|---|---|
| **FRET** | Förster resonance energy transfer |
| **$GABA_A$** | γ-aminobutyric acid A |
| **GC** | Guanylyl cyclase |
| **GDP** | Guanosine diphosphate |
| **GFP** | Green fluorescent protein |
| **GPCR** | G protein-coupled receptor |
| **GTP** | Guanosine triphosphate |
| **HBSS** | HEPES buffered saline solution |
| **HEK** | Human embryonic kidney |
| **HIF-1** | Hypoxia-inducible factor 1 |
| **HIF-1α** | Hypoxia-inducible factor 1α |
| **HR** | Heart rate |
| **I.U.** | Industrial units |
| **i.v.** | Intravenous |
| **IL-6** | Interleukin 6 |
| **$IP_3$** | Inositol 1,4,5-trisphosphate |
| **$K_{ATP}$** | ATP-sensitive $K^+$ |
| **KDR** | Kinase insert domain |
| **KIT** | Stem-cell growth factor receptor |
| **LB** | Luria broth |
| **LD** | Lumen diameter |
| **L-NAME** | $N^G$-nitro-L-arginine methyl ester |
| **MAP** | Mean arterial pressure |
| **MAPK** | Mitogen-activated protein kinase |
| **MPI** | Myocardial perfusion imaging |
| **mRNA** | Messenger ribonucleic acid |
| **NA** | Nucleus ambiguus |
| **NACWO** | Named animal care & welfare officer |
| **NC3R** | The national centre for the replacement, refinement and reduction of animals in research |
| **NFAT** | Nuclear factor of activated T-cells |
| **NF-κB** | Nuclear factor κ-light-chain-enhancer of activated B cells |
| **NLuc** | Nano luciferase |
| **NO** | Nitric oxide |
| **NSAID** | Non-steroidal anti-inflammatory drug |
| **NTS** | Nucleus tractus solitarius |
| **NVS** | Named veterinary surgeon |
| **PBS** | Phosphate buffered saline |
| **PDE** | Phosphodiesterase |
| **PDGFR** | Platelet-derived growth factor receptor |
| **PDL** | Poly-D-lysine |
| **PE** | Polyethylene |
| **PET** | Positron emission tomography |
| **PG** | Prostaglandin |

| | |
|---|---|
| **PGIS** | Prostaglandin I2 synthase |
| **PI3K** | Phosphoinositide 3-kinase |
| **PIL** | Personal license |
| **$PIP_2$** | Phosphatidylinositol 4,5-bisphosphate |
| **PKA** | Protein kinase A |
| **PKC** | Protein kinase C |
| **PKCγ** | Protein kinase C γ |
| **PLC** | Phospholipase C |
| **PPL** | Project license |
| **PRF** | Pulse repetition frequency |
| **RET** | Resonance energy transfer |
| **RNA** | Ribonucleic acid |
| **RTK** | Receptor tyrosine kinase |
| **RTKI** | Receptor tyrosine kinase inhibitor |
| **RVLM** | Rostral ventrolateral medulla |
| **SAN** | Sinoatrial node |
| **SEM** | Standard error of the mean |
| **SPECT** | Single-photon emission computed tomography |
| **SV40** | Simian virus 40 |
| **TRPC** | Transient receptor potential canonical |
| **VC** | Vascular conductance |
| **VEGF** | Vascular endothelial growth factor |
| **VEGF-A** | Vascular endothelial growth factor A |
| **VEGF-C** | Vascular endothelial growth factor C |
| **VEGF-D** | Vascular endothelial growth factor D |
| **VEGFR** | Vascular endothelial growth factor receptor |
| **VEGFR1** | Vascular endothelial growth factor receptor 1 |
| **VEGFR2** | Vascular endothelial growth factor receptor 2 |
| **VEGFR3** | Vascular endothelial growth factor receptor 3 |
| **VGSC** | Voltage-gated sodium channels |
| **XAC** | Xanthine amine congener |

## vi. Chemical Compound Abbreviations

| Salt (If Present) | Thesis Short Version | Chemical Name |
|---|---|---|
| **Adenosine** | Adenosine | 9-β-D-Ribofuranosyl-9H-purin-6-amine |
| **BAY 60-6583** | BAY 60-6583 | 2-[[6-Amino-3,5-dicyano-4-[4-(cyclopropylmethoxy)phenyl]-2-pyridinyl]thio]-acetamide |
| **CCPA** | CCPA | 2-Chloro-N6-cyclopentyladenosine |
| **CGP 20712A Dihydrochloride** | CGP 20712A | 1-[2-((3-Carbamoyl-4-hydroxy)phenoxy)ethylamino]-3-[4-(1-methyl-4-trifluoromethyl-2-imidazolyl)phenoxy]-2-propanol dihydrochloride |
| **CGS 21680 Hydrochloride** | CGS 21680 | 4-[2-[[6-Amino-9-(N-ethyl-β-D-ribofuranuronamidosyl)-9H-purin-2-yl]amino]ethyl]benzenepropanoic acid hydrochloride |
| **Forskolin** | Forskolin | (3R,4aR,5S,6S,6aS,10S,10aR,10bS)-5-(Acetyloxy)-3-ethenyldodecahydro-6,10,10b-trihydroxy-3,4a,7,7,10a-pentamethyl-1H-naphtho[2,1-b]pyran-1-one |
| **HEPES** | HEPES | 4-(2-hydroxyethyl)-1-piperazineethanesulfonic acid |
| **ICI 118,551 Hydrocholoride** | ICI 118,551 | (±)-erythro-(S*,S*)-1-[2,3-(Dihydro-7-methyl-1H-inden-4-yl)oxy]-3-[(1-methylethyl)amino]-2-butanol hydrochloride |
| **NECA** | NECA | 1-(6-Amino-9H-purin-9-yl)-1-deoxy-N-ethyl-β-D-ribofuranuronamide |
| **Propranolol Hydrochloride** | Propranolol | (RS)-1-[(1-Methylethyl)amino]-3-(1-naphthalenyloxy)-2-propanol hydrochloride |
| **PSB 1115** | PSB 1115 | 4-(2,3,6,7-Tetrahydro-2,6-dioxo-1-propyl-1H-purin-8-yl)-benzenesulfonic acid |
| **PSB 603** | PSB 603 | 8-[4-[4-(4-Chlorophenzyl)piperazide-1-sulfonyl)phenyl]]-1-propylxanthine |
| **SCH 58261** | SCH 58261 | 2-(2-Furanyl)-7-(2-phenylethyl)-7H-pyrazolo[4,3-e][1,2,4]triazolo[1,5-c]pyrimidin-5-amine |
| **Sunitinib Malate** | Sunitinib | N-[2-(Diethylamino)ethyl]-5-[(Z)-(5-fluoro-1,2-dihydro-2-oxo-3H-indol-3-ylidine)methyl]-2,4-dimethyl-1H-pyrrole-3-carboxamide (2S)-2-hydroxybutanedioate salt |

# Table of Contents

# 1 General Introduction

The work detailed in this thesis first considers the haemodynamic consequences of adenosine $A_{2A}$ and $A_{2B}$ receptor ligand administration in conscious, freely moving rats. To provide a detailed context of these results, the introduction first aims to introduce the role of adenosine (**1.1**), its endogenous production (**1.1.1**), its role in the cardiovascular system (**1.1.4**, **1.1.5**) and the current clinical uses of targeting adenosine receptors in the cardiovascular system (**1.1.6.1**). This introduction will then focus on the known roles of the two $A_2$ receptors in the cardiovascular system and the therapeutic potential of targeting these two receptors (**1.1.6.2**). This review will emphasise the known effects of adenosine receptors in the cardiovascular regions investigated during these studies: the kidney, the mesentery and the hindquarters. This introduction aims to provide the background information required to understand the context behind the studies detailed in this thesis, justify why they were undertaken and detail the project's primary goals.

An advantage of the *in vivo* haemodynamic model that was used over *ex vivo* and *in vivo* studies using anesthetised animals was that during these studies, the cardiovascular effects of drug administration were measured in conscious rats, with intact cardiovascular systems under full homeostatic reflex control (**2.1**). A major homeostatic reflex activated due to acute perturbations to mean arterial blood pressure is the baroreflex, which is under the control of the autonomic nervous system, and as such, the physiological responses activated by the sympathetic nervous system are mediated by catecholamines acting at adrenoreceptors. Results detailed in this thesis indicated that $A_2$ receptor activation might cause the activation of the baroreflex system, and that sympathetic drive could be involved in this response (**4.4**). To test this hypothesis, experiments were undertaken using the administration of β-antagonists prior to the administration of adenosine $A_2$ receptor ligands (**4.3.1**). To understand the context of the results of the experiments detailing β-antagonism, the baroreflex system is detailed in this introduction (**1.2**).

Based on what is known in the literature (**1.1.6.2**), and the results of experiments detailed in this thesis (**3.3.1**), it is hypothesised that $A_{2A}$ receptor agonism might be clinically useful to reduce blood pressure and restore blood flow to vascular beds in disease states, and thus $A_{2A}$ receptor agonism might have utility in conditions that involve high blood pressure associated with a reduced blood flow to regional

vascular beds (**5.1**). A condition in which this has been demonstrated to be the case is hypertension induced by receptor tyrosine kinases inhibitors (RTKIs), which are utilised in the clinic as chemotherapeutic agents. To test this hypothesis, the ability of $A_{2A}$ receptor agonism to temporarily relieve the hypertensive effects of the RTKI, sunitinib, were investigated. To give context and justification to these studies, the background behind RTKIs, and their ability to cause deleterious hypertension and reduced vascular flow are introduced (**1.3**), along with an introduction to sunitinib (**1.3.3**). Following this, the introduction will cover a key receptor tyrosine kinase (RTK) that is inhibited by sunitinib, vascular endothelial growth factor receptor 2 (VEGFR2) (**1.3.2**) and discuss what is known about the signalling interactions between this RTK and adenosine receptors. Finally, what is currently known about the oligomerisation of both VEGFR2 and adenosine $A_2$ receptors will be discussed (**1.4**), giving background to studies completed in this thesis exploring the potential interactions between VEGFR2 and $A_{2A}$ receptors (**5.3.2**).

# 1.1 Introduction to Adenosine Signalling

## 1.1.1 Adenosine Generation & Metabolism

Adenosine is a purine nucleoside comprised of a molecule of adenine attached to a ribose sugar via a β-N9-glycosidic bond (King et al., 2006). Adenosine is an autacoid because it is synthesised inside and outside of cells for immediate use and is not stored in vesicles for future release (Rouquette et al., 2019). Adenosine has a short half-life of less than 10 s *in vivo* due to rapid enzymatic degradation, both extracellularly and intracellularly, to inosine by adenosine deaminase or to adenosine monophosphate (AMP) by adenosine kinase (**Figure 1**) (Moser et al., 1989, King et al., 2006). In the cell, AMP can be phosphorylated to generate the cellular fuel adenosine triphosphate (ATP) (**Figure 1**) (Rouquette et al., 2019).

Under physiological conditions, intracellular adenosine is derived mainly from S-adenosylhomocysteine via S-adenosylhomocysteine hydrolase (Antonioli et al., 2013b). Most, and possibly all, cells possess equilibrative nucleoside transporters (ENTs), membrane-spanning proteins that extrude intracellular nucleosides, including adenosine (King et al., 2006, Boswell-Casteel and Hays, 2017), and because of this, there will always be adenosine in the extracellular space. The adenosine concentration in the extracellular space has been estimated to be 30-200 nM under normal physiological conditions (Fredholm et al., 2011).

Extracellular adenosine binds to adenosine receptors, which are the focus of the thesis (**1.1.2**). Adenosine and the receptors that it binds are involved in the regulation of every organ system in the body, most notably the cardiovascular, nervous, and immune systems (Hasko et al., 2018). Adenosine is known as a ‘retaliatory metabolite’ because it is rapidly generated in response to detrimental cellular conditions such as inflammation, hypoxia, ischaemia or tissue damage; under such conditions, extracellular levels of adenosine increase, reaching the micromolar range (Hasko et al., 2018). Extracellular adenosine can increase substantially due to two different mechanisms: intracellular formation and export via the aforementioned ENTs or formation in the extracellular space from adenine nucleotides that have been released from cells (Fredholm et al., 2011). Under pathological conditions, a significant route of extracellular adenosine accumulation stems from increased extracellular dephosphorylation of ATP, which is converted

sequentially by ecto-nucleotide triphosphate diphosphohydrolase-1 (CD39) and ecto-5′-nucleotidase (CD73) into adenosine (**Figure 1**) (Antonioli et al., 2013c).

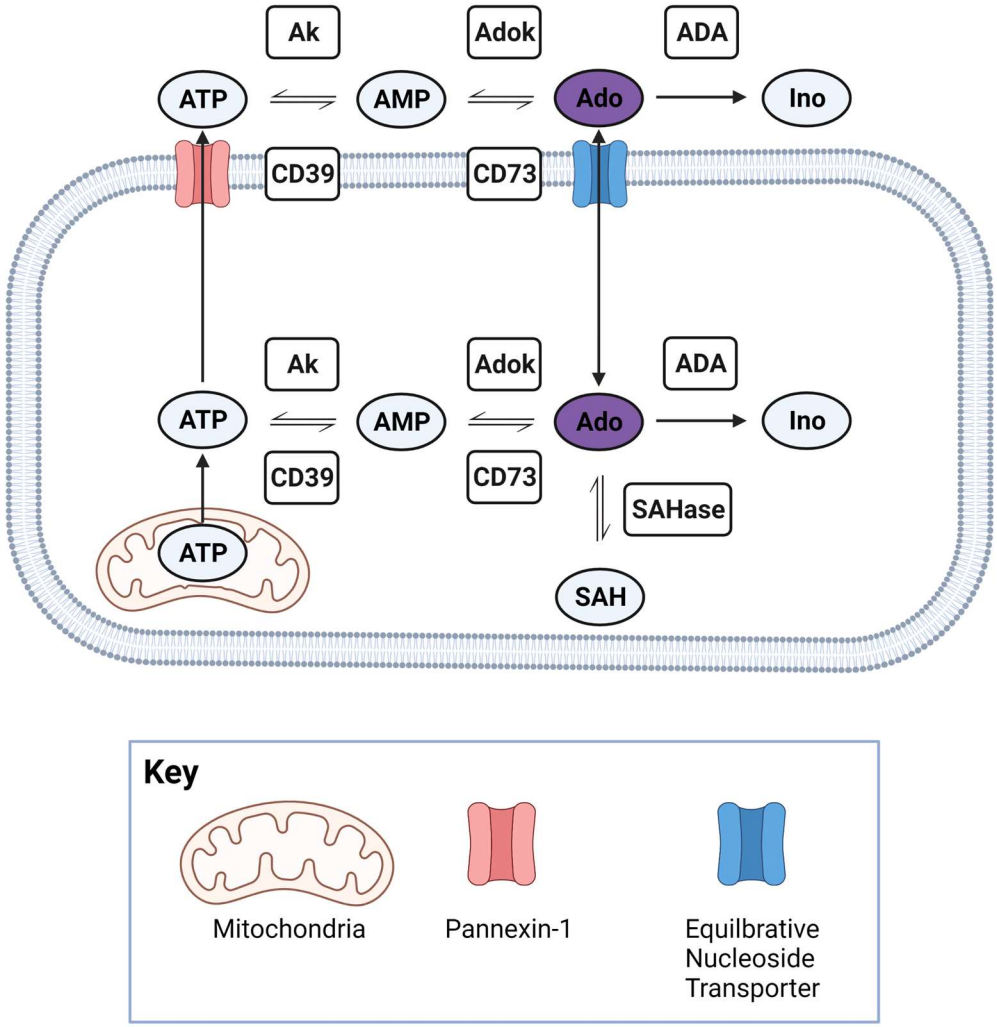


**Figure 1 The Pathways of Cellular Adenosine Metabolism.** Adenosine is generated by hydrolysis of AMP or SAH, via CD73 or SAHase, respectively. AMP is generated both intra- and intercellularly by the hydrolysis of ATP by CD39. ATP is generated in the mitochondria by oxidative phosphorylation. ATP is exported from the cell by the ATP binding cassette transporter Pannexin-1. Adenosine is transported in or out of the cell depending on its concentration gradient by equilibrative nucleoside transporters. Adenosine can be converted by AdoK and ADA into AMP and inosine, respectively. **Abs. ADA**-Adenosine deaminase**, Ado**- Adenosine, **Adok**- adenosine kinase, **AK**-Adenylate kinase, **AMP**-adenosine monophosphate, **ATP**- adenosine triphosphate, **CD39**- ecto-nucleotide triphosphate diphosphohydrolase-1, **CD73**- ecto-5′-nucleotidase, **Ino**- Inosine, **SAH**- S-Adenosylhomocysteine, **SAHase**- S-adenosylhomocysteine hydrolase. *Figure created with BioRender.com*

### 1.1.2 Adenosine Receptors

Extracellular adenosine regulates essential cellular processes by binding to a family of four class A G protein-coupled receptors (GPCRs): the $A_1$, $A_{2A}$, $A_{2B}$ and $A_3$ receptors (Fredholm et al., 2011). These receptor subtypes allow a vast range of differential signalling responses to adenosine due to different cell types expressing different combinations of adenosine receptors.

All GPCRs, including the adenosine receptors, have a characteristic structure of seven transmembrane-spanning helices, with each helix comprised of between 20–27 amino acids, a short membrane-associated helix (helix 8), an extracellular amino-terminus (N-terminus), a cytosolic carboxy-terminus (C-terminus), as well as three intracellular and three extracellular loops (Piirainen et al., 2011).

The ADORA genes code for the adenosine receptors in humans (Fredholm et al., 2011). All four human adenosine receptor genes contain a single intron in their coding sequences (Ren and Stiles, 1994, Jacobson et al., 1995, Murrison et al., 1996, Peterfreund et al., 1996). The overall sequence similarity between adenosine receptors is relatively high (Piirainen et al., 2011). Within the subtypes, adenosine $A_{2A}$ and $A_{2B}$ receptors have high sequence identity between themselves, and the $A_1$ and $A_3$ receptors also have high sequence similarities (Piirainen et al., 2011). In humans, there is a 59% similarity between the $A_{2A}$ and $A_{2B}$ receptors, and a 49% amino acid sequence similarity between $A_1$ and $A_3$ receptors (Jacobson and Gao, 2006).

The differences in the molecular structure of each adenosine receptor subtype cause them to have a unique pharmacological profile regarding ligand binding, activation, and G protein coupling. Most of the orthosteric binding site residues engaged by adenosine are conserved between the four receptor subtypes (Lane et al., 2011, Lebon et al., 2011). Beyond the orthosteric binding pocket, however, the extracellular loops of the adenosine receptors play a critical role in ligand binding and receptor activation (Peeters et al., 2011). In adenosine receptors, extracellular loop 2 (ECL2) is the largest and most diverse of the three extracellular loops and has been associated with determining ligand selectivity within the subfamily (Olah et al., 1994, Seibt et al., 2013, Geldenhuys et al., 2017, De Filippo et al., 2020). It has been shown that the ECL2 loop contributes directly to the binding of ligands by helping to form part of the orthosteric binding cavity of adenosine receptors (Lebon et al., 2015, Carpenter and Lebon, 2017).

The affinity of adenosine to the human $A_1$, $A_{2A}$, and $A_3$ receptors is approximately equal, however, the affinity of adenosine to the $A_{2B}$ receptor is approximately 50 times lower than its affinity to the other adenosine receptor subtypes (Fredholm et al., 2001). Despite differing affinity, the $A_{2A}$ receptor and $A_{2B}$ receptor have similar orthosteric ligand binding sites (Jaakola et al., 2010, Fredholm et al., 2011, El Maatougui et al., 2016). Analysis of the human $A_{2A}$ and $A_{2B}$ receptors show that most of the substantial differences in the amino acid sequences between the two receptors are found in the loop regions, particularly in the ECL2 region (Schiedel et al., 2011). Mutagenesis studies swapping around $A_{2A}$ and $A_{2B}$ receptor ECL2 regions to create hybrid receptors have demonstrated that ECL2 determines high $A_{2A}$ receptor affinity and low $A_{2B}$ receptor affinity to adenosine (Seibt et al., 2013, De Filippo et al., 2020).

Adora genes code the four adenosine receptors in rats (Fredholm et al., 2011). The rat $A_{2A}$ receptor is comprised of 410 amino acids, compared to the 412 amino acids of the human $A_{2A}$ receptor (**7.1.1.2**), with the receptors sharing an 82% sequence homology (Le et al., 1996, Chu et al., 1996, Alnouri et al., 2015). The rat $A_{2B}$ receptor is comprised of 332 amino acids (**7.1.1.2**), which is the same number as the human $A_{2B}$ receptor, with the receptors sharing 86% sequence homology (Pierce et al., 1992, Stehle et al., 1992, Alnouri et al., 2015). Differences in the human and rat versions of the receptors can lead to differing affinities for pharmacological ligands to these receptors (Alnouri et al., 2015). Therefore, it is important not to take a ligand's specificity for granted and to check for species differences when working *in vivo*.

### 1.1.3 Adenosine Receptor Intracellular Signalling Pathways

GPCRs couple to heterotrimeric G proteins comprising of α, β and γ subunits (Oldham and Hamm, 2008). G proteins are molecular switches that initiate and regulate intracellular signalling cascades via the enzymatic conversion of guanosine triphosphate (GTP) into guanosine diphosphate (GDP) (Oldham and Hamm, 2008). In humans, there are known to be 21 different α subunits, which fall into four different families, $\alpha_s$, $\alpha_i$, $\alpha_q$ and $\alpha_{12}$ (Downes and Gautam, 1999, Oldham and Hamm, 2006).

$A_1$ and $A_3$ receptors are $G_i$-coupled and mediate responses via inhibition of adenylyl cyclase (AC), which is an enzyme that produces intracellular cyclic adenosine monophosphate (cAMP), and thus inhibition of AC decreases cAMP concentrations. On the other hand, $A_{2A}$ and $A_{2B}$ receptors are $G_s$-coupled and mediate their effects via stimulation of AC activity, increasing intracellular cAMP levels (**Figure 2**) (Antonioli et al., 2019).

Additionally, $A_1$ and $A_3$ receptor stimulation leads to $G_{\beta\gamma}$ subunit activation of phospholipase C (PLC), which causes the cleavage of phosphatidylinositol 4,5-bisphosphate ($PIP_2$) into diacyl glycerol (DAG) and inositol 1,4,5-trisphosphate ($IP_3$). $IP_3$ then causes the release of $Ca^{2+}$ from intracellular stores (Fredholm et al., 2000, Jacobson and Gao, 2006). $A_{2B}$ receptors can also cause PLC activation and $Ca^{2+}$ release, but through the alternative pathway of $G_q$ regulation (Klinger et al., 2002, Antonioli et al., 2013a).

Regulation by adenosine receptors of protein kinase C (PKC) by localised $Ca^{2+}$ concentrations, and protein kinase A (PKA) by localised cAMP concentrations, triggers downstream signalling cascades that can modulate the transcription of genes involved in cell regulation. For example, adenosine receptors have been demonstrated to affect nuclear factor κ-light-chain-enhancer of activated B cells (NF-κB), cyclic adenosine monophosphate response element-binding protein (CREB), and hypoxia-inducible factor 1 (HIF-1) (Merighi et al., 2005, Gessi et al., 2010, Borea et al., 2016). Additionally, it has been reported that $A_{2B}$ receptors can regulate the production of eicosanoids by exerting influence on the arachidonic acid cascade, leading to the release of prostanoids that activate the thromboxane receptor, which can cause vasoconstriction (Donoso et al., 2005).

All adenosine receptors are coupled via $G_{\beta\gamma}$ subunit activation to pathways involving the mitogen-activated protein kinase (MAPK) protein family, and these include the phosphorylation of extracellular signal-regulated kinase 1 (ERK1), extracellular signal-regulated kinase 2 (ERK2), and p38 MAPK (Schulte and Fredholm, 2000, Schulte and Fredholm, 2003, Jacobson and Gao, 2006, Antonioli et al., 2013a).

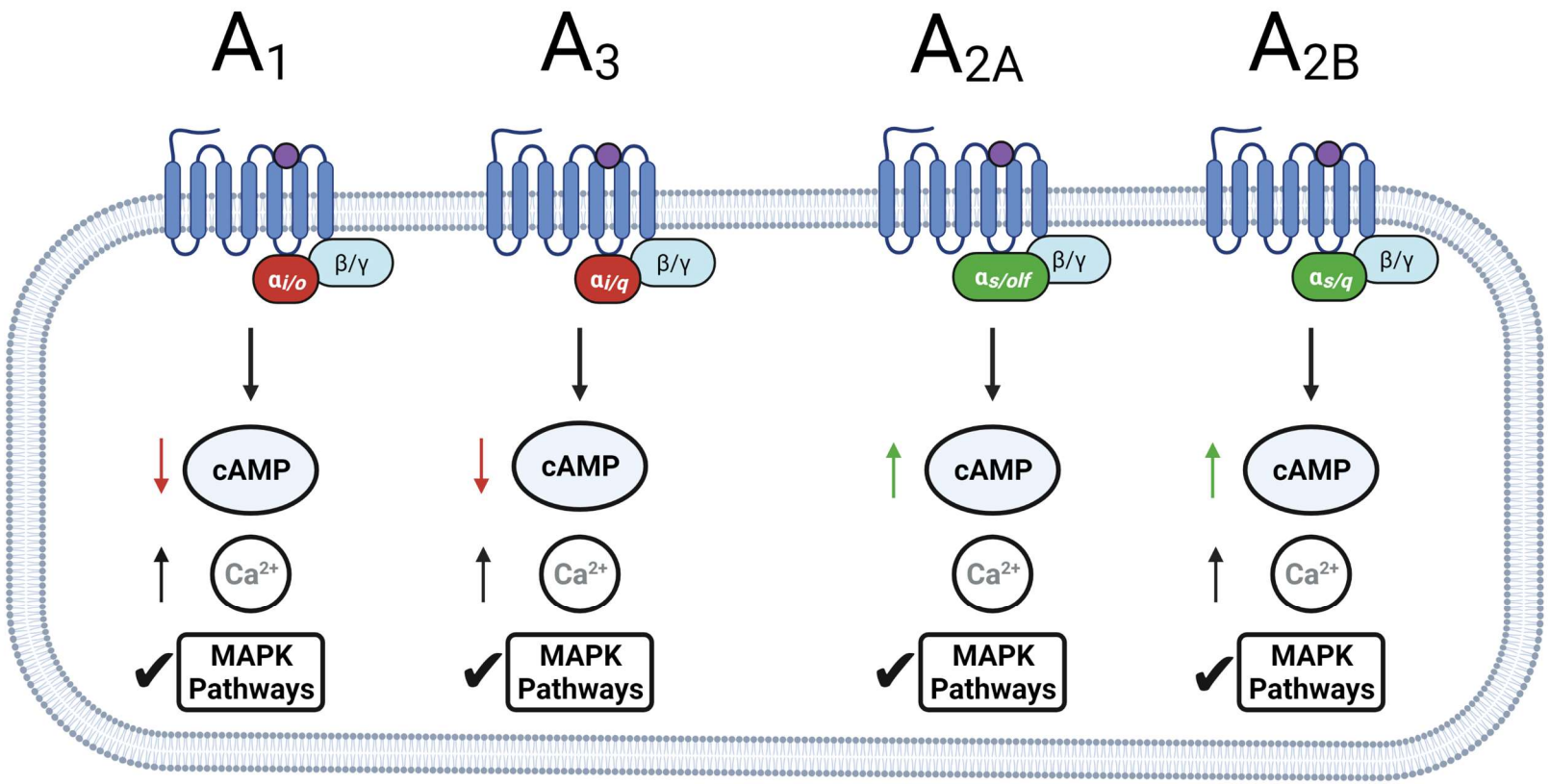


**Figure 2 The Main Signalling Transduction Pathways Activated by the Four Adenosine Receptors.** $A_1$, $A_{2A}$, $A_{2B}$ and $A_3$ receptors are activated by extracellular adenosine (purple). $A_{2A}$ and $A_{2B}$ receptors are coupled to $G_s$ proteins, which lead to adenylyl cyclase (AC) activation and cyclic AMP (cAMP) increases. Conversely, $A_1$ and $A_3$ receptors are coupled to $G_i$ proteins which inhibit AC and decrease cAMP. Additionally, $A_{2B}$ and $A_3$ receptors have been reported to couple with $G_q$ proteins, and $A_1$ receptors with $G_o$ proteins, with both sets of couplings initiating pathways that lead to intracellular $Ca^{2+}$ release from intracellular stores. All four adenosine receptors are known to activate pathways involving mitogen-activated protein kinases (MAPKs). **Abs. $Ca^{2+}$**- Ionic Calcium, **cAMP**- Cyclic adenosine monophosphate, **MAPK**- Mitogen-activated protein kinase. *Figure created with BioRender.com*

### 1.1.4 Adenosine Receptor Expression in the Cardiovascular System

In the cardiovascular system, the $A_1$ receptor is found in vascular smooth muscle and endothelial cells (Lynge and Hellsten, 2000). $A_1$ receptors are also present in pacemaker cells of both the sinoatrial node (SAN) and atrioventricular (AV) node (Lou et al., 2014, Li et al., 2017). The $A_{2A}$ receptor is highly expressed in all cardiovascular tissues, including the heart vasculature, cardiomyocytes and pacemaker cells (Hove-Madsen et al., 2006, Fredholm et al., 2011, Li et al., 2017, Boknik et al., 2021). Functional $A_{2B}$ receptors have been found in fibroblasts (Chen et al., 2004) and myocardial cells (Liang and Haltiwanger, 1995). High levels of $A_{2B}$ receptor expression are found throughout the vasculature, both in smooth muscle and endothelial cells, with the $A_{2B}$ receptor demonstrated to be extensively distributed throughout the vasculature of most organs, including the heart, lung, brain, pancreas, retina, liver, kidney and large intestine (Dixon et al., 1996, Yang et al., 2006, St Hilaire et al., 2008, Maas et al., 2010, Teng et al., 2013). Low levels of the $A_3$ receptor have been found in the aorta (Gessi et al., 2008). In cardiomyocytes, there is no direct evidence of the presence of $A_3$ receptors, however, studies have reported that the $A_3$ receptor is responsible for cardioprotection in a range of species and models, in addition to isolated myocardial muscle preparations and isolated cardiomyocytes, suggesting the receptor is present at low levels (Peart and Headrick, 2007).

The expression of adenosine receptors can vary in a cellular bed, even amongst cells of the same type. For example, heterogeneous cell differences in adenosine $A_1$ receptor expression across the SAN complex have been discovered (Li et al., 2017). A potential cause of total SAN failure is blockade by adenosine, its effects mediated mainly by the dromotropic (the velocity in which the electrical impulse is propagated across the node) actions of $A_1$ receptor activation; if the effects of adenosine block the lead pacemaker, then normally redundant backup pacemaker cells, expressing a lower level of the $A_1$ receptor, will take over as the lead pacemaker to protect against total SAN arrest (Li et al., 2017, Kalyanasundaram et al., 2019).

Changes in adenosine receptor expression have been demonstrated to be important to disease states. For example, overexpression of $A_1$ receptors can induce cardiomyopathies such as cardiac dilatation and hypertrophy (Funakoshi et al., 2006). Additionally, overexpression of $A_1$ receptors in failing hearts has been demonstrated to cause a decrease in SAN automaticity, decreasing heart rate, which has a detrimental impact to cardiac output, and can exacerbate conduction abnormalities, causing atrial fibrillation (Lou et al., 2014, Kalyanasundaram et al., 2019). Another example is that patients with coronary artery disease (CAD) have been shown to have a lower basal expression of the $A_{2A}$ receptor in their coronary arteries compared to healthy adults (Guieu et al., 2015, Paganelli et al., 2018). Finally, it has been shown in spontaneously hypertensive rats that $A_3$ receptor downregulation could contribute to essential hypertension, although the mechanism of action for this is currently unclear (Ho et al., 2016).

Adenosine receptor expression has been demonstrated to be a dynamic process. For example, it has been shown that $A_1$ receptor expression can be upregulated by long-term activation of the $A_{2A}$ receptor (Brito et al., 2012). Also, excess extracellular adenosine has been shown to lead to both $A_{2B}$ receptor activation and expression upregulation (Sorrentino and Morello, 2017, Yu et al., 2020). Furthermore, $A_{2B}$ receptors on cancer-associated fibroblasts have been shown to upregulate the generation of adenosine, leading to a feed-forward positive feedback circuit of extracellular adenosine generation, causing a higher expression of $A_{2B}$ receptors (Yu et al., 2020).

### 1.1.5 Adenosine Signalling in Cardiovascular Regulation

Adenosine was first identified as a modulator of heart rate, blood pressure and coronary vascular tone in 1929, being described as a potent vasodilator-like molecule (Drury and Szent-Györgyi, 1929). Adenosine is known to cause a decrease in systemic arterial blood pressure through these vasodilatory effects (Zhang et al., 1991).

The activation of $A_{2A/2B}$ receptors located on both vascular endothelial and vascular smooth muscle cells are known to cause vasodilatory effects (Lewis et al., 1994, Leal et al., 2008). In endothelial cells, this is due to the activation of $G_{S,}$ proteins, which triggers nitric oxide (NO) release by activating the AC-cAMP-PKA pathway, with PKA activating endothelial nitric oxide synthase (eNOS) to generate NO from L-arginine (**Figure 3**) (Ray and Marshall, 2006, El-Gowelli et al., 2013). NO is a potent regulator of the vascular tone; it mediates vasodilation by stimulating soluble guanylyl cyclase (GC) and increasing cyclic guanosine monophosphate (cGMP) in smooth muscle cells, which causes their relaxation (**Figure 3**) (Förstermann and Sessa, 2012). Additionally, activation of $A_{2A/2B}$ in vascular smooth muscle cells activates the AC-cAMP-PKA pathway, with PKA in this cell type leading to downstream phosphorylation and subsequent opening of $K^+$ channels; the opening of these channels causes $K^+$ to leave the cell down its concentration gradient, which, in turn, causes cellular hyperpolarisation and subsequent vasodilatation (**Figure 3**) (Ko et al., 2008, Sanjani et al., 2011, El-Gowelli et al., 2013). In contrast to $A_{2A/2B}$ receptors, $A_1$ and $A_3$ receptors work to directly oppose the effects of $A_{2A/2B}$ receptor-induced vasodilation through coupling to $G_{i/o}$, causing inhibition of AC, deactivating the AC-cAMP-PKA pathway discussed above, and thus causing subsequent vasoconstriction (Mustafa et al., 2009, Ponnoth et al., 2009). The result of these receptor couplings means that although adenosine is known for its vasodilatory effects, it can, in some cases, act as a vasoconstrictor, depending on its interaction with specific receptor subtypes, adenosine plasma levels and the location of the vasculature affected. The cardiovascular effects of adenosine in the regions of the body investigated during experiments conducted in this thesis will now be discussed in detail.

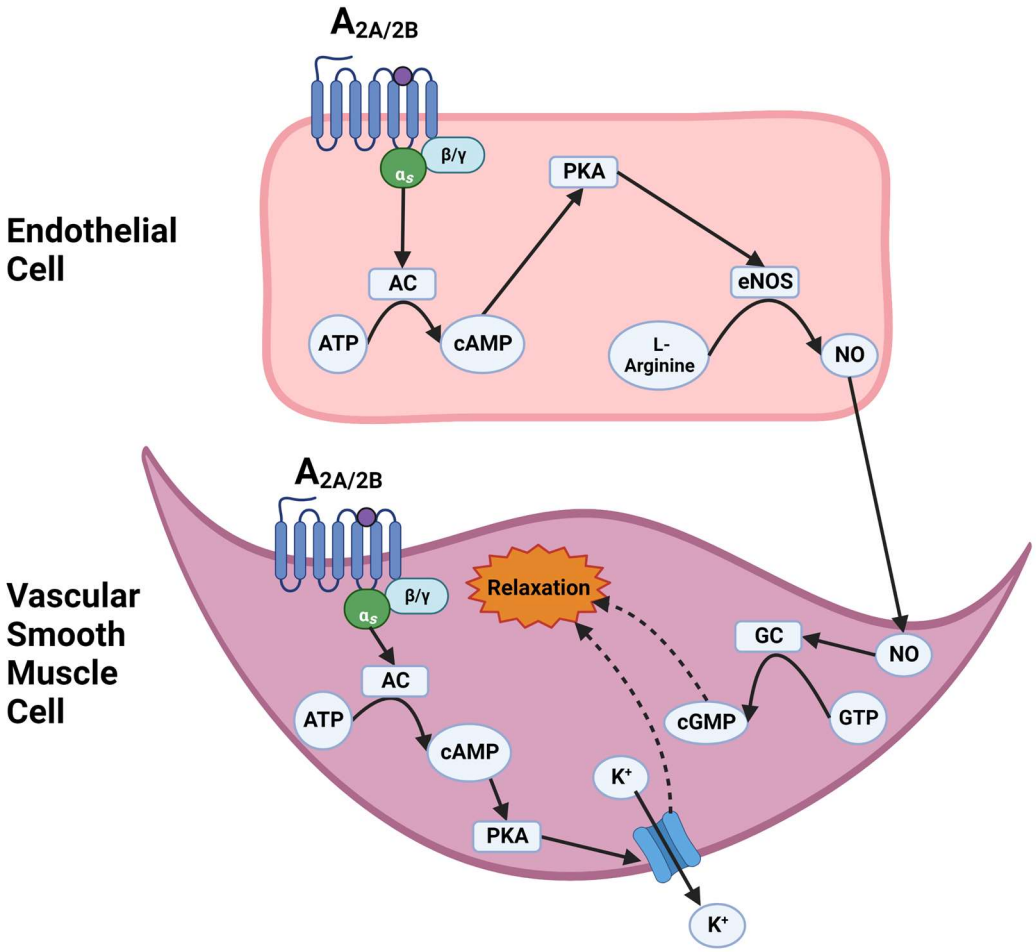


**Figure 3 Activation of Adenosine $A_{2A}$ or $A_{2B}$ Receptors cause Relaxation of Vascular Smooth Muscle Cells.** The activation of the two $A_2$ receptors located in both vascular endothelial and vascular smooth muscle cells are known to cause vasodilatory effects by $A_2$ receptors. In endothelial cells, activation of $G_S$, triggers NO release by activating the AC-cAMP-PKA pathway, with PKA activating eNOS, causing the generation of NO from L-arginine. NO causes smooth muscle relaxation by stimulating soluble GC which increases cyclic GMP resulting in relaxation. Additionally, direct activation of $A_2$ receptors in vascular smooth muscle cells activates the AC-cAMP-PKA pathway, with PKA in this cell type leading to downstream phosphorylation and subsequent opening of $K^+$ channels; causing $K^+$ to leave the cell down its concentration gradient, which, in turn, causes cellular hyperpolarisation and subsequent relaxation. **Abs. PKA-** Protein Kinase A**, eNOS-** Endothelial nitric oxide synthase**, AC-** Adenylyl cyclase**, cAMP-** Cyclic adenosine monophosphate**, cGMP-** Cyclic guanosine monophosphate**, GC-** guanylate cyclase**, NO-** Nitric oxide. *Figure created with BioRender.com*

#### 1.1.5.1 Adenosine Signalling in the Heart

Adenosine has an effect on the heart that is cell-type dependent. In the coronary system, which is the blood vessels that supply the heart, the $A_{2A}$ receptor is the principal adenosine receptor subtype responsible for coronary blood flow regulation, exerting its effects on both the vascular endothelium and vascular smooth muscle cells, causing both endothelium-dependent and endothelium-independent vasodilation (Lewis et al., 1994, Shryock et al., 1998, Leal et al., 2008, Mustafa et al., 2009). $A_{2B}$ receptor activation has been reported not to cause any effect on the dilation of coronary arteries in the guinea pig heart (Martin et al., 1993); however, a knockout mouse study found $A_{2B}$ receptors to cause vasodilation in the coronary arteries (Berwick et al., 2010). The $A_1$ receptor has been demonstrated to counter the effects of the $A_{2A}$ receptor and cause vasoconstriction in coronary arteries (Ponnoth et al., 2009).

Adenosine exerts a negative chronotropic effect by automaticity suppression of cardiac pacemaker cells that make up the SAN and a negative dromotropic effect by slowing the conduction time through the AV node; both of these effects are due to activation of $A_1$ receptors found on the pacemaker cells (Mustafa et al., 2009, Eltzschig, 2013, Li et al., 2017).

On atrial myocardial cells, negative inotropic (strength of contraction) effects are reported that are related to $A_1$ receptor stimulation (Burnstock and Meghji, 1983, Belardinelli and Isenberg, 1983) (**Figure 4**). On the other hand, adenosine exerts an indirect positive inotropic effect through endothelial independent vasodilation in the coronary circulation, which leads to an increase in coronary flow, and a subsequent increase in cardiac output due to Gregg's phenomenon (Goto et al., 1991). Gregg's phenomenon is the observation that increases in coronary perfusion cause an increase in cardiac strength (Gregg, 1963); this is thought to occur because the filling of the intramyocardial coronary vasculature stretches the surrounding cardiomyocytes, which leads to an increase in contractile force via the Frank-Starling mechanism, although current research into the phenomenon appears to be lacking (Dijkman et al., 1997). Unlike the $A_1$ and $A_{2A}$ receptors, activation of the $A_{2B}$ receptor seemingly causes minimal direct physiological effects on the heart (Liu et al., 2010, Maas et al., 2010).

#### 1.1.5.2 Adenosine Signalling in Renal Vascular Beds

The kidneys are filters that control the blood's volume and electrolyte composition, and remove toxins from the body. In the kidney, the vasculature functions to both filter the blood and deliver blood to the kidney. The blood is supplied to the kidney by the main renal artery which branches into progressively smaller vessels that supply afferent arterioles that feed blood into the glomerular capillaries situated in the Bowman's capsule of the nephron, where the blood is filtered by a unique double capillary bed system, which ends in the capillaries found in each glomerulus forming together into the efferent arterioles in the glomerulus, which supply the kidney with blood (Chade, 2013).

Juxtaglomerular cells of the afferent arteriole are baroreceptors that sense renal perfusion pressure (Gomez and Sequeira Lopez, 2009). When blood pressure falls, renin is released, and when blood pressure is high, renin release is inhibited (Gomez and Sequeira Lopez, 2009, Harrison-Bernard, 2009). It has been demonstrated that at high pressures, the formation and action of adenosine are critical to baroreceptor-mediated inhibition of renin release from juxtaglomerular cells through actions at the $A_1$ receptor (Schweda et al., 2005, Gomez and Sequeira Lopez, 2009). This is thought to be due to the $A_1$ receptor activating $Ca^{2+}$-permeable nonselective cation channels known as transient receptor potential canonical (TRPC) channels (Ortiz-Capisano et al., 2013). $A_{2A}$ and $A_{2B}$ receptors are not thought to have a direct effect on renin release (Ortiz-Capisano et al., 2013).

In the renal vasculature, in *ex vivo* rat kidneys, adenosine can cause vasoconstriction in the afferent arterioles at a micromolar range through activation of $A_1$ receptors, but vasodilation at higher concentrations above 10 μM through activation of $A_2$ receptors (Tang et al., 1999). $A_{2B}$ receptor activation has been demonstrated to be the major driver of $A_2$ receptor vasodilation in the afferent arterioles, with $A_{2A}$ receptors demonstrated only to have a minor role in the functional vasodilatory response (Martin and Potts, 1994, Feng and Navar, 2010, El-Gowelli et al., 2013) (**Figure 4**). It has been demonstrated that rat *in vivo* renal vascular flow is increased on the administration of adenosine and the non-selective adenosine agonist NECA, but $A_1$ receptor agonists cause a decrease in renal vascular flow (Gardiner et al., 1991, Jolly et al., 2008, Cooper et al., 2020) (**Figure 4**).

#### 1.1.5.3 Adenosine Signalling in Mesenteric Vascular Beds

The mesentery is an organ that holds the intestines in place from the posterior abdominal wall and is vital to the supply of blood to the intestines via the superior and inferior mesenteric arteries that branch off the descending aorta (Coffey and O'Leary, 2016).

Adenosine is known to have an important role in the regulation of the mesenteric circulatory system. Adenosine is involved in the vasodilatory response due to post-prandial hyperaemia, which is an increase in blood flow to the gut after eating to modulate intestinal blood flow in accordance with the nutritional needs of the gut (Sawmiller and Chou, 1988, Sawmiller and Chou, 1992). It is also involved in producing vasodilations in response to reactive hyperaemia in the mesentery, which is increased blood flow after a period of transient ischaemia (Sawmiller and Chou, 1992). Finally, there is evidence that adenosine is involved in pressure-flow autoregulation of the mesenteric circulation, especially when the gut is full, to keep the flow constant through the organ in response to pressure changes (Granger and Norris, 1980, Lautt, 1986).

Adenosine is known to cause increases in superior mesenteric arterial conductance (Zhang et al., 1991). $A_{2A}$ receptor activation has been demonstrated to cause vasodilation in mesenteric arterial beds (Hiley et al., 1995) (**Figure 4**). $A_{2B}$ receptor activation has also been reported to cause vasodilation in the arteries comprising the mesenteric arterial bed (Rubino et al., 1995, Tabrizchi and Lupichuk, 1995, Teng et al., 2013) (**Figure 4**). It has been demonstrated that rat *in vivo* mesenteric vascular flow is increased by the administration of adenosine and the non-selective adenosine agonist NECA but is decreased by the administration of the $A_1$ receptor agonist CCPA (Gardiner et al., 1991, Jolly et al., 2008, Cooper et al., 2020) (**Figure 4**).

#### 1.1.5.4 Adenosine Signalling in Hindquarters Vascular Beds

The hindquarters are the hind legs and adjoining parts of a quadruped, such as a rat. They represent and correspond to the human legs, buttocks and genital areas. The blood supply for these areas is from the descending abdominal aorta, which bifurcates into the iliac artery that runs down each side of the body into the legs (Laughlin and Ripperger, 1987).

It has been previously demonstrated that rat *in vivo* hindquarters vascular flow is increased by the administration of adenosine and the non-selective adenosine agonist NECA (Gardiner et al., 1991, Jolly et al., 2008). *In vivo* studies have demonstrated that $A_2$ receptors cause vasodilatory effects in the hindquarters vascular beds (Barrett et al., 1992, Barrett et al., 1993, Bivalacqua et al., 2002), specifically the $A_{2A}$ receptor (Bryan and Marshall, 1999) (**Figure 4**). In contrast to the other vascular beds described, the $A_1$ receptor is reported to cause vasodilation in the hindquarters vascular bed (Bryan and Marshall, 1999, Bivalacqua et al., 2002) (**Figure 4**). It has also been demonstrated *in vivo* that rat hindquarters flow is increased by the administration of the $A_1$ receptor agonist CCPA (Cooper et al., 2020) (**Figure 4**). Interestingly, and perhaps paradoxically, $A_1$ receptor-mediated vasodilation has been demonstrated to be dependent on AC-cAMP generation (Bivalacqua et al., 2002), which is the opposite of what occurs at the renal and mesenteric vascular beds mentioned previously and perhaps would not be expected as the $A_1$ receptor is $G_i$ linked. The mechanism of $A_1$ receptor-mediated vasodilation has been suggested to be due to vasodilatation in the resistance arteries supplying skeletal muscle through ATP-sensitive $K^+$ ($K_{ATP}$) channels promoting $K^+$ efflux, and prostaglandin (PG) and NO production (Bryan and Marshall, 1999, Ray and Marshall, 2006). In contrast, Bivalacqua *et al.* 2002 reported that the mechanism of $A_1$ receptor-mediated dilation in the hindquarters of cats was not dependent on NO, PG, or $K_{ATP}$ channels, and so the exact mechanisms of this are yet to be fully understood (Bivalacqua et al., 2002).

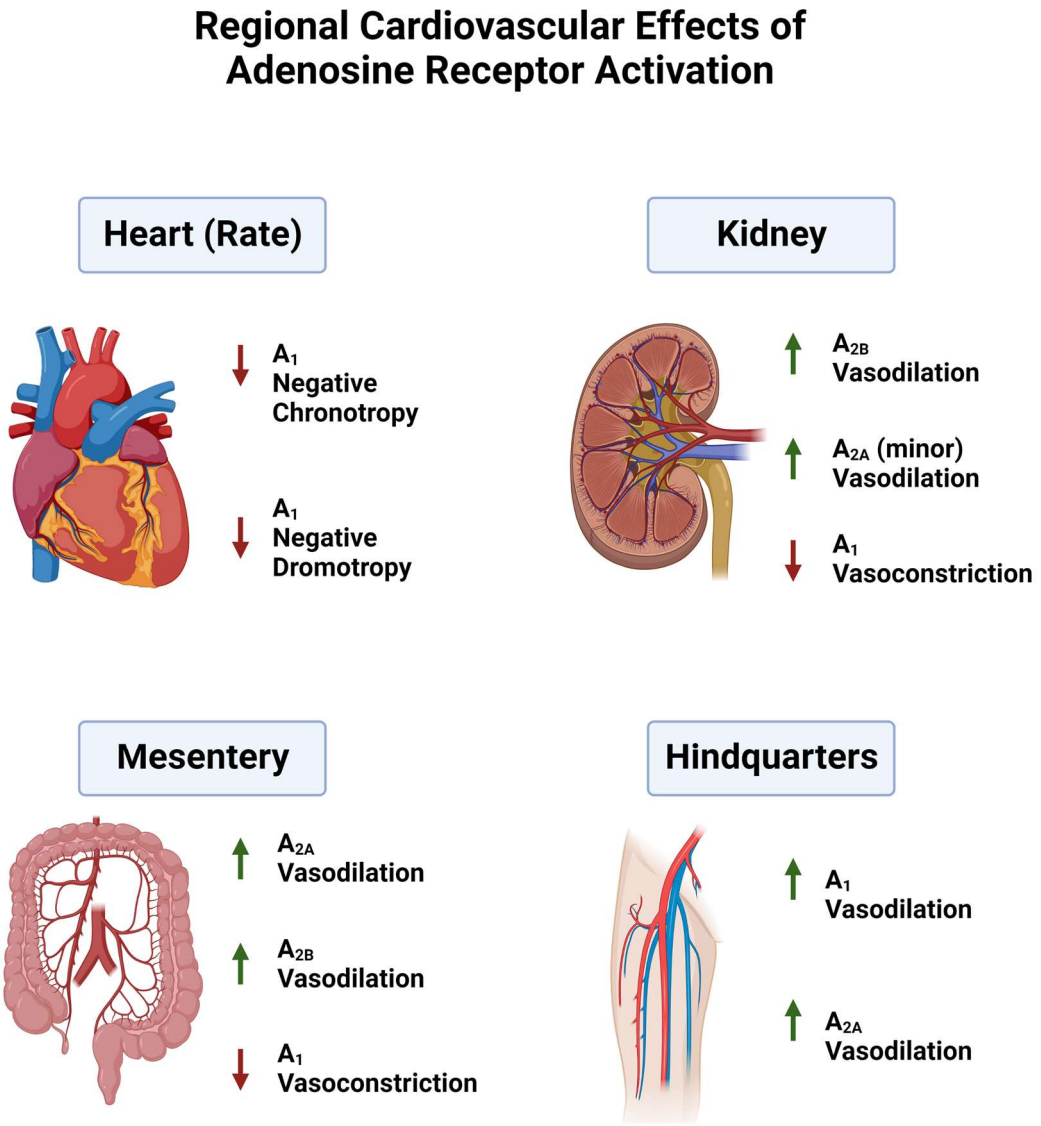


**Figure 4 The Physiological Consequences of Adenosine Receptor Activation on Heart Rate and the Vasculature Beds of the Kidneys, Mesentery and Hindquarters.** Adenosine $A_1$ receptors influence the heart's rate (chronotropy) and electrical conduction speed (dromotropy). In the renal vascular beds, adenosine $A_{2B}$ receptors, and to a lesser extent, $A_{2A}$ receptors induce vasodilation, whereas $A_1$ receptors induce vasoconstrictions. In the mesentery, $A_{2A}$ and $A_{2B}$ receptors have been shown to cause vasodilations, whereas $A_1$ receptors induce vasoconstrictions. In the vascular beds of the hindquarters, both $A_1$ and $A_{2A}$ receptors have been demonstrated to induce vasodilations. *Figure created with BioRender.com.*

## 1.1.6 Adenosine Signalling in Cardiovascular Disease

### 1.1.6.1 Current Cardiovascular Clinical Uses of Adenosine Agonists

As described in section **1.1.1**, adenosine has a metabolic half-life of under 10 seconds *in vivo,* which makes the effects of an adenosine intravenous (i.v.) bolus short-lived (Moser et al., 1989). This unique property of adenosine allows it to be used as a 'shock agent' to terminate certain cardiac arrhythmias, such as conditions that cause supraventricular tachycardia or as a diagnostic 'stress test' during myocardial perfusion imaging (MPI) studies at doses that would otherwise be toxic if maintained.

Continuous adenosine infusion can be used in conjunction with a radiotracer in stress/rest MPI studies to diagnose CAD and damage to the myocardium. MPI studies use positron emission tomography (PET) or single-photon emission computed tomography (SPECT) imaging of a patient's heart before and after either exercise or pharmacological stressor (adenosine) to determine the effect of physical stress on the blood flow through the coronary arteries of the heart (Lieu et al., 2007). During MPI, adenosine increases blood flow in the myocardium. If the patient has a healthy coronary flow, this increase can be as much as five-fold the resting value, whereas, in a patient with an impaired flow reserve due to cardiovascular disease, the adenosine-mediated increases in blood flow are reduced (Lieu et al., 2007).

An alternative to adenosine used in MPI studies is Regadenoson (CVT3146), which is an adenosine receptor agonist that is functionally selective for the $A_{2A}$ receptor over the other three adenosine receptors (Gao et al., 2001, Lieu et al., 2007). Regadenoson is not a substrate for adenosine deaminase, unlike adenosine, and thus is not rapidly metabolised in the body (Gupta and Bajaj, 2018). Regadenoson has a terminal half-life of approximately an hour and is mostly (58%) excreted by the kidneys (Gordi et al., 2006, Al Jaroudi and Iskandrian, 2009). Furthermore, because Regadenoson is $A_{2A}$ receptor-selective, it causes less undesirable side effects to the patient during MPI studies than adenosine, including reduced AV block (Al Jaroudi and Iskandrian, 2009).

An additional use of adenosine is as an antiarrhythmic agent for investigating and treating certain types of tachycardia (Eltzschig, 2013). Adenosine is considered a class V antiarrhythmic agent, as it falls outside the other classes of the Vaughan-Williams classification of antiarrhythmic agents (Cobbe, 1987). An adenosine bolus will cause the heart to enter ventricular asystole for a few seconds by causing a brief blockade of the AV node, preventing nodal conduction pathways. This blockade is caused by the activation of $A_1$ receptors on cardiac pacemaker cells (Eltzschig, 2013, Li et al., 2017, Kalyanasundaram et al., 2019). This block can unmask and identify arrhythmias if they are present, such as Wolff-Parkinson-White syndrome, a condition in which an additional electrical conduction pathway is present in the heart that allows conduction to bypass the AV node and travel straight from the atria to the ventricles, which will be clear on an electrocardiogram (ECG) in the presence of AV block (Al-Khatib and Pritchett, 1999). This brief AV block can also be used to terminate re-entrant arrhythmias that involve the AV node, such as supraventricular tachycardia, were electrical activity re-enters the atria via the ventricles, causing a self-sustaining electrical loop (Zehender et al., 1996, Mallet, 2004, Neumar et al., 2010).

### 1.1.6.2 Therapeutic Potential of Adenosine $A_2$ Receptors in Cardiovascular Disease

Currently, short-acting adenosine and Regadenoson are the only adenosine agonists approved for clinical use (**1.1.6.1**). However, targeting all four adenosine receptors has been shown to have therapeutic potential, and thus new ligands are under development to potentially treat a range of conditions (Jacobson et al., 2019).

Although all four adenosine receptors show therapeutic potential, work for studies in this thesis has focused on the $A_2$ receptors and their role in the cardiovascular system. One potential clinical use for adenosine agonists is cardioprotection (Hisatome, 2007, Busse et al., 2016, Alencar et al., 2017). Adenosine has been demonstrated to be cardioprotective, protecting from cardiovascular damage caused by ischaemia/reperfusion injury, with endogenous synthesis of adenosine after myocardial infarction demonstrated to protect the heart from excess damage (Hisatome, 2007, Busse et al., 2016, Alencar et al., 2017). Furthermore, studies have demonstrated that activation of the $A_{2A}$ receptor is a vital component in bringing about this cardioprotection, with the heart protected during ischaemia/reperfusion injury caused by myocardial infarction by activating the $A_{2A}$ receptor prior to or during reperfusion (McIntosh and Lasley, 2012, Borea et al., 2016, da Silva et al., 2017).

There is also significant evidence that adenosine represents a potent modulator of cardiac myocyte hypertrophy and could help in diseases associated with pathological cardiac remodelling, such as heart failure (Wakeno et al., 2006, Xia et al., 2007, Chuo et al., 2016, da Silva et al., 2017). A reduction in the expression of ventricular $A_{2A}$ receptors has been reported in patients with chronic heart failure (Asakura et al., 2007). Additionally, the activation of adenosine receptors plays a crucial role in preventing renal failure due to conditions causing hypoxia or ischaemia by promoting renal perfusion (Yap and Lee, 2012, Borea et al., 2018).

As for the $A_{2A}$ receptor, $A_{2B}$ receptor activation has been demonstrated to be cardioprotective in ischaemia-reperfusion injury, as detailed above (Kuno et al., 2007, Eltzschig et al., 2014, Tian et al., 2015, Lasley, 2018, Ni et al., 2018).

The $A_{2B}$ receptor has been shown to increase the activity of cardiac fibroblasts, which have an essential role in the production of the extracellular matrix of the heart, which is crucial for maintaining its structural integrity (Camelliti et al., 2004, Souders et al., 2009). As a result, the $A_{2B}$ receptor has been shown to be a promoter of cardiac fibrosis, and $A_{2B}$ receptor blockade has been shown to be beneficial in *in vivo* models of pathogenic cardiac remodelling and fibrosis, improving cardiac function by preventing the remodelling and fibrogenesis that occurs following $A_{2B}$ receptor activation that occurs in heart failure (Toldo et al., 2012, Zhang et al., 2014, Francis et al., 2016, Stuart et al., 2016).

$A_{2A}$ and $A_{2B}$ receptors are promising targets for a wide range of cardiovascular diseases, particularly acute kidney injury and hypertension (Yap and Lee, 2012, Borea et al., 2018, Jamwal et al., 2019). Activation of $A_{2B}$ receptors has been demonstrated to play an important role in both renal and mesenteric ischaemic reperfusion injury by improving capillary flow in these regions (Grenz et al., 2008, Hart et al., 2009). $A_{2B}$ receptor agonism has been demonstrated to attenuate ischaemic kidney injury in a mouse model (Grenz et al., 2008).

Both $A_2$ receptors promote vasodilatation, and, as a result, $A_{2A}$ and $A_{2B}$ receptors are potential targets for the treatment of hypertension (Jacobson and Gao, 2006, Borea et al., 2018, Jamwal et al., 2019). $A_{2A}$ receptor activation has been shown to cause vasodilation that induces hypotension in the rat (Alberti et al., 1997). Systemic administration of non-selective adenosine $A_{2A/2B}$ receptor agonists produces hypotension that is believed to be a direct consequence of vasodilation induced by $A_{2A/2B}$ receptor activation, caused by the indirect effect of causing increases in renal blood flow, which causes subsequent sodium excretion, which reduces blood pressure (Evoniuk et al., 1987, Mathôt et al., 1995, Lai et al., 2006, Feng and Navar, 2010).

Evidence shows that $A_{2A}$ receptor activation can increase sympathetic reflex activity, which regulates heart rate and vascular conduction throughout the body (Alberti et al., 1997, El-Mas et al., 2011, Minic et al., 2015). $A_{2B}$ receptors are also found in an area of the brain that influences sympathetic reflex activity (Bauer et al., 1988, Lee and Koh, 2009). These effects will be discussed in detail in the subsequent section (**1.2**). Understanding how sympathetic reflexes interplay with the haemodynamic response to $A_2$ receptor activation is crucial as they may change the physiological effects of adenosine $A_2$ receptor activation *in vivo* and thus influence the therapeutic potential of adenosine $A_2$ receptor ligands.

## 1.2 Homeostatic Regulation of Blood Pressure: the Importance of the Baroreflex

The arterial baroreflex is a critical neural reflex that enacts short-term fine regulation of blood pressure by inducing rapid changes in heart rate (HR) and peripheral vascular resistance (Kougias et al., 2010). The continuous sensation of blood pressure by tonic arterial baroreceptors situated in the carotid sinus and the aortic arch is transmitted to the Nucleus Tractus Solitarius (NTS) situated in the medulla oblongata via the glossopharyngeal nerve (IX) and the vagus nerve (X), respectively (**Figure 5**). Increases in arterial blood pressure will cause an increase in baroreceptor activation and rate of impulse firing. In contrast, the opposite is true with decreases in arterial blood pressure, resulting in a decrease in baroreceptor activation and, as a result, a reduction in NTS stimulation.

Excitatory projections from the NTS stimulate the caudal ventrolateral medulla (CVLM). Inhibitory projections from the CVLM inhibit the rostral ventrolateral medulla (RVLM); this then leads to the reduction of excitation of neurons in the spinal intermediolateral grey column, which causes a reduction in the sympathetic output to the heart and blood vessels by post-ganglionic sympathetic neurons that release noradrenaline (**Figure 5**). Excitatory projections from the NTS also stimulate the Nucleus Ambiguus (NA), which causes an increase in parasympathetic output to the heart by post-ganglionic parasympathetic neurons that release acetylcholine (ACh) (**Figure 5**) (Suarez-Roca et al., 2021). As a result, increases in blood pressure are corrected by decreases in sympathetic outflow to the heart and vasculature and increases in parasympathetic outflow to the heart. Decreases in blood pressure are corrected by increased sympathetic outflow to the heart and vasculature and decreased parasympathetic outflow to the heart.

### 1.2.1 Pharmacology of the Baroreflex

The physiological responses to sympathetic outputs under the control of the baroreflex result from the binding of the catecholamines noradrenaline and adrenaline to adrenoceptors (Barki-Harrington et al., 2004). In particular, $\beta_1$ and $\beta_2$ adrenoceptors have central roles in regulating cardiovascular homeostasis (Chruscinski et al., 2001, Ali et al., 2020). It is well established that $\beta_1$ adrenoceptors mediate heart rate responses to noradrenaline and adrenaline, with $\beta_2$ mediating inotropy due to actions on cardiac myocytes and vasculature tone on blood vessels (Schäfers et al., 1994, Bristow, 2011).

$\beta_1$ adrenoceptors are also expressed in the kidneys, where they stimulate renin secretion (Osborn et al., 1981, Jacob et al., 2005). $\beta_1$ blockade has been demonstrated to cause a decrease in plasma renin activity (Petersen et al., 2012). Renin acts via the renin-angiotensin-aldosterone system to regulate blood volume and subsequently influence blood pressure (Saxena, 1992).

The baroreflex has been shown to have a sizeable sympathetic influence over the blood vessels of the mesentery, which has been demonstrated to be important in maintaining blood pressure when moving from a supine to a standing position, and can be perturbed in patients with orthostatic hypotension (Fujimura et al., 1997, Low and Singer, 2008).

### 1.2.2 Adenosine Receptors and the Baroreflex

Adenosine receptors have been shown to interact with and affect the baroreflex. Adenosine has been shown to activate sympathetic afferent nerve terminals in the kidney and heart leading to stimulatory effects in these areas (Cox et al., 1989, Katholi et al., 1984).

There is evidence of $A_{2A}$ receptors in the NTS that mediate control of baroreflex activity (El-Mas et al., 2011, Minic et al., 2015). $A_{2A}$ receptors have been demonstrated to sensitise the reflex for bias toward sympathetic stimulation of the kidneys (Ichinose et al., 2009). $A_{2A}$ receptor activation has been demonstrated in the rat to cause a marked increase in HR that is consistent with increases in reflex sympathetic nervous activity (Alberti et al., 1997).

In contrast, $A_1$ receptors inhibit glutamatergic transmission in the NTS, reducing the baroreflex stimulus-response (Scislo et al., 2008). Additionally, cardiac $A_1$ receptor activation has been found to cause the attenuation of the stimulatory actions of catecholamines on the heart (Fraser et al., 2003, Zablocki et al., 2004).

Finally, $A_{2B}$ receptors situated in the posterior hypothalamus, an area of the brain that influences the NTS and baroreflex, have been demonstrated to be involved in cardiac regulation (Bauer et al., 1988, Lee and Koh, 2009).

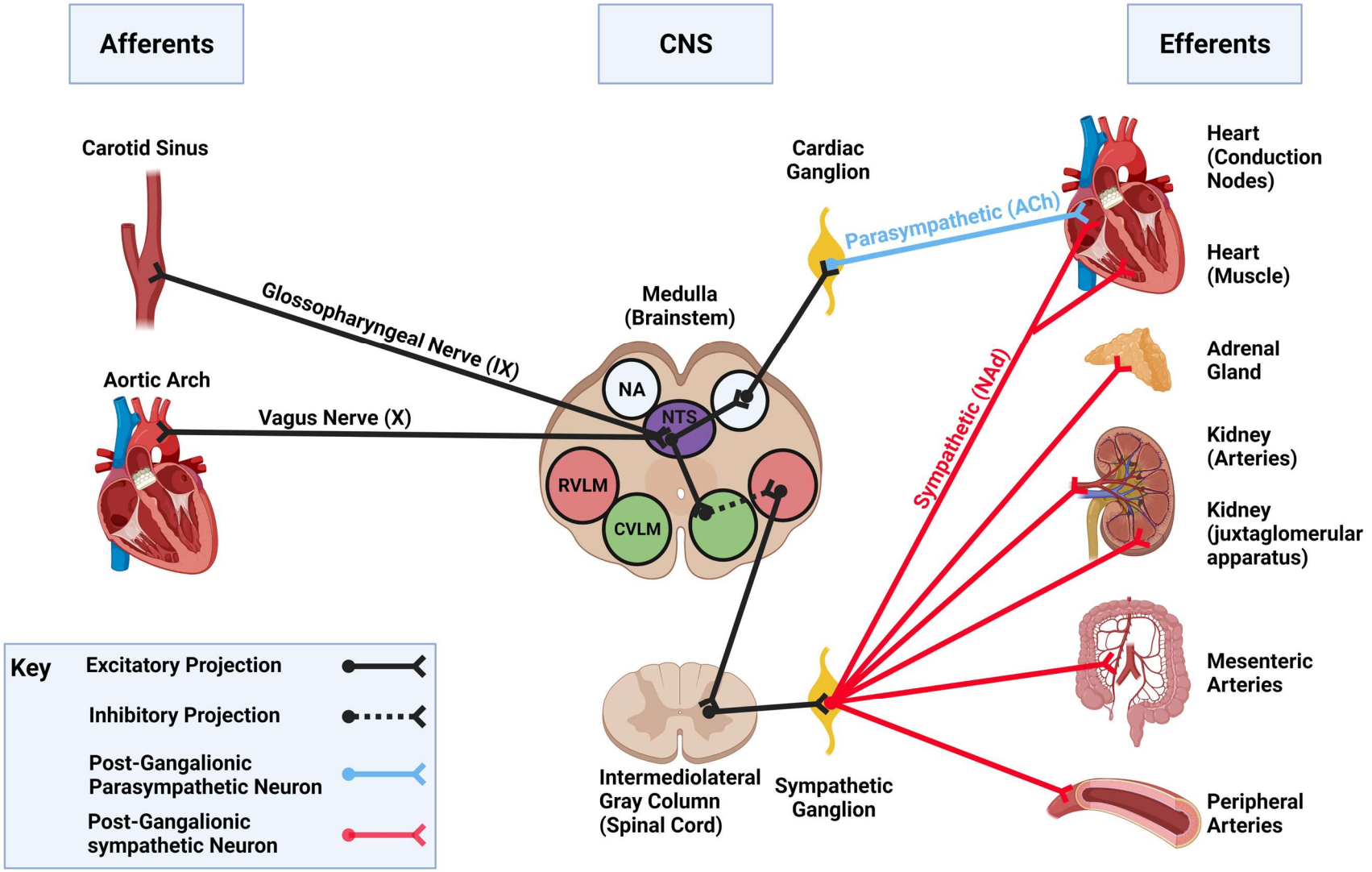


**Figure 5 Neuronal Circuitry of the Baroreflex Arc.** Pressure is sensed by baroreceptors that are located in the carotid sinus and aortic arch and the signal is transferred by the NTS via the afferent glossopharyngeal nerve and vagus nerve, respectively. Excitatory projections from the NTS ascend to other centres in the medulla that lead to sympathetic and parasympathetic efferents being projected to target organs. **Abs. ACh**- Acetylcholine, **CNS**-Central Nervous System, **CVLM**- Caudal Ventrolateral Medulla, **NA**- Nucleus Ambiguus, **NAd**- noradrenaline, **NTS**- Nucleus Tractus Solitarius, **RVLM**- Rostral Ventrolateral Medulla, **SAN**- sinoatrial node. *Figure created with BioRender.com*

# 1.3 The Effects of Receptor Tyrosine Kinase Inhibitors on the Cardiovascular System

As discussed earlier in the introduction, adenosine $A_2$ receptor agonists are known to increase blood flow to vascular beds (**1.1.5**). RTKIs are anti-cancer agents that are known to cause hypertension (Davis et al., 2011) (**1.3.1.1**). A proposed mechanism for the production of this hypertension is through increasing vascular resistance in vascular beds. Research in **chapter 5** of this thesis investigates if $A_{2A}$ receptor activation could lower the blood pressure of rats that have developed hypertension due to the RTKI sunitinib, a drug currently used in the clinic against a range of cancers (**1.3.3**). Sunitinib was chosen for this study due to its extensive clinical use, its well-documented ability to cause hypertension and cardiovascular disease, and from a practical point of view, its solubility in the vehicle used *in vivo* (**1.3.3**).

This introduction aims to introduce the challenges associated with RTKI-induced hypertension, so that a potential solution to this problem, the treatment with $A_{2A}$ receptor agonists, can be examined in **chapter 5**. In this section of the introduction, RTKs will be introduced to provide the background knowledge required to understand some of the mechanisms involved in RTKI-induced hypertension, examining vascular endothelial growth factor (VEGF) receptor blockade, which is thought to be a critical component in the development of this hypertension.

### 1.3.1 Introduction to Receptor Tyrosine Kinases

Tyrosine kinases are enzymes that transfer a phosphate group from a donor substrate, ATP, to a tyrosine residue of an acceptor substrate. There are 90 tyrosine kinases encoded into the human genome, of which 58 are receptors, known as RTKs, that are further divided into around 20 subfamilies (Robinson et al., 2000, Blume-Jensen and Hunter, 2001, Manning et al., 2002).

RTKs all share a similar structure comprised of an extracellular N-terminal ligand-binding domain, a transmembrane helix domain, and an intracellular C-terminal tyrosine kinase domain (**Figure 6**) (Hubbard, 1999, Gotink and Verheul, 2010). In addition, RTKs typically function as a dimer, cooperativity across the intracellular kinase domains of the two monomers, allows cross-monomer phosphorylation (Lemmon and Schlessinger, 2010). Classically it was thought that ligand binding led to RTK dimerisation; however, it has now been shown that some RTKs exist as dimers in the absence of ligand (Paul and Hristova, 2019). For example, evidence is emerging that VEGFR2 dimerisation occurs without ligand binding, but also is significantly increased by ligand binding (Sarabipour et al., 2016, King and Hristova, 2019).

RTK signalling is involved in mediating and controlling a wide range of complex biological functions including cell growth, angiogenesis and cell survival (Du and Lovly, 2018). Due to the modulation of these essential functions, dysfunctional RTK signalling contributes to many cancers; RTKs are estimated to be mutated or overexpressed in around 30% of human cancers (Lu et al., 2001). As such, RTKs are prime targets for anti-cancer therapies (Pottier et al., 2020).

Angiogenesis has a key role in the facilitation of tumour proliferation, as new blood vessels are required for the growth of a tumour to supply nutrients and oxygen to the cancerous cells (Verheul et al., 2004).

Vascular endothelial growth factor A (VEGF-A) is the critical mediator of angiogenesis and signals primarily through VEGFR2. VEGF-A secreted by tumour cells stimulates the proliferation and survival of endothelial cells, leading to the formation of new blood vessels (Nagy et al., 2009, Ferrara, 2010).

Alongside VEGF, other RTK signalling pathways have been found to have a major roles in angiogenesis and tumour progression. For example, platelet-derived growth factor receptors (PDGFRs), which signal for the recruitment of smooth muscle cells and pericytes to the new vasculature, are essential for the creation of a functional vasculature (Jain, 2003). Other important RTKs identified to play an angiogenic role include the stem-cell growth factor receptor (KIT) and fms-related tyrosine kinase 3 (FLT3) (Faivre et al., 2007).

#### 1.3.1.1 Receptor Tyrosine Kinase Inhibitors: Therapeutic Uses and Cardiovascular Side Effects

RTKIs are widely used anti-cancer agents that block the catalytic function of RTKs, preventing ATP-dependent phosphorylation. RTKIs block ATP binding to the highly conserved kinase domain of these receptors; because of this, most small molecule inhibitors are multi-targeted and inhibit numerous kinases, such as members of the VEGFR and PDGFR families (Davis et al., 2011). This kind of indiscriminate inhibition has the advantage of casting a wide net to hopefully be effective at blocking angiogenesis in cancer; however, the drawbacks are the increased risk of drug toxicity and the potential for severe side effects for patients undergoing RTKI therapy, including cardiotoxicity associated with hypertension, hypothyroidism and hematologic, gastrointestinal and dermatologic toxicities (Aparicio-Gallego et al., 2011).

### 1.3.2 Introduction to VEGF Receptors

Vascular Endothelial Growth Factor Receptors (VEGFRs) are RTKs that are known to dimerise in both the presence and absence of ligand binding (**1.3.1**) (Roskoski, 2008, Sarabipour et al., 2016, King and Hristova, 2019). VEGF acts through three structurally related VEGFRs, denoted 1-3. Although not always the case, Vascular Endothelial Growth Factor Receptor 1 (VEGFR1) is typically the dominant VEGF receptor expressed in macrophages, VEGFR2 is typically the dominant VEGF receptor expressed in vascular endothelial cells, and Vascular Endothelial Growth Factor Receptor 3 (VEGFR3) is typically the dominant VEGF receptor expressed in lymphatic endothelial cells (Koch and Claesson-Welsh, 2012).

The kinase domain for VEGFRs differ from the typical RTK previously described (**1.3.1**). In VEGFRs, the kinase domain has a split structure with N- and C-terminal lobes with the ATP-binding cleft located between them (Liu and Gray, 2006). Upon receptor activation by ligand binding, the split kinase domain undergoes conformational changes that facilitate and stabilises ATP binding into the ATP binding cleft between the split N- and C- kinase domains (**Figure 6**) (Sarabipour et al., 2016). VEGFR kinase activation leads to auto- or trans-phosphorylation of tyrosine residues on the monomers of the receptor dimer itself, as well as the phosphorylation of tyrosine residues on downstream signal transducers (Koch and Claesson-Welsh, 2012).

The RTK VEGFR2 is the best understood VEGF receptor and is coded in humans by the Kinase Insert Domain (KDR) gene (Terman et al., 1992). VEGFR2 can be found as a homodimer in the absence of ligand (Sarabipour et al., 2016). VEGFR2 binds VEGF-A with nanomolar binding affinity (King and Hristova, 2019, Peach et al., 2019).

VEGFR2 plays an essential role in endothelial differentiation and proliferation as well as vascular permeability and a wide range of other endothelial cell activities, including cell survival, motility, and transcriptional activation (Ito et al., 1998, Koch and Claesson-Welsh, 2012). VEGFR2 is critical for vascular development, as gene inactivation of VEGFR2 results in early embryonic lethality (Shalaby et al., 1995).

#### 1.3.2.1 The Effect of VEGF on Blood Pressure Regulation

VEGF is a potent vasodilator (Ku et al., 1993). When administered centrally, the net result of treatment with VEGF is hypotension (Yang et al., 1996). It is believed that VEGF-A caused vasodilation due to the stimulation of NO production from endothelial cells, signalling through VEGFR2 (**Figure 3**) (Zachary and Gliki, 2001, Itoh et al., 2002). VEGF stimulation of NO production is thought to involve both $Ca^{2+}$ dependant mechanisms through activation of phospholipase C γ (PLCγ), and $Ca^{2+}$ independent signalling mechanisms through phosphoinositide 3-kinase (PI3K)-Akt pathways (**Figure 6**) (Zachary and Gliki, 2001). Additionally, VEGF stimulates the production of prostacyclin through PKC-mediated activation of the arachidonic acid cascade leading to prostacyclin synthesis by prostaglandin I2 synthase (PGIS) (**Figure 6**) (Gliki et al., 2001, Zachary and Gliki, 2001).

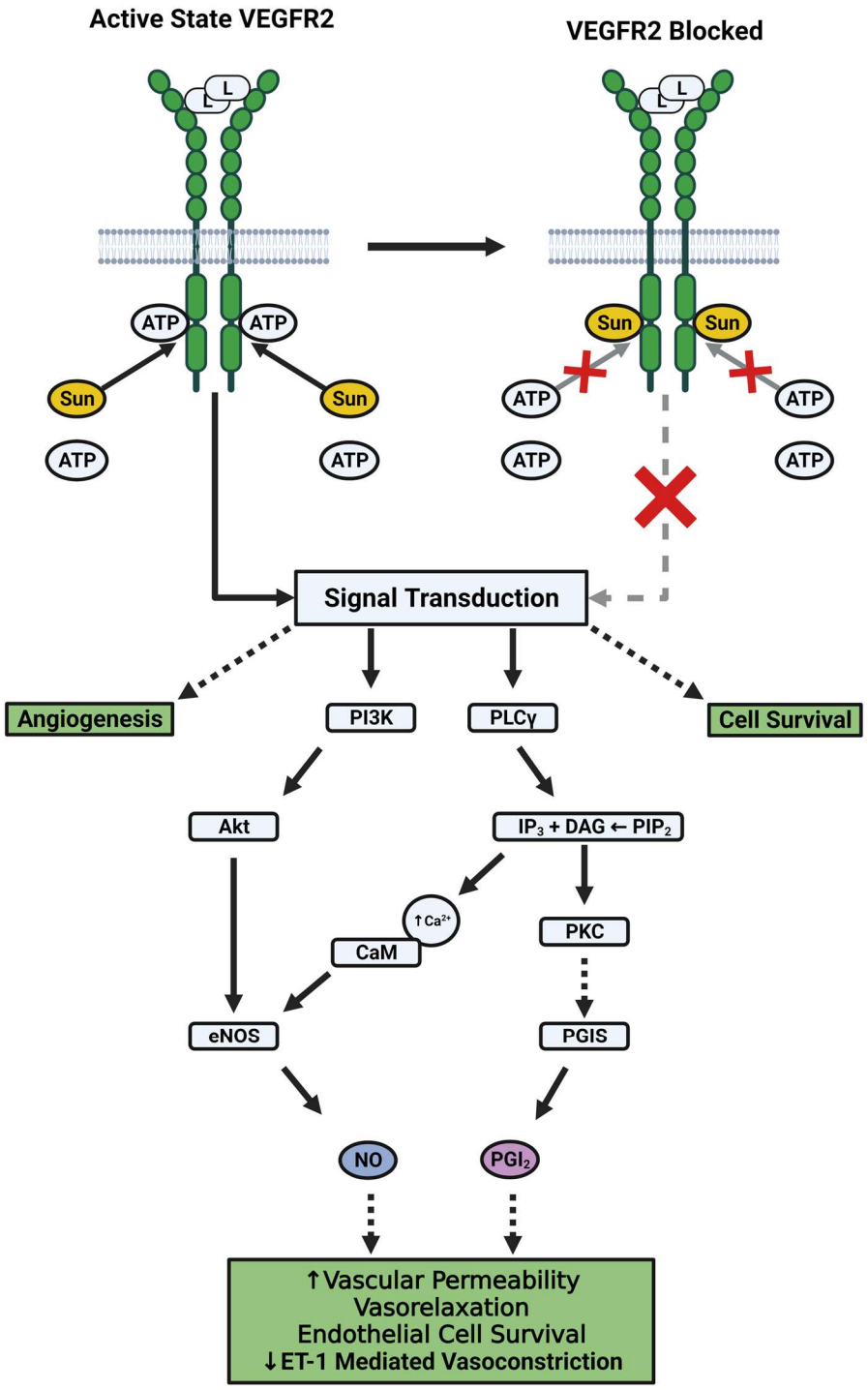


**Figure 6 Vascular Endothelial Growth Factor 2 Signal Transduction Cascades and Receptor Blockade by Sunitinib.** Upon ligand binding, conformational changes facilitate ATP binding into the ATP binding cleft. VEGFR2 kinase activation leads to the phosphorylation of tyrosine residues on downstream signal transducers, triggering signalling cascades that can lead to NO and $PGI_2$ release. Sunitinib competes reversibly for the ATP binding cleft of active VEGFR2, blocking receptor signalling. **Abs. ATP**- adenosine triphosphate, **$Ca^{2+}$-** ionic calcium**, CaM-** Calmodulin**, DAG-** Diacylglycerol, **eNOS**- Endothelial nitric oxide synthase, **ET-1**- endothelin-1, **L**- Ligand, **NO**- Nitric oxide, **PGI2**- Prostaglandin I2 (prostacyclin), **PGIS**- prostaglandin I2 (prostacyclin) synthase, **PI3K**- Phosphoinositide 3-kinase, **$PIP_2$**- Phosphatidylinositol 4,5-bisphosphate, **PKC**- protein kinase C, **PLCγ**- Phospholipase C gamma, **Sun**- Sunitinib **VEGFR2**- Vascular Endothelial Growth Factor 2. *Figure created with BioRender.com*

#### 1.3.2.2 The Cardiovascular Side Effects of Anti-VEGF Signalling

VEGFR2 represents an important drug target for cancer angiogenesis (Peach et al., 2018). Inhibitors of VEGFR2 activity, including anti-VEGF-A and anti-VEGFR2 monoclonal antibodies and small molecule RTKIs (**1.3.1.1**) have been developed to interfere with tumour angiogenesis (Hegde et al., 2018, Peach et al., 2018).

VEGFR2 inhibitors are inherently toxic due to the on-target side effects, including renal damage and proteinuria, as well as hypertension (Lankhorst et al., 2014, Ollero and Sahali, 2014). It has been shown that VEGF inhibition decreases NO production, leading to vasoconstriction, elevated peripheral vascular resistance, and hypertension (Facemire et al., 2009). In addition, there is growing evidence that anti-VEGF therapies cause an increase in endothelin-1 (ET-1), a potent vasoconstrictor that has been demonstrated to be involved in anti-VEGF induced renal injury and increases in blood pressure (Bhargava, 2009, Lankhorst et al., 2014).

Therapies that target VEGF cause hypertension in 30% to 80% of patients, and this hypertension can be resistant to standard anti-hypertensive medication (Robinson et al., 2010b). If left unsuccessfully treated, this severe clinical hypertension (grade 3 and above*) can lead to ischaemic vascular events, left ventricular dysfunction, heart failure or thrombo-haemorrhagic phenomena after longer-term exposure over several months (Katsi et al., 2014, Abi Aad et al., 2015). For example, Bevacizumab, which is a VEGF-A blocking recombinant humanised monoclonal antibody, causes hypertension in 36% of patients treated with the drug, with up to 22% reporting serious high grade (3-4) hypertension (Zhu et al., 2007, Ranpura et al., 2010, Li and Kroetz, 2018).

**Clinical hypertension is commonly assessed on a 1-5 scale defined by the National Cancer Institute's Common Terminology Criteria for Adverse Events, with grades 3–4 considered high-grade hypertension (Chen et al., 2012).*

### 1.3.3 Introduction to Sunitinib: an RTKI Currently Used in the Clinic

Sunitinib malate (SU11248, Sutent- Pfizer) is an oral multitargeted tyrosine kinase receptor inhibitor with antiangiogenic and antitumor activities against a broad range of malignancies (Goodman et al., 2007, Motzer et al., 2017, Vivanet et al., 2022). Sunitinib is a type I kinase inhibitor, meaning that it recognises the active form of the kinase and competes with ATP for the ATP-binding site of the kinase (Zhang et al., 2009). Sunitinib has been demonstrated to inhibit a selection of RTKs that are important in cell growth and angiogenesis, including VEGFRs1-3, PDGFR α & β, KIT and FLT3 (Abrams et al., 2003, Mendel et al., 2003, Faivre et al., 2007).

Sunitinib has seen longstanding clinical use, having been on the market since 2007, and is approved for treating advanced renal cell carcinomas, gastrointestinal stromal tumors and pancreatic neuroendocrine tumors (Goodman et al., 2007, Motzer et al., 2017, Vivanet et al., 2022).

Sunitinib is known to cause a large number of cardiovascular side effects. Many of these are thought to be due to the on-target blockage of VEGF signalling, described previously (**1.3.2.2**) (**Figure 6**). These side effects include hypertension in 30% of patients treated with this drug, with over a third of those developing severe grade 3-4 hypertension (Rixe et al., 2007, Motzer et al., 2009, Aparicio-Gallego et al., 2011, Lankhorst et al., 2014, Ollero and Sahali, 2014). Hypertension has even been shown to be a predictive factor of sunitinib activity and effectiveness against metastatic renal cell carcinomas (Rixe et al., 2007). Sunitinib is also known to cause left ventricular dysfunction and myocardial ischaemia, which can cause heart failure, as well as renal damage and proteinuria (Aparicio-Gallego et al., 2011).

## 1.4 Adenosine and VEGF Signalling Crosstalk

Growing evidence suggests significant crosstalk between GPCRs and RTKs, with both classes of receptor working synergistically to control complex mechanisms, resulting in the tight regulation of biological processes (Liebmann and Bohmer, 2000, Natarajan and Berk, 2006, Pyne and Pyne, 2011).

Adenosine receptors and vascular endothelial growth VEGF receptors collaborate to promote cell growth, survival, proliferation and migration, but also tumour metastasis, and are both involved in wound healing and tissue remodelling (Adair, 2005, Escudero et al., 2014). Adenosine is involved in enhancing VEGF-driven angiogenesis in both physiological and pathophysiological states (Feoktistov et al., 2009, Acurio et al., 2017). All of the adenosine receptors have been found to upregulate VEGF production, with the receptor responsible being tissue or cell dependant (Clark et al., 2007, Ryzhov et al., 2008, Escudero et al., 2014, Rudich et al., 2015). A proposed mechanism of action of adenosine-mediated VEGF production is through adenosine receptor-mediated stimulation of hypoxia-inducible factor 1α (HIF-1α) expression (Merighi et al., 2005, Gessi et al., 2010). HIF-1α acts in the nucleus to induce the production of various factors, including VEGF (Ke and Costa, 2006). $A_{2A}$ receptor activation can mediate cell proliferation and migration, and, additionally, the synthesis of pro-angiogenic factors, including VEGF, in endothelial cells (Escudero et al., 2014). $A_{2B}$ receptors have long been known to stimulate VEGF production and angiogenesis in various cell types, including cardiac mesenchymal stem-like cells (Ryzhov et al., 2012, Merighi et al., 2015) and endothelial cells (Grant et al., 1999, Feoktistov et al., 2002).

### 1.4.1 Introduction to Receptor Oligomerisation and Cooperation

A way in which receptors crosstalk is by dynamic receptor oligomerisation on plasma membranes (Rozenfeld and Devi, 2010). A growing number of studies hint at a relationship between oligomerisation and function of GPCRs, and strengthen the view that receptor assembly into dimers or even higher power oligomers play an important role in the regulation of protein function (Gahbauer and Bockmann, 2016). Studies have shown that receptor heteromerisation can change G protein coupling for the oligomerised receptors. In some cases, this change is to the extent of coupling to the G protein, but in others, this is a complete change in the nature of the coupled G protein (Rozenfeld and Devi, 2010). For example, heteromerisation between $D_1$-$D_2$ dopamine receptors has been shown to cause a switch from a $G_s$- ($D_1$ receptor), or $G_i$-($D_2$ receptor) mediated pathway, to a $G_q$-mediated pathway (Rashid et al., 2007).

Like other class A GPCRs, adenosine receptors have been thought to occur exclusively in a monomeric state (White et al., 2007, Whorton et al., 2007). More recently, however, evidence is accumulating that adenosine receptors can form dimeric, or even higher-order oligomeric structures, that may have significant pharmacological consequences to cellular signalling (Gahbauer and Bockmann, 2016).

It is established that RTKs exist as dimers or can be induced to dimerise following the binding of their cognate ligand (Bessman et al., 2014, Freed et al., 2015). Studies utilising purified extracellular domains of VEGFR2 have provided evidence for VEGF-A induced receptor homodimerisation (Dosch and Ballmer-Hofer, 2010, Brozzo et al., 2012, Markovic-Mueller et al., 2017). However, pre-formed VEGFR2 dimers have also been shown to exist *in vitro* in the absence of VEGF, with the dimer stabilised further upon ligand binding through several points of contact between the different receptor domains (Sarabipour et al., 2016).

## 1.4.1.1 Adenosine Receptor Oligomerisation

### 1.4.1.1.1 Adenosine $A_2$ Receptor Homodimers

There is currently evidence in the literature for $A_{2A}$ (Canals et al., 2004, Briddon et al., 2008, Schonenbach et al., 2016) receptor homodimers, but not currently for $A_{2B}$ receptor homodimers.

### 1.4.1.1.2 Adenosine $A_2$ Receptor Heterodimers

There is evidence for $A_1$-$A_{2A}$ receptor-receptor heterodimerisation, and the two receptors have been found to colocalise in striatal glutamatergic nerve terminals, both pre- and post-synaptically (Ciruela et al., 2006, Briddon et al., 2008). Additionally, cooperativity across the oligomeric interface has been reported for this receptor pair (Ciruela et al., 2006). Radioligand binding studies in isolated cell membranes have demonstrated that agonist binding to the adenosine $A_{2A}$ receptor influences the affinity of a radiolabelled $A_1$ agonist for the adenosine $A_1$ receptor, but not *vice versa* (Ciruela et al., 2006).

Adenosine $A_{2A}$-$A_{2B}$ receptor-receptor heteromeric complex formation has recently been described (Hinz et al., 2018). Hinz *et al*. 2018 reported dramatically altered pharmacology of the $A_{2A}$ receptor when co-expressed with the $A_{2B}$ receptor in recombinant, as well as in native cell lines (Hinz et al., 2018). In the presence of activated $A_{2B}$ receptors, $A_{2A}$ receptor-selective ligands have been shown to lose high-affinity binding to $A_{2A}$ receptors and display sharply reduced potency in causing cellular cAMP accumulation (Hinz et al., 2018).

A well studied receptor combination is adenosine $A_{2A}$ receptor- dopamine $D_2$ receptor, with a large body of evidence confirming its existence (Hillion et al., 2002, Canals et al., 2003, Vidi et al., 2008). Recent studies show that $A_{2A}$ and $D_2$ receptors predominantly form heteromers in the striatum, which may constitute a target for the treatment of Parkinson's disease. Drugs with dual target profiles targeting adenosine $A_{2A}$ and dopamine $D_2$ receptors are currently under investigation as potential treatments (Taura et al., 2018, Shao et al., 2018, Borroto-Escuela and Fuxe, 2019).

### 1.4.1.2 VEGFR2 Receptor Oligomerisation

#### 1.4.1.2.1 VEGFR2 Receptor Heterodimers

Heterodimerisation has been reported between VEGFR2 and other VEGF Receptors. It has been found that VEGFR1–VEGFR2 heterodimers inhibit VEGF-A signalling at VEGFR2 by suppressing VEGFR2 phosphorylation and subsequent signalling via the PI3K pathway (Cai et al., 2017). Additionally, VEGF-A, vascular endothelial growth factor C (VEGF-C), and vascular endothelial growth factor D (VEGF-D) have been demonstrated to induce heterodimerisation of VEGFR2 and VEGFR3 (Alam et al., 2004, Nilsson et al., 2010).

Additionally, oligomeric complexes involving the RTK VEGFR2 and the GPCR $\beta_2$ adrenoceptor have been reported, with these complexes induced by agonist treatment at either receptor (Kilpatrick et al., 2019). Furthermore, it has been shown that this oligomeric structure has functional implications for the paired receptors. The coupling of $\beta_2$ to β-arrestin2 has been shown to be prolonged by VEGFR2 activation (Kilpatrick et al., 2019).

## 1.4.2 Could Adenosine Receptors and VEGFR2 Form Functional Heterodimers?

As discussed previously, VEGF and adenosine signalling are linked, and crosstalk between the signalling pathways induced by VEGF receptor and adenosine receptor signalling is plausible. Both VEGFR2 and adenosine $A_2$ receptors form dimers (**1.4.1.1**, **1.4.1.2**). Adenosine $A_{2A}$ has been shown to form complexes with a GPCR outside of the adenosine receptor family (the $D_2$ receptor), and VEGFR2 has been shown to bind to a GPCR, the $\beta_2$ adrenoceptor, so it is plausible that VEGFR2 may form oligomers with different GPCRs, such as with adenosine $A_2$ receptors (**1.4.1.1.2**, **1.4.1.2.1**).

# 1.5 Thesis Research Aims by Chapter

**Chapter 3**: The adenosine $A_2$ receptors are exciting targets for novel treatments in the cardiovascular system, including treatments for diseases that involve renal and mesenteric vascular beds (**1.1.6.2**). Both receptors cause vasodilation in regional vascular beds, and the $A_{2A}$ receptor is associated with the generation of hypotension (**1.1.5**). However, the relative extent to which each $A_2$ receptor contributes to vasodilatation in different vascular beds has not been investigated in a holistic *in vivo* model. Research detailed in this thesis will investigate regional haemodynamic consequences of adenosine $A_{2A}$ and $A_{2B}$ receptor signalling using a conscious, freely moving rat model. In addition, the selectivity and action of the ligands used *in vivo* will be investigated using *in vitro* bioluminescent resonance energy transfer (BRET) based proximity assays and cAMP accumulation assays.

**Chapter 4**: There is evidence that $A_2$ receptors may, directly and indirectly, influence the baroreflex system (**1.2.2**). To understand how the response of $A_2$ receptor activation might be influenced by this system, the investigation into $A_2$ receptor activation was expanded to examine the secondary involvement of β adrenoceptors in the cardiovascular response to $A_{2A}$ and $A_{2B}$ receptor signalling. This research is important to understand how adenosine $A_2$ receptors affect homeostatic reflexes, as this would be the case if the receptors were targeted in the clinic, thus providing critical novel insights that will inform the use of $A_2$ receptor ligands as drug targets.

**Chapter 5**: There is clear overlap and synergism between the physiological effects of adenosine and VEGF in how they affect the cardiovascular system (**1.4**).

In this chapter, *in vitro* work will investigate if VEGF signalling via VEGFR2 (**1.3.2**) influences cAMP accumulation caused by $A_{2A}$ receptor activation (**1.1.3**). A way in which receptors influence other receptors' signalling is by forming receptor oligomers (**1.4.1**, **Figure 2**). Both VEGFR and adenosine receptors readily form dimers, and thus it is plausible that VEGFR2 could form oligomers with adenosine $A_2$ receptors (**1.4.2**). *In vitro* experiments investigating the colocalisation of VEGFR2 and $A_2$ receptors were undertaken to investigate this possibility.

Sunitinib is an important RTKI used clinically that, like many drugs in its class, comes with unwanted cardiovascular side effects, including hypertension that is resistant to standard anti-hypertensive treatments (**1.3.3**). Research into the cause of sunitinib-induced hypertension and how to relieve it is thus critical and could

save lives in the clinic. It has been demonstrated *in vivo* that other multitargeted tyrosine kinase receptor inhibitors, such as cediranib, cause a reduction in vascular conductance in mesenteric and hindquarters vascular beds and, to a lesser degree, renal vascular beds (Carter et al., 2017). Moreover, this reduction in vascular conductance and hypertension has been demonstrated to be resistant to anti-hypertensive antagonism of ET-1 receptors, or α and β adrenoceptors (Carter et al., 2017). Work in this thesis will first investigate if hypertension caused by sunitinib follows the same pattern as other RTKIs, such as cediranib, in causing a reduction in vascular conductance across the renal, mesenteric and hindquarters vascular beds. Following this, experiments will be conducted to see if sunitinib-induced hypertension could be relieved by an $A_{2A}$ agonist, reversing the detrimental effects of sunitinib on vascular conductance at these regional beds. An $A_{2A}$ agonist was selected over an $A_{2B}$ receptor agonist because $A_{2A}$ agonism was demonstrated to cause hypotension in **Chapters 3 & 4**, whereas $A_{2B}$ receptor agonism did not.

# 2 Materials & Methods

# 2.1 Materials & Methods: *In Vivo*

## 2.1.1 *In Vivo Methods*: Measuring Regional Haemodynamic Changes in Conscious Rats

### 2.1.1.1 Measuring Regional Haemodynamic Changes in Conscious Rats: Technique History & Overview

Hartley and Cole developed the use of pulsed Doppler flowmetry to measure regional blood flow in animals in 1974 for use in dogs (Hartley and Cole, 1974). The technique was further refined for use in rats by Haywood *et al.* in 1981 (Haywood et al., 1981). This project employs a single *in vivo* approach originally developed and validated in Nottingham by Sheila M. Gardiner and Terence Bennett, using miniature ultrasonic pulsed Doppler flow probes to measure blood flow in three separate regional beds (Gardiner and Bennett, 1988). This haemodynamic technique incorporates implanted intra-arterial catheters to allow the calculation of HR and mean arterial pressure (MAP) (**2.1.3.1**), alongside pulsed Doppler flowmetry probes (**2.1.3.2**) to allow changes in vascular conductance (VC) across multiple regional vascular beds to be calculated, in conscious freely moving rats. This haemodynamic model also utilises implanted intravenous catheters to allow responses to pharmacological agents to be explored, without disturbing the animal.

#### 2.1.1.2 Measuring Regional Haemodynamic Changes in Conscious Rats: Technique Advantages

##### 2.1.1.2.1 Haemodynamic Technique Advantages: The Use of Miniaturized Pulsed Doppler Flow Probes

A significant advantage of this technique is the miniature size of the pulsed Doppler probes used. An alternative technique to measure blood flow is electromagnetic flowmetry; which requires bulkier probes with larger diameter wires, making the technique more suitable for use in unconscious haemodynamic studies, and not as practical for use in conscious rats (Haywood et al., 1981, Mitchell et al., 1994). An additional advantage over electromagnetic flowmetry is that by the nature of the pulsed Doppler technique, a reading for zero flow does not have to be determined by potentially damaging vessel occlusion, whereas it does in electromagnetic flowmetry (Kolin et al., 1964, Haywood et al., 1981). Another method to measure blood flow is with continuous-wave transonic Doppler probes with independent sender and receiver crystals (Reeder et al., 1986). Unfortunately, this technique also requires bulker probes than the pulsed Doppler method, and obtaining the correct orientation of both crystals can prove difficult (Haywood et al., 1981).

A further advantage of this ultrasonic pulsed Doppler flowmetry-based technique is that because the probes are miniature and the wires thin, they can be easily placed around small vessels, such as the rat renal artery (Haywood et al., 1981). In addition, because the probes are small, this technique can simultaneously measure the responses in three separate vascular beds in a rat. Even the latest generation of telemetric transonic Doppler probes available on the commercial market can only currently measure from two vascular beds simultaneously in a rat, making the Doppler technique still cutting edge to this day (Gardiner and Bennett, 1988, Arnall et al., 2017, Van Daele et al., 2022).

Being able to measure VC simultaneously through three separate regional vascular beds is especially valuable because vascular beds can respond differentially and sometimes in opposing ways to pharmacological stimuli. For example, sibutramine, a serotonin and noradrenaline reuptake inhibitor, causes an

increase in VC in celiac and mesenteric vascular beds, while simultaneously causing a decrease in VC in vascular beds situated in the hindquarters (Woolard et al., 2004). Theoretically, a drug may cause limited effects on blood pressure or HR and yet cause substantial haemodynamic changes due to a balance of vasoconstrictor effects in some vascular beds, together with vasodilator effects in others; haemodynamics effects that otherwise could be missed if changes to regional haemodynamics were not measured across multiple vascular beds.

#### 2.1.1.2.2 Haemodynamic Technique Advantages: The Use of Conscious Rats

Another significant benefit to this ultrasonic pulsed Doppler flowmetry-based technique is that the rats are conscious, and thus there is an absence of any effects caused by anaesthetics. Most anaesthetic drugs depress cardiovascular function, commonly causing a reduction in HR and the force of cardiac contraction (Flecknell, 2015). Additionally, anaesthetics and analgesics commonly used during anaesthesia, such as opioids, can cause respiratory depression, which can lead to hypoxia and hypercapnia, which can have profound haemodynamic effects, such as causing an increase in HR and systemic vasodilatations (Boom et al., 2012). In severe causes of hypoxia, constriction of the peripheral vasculature can occur to redistribute oxygen delivery to the most critically dependent organs (Boom et al., 2012, Heinonen et al., 2016).

Drugs given under anaesthetic protocols can also interfere with important homeostatic reflexes, such as the baroreflex (**1.2**), which helps maintain constant blood pressure (Tank et al., 2004). For example, a commonly used sedative agent in rats is medetomidine, an $\alpha_2$ adrenoceptor agonist (Kint et al., 2020). Metetomidine, through activation of central $\alpha_2$ adrenoceptors found in the NTS of the central nervous system, can augment parasympathetic tone and enhance baroreceptor reflex sensitivity, leading to bradycardia and a reduction in the output of the heart (Fischetti et al., 1994, Hayward et al., 2002, Sinclair, 2003, Tank et al., 2004) (**1.2**). However, acting contrary to these effects, $\alpha_2$ receptors in the periphery can cause vasoconstrictions in vascular beds, leading to hypertension at sedative doses of medetomidine (Sinclair, 2003).

To conclude, due to the profound haemodynamic changes that anaesthesia can induce, pharmacological studies conducted under anaesthesia risk producing results that are not demonstrative of normal physiological conditions as the cardiovascular system is already highly perturbed from its regular state. The pulsed Doppler flowmetry-based technique used in this thesis involves conscious, freely moving rats and does not suffer from these drawbacks. The animal is in a normal physiological state throughout the experiment; it has been demonstrated that there are no changes to the haemodynamic variables measured across 4 study days in control groups receiving only vehicle treatments with this flowmetry-based technique (Gardiner et al., 2010, Carter et al., 2017).

### 2.1.2 *In Vivo* Methods: Exploring the Haemodynamic Effects of Ligands

In the studies detailed in this thesis, the continuous measurement of Doppler shift in three distinct vascular beds (kidney, mesentery and hindquarters), alongside continuous arterial pressure measurements, were taken to elucidate the cardiovascular effects of ligands in conscious, freely moving rats. This technique allows for the evaluation of an impact of a ligand on the cardiovascular system in an animal with full autonomic regulation. Overall, this technique helps to elucidate the integrated haemodynamic effects of drug action generating powerful *in vivo* data relating to meaningful physiological effects in conscious, freely moving rats (Gardiner and Bennett, 1988, Woolard et al., 2004, Cooper et al., 2018).

## 2.1.3 *In Vivo* Methods: Technique Details

### 2.1.3.1 Haemodynamic Technique Details: Measuring Blood Pressure

In this *in vivo* method, blood pressure is measured continuously using a fluid-filled arterial catheter connected to a transducer. Originally validated by Gardiner *et al.* (Gardiner et al., 1980), the arterial catheter comprises two different sizes and types of tubing. A small flexible length (~7.0 cm) of narrow-bore polyethylene (PE) tubing (Braintree Scientific, lumen diameter (LD) $PE_{10}$- 0.28 mm) is connected to a much longer length (100 cm) of wider, less flexible and thicker nylon tubing (Braintree Scientific, lumen diameter $PE_{50}$- 0.58 mm) (**Figure 7**). The catheter is known as a $PE_{50}/PE_{10}$ catheter. The flexible narrow-bore tubing of this $PE_{50}/PE_{10}$ catheter is suitably small enough to allow insertion into the distal abdominal aorta via the ventral caudal artery situated in the tail of the rat (Gardiner et al., 1980).

The dynamic response of a catheter system is largely determined by a combination of its length and lumen diameter. Catheters exclusively made using lengths of tubing with too wide a lumen can suffer from resonance phenomena, resulting in a distortion or amplification of the pressure pulse (Van Vliet et al., 2000). For example, in a rat system, the $PE_{50}/PE_{10}$ catheter introduced above was compared to a catheter created exclusively from $PE_{50}$. The $PE_{50}$ catheter showed distortion and overshoot of the pressure trace compared to the $PE_{50}/PE_{10}$ catheter (Schenk et al., 1992).

There are, however, trade-offs that makes the $PE_{10}$ tubing unsuitable to be the entire length of the catheter. Damping of the pressure signal occurs which is inversely proportional to the catheter diameter, and too narrow a catheter can reduce the dynamic sensitivity of the measurement system (Van Vliet et al., 2000). Rigidity also affects damping; the less rigid the catheter, the more signal damping occurs (Schenk et al., 1992). For the $PE_{50}/PE_{10}$ catheter system, most of the damping has been demonstrated to be caused by the short ~7 cm of narrow-bore tubing, not from the 100 cm of $PE_{50}$ tubing (Schenk et al., 1992). If the whole catheter were created from $PE_{10}$, the signal would be excessively dampened. This $PE_{50}/PE_{10}$ catheter provides a fusion of tubing sizes that provides optimum dynamic sensitivity with minimal dampening effects (Schenk et al., 1992).

The catheter is connected to a pressure transducer system via a stainless steel needle and a 3-way tap (**Figure 8**). The transducer system comprises of a displacement dome filled with degassed double-distilled water incorporating a Bell and Howell type 4-42 pressure transducer, connected to a transducer amplifier (model 13-4615-50; Gould, Cleveland, Ohio, USA), which is itself sequentially connected to a computer running custom modified software (Instrument Development Engineering Evaluation, IdeeQ version 2.5; Maastricht Instruments, Maastricht, The Netherlands) (**Figure 8**). The 3-way tap allows the transducer to be temporally disconnected, and heparinised saline (40 Industrial Units (I.U.) /mL, ~0.2 mL) flushed through the arterial line as a bolus to prevent the loss of line patency due to the formation of blood clots. This catheter system has been tested and verified to measure pressure accurately at the frequencies of the signal generated by a rat heart (around ~5 Hz at rest, 300 beats $min^{-1}$) (Gardiner et al., 1980).

When pressure is not being measured, the catheter is connected to a fluid-filled swivel, which is made in-house, to the specifications found in Brown *et al.* 1976 (Brown et al., 1976), which is itself connected to a pump delivering a constant infusion of heparinised saline (20 I.U. /mL, 0.4 ml/hr) to keep the catheter patent. Briefly, the fluid-filled swivel is created from the body of a 3.0 mL plastic syringe with a 22 gauge hypodermic needle inside, which freely rotates and forms the bearing (**Figure 7**). The swivel ensures the catheter lines do not get tangled when the rat moves around the cage.

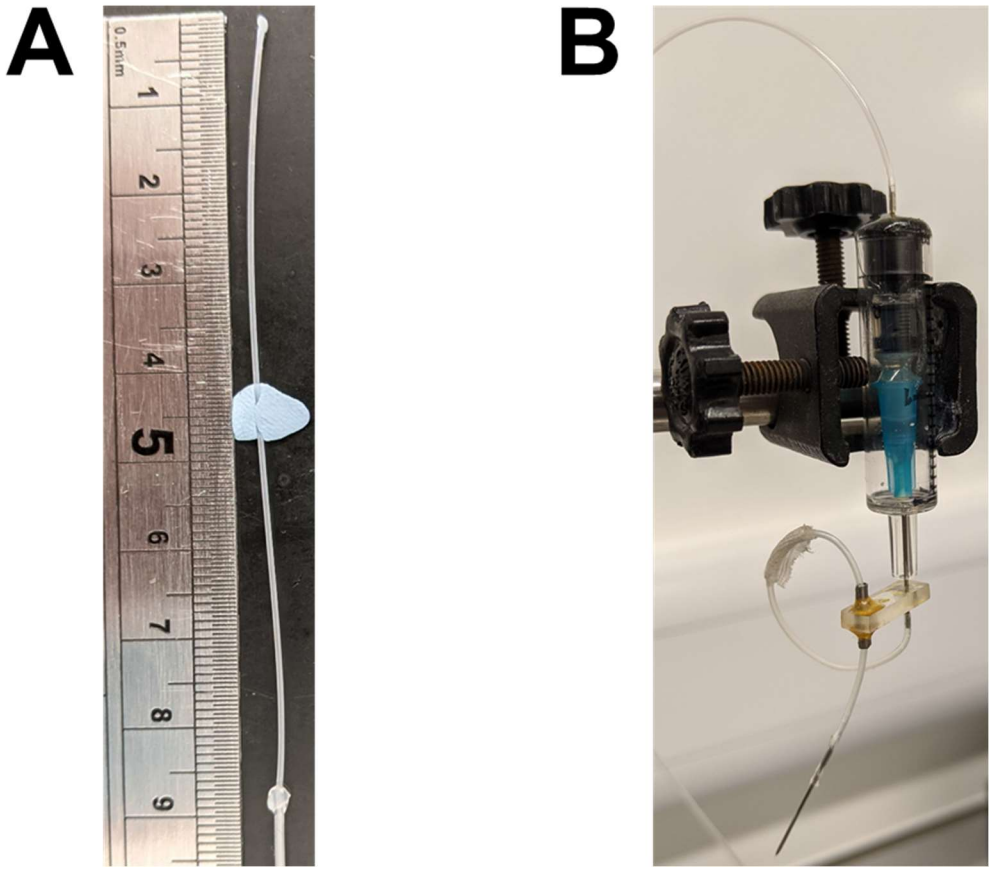


**Figure 7 Photographs of the Catheter and the Swivel Pivot System. A)** The catheter system to measure blood pressure is comprised of a small flexible length (~7.0 cm) of narrow-bore polyethylene tubing (lumen diameter $PE_{10}$- 0.28 mm) connected to a much longer length (100 cm) of wider, less flexible and thicker nylon tubing (lumen diameter $PE_{50}$- 0.58 mm). **B)** A fluid-filled swivel is attached to keep the catheter system patent when not in use, allowing the constant infusion of heparinised saline via an infusion pump. In addition, the swivel ensures that the line does not get tangled when the rat moves around the cage. The fluid-filled swivel is made from the body of a 3 mL plastic syringe with a 22 gauge hypodermic needle inside, which freely rotates and forms the bearing.

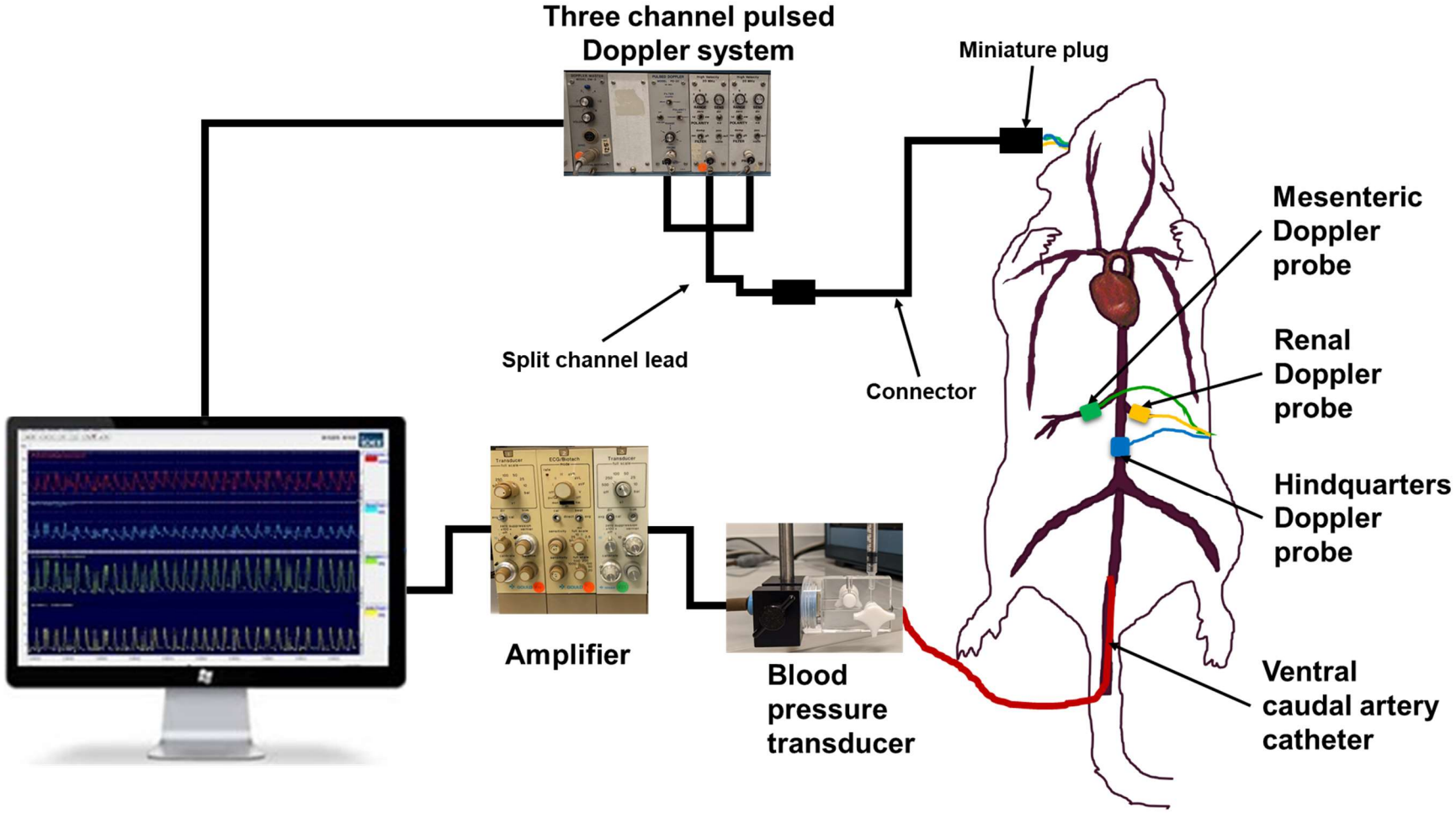


**Figure 8 Schematic Overview: Measuring Regional Haemodynamics Using Doppler Flowmetry.** In brief, under surgery, pulsed Doppler flow probes are placed around three major arteries supplying the left kidney, the mesentery and the hindquarters, with the wires of these probes tunnelled to the back of the rat's neck. These wires are soldered into a plug connected to a three-channel pulsed Doppler system via a connector and split channel lead. In addition, an arterial catheter is advanced up the ventral caudal artery, allowing simultaneous blood pressure measurements to be taken via a blood pressure transducer and pressure amplifier. The amplifier and the Doppler system are connected to a computer running bespoke software (IdeeQ) to allow real-time visualisations of the collected data.

#### 2.1.3.2 Haemodynamic Technique Details: Measuring Changes to Regional Blood Flow

The sound emitted from a source is measured at a frequency that depends on the observer's relative velocity. The change in frequency of the sound from its rest frame value can be used to determine the observer's velocity; this is known as the Doppler effect (Censor, 1984). The ultrasound probes used for this *in vivo* method work on this principle (Gardiner and Bennett, 1988).

This technique's detection system utilises a pulsed Doppler flowmeter to distinguish changes in erythrocyte velocity (Gardiner and Bennett, 1988). The probes used for this pulsed Doppler flowmeter are created in-house, based on the design suggested by Haywood and colleagues (Haywood et al., 1981). The probes consist of a single piezoelectric crystal, 1 mm in diameter, attached to insulated silver-plated copper wires (36 AWG) (Crystal Biotech Inc.), which is mounted inside silastic tubing and surrounded by a cuff created from soft silastic material which creates a lumen for which the blood vessel is to be placed inside (**Figure 9**). The crystal is fixed in place within the probe at 45° to the axis of blood flow, and an acoustic sound baffle is created out of syrofoam around the back and sides of the silastic tubing to prevent interference caused by the detection of flow in the surrounding tissues (Haywood et al., 1981, Gardiner et al., 1990) (**Figure 9**). Silk sutures (6/0) are put in place at the top of this silastic lumen to allow the probe to be tied around the blood vessel. Probes are customed-made for use on different vessels, with probes for the renal and superior mesenteric arteries made with a lumen diameter of ~1.0 mm, while probes to be implanted around the descending aorta made with a lumen diameter of ~1.7 mm. In the setup described, the probes are connected to a transducer amplifier (Model 13-4615-50; Gould, Cleveland, OH, USA), a Doppler flowmeter (Crystal Biotech, Holliston, MA, USA), and a VF-1 mainframe (pulse repetition frequency 125 kHz) fitted with high-velocity (HVPD-20) modules (**Figure 8**).

The piezoelectric crystal in the probe emits a short burst of pulsed ultrasonic energy (20 MHz), which insonifies a section of the blood vessel held within the probe lumen. Following a short delay, the signal is reflected from moving erythrocytes found in the vessel and is detected by the same crystal (**Figure 10**). The sound reflected back from the moving erythrocytes is at a slightly different frequency than the transmitted sound due to the Doppler effect (Routh, 1996). The returning sound received by the flowmeter is measured by comparing the phase difference of the returning sound against a reference signal, and by doing this, the Doppler shift is detected. The Doppler shift can be described by the following Doppler equation.

$$\Delta_f = 2f_o\, V/c\, cos\theta$$

***$\Delta_f$- Doppler frequency difference, $f_o$- frequency of transmitted signal; V- velocity of the blood; c- velocity of sound in the blood; θ- the angle between the crystal and blood vessel***

In the cuff, the angle (**θ**) of the crystal remains constant at ~45° (**Figure 9**). The frequency of the transmitted signal ($\mathbf{f_o}$) and velocity of sound in the blood (**c**) are also constants- meaning that the Doppler frequency difference ($\mathbf{\Delta_f}$) is directly proportional to the velocity of the erythrocytes, which are travelling at the same speed as the blood of which they suspended in (**Figure 9**). When the probes are chronically implanted, a fibrous capsule grows around the cuff and the vessel, preventing vessel diameter changes beneath the probe, and because the blood vessel's diameter beneath the probe remains constant, changes in Doppler shift give an index of blood flow into the regional vascular beds downstream of the probe (Hartley and Cole, 1974, Haywood et al., 1981).

The system has been modified to operate at a pulse repetition frequency (PRF) (which is the number of times the crystal transmits and receives sound in 1 second) of 125 kHz, which is equal to once every 8 μs (**Figure 10**). The standard 62.5 kHz for these Crystal Biotech VF1 systems is not used to avoid the effects of aliasing, where high-velocity signals appear as lower or reversed frequencies (Gardiner et al., 1990). Aliasing effects are explained by the Nyquist theorem, which states that correct reproduction of analogue-to-digital signals requires that the sampling frequency, which in this case is the PRF, must be greater than half the maximum frequency response. Accordingly, aliasing effects occur when the frequency of the Doppler shift of the reflected sound exceeds half the PRF; above this limit, high-velocity signals are aliased and erroneously appear as lower or reversed frequencies (Nyquist, 1928). Aliasing occurs when the sampling rate is too slow and misses out on key information from the analogue signal.

Gardiner *et al.* showed that, in conscious rats implanted with aortic pulsed Doppler flow probes and treated with nitroprusside or methoxamine, a standard PRF of 62.5 kHz was insufficient to accurately measure changes in Doppler shift due to aliasing of the Doppler signal at high velocities (Gardiner et al., 1990). In this system, only spectral components up to 31.25 kHz could be measured. By modifying this system and increasing the PRF to 125 kHz, the high-velocity component of the signal can be included, up to 62.5 kHz. Therefore the experiments outlined in this thesis use a high-velocity module with a PRF of 125 kHz for all vascular beds, ensuring that aliasing does not occur under any experimental conditions (Hartley, 1981, Gardiner et al., 1990).

The time between transmission and the measured ultrasound signal can be adjusted using a range gate control on the pulsed Doppler flowmeter. This adjustment alters the distance from the crystal to the object from which reflected sound is measured. Adjusting the signal allows the velocity of blood cells in the centre of the vessel, where velocity is at its highest, to be sampled by adjusting the range control to give a maximum signal (**Figure 10**).

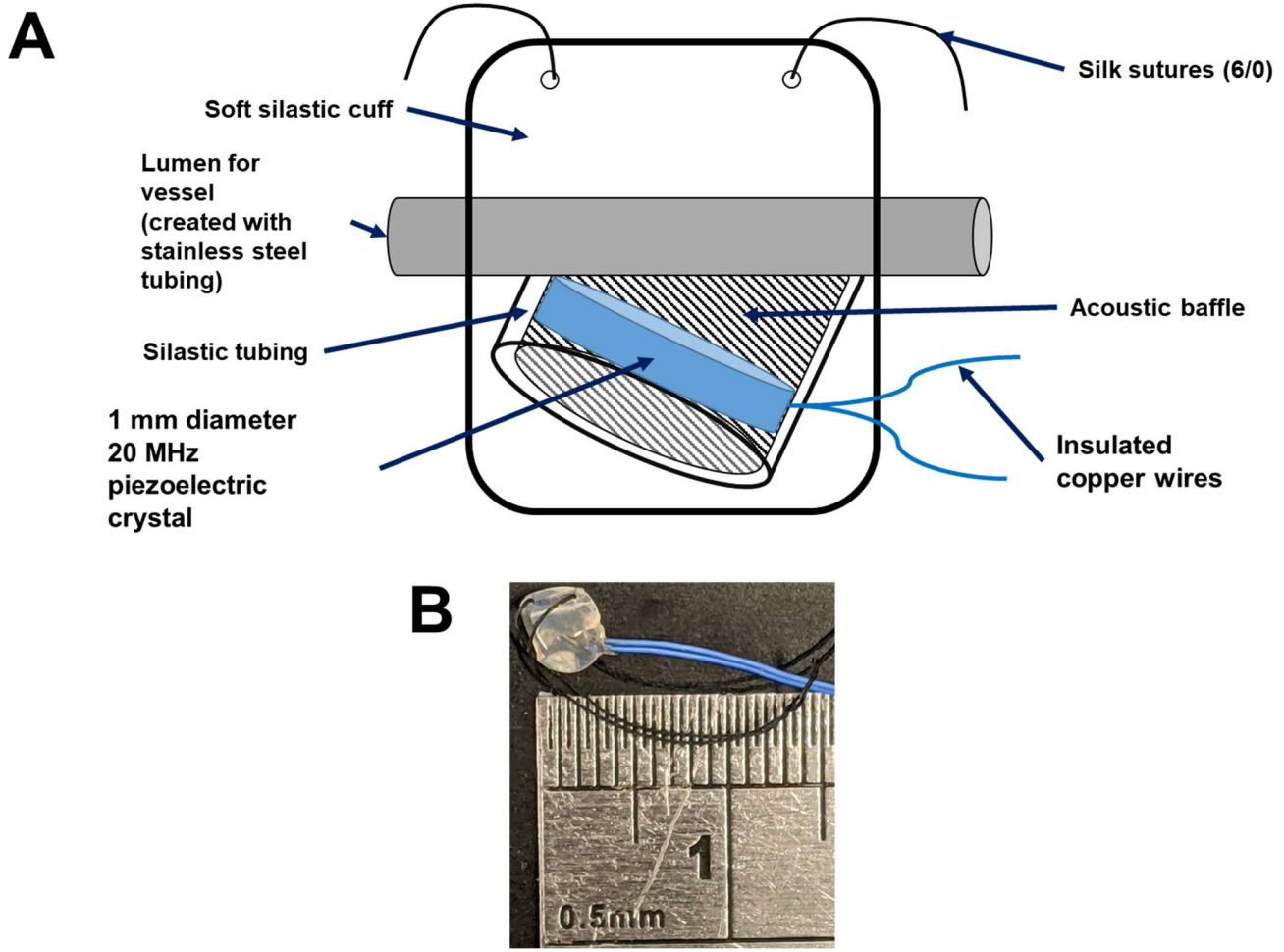


**Figure 9 The Miniaturised Pulsed Doppler Flow Probe. A)** Schematic representation of the miniaturised ultrasonic pulsed Doppler flow probe, made in-house. A 1 mm diameter 20 MHz piezoelectric crystal with insulated copper wires is housed inside silastic tubing, designed to sit at a 45° angle to the blood vessel lumen. The back and sides around the crystal are covered with an acoustic baffle to prevent interference from surrounding blood vessels. A soft silastic cuff is created with the aid of a section of stainless steel tubing to encase the probe and allow the creation of a lumen for the vessel to sit in. Silk sutures (6/0) are tied into the silastic cuff to allow the probe to be fastened around an artery. **B)** A photograph of the probe described in **A)**, next to a ruler, to reference size.

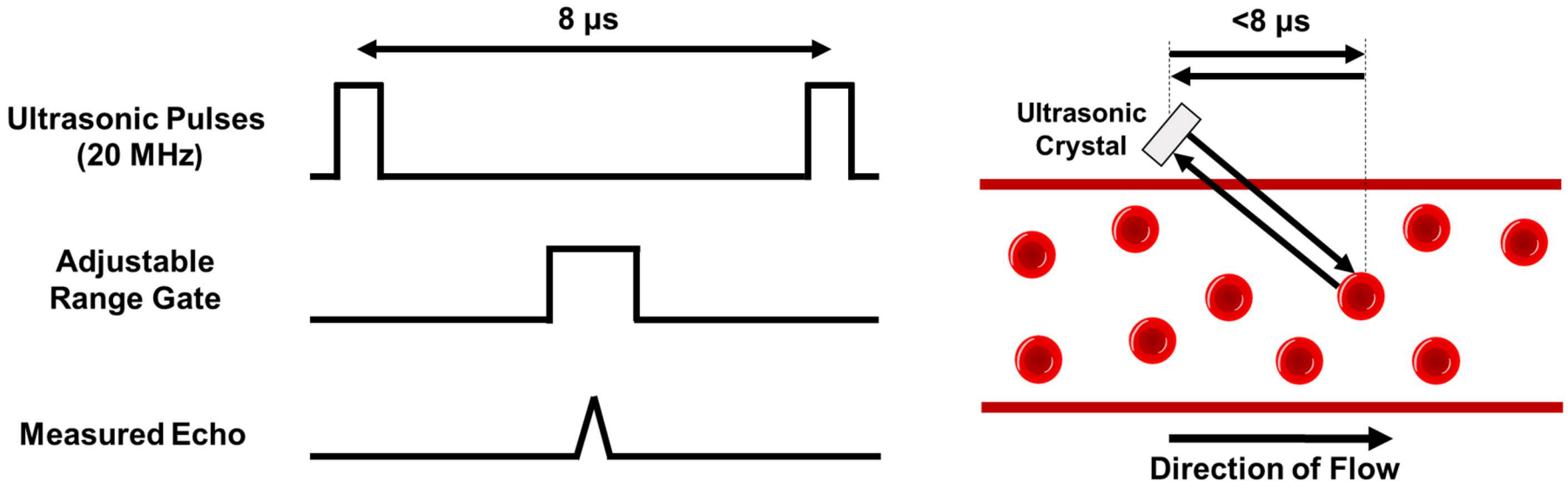


**Figure 10 Diagram of the 20 MHz Pulsed Doppler System.** The pulsed ultrasonic crystal used in this method has a pulse repetition frequency (PRF) of 125 Hz, meaning that the crystal isonifies the blood vessel held in the probe cuff every 8 µs, with a 20 MHz sound wave. In the vessel, the 20 MHz sound wave reflects off moving erythrocytes in the blood, which due to the Doppler effect, changes the frequency of the ultrasound wave in proportion to the speed of the erythrocytes. The sound wave must be reflected and returned to the crystal within 8 µs before the next pulse of ultrasound is admitted by the crystal to be measured correctly by the crystal. Erythrocytes flow faster in the centre of the vessel than at the edges. The Doppler system's range gate is a tunable filter that only measures sound reflected a certain time after the ultrasonic pulse, which effectively allows the Dopper device to be tuned to receive sound from a source closer or further away from the probe, allowing the measured echo to be tuned to detect the speed only from the erythrocytes flowing fastest in the vessel's centre.

### 2.1.3.3 Haemodynamic Technique Details: Calculating Regional Vascular Conductance

Vascular conductance (VC) is the ease with which blood flows through the circulation, or when applied to this *in vivo* Doppler technique, the ease with which blood flows through the regional microvascular beds downstream of the Doppler flow probe. VC is the reciprocal of vascular resistance.

The VC of a vascular bed is equal to the blood flowing through the vascular bed divided by the pressure of the blood (Gardiner and Bennett, 1988). Doppler shift in this experimental set-up is directly proportional to the blood flow through the artery (**2.1.3.2**). Additionally, the mean arterial pressure is also directly proportional to the blood flow through an artery. For this experimental setup, VC in regional arterial beds downstream of the Doppler flow probe is thus directly proportional to the Doppler shift (**2.1.3.2**), divided by the mean arterial pressure (**2.1.3.1**). By calibrating a baseline recording to zero, percentage changes in VC can thus be calculated using this technique.

$$\textbf{Vascular Conductance} = \textbf{Blood Flow} / \textbf{Blood Pressure}$$

$$\text{Doppler Shift} \propto \text{Blood Flow}$$

$$\%\Delta\textbf{Vascular Conductance} = \%\Delta(\textbf{Doppler Shift} / \textbf{Mean Arterial Pressure})$$

An increase in VC indicates vasodilation in the microvascular beds downstream of the probe. A decrease in VC indicates vasoconstrictions in the microvascular beds downstream of the probe.

## 2.1.4 *In Vivo* Methods: Materials Used

### 2.1.4.1 Materials Used: Veterinary Medications

| Resource | Use | Pharmacology | Manufacturer |
|---|---|---|---|
| **Atipamezole Hydrochloride (Sedastop®)** | Anaesthetic Reversal Agent | Adrenergic $\alpha_2$ Receptor Antagonist | Animalcare Ltd. (York, UK) |
| **Buprenorphine (Buprecare®)** | Anaesthetic Reversal Agent and Analgesic | Opioid Partial Agonist | Animalcare Ltd. (York, UK) |
| **Eye Gel (Lubrithal®)** | Eye Lubricant for Surgery | N/A | Dechra (Northwich, UK) |
| **Fentanyl Citrate** | Anaesthetic & Analgesic | Opioid Agonist | Martindale Pharmaceuticals (Essex, UK) |
| **Heparin Sodium** | Anticoagulant | Antithrombin III Inhibitor | Wockhardt (Wrexham, UK) |
| **Lidocaine** | Local Anaesthetic | $Na^+$ Channel Blocker | Antigen Pharmaceuticals (Southport, UK) |
| **Medetomidine Hydrochloride (Sedastart®)** | Anaesthetic and Analgesic | Adrenergic α2 Receptor Agonist | Animalcare Ltd. (York, UK) |
| **Meloxicam (Metacam®)** | Analgesic | COX Inhibitor | Boehringer Ingelheim Animal Health UK (Berkshire, UK) |
| **Pentobarbitone (Euthatal®)** | Schedule 1 Overdose Anaesthetic | $GABA_A$ Receptor Potentiator | Alstoe Animal Health (York, UK). |
| **Plasmin** | Clot-busting Enzyme | Serine Protease | Millipore/ Merck KGaA (Darmstadt, Germany) |
| **Water for Injections** | Drug Diluent | N/A | Hameln Pharmaceuticals (Gloucester, UK) |

**Table 1 Veterinary Drugs and Medications Used During Surgery, Surgical Aftercare, and Catheter Patency Maintenance After Insertion. Abbreviations: COX-** cyclooxygenase**, GABA-** γ-aminobutyric acid.

## Anaesthetic Agents

**Medetomidine:** Medetomidine is a sedative and analgesic commonly used in veterinary medicine (Giovannitti et al., 2015, Bennett and Restitutti, 2016). It is comprised of a racemic mixture of two optical stereoisomers: dexmedetomidine, the active enantiomer, and levomedetomidine, the inactive enantiomer (Bennett and Restitutti, 2016). Medetomidine is a selective $\alpha_2$ adrenoceptor agonist (Giovannitti et al., 2015). $\alpha_2$ activation causes inhibition of norepinephrine release from presynaptic neurons, which, in the central nervous system, causes sedation via the locus coeruleus and analgesia via the dorsal horn (Giovannitti et al., 2015).

**Fentanyl:** Fentanyl is a synthetic opioid and full agonist of the μ opioid receptor. Fentanyl causes analgesia and anaesthesia primarily by activating opioid receptors distributed throughout the central nervous system and within peripheral neural tissues (Stanley, 2014). Within the central nervous system, activation of the μ opioid receptors in the midbrain reduces nociceptive transmission from the periphery to the thalamus, reducing pain sensation (Pathan and Williams, 2012).

## Local Anaesthetics

**Lidocaine:** Lidocaine is a local anaesthetic. The primary mechanism of action of lidocaine is through the blockade of voltage-gated sodium channels (VGSCs) found on nerve cells, leading to reversible inhibition of action potential propagation. Thus when given locally, lidocaine causes a confined blockade of nervous system function, which is required for nociceptive signalling, thus leading to local anaesthesia (Hermanns et al., 2019).

## Reversal Agents

**Atipamezole:** Atipamezole is an $\alpha_2$-adrenoceptor antagonist commonly used to effectively reverse the effects of medetomidine (Virtanen, 1989, Giovannitti et al., 2015, Bennett and Restitutti, 2016). Atipamezole does not interfere with the analgesic effect of buprenorphine and is thus suitable for use in combination with it (Izer et al., 2014).

**Buprenorphine:** Buprenorphine is a semi-synthetic analgesic opioid derived from thebaine, an alkaloid found in the opium poppy *Papaver somniferum* (Welsh and Valadez-Meltzer, 2005). Buprenorphine exerts most of its effects at the μ opioid receptor, where it is a partial agonist (Virk et al., 2009). Because of its relatively decreased activation compared to full μ agonists, there is a plateau of receptor activation where there is no further physiological effect from increases in dose, causing the analgesic effects of buprenorphine to have a ceiling effect (Bloms-Funke et al., 2000, Welsh and Valadez-Meltzer, 2005). Buprenorphine has a high affinity and slow dissociation from μ opioid receptors, making buprenorphine suitable to compete with and reverse the effects of other opioids, such as fentanyl (Welsh and Valadez-Meltzer, 2005).

## Post-operative Analgesics

**Meloxicam:** Meloxicam is a non-steroidal anti-inflammatory drug (NSAID) with selective inhibition of cyclooxygenase-2 (COX-2) over cyclooxygenase-1 (COX-1) (Ogino et al., 1997). Inhibition of cyclooxygenase (COX) is central to the anti-inflammatory actions of NSAIDs, as COX is involved in the production of pro-inflammatory prostaglandins that cause vasodilation and pain (Wallace, 2013).

## Anti-Blood Clotting Agents

**Heparin:** Heparin is an anticoagulant glycosaminoglycan composed of chains of alternating residues of D-glucosamine and uronic acid (Hirsh et al., 1995). Heparin is a heterogeneous mix of molecular sizes and structures, with the anticoagulant activity of heparin dependent on the presence of a unique pentasaccharide present in only 1/3 of heparin molecules, which has a high-affinity binding to antithrombin III (ATIII) (Andersson et al., 1979, Rosenberg and Rosenberg, 1984). Binding to ATIII produces a conformational change that accelerates its ability to inactivate the coagulation enzymes thrombin (factor IIa), factor IXa and factor Xa (Hirsh et al., 1995).

**Plasmin:** Plasmin is a potent and reactive serine protease (Deryugina and Quigley, 2012). Plasmin facilitates the proteolysis of fibrin, which causes the breakdown of blood clots (Chapin and Hajjar, 2015).

# Schedule One Anaesthetic

**Pentobarbitone:** Pentobarbitone is a barbiturate anaesthetic that acts at the γ-aminobutyric acid A ($GABA_A$) channel (Muroi et al., 2009). The pharmacological action of pentobarbitone is complex, and depending on its concentration, pentobarbital can potentiate, activate, or block $GABA_A$ (Muroi et al., 2009). Pentobarbitone causes cardiorespiratory depression due to inhibitory action in the medulla oblongata, which rapidly causes cardiorespiratory failure and death if administered at a lethal dose (Yamada et al., 1983).

### 2.1.4.2 Materials Used: Vehicle Reagents

| Reagent | Manufacturer | Catalogue Number |
|---|---|---|
| **Propylene Glycol** | Sigma-Aldrich (Gillingham, UK) | Cat #P4347 |
| **Saline (Sodium Chloride 0.9 % w/v)** | Baxter (Newbury, UK) | N/A |
| **Tween 80** | Sigma-Aldrich (Gillingham, UK) | Cat #P1754 |

**Table 2 Reagents Used to Create the Inert Vehicle Used for i.v Drug Administration.**

### 2.1.5 *In Vivo* Methods: Surgical Procedures

All procedures were approved by the Animal Welfare and Ethical Review Body (University of Nottingham, establishment license (X653228F4); which has representation from The National Centre for the Replacement, Refinement and Reduction of Animals in Research (NC3R)) and performed in keeping with the Animals (Scientific Procedures) Act (1986) UK, under Home Office Project License (PPL) (PFOF2A6EC) and Personal License (PIL) authority for all members of the *in vivo* research team (Edward Wragg: 1830EA5D0). For the studies mentioned in this thesis, the data from 132 rats are reported. The results are reported following the Animal Research: Reporting of *In Vivo* Experiments (ARRIVE) guidelines for experiments involving animals (Kilkenny et al., 2010) and the editorial on reporting animal studies with the recommendations made by the British Journal of Pharmacology (McGrath and Lilley, 2015).

Adult male Sprague-Dawley rats (Charles River, Margate, UK), weighing 350-450 g at the commencement of the study, were pair housed in individually ventilated cages prepared with bedding material and enrichment. Cages were held in a temperature-controlled (21-23°C) environment with a 12-hour light-dark cycle (lights on 06:00-18:00); rats received access to food (18% Protein Rodent Diet; Envigo, Madison WI, USA) and water *ad libitum*, arriving at the animal house at least seven days before any surgical intervention. Welfare checks were carried out daily before surgery by a Named Animal Care & Welfare Officer (NACWO).

Doses for pharmacological agents used during surgery were as recommended in *Laboratory Animal Anaesthesia, Fourth Edition* (Flecknell, 2015). Surgery was conducted under general anaesthesia provided by fentanyl citrate and medetomidine hydrochloride (both 300 µg/kg, i.p., supplemented if required). The depth of anaesthesia was assessed by monitoring toe pinch withdrawal. Upon completion of the surgery, reversal of anaesthesia and postoperative analgesia were provided by atipamezole hydrochloride (1.0 mg/kg, s.c.) and buprenorphine (30 µg/kg, s.c.), with additional analgesia (meloxicam, 1.0 mg/kg/day, s.c.) given before the start of the surgical procedure and also daily for a further three days post-operation. The *in vivo* technique described requires two rounds of surgery, the first round for the implantation of the Doppler flow probes, and the second for intra-arterial and i.v. catheter insertion.

#### 2.1.5.1 Surgical Procedures: Surgery 1- Doppler Flow Probe Implantation

Rats were anaesthetised as previously described (**2.1.5**). Under anaesthesia, a midline abdominal incision was made, and the body wall opened. The intestines were lifted out of the body cavity into a saline-dampened tissue and laid to the side of the rat. The left renal artery (supplying the left kidney), the superior mesenteric artery (supplying the mesentery), and the distal/descending abdominal aorta below the level of the ileocecal artery (supplying the hindquarters) were cleared, and miniature pulsed Doppler flow probes placed and sutured around them (**Figure 11**). The intestines were put back in place, and the probe wires sutured to the left abdominal wall and tunnelled subcutaneously via the left flank to the posterior of the neck. The wires were then secured with a suture and taped to the nape of the neck, leaving about 0.5 cm in length protruding from the skin( **Figure 11**). Excess wire was coiled and sewn into a pouch beneath the skin on the left flank. All incisions were closed, and, following surgery, anaesthesia was reversed, and postoperative analgesia was given as previously described (**2.1.5**).

Following surgery, animals were returned to warmed cages containing recovery bedding with access to food and water *ab libitum*. Animals were closely monitored post-surgery, with welfare checks carried out every 15 minutes. After a minimum of 3 hours of observations and on confirmation that the rat had recovered successfully, the animal was returned to the holding room. The following morning, the rat was housed back into pairs with its original cage mate, who also underwent the surgery.

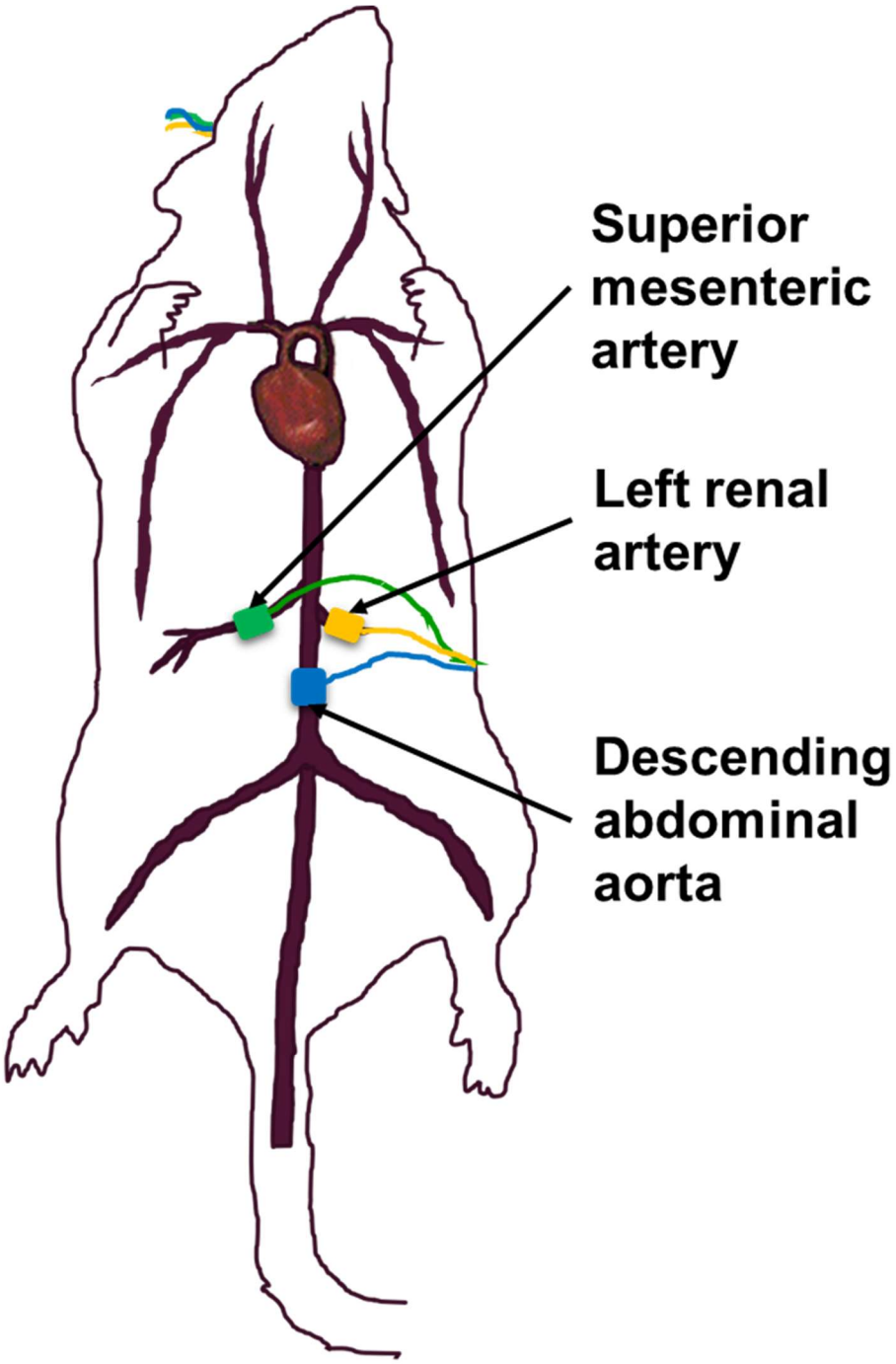


**Figure 11 Schematic Detailing the Location of Doppler Probes Implanted During Surgery.** Under anaesthetic, miniaturised pulsed Doppler flow probes are placed around the left renal artery, the superior mesenteric artery, and the descending abdominal aorta of the rat. The probes are tied shut using a suture, securing them in place. The probe wires are then tunnelled subcutaneously to the back of the neck, secured with a suture, and taped to the nape of the neck, leaving about 0.5 cm in length protruding from the skin. The excess wire from the probes is coiled and sewn into a pouch beneath the skin on the left flank.

### 2.1.5.2 Surgical Procedures: Surgery 2- Intravascular Catheter Implantation

Catheter implantation surgery commenced 11-13 days after Doppler flow probe implantation and after a satisfactory welfare check from the Named Veterinary Surgeon (NVS) or NACWO. Under anaesthesia, as previously described (**2.1.5**), before vessel catheterisation, the Doppler probe wires were released from the skin at the neck, and the signals checked before the wires were soldered into a miniature plug (Omnetic Connector Corporation, USA) (**Figure 12C**).

Before cannulation, all catheters were pre-filled with heparinised saline (20 I.U. /mL). Local anaesthetic (lidocaine, 0.5% w/v solution) was applied dropwise to all vessels exposed during these procedures. First, an incision was made into the neck, and the right jugular vein exposed. The rostral end of the vein towards the head was then ligated with a suture, and a small incision made into it. Next, three polyethylene catheters (Braintree Scientific, LD 0.28 mm, 100 cm in length, total lumen dead-space 0.1 mL) were inserted approximately 2 cm into the vein and tied in place. The i.v. catheters were then tunnelled subcutaneously to the back of the neck, before the initial incision was sutured shut.

Following insertion of the i.v. catheters, an incision was made on the underside of the tail to insert an intra-arterial catheter (**2.1.3.1**). The ventral caudal artery was exposed, and the caudal end ligated. An incision was made in the vessel, and the narrow portion of the catheter passed into it; the catheter was then advanced into the distal abdominal aorta. The catheter was tied in place and tunnelled subcutaneously to the same exit site at the back of the neck as the i.v. catheters before the tail incision was sutured shut.

The miniature plug soldered previously was mounted onto a custom-designed harness fitted and worn by the rat (**Figure 12A**). The catheters were then fed through a protective flexible metal spring secured to the harness and attached to a counter-balanced pivot system (**Figure 12B**). A connecting extension lead was then attached to the miniature plug and taped to the spring (**Figure 12C,D**). Finally, reversal of anaesthetic and analgesia was administered as previously described (**2.1.5**) and the animals singly housed with access to food and water *ab libitum*.

The arterial catheter line was connected to a fluid-filled swivel for continuous infusion of heparinised saline (20 I.U./mL, 0.4 mL/h) to preserve patency (**2.1.3.1**, **Figure 7**). This harness system allows the rat free movement in their cages. Animals were closely monitored post-surgery, with welfare checks carried out every 15 minutes. In addition, 4.5 hours after the surgery, a top-up dose of buprenorphine (15 µg/kg, s.c.) was given as an analgesic. The rat was observed for a minimum of 5 hours post-surgery until confirmed that the rat had successfully recovered.

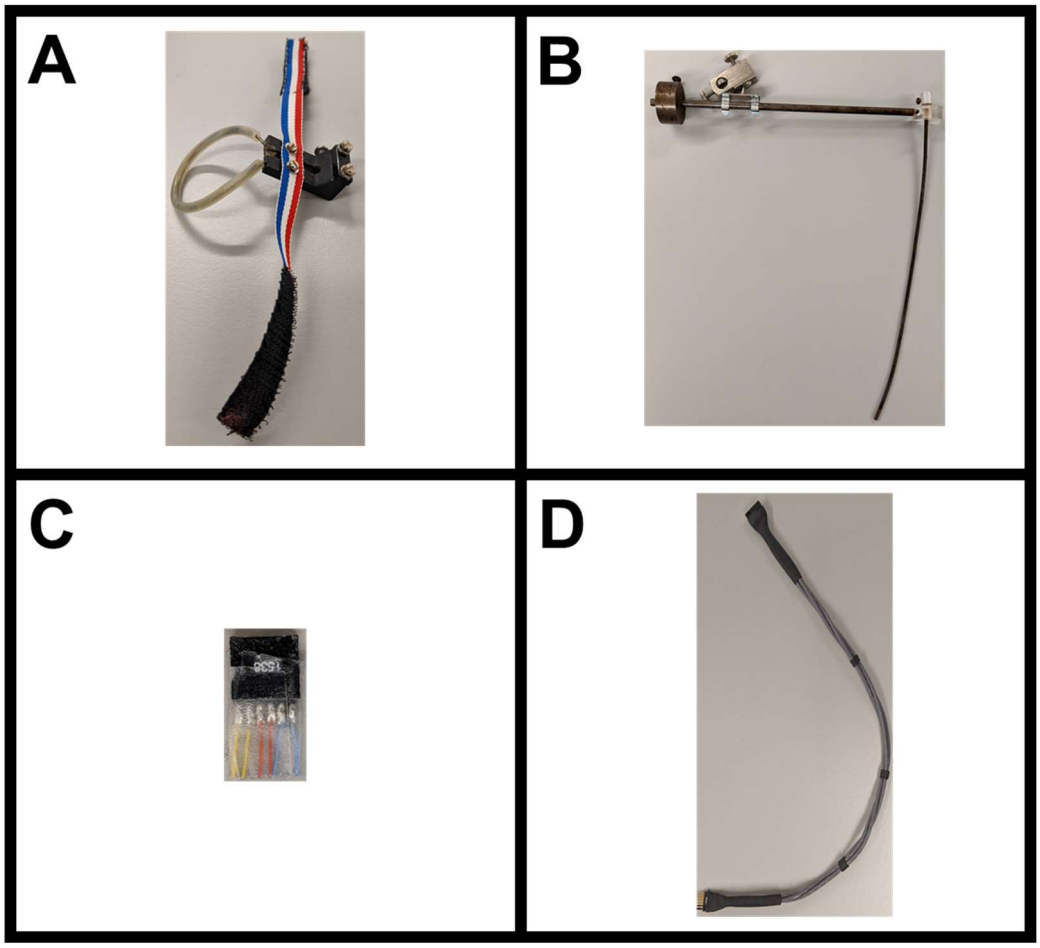


**Figure 12 Photograph Showing the Harness, Spring and Counterbalance System for the Haemodynamic Technique.** The rat wore a custom-designed harness (**A**), which protects the wires and catheters which protrude from the nape of the neck from damage. Catheters were advanced up a metal spring (**B**), protecting them from kinks and damage. Wires from the Doppler flow probes were soldered into a miniature plug (**C**), and a connector (**D**) from the plug to the top of the cage was fastened to the spring with surgical tape. The spring is held with a counterbalance arm (**B**), connected to a support that prevents the spring from draping down, but allows the rat complete movement around the cage.

### 2.1.6 *In Vivo* Methods: Data Collection

Cardiovascular variables of arterial blood pressure (used to calculate HR and MAP), and renal, mesenteric, and hindquarters Doppler shifts were recorded using bespoke software (Instrument Development Engineering Evaluation, IdeeQ version 2.5; Maastricht Instruments, Maastricht, The Netherlands). Raw data were sampled by IdeeQ every 2 ms, averaged, and digitally stored every cardiac cycle.

For all *in vivo* experiments, time-averaged data are shown as changes from baseline [Δ(HR (beats/min); ΔMAP (mmHg); ΔVC (%)]. Statistical analysis for group comparisons of animals was performed on the average changes over specified time periods. Statistical and graphical analysis was performed with Biomedical software version 3.4 (Medical Physics, University of Nottingham, UK) and Prism software version 9.2.0 (GraphPad Software, San Diego, CA, USA). Biomedical software tabulates the raw data, including VCs for each vascular bed and calculates the change and % change across time for HR, blood pressure, and the three reported VCs.

Changes in mean Doppler shift signals were taken as indices of flow changes (**2.1.3.2**). MAP and mean Doppler shift signals were used to calculate percentage changes in VCs for each specified time period (**2.1.3.3**). For the graphical representation of each experiment, all variables were presented on the same X-axis length and scale.

The Y-axis for all cardiovascular variables were appropriately scaled to the magnitude (range) of the effect. A minimum scale size was applied for each variable to ensure that the graphs did not misrepresent small effects that were not physiologically relevant and that the studies were not powered to detect (**2.1.7**). The minimum range of the Y-axis for each of the variables was as follows: ΔHR- 50 bpm, ΔMAP- 20 mmHg, ΔVC- 20%.

The length of the Y-axis for graphs presenting ΔHR and ΔMAP were equal for both variables and fixed regardless of the range represented on each axis (Δ(beats/min) and Δ(mmHg), respectively), with the length of both Y-axis' equalling L. The length of each of the Y-axis for each of the three reported ΔVCs was variable and directly proportional to the range (±Δ%) represented on the axis in comparison to the range (±Δ%) represented on the axis' of the other reported ΔVCs. All three VCs shared a total length of Y-axis equalling 3L, divided out in proportion to the range represented on each ΔVC Y-axis.

Each animal represented one experimental unit (n). All results shown are an average of the means for each 'n' number. Error bars are + or - SEM for all graphs presented.

### 2.1.7 *In Vivo* Methods: Statistical Analysis

Prior to the work detailed in this thesis, to minimise the number of animals used for these studies, power calculations were carried out by Prof Jeanette Woolard (the PPL holder) to estimate the group size required to measure a clinically relevant change in blood pressure (>10 mmHg) and in regional changes to blood flows (>10%) (80%, p=0.05, effect size of 10 mmHg, SD=8.48, paired T-test). Based on both previous experience from the research group, and the results of the NC3R's Experimental Design Assistant tool, which guides researchers through the design and analysis of *in vivo* experiments, eight animals per group were found to be appropriate (Percie du Sert et al., 2017).

For some animals, one or up to two Doppler probe signals were lost during the experiment due to damage to the probe, its wires, or changes to its positioning relative to the blood vessel in the rat. Rats without complete sets of signals were still included in the study to reduce the use of animals. For each experiment, a minimum of six working signals for each vascular bed measured was required; if this was not reached, additional rats were added to the study. Because of this requirement, and the loss of some animals due to attrition, which is to be expected with research of this nature, the final n number for each experiment varied between eight and ten.

Nonparametric tests were completed in all instances because the *in vivo* data could not be assumed to be normally distributed, there was considerable variability in these studies, so outliers were hard to identify, and homoscedasticity (equality of variances) could not be assured between groups as variances in treatment groups exerting a large effect were generally greater than those of a control group (Gosselin, 2019). Statistical analysis was performed with Biomedical software version 3.4 (Medical Physics, University of Nottingham, UK) and Prism software version 9.2.0 (GraphPad Software, San Diego, CA, USA).

For statistical analyses for the individual *in vivo* studies conducted throughout this thesis, a value of $p<0.05$ was considered significant. Therefore, if a value of $p<0.05$ was achieved, it is denoted by a single symbol specific to the statistical test conducted. Where data from individual studies were combined for analysis, as was the case when multiple studies started with a dose of the same antagonist, a value of $p<0.01$ was considered significant because, on review, the original p-value used for the individual studies was not optimal for use with the high n numbers of the combined datasets. To ensure full transparency the original datasets ($p<0.05$) are presented in the thesis appendix (**7.2**).

For all experiments, for each specified time point (**2.1.6**), a Friedman test (a nonparametric, repeated-measures analysis of variance test) was used for within-group comparisons compared to the baseline to ascertain if there was a significant difference between the time point and the baseline recording at time 0 for the rats at rest before treatment.

For experiments in which each animal underwent repeated experimental measures on day one and day three, with a washout on day two, each animal could act as its own paired control (**2.1.8**, **3.2.1.3**, **4.2.1.4, Figure 13**). Because of this, a Wilcoxon signed-rank matched-pairs test (a nonparametric test) was conducted for within-group comparisons between different dosing treatment regimens at each specified time point to ascertain if there was a significant difference between the two different treatment conditions at each time point.

For experiments where a 3-day protocol was followed with no repeated measures (**5.2.1.2**), Mann-Whitney U tests (a nonparametric test) were conducted for between-group comparisons between two different dosing treatment regimens at each specified time point to ascertain if there was a significant difference between two groups at that given time point.

## 2.1.8 *In Vivo* Methods: Experimental Overview

Experiments began the day after the second surgery (**2.1.5.2**), following a satisfactory welfare check by the NACWO, with animals conscious and unrestrained in home cages with free access to food, water and environmental enrichment.

Drugs were administered through the three i.v. catheters inserted during the second round of surgery (**2.1.5.2**), which allowed for concurrent administration of drugs, minimised disruption to the rat, and allowed for measurement of the drug effects straight after dosing. The i.v. lines were checked for patency by flushing ~0.2 mL heparinised saline (20 I.U. /mL) through the line before starting the day's experiments. Lines were also flushed through with ~0.2 mL heparinised saline (20 I.U. /mL) after completion of the experimental day, removing any residual traces of ligand and helping to maintain the lines' patency.

Before starting a day's experiments, the arterial line was disconnected from the pump and swivel system (**Figure 7**) and connected to the pressure transducer dome (**2.1.3.1**). Heparinised saline (40 I.U. /mL, ~0.2 mL) was flushed through the arterial line to prevent the catheter from losing patency (**2.1.3.1**) approximately every 10 minutes. If at the start of the day the arterial line was blocked or the signal was excessively dampened, the clot-busting enzyme plasmin (**2.1.4.1**) was made up to 1.0 I.U./mL in heparinised saline (40 I.U. /mL) and given in 0.2 mL bolus' over 10 min. Additionally, the Doppler flowmeter was connected to the connector (**2.1.5.2**) (**Figure 12D**), and the Doppler system (**2.1.3.2**) calibrated before starting the day's experiments.

The vehicle used as a drug dilutant and control for all experiments was sterile saline with 5% polyethene glycol (v/v) and 2% Tween 80 (v/v). This vehicle is referred to throughout this thesis as the 'vehicle'. Drugs were dissolved in this vehicle with the assistance of sonication when required.

Each experiment lasted three days. At the end of each experiment, rats were euthanised by an Animals (Scientific Procedures) Act 1986 Schedule One procedure. This procedure was an anaesthetic overdose (Euthatal/Dolethal, ~60–80 mg, i.v.) followed by exsanguination.

It has been demonstrated previously that with this technique, rats undergoing treatment regimes consisting only of vehicle administration do not have significant haemodynamic changes over the course of a four-day study (Gardiner et al., 2010, Carter et al., 2017), implying that when the study begins 24 hours after surgery, the effects of that surgery, including from the anaesthetics used, are negligible. It also implies that the method does not result in significant cardiovascular changes for the rat throughout the duration of the study.

In addition, the studies were designed to account for any variation caused over the course of the study. In **chapters 3** and **4**, experiments were conducted in which each animal underwent repeated experimental measures on days one and three, with a washout on day two, with each animal acting as its own paired control (**3.2.1.3**, **4.2.1.4**). The animals were randomly allocated based on a study-independent identification number assigned to the rat on entry into the animal unit into two groups, with each group receiving different conditions on day 1, before swapping conditions for day 3 (**Figure 13**).

In **chapter 5**, experiments in which repeated experimental measures were not used. Variation throughout the study was accounted for by comparing the study group to a vehicle control group. Rats were randomly allocated based on a study-independent identification number assigned to the rat on entry into the animal unit into a group undergoing drug treatment or a group undergoing vehicle control.

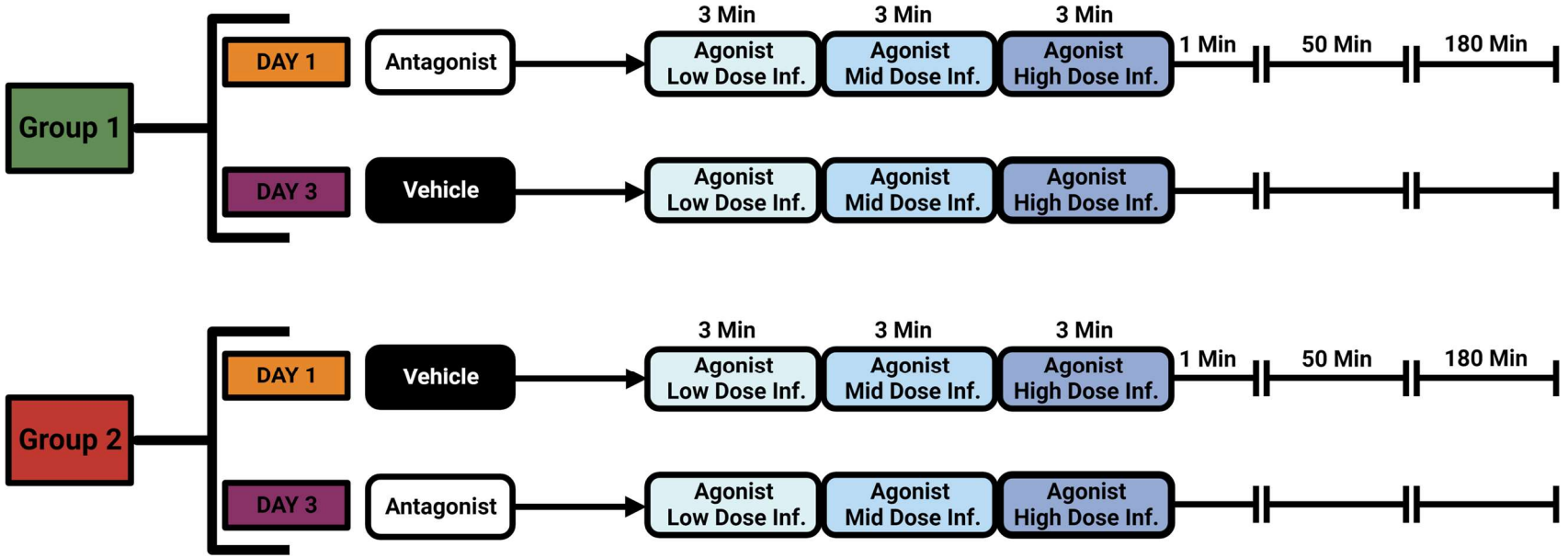


**Figure 13 Generalised Adminstration Schematic for *In Vivo* Experiments with Repeated Experimental Measures.** Experiments explored the effect of an agonist in the presence or absence of an antagonist.

### 2.1.9 *In Vivo* Methods: Drugs Used *In Vivo*

A comprehensive list of compounds and suppliers can be found in the in vitro section of the methodology (**2.2.1.4.3**). Please note, for the drugs used *in vivo*, drug doses are given as units of mass of the drug divided by the mass of the animal, as convention dictates. The mass of the drug refers directly to the amount of the specific pure powdered compound used for the experiment, which is commonly a salt. Because of this, it is important to note that for these experiments, the mass given for each drug includes the ionic drug and its ionic non-drug counterpart. Where this is the case, and to make for a straightforward read, only the ionic drug is mentioned throughout this thesis. The drugs used for *in vivo* experiments in this chapter and their corresponding salts are detailed in the preliminary matter of the thesis (**vi**).

# 2.2 Materials & Methods: *In Vitro*

## 2.2.1 *In Vitro* Methods: Materials Used

### 2.2.1.1 *In Vitro* Materials: Lab Plasticware

| Reagent or Resource | Manufacturer | Catalogue Number |
|---|---|---|
| **White 96-well Plates** | Greiner Bio-One (Stonehouse, UK) | 655089 |
| **BackSeal, (96-well plate) Backing Tape, White** | PerkinElmer Inc (Massachusetts, USA) | 6005199 |
| **TC Flask T25, Standard Vented Cap** | Sarstedt AG & Co. KG (Nümbrecht, Germany) | 83.3910.002 |
| **TC Flask T75, Standard Vented Cap** | Sarstedt AG & Co. KG (Nümbrecht, Germany) | 83.3911.002 |
| **TC Flask T175, Standard Vented Cap** | Sarstedt AG & Co. KG (Nümbrecht, Germany) | 83.3912.002 |
| **Corning® Tissue Culture-Treated Dish 100 mm x 20 mm** | Corning (Deeside, UK) | 430167 |
| **Nalgene Cryogenic Vial (2.0 mL)** | Thermo Fisher Scientific (Loughborough, UK) | 5000-0020 |

**Table 3 Lab Plasticware used for *In Vitro* Experiments.**

## 2.2.1.2 *In Vitro* Materials: Tissue Culture

### 2.2.1.2.1 *In Vitro* Tissue Culture: Cell Lines

| Reagent or Resource | Manufacturer | Catalogue Number |
|---|---|---|
| **Human: GloSensor™ cAMP HEK 293 Cell Line (female)** | Promega Corporation (Wisconsin, USA) | E1261 |
| **Human: HEK 293T cells (female)** | ATCC (Virginia, USA) | CRL-3216 |

**Table 4 Cell Lines used for *In Vitro* Experiments.** Abbreviations: **cAMP-**cyclic adenosine monophosphate, **HEK 293T-** Human embryonic kidney 293T cells, **ATCC-** American Type Culture Collection

### 2.2.1.2.2 *In Vitro* Tissue Culture: Tissue Culture Reagents

| Reagent or Resource | Manufacturer | Catalogue Number |
|---|---|---|
| **Dulbecco's Modified Eagle's Medium (DMEM)- High Glucose** | Sigma-Aldrich (Gillingham, UK) | D6429 |
| **Dulbecco's Phosphate Buffered Saline (PBS)** | Sigma-Aldrich (Gillingham, UK) | D8537 |
| **Foetal Bovine Serum** | Sigma-Aldrich (Gillingham, UK) | F2442 |
| **Poly-D-Lysine Hydrobromide** | Sigma-Aldrich (Gillingham, UK) | P5407 |
| **Trypsin-EDTA solution (x10)** | Sigma-Aldrich (Gillingham, UK) | T4174 |
| **Fisherbrand™ Sterile PES Syringe Filter** | Thermo Fisher Scientific (Loughborough, UK) | 15206869 |

**Table 5 Tissue Culture Reagents used for *In Vitro* Experiments.** Abbreviations: **PES-** polyethersulfone

### 2.2.1.3 *In Vitro* Materials: Transient Transfections

#### 2.2.1.3.1 *In Vitro* Transient Transfections: DNA Amplification

| Reagent or Resource | Manufacturer | Catalogue Number |
|---|---|---|
| **PureYield™ Plasmid Maxiprep System** | Promega Corporation (Wisconsin, USA) | A2393 |
| **Subcloning Efficiency™ DH5α™ Chemically Competent Cells** | (Invitrogen) Thermo Fisher Scientific (Loughborough, UK) | 18265-017 |
| **Luria Broth (Lennox)** | Sigma-Aldrich (Gillingham, UK) | L3022 |
| **Luria Broth with Agar (Lennox)** | Sigma-Aldrich (Gillingham, UK) | L2897 |
| **Kanamycin sulphate** | Gibco™, Thermo Fisher Scientific (Loughborough, UK) | 11815-024 |
| **Ampicillin Sodium Salt** | PanReac Química SLU (Barcelona, Spain) | A0839 |
| **Petri Dish 92x 16mm with ventilation cams** | Sarstedt AG & Co. KG (Nümbrecht, Germany) | 82.1473 |

**Table 6 Reagents and Resources Required for DNA Amplification Techniques.**

#### 2.2.1.3.2 *In Vitro* Transient Transfections: Transfection Reagents

| Reagent or Resource | Manufacturer | Catalogue Number |
|---|---|---|
| **FuGENE® HD Transfection Reagent** | Promega Corporation (Wisconsin, USA) | E2312 |
| **Opti-MEM® Reduced Serum Medium** | Thermo Fisher Scientific (Loughborough, UK) | 31985-062 |

**Table 7 Transfection Reagents used for *In Vitro* Experiments.**

## 2.2.1.4 *In Vitro* Materials: Experimental Materials

### 2.2.1.4.1 *In Vitro* Experimental Materials: Buffer Components

| HEPES Buffered Saline Solution Additive | Manufacturer | Catalogue Number |
|---|---|---|
| **Bovine Serum Albumin** | Sigma-Aldrich (Gillingham, UK) | A7030 |
| **Dimethyl Sulfoxide (DMSO) (ReagentPlus® ≥99.5%)** | Sigma-Aldrich (Gillingham, UK) | D5879 |

**Table 8 Buffer Components used for *In Vitro* Experiments.**

### 2.2.1.4.2 *In Vitro* Experimental Materials: Experimental Assay Reagents

| Reagent or Resource | Manufacturer | Catalogue Number |
|---|---|---|
| **Nano-Glo® Luciferase Assay (Nano-Glo® Substrate, [Furimazine])** | Promega Corporation (Wisconsin, USA) | N1130 |
| **GloSensor™ cAMP Reagent** | Promega Corporation (Wisconsin, USA) | E1291 |
| **SNAPTag® AlexaFlour 488 membrane impermeant substrate** | New England Biolabs | S9124S |

**Table 9 Experimental Assay Reagents used for *In Vitro* Experiments.**
Abbreviations: **cAMP-** cyclic adenosine monophosphate.

#### 2.2.1.4.3 *In Vitro* Experimental Materials: Pharmacological Ligands

| Ligand | Pharmacological Action | Manufacturer | Catalogue Number |
|---|---|---|---|
| **Adenosine** | Non-selective Adenosine Receptor Agonist | Fisher Scientific (Loughborough, UK) | 10377580 |
| **BAY 60-6583** | Selective $A_{2B}$ Receptor Partial Agonist | Tocris Bioscience (Bristol, UK) | 4472 |
| **CA200645** | Adenosine Receptor Fluorescence labelled Antagonist | Hello Bio (Bristol, UK) | HB7812 |
| **CGP 20712A Dihydrochloride** | Selective $\beta_1$ Receptor Antagonist | Tocris Bioscience (Bristol, UK) | 1024 |
| **CGS 21680 Hydrochloride** | Selective $A_{2A}$ Receptor Agonist | Tocris Bioscience (Bristol, UK) | 1063 |
| **ICI 118,551 hydrochloride** | Selective $\beta_2$ Antagonist | Tocris Bioscience (Bristol, UK) | 0821 |
| **Forskolin** | Adenylyl cyclase activator | Tocris Bioscience (Bristol, UK) | 1099 |
| **Propranolol Hydrochloride** | Non-Selective β antagonist | Tocris Bioscience (Bristol, UK) | 0624 |
| **PSB 1115** | Selective $A_{2B}$ Receptor Antagonist | Tocris Bioscience (Bristol, UK) | 2009 |
| **PSB 603** | Selective $A_{2B}$ Receptor Antagonist | Tocris Bioscience (Bristol, UK) | 3198 |
| **SCH 58261** | Selective $A_{2A}$ Receptor Antagonist | Sigma-Aldrich (Gillingham, UK) | S4568 |
| **Sunitinib Malate** | Receptor Tyrosine Kinase Inhibitor | Fisher Scientific (Loughborough, UK) | AC462640010 |
| **Recombinant Human VEGF-$A_{165}$a** | Protein VEGF Receptor Agonist. | R&D Systems (Abingdon, UK) | 293-VE-500 |

**Table 10 Ligands used for In Vivo and *In Vitro* Experiments.**

## 2.2.2 *In Vitro* Methods: Tissue Culture

### 2.2.2.1 Tissue Culture Background: Human Embryonic Kidney 293 Cell Lines

Human Embryonic Kidney (HEK) 293 cell lines were used for the *in vitro* experiments presented in this thesis. HEK 293s are an extensively used immortalised cell line family, originally derived from the kidney of a human aborted female embryo that was transfected with sheared human adenovirus type 5 deoxyribonucleic acid (DNA), causing expression of the E1A adenovirus gene (Graham et al., 1977, Lin et al., 2014). The presence of this gene allows for the rapid upregulation of a selection of viral promoters, enabling these cells to manufacture high levels of proteins expressed with these promoters (Graham et al., 1977, Lin et al., 2014). Additionally, the adenovirus gene E1B was transfected into the original HEK 293 cell line, which inhibits apoptosis, helping to immortalise the cell line to allow it to grow successfully in culture (Berk, 2005). Cells of the HEK 293 family are easy to grow, respond well to freezing, and are efficiently transfected with recombinant proteins, making HEK 293 cell lines versatile workhorses with many applications in molecular biology (Thomas and Smart, 2005).

Numerous variants of the original HEK 293 line have been generated to optimise the line for various conditions and uses (Yuan et al., 2018). HEK 293T cells were used for work in this thesis. Known initially as 293/*tsA1609*neo cells, HEK 293T cells are engineered to express a plasmid encoding a temperature-sensitive mutant of the simian virus 40 (SV40) large T antigen (DuBridge et al., 1987). The presence of this viral protein enhances the transfection of expression vectors engineered to express the viral promoter SV40 origin of replication (Lin et al., 2014, Yuan et al., 2018). A potential drawback of the viral promoter SV40 is its ability to bind to and suppress p53, a cellular tumour suppressor protein, which is important in maintaining genome integrity (Lilyestrom et al., 2006). As a result of p53 suppression, HEK 293T cells have been shown to be more susceptible to genetically differentiating away from the original clone, although this has been demonstrated to not be a problem under standard laboratory use (Lin et al., 2014). Also used in this thesis for experiments investigating cAMP accumulation was a clonal HEK 293 cell line acquired from Promega, referred to as HEK 293G, which stability express a GloSensor™ cAMP plasmid, encoding a protein that dynamically

senses cellular cAMP levels (**2.2.7.1.2**, **Figure 21**). This HEK 293G cell line has endogenous $A_{2A}$ and $A_{2B}$ receptor expression, resulting in cAMP accumulation upon ligand stimulation (Goulding et al., 2018).

#### 2.2.2.2 Tissue Culture: HEK 293 Cell Line Maintenance

HEK 293T and HEK 293G cell lines used throughout this thesis had similar morphology and required the same maintenance and media for growth (**2.2.2.1**). HEK 293 cell lines were grown in high-glucose Dulbecco's Modified Eagle's Medium (DMEM) containing 2.0 mM L-glutamine, complemented with 10% Fetal Bovine Serum (FBS) as a growth supplement. This culture media contained all the essential inorganic salts, amino acids, vitamins and pyruvate required for cell survival, as well as fetal growth factors to stimulate cell growth and division. DMEM contained a bicarbonate buffering system that is $CO_2$ sensitive and the pH indicator phenol red, which gives a visible indication of the pH of the solution, with red being pH 7.4.

HEK cell lines were maintained in T75 flasks in incubators at 37°C with humidified atmospheric air supplemented with 5% $CO_2$. Both HEK 293 cell lines used for experimental work formed adherent monolayers to the bottom surface of the container in which they were propagated.

Cell morphology and confluence were checked daily using an inverted microscope (Zeiss, Primovert) with a Plan Apochromat 10X objective lens. Cells were passaged at 70-80% confluency to ensure cell viability and health by maintaining the cells in logarithmic phase growth. To maintain a sterile environment, tissue culture was performed in a Microbiological Safety Cabinet (TriMAT Class II; Contained Air Solutions, UK). All media were stored at 4°C and warmed to room temperature before use. To create a new passage the old medium was removed from the T75 flask, and the cells rinsed with 2 mL Dulbecco's Phosphate Buffered Saline (PBS) to remove traces of the old medium and any cells not adherent to the flask. Next, cells were detached from the flask and separated from each other by incubation for 5 min at room temperature with 1 mL of 1x porcine trypsin solution with ethylenediaminetetraacetic acid (EDTA). The 1x solution was created from a 10x solution using PBS as the dilutant. Trypsin is a proteolytic serine protease that cleaves adhesion molecules that hold cells to each other and the flask (Polgár, 2005). EDTA is a hexadentate chelating agent added to the trypsin mixture to bind any remaining $Ca^{2+}$ and $Mg^{2+}$ ions following the PBS wash, which disrupts ion-dependent protein-protein interactions that hold cells together (Alberts et al., 2002). The cell suspension was centrifuged at 1000 rpm for 5 min, the supernatant discarded, and the pellet containing the cells resuspended in 5 mL of the culture

media. Cells were then passaged into new T75 flasks containing 20 mL of the culture media, typically seeding the new flasks using a fifth, a tenth, or twentieth of the resuspend culture media, depending on when the flask was required for experimental use.

For cell line freezing (**2.2.2.3**), new T175 flasks containing 40 mL of the culture media were seeded using a fifth of the suspended culture media. For cell line recovery (**2.2.2.4**), T25 flasks were used. For passaging, these flasks were treated the same as the T75 flasks described above, apart from that the cells were removed from the plate with 0.75 mL trypsin solution instead of 1 mL.

### 2.2.2.3 Tissue Culture: HEK 293 Cell Line Freezing

Multiple passages of the HEK cell lines used throughout this thesis (**Table 4**) were stored frozen for future use. The cells lines were temporarily stored at -80°C or in vapour phase liquid nitrogen for long-term storage (Isothermal V3000-EHAB/C, Custom Biogenic System, USA). Cells were frozen in a cryopreservation media containing 90 % FBS and 10% dimethylsulfoxide (DMSO) to reduce cellular damage and lysis during freezing and thawing. Before use, potential contaminants were removed from the cryopreservation medium by filter sterilisation using a 0.2 µm filter. FBS protects the cells from cellular stress, and DMSO prevents the formation of ice crystals that can pierce the plasma membrane and cause cell lysis (Chaytor et al., 2011).

Before freezing, cells were bulked up in a T175 flask (**2.2.2.2**). These flasks were trypsinised as previously described for a T75 flask (**2.2.2.2**), however, due to the increase in flask size, they were rinsed with 5 mL PBS instead of 2 mL, the cells removed from the plate with 3 mL of the 1x trypsin solution instead of 1 mL, and the detached cells resuspend in 20 mL the culture media instead of 10 mL.

The cell pellet was then resuspended in 4 mL cryopreservation media, with 1 mL of the resuspension media aliquoted into four 2.0 mL cryogenic storage vials. Optimal cell freezing is slow to reduce the formation of intracellular ice crystals that are fatal upon thawing; to slow the freezing rate vials were placed in a Mr Frosty™ freezing container (Nalgene, Thermo Fisher Scientific, UK) and frozen to -80°C (Pegg, 2007). Once frozen to -80°C, cells were transferred to the liquid nitrogen vapour phase for long-term storage.

### 2.2.2.4 Tissue Culture: HEK 293 Cell Line Recovery from Frozen

To recover a frozen cell line, a previously frozen aliquot (**2.2.2.3**) was removed from storage and rapidly thawed. 1 mL of cell culture media (DMEM with FBS, as described previously (**2.2.2.2**) was added to the frozen aliquot. Once defrosted, the aliquot was suspended in 10 mL cell culture media and seeded into a small T25 flask (25 $cm^2$ surface area), selected to allow cells to establish contact with each other, encouraging recovery and growth. 24 hours following the seeding of the flask, the media in the flask was exchanged with 10 mL of fresh cell culture media to remove dead cells and the remaining DMSO found in the aliquot. When the cells had suitability recovered and grown back to 60% confluency, the original T25 was then passaged into a T75, as described previously (**2.2.2.2**). After an additional few passages of growth, the cell line was fully recovered and ready for experimental use.

### 2.2.2.5 Tissue Culture: Seeding of HEK 293 Cells into Tissue Culture Dishes or T25 Flasks

The required HEK 293 cell line was grown in a T75 flask until ~70% confluent before the cells were washed, detached from the flask, resuspended, and centrifuged as described previously (**2.2.2.2**). The supernatant was discarded, and the cell pellet further resuspended in 10 mL cell culture media (DMEM + FBS, as previously described (**2.2.2.2**). To ensure experiments used cells at optimal confluency and number for transfection and further plating, the cell density of the sample was determined using the average cell count calculated with a haemocytometer (BRAND® counting chamber, BLAUBRAND® Neubauer improved, BR717805, Sigma-Aldrich, UK), averaged over two independent readings. Cells were then diluted into 15 mL of fresh culture medium per tissue culture dish (surface area 55 $cm^2$) or T25 flask (surface area 25 $cm^2$) required, at the required density unique to each experiment.

## 2.2.3 *In Vitro* Methods: Molecular Biology

Constructs containing receptors genetically engineered to encode N-terminal tags were utilised to explore the function of receptors *in vitro*. These receptors were expressed in HEK 293 cell lines (**2.2.2.1**) using plasmid expression vectors.

All receptor constructs used for work detailed in this thesis were kindly donated by other researchers (detailed below). As such, the key background for these constructs will be covered in this thesis, but not their creation. Peptide sequences for receptors and there associated enhancer region, tags and linkers are provided in the appendix (**7.1**).

### 2.2.3.1 Molecular Biology: Expression Vectors

Plasmid gene expression vectors were used to encode the modified receptors of interest (**2.2.3.2**) to facilitate the amplification of the complementary deoxyribonucleic acid (cDNA) (**2.2.3.3**) and its successful transfection (**2.2.4.1**), transcription, translation and cell surface expression of the encoded recombinant receptor in HEK 293 cells.

Each plasmid expression vector contained promoters to facilitate the initiation of transcription, such as the human cytomegalovirus (CMV) promoter, which enhances transcription in mammalian cell lines (**Figure 14**). All of the expression vectors used also contained an SV40 polyadenylation sequence tail to protect the generated messenger ribonucleic acid (mRNA) from degradation (van den Hoff et al., 1993) (**Figure 14**). Additionally, each vector contains a Kozak consensus sequence motif which is a site to initiate translation of the plasmid cDNA (Kozak, 1987) (**Figure 14**). The export of the translated protein to the plasma membrane was enhanced using a signal sequence inserted just before the N-terminal tag on each receptor. This signal sequence was either derived from the interleukin 6 (IL-6) gene for VEGFR2 constructs (**7.1.2.1**, **Figure 14B**) or the murine serotonin 5-hydroxytryptamine 3A (5-HT3A) signal sequence for adenosine receptor constructs (**7.1.1.1**, **Figure 14A**). Outside of the open reading frame, which encodes the tagged receptor, expression vectors encoded antibiotic resistance genes (**Figure 14**). These included resistance genes against antibiotics that kill non-resistant gram negative bacteria, such as kanamycin or ampicillin, allowing for selection to be used in bulking up the cDNA construct for use (**2.2.3.3**). An

additional antibiotic resistance gene was also present in all the plasmids, providing resistance to geneticin (G418) to allow selection to be used to create cell lines that express the recombinant tagged receptor (**Figure 14**).

## 2.2.3.2 Molecular Biology: Tagged Receptors

### 2.2.3.2.1 Rat NLuc-$A_{2A}$ and NLuc-$A_{2B}$ Receptors

Constructs were created and kindly donated for use by Dr Mark Soave (University of Nottingham). The creation of these constructs was described previously (Cooper et al., 2022). In brief, rat (*Rattus norvegicus*) $A_{2A}$ and $A_{2B}$ receptor cDNA was cloned into a pcDNA3.1 expression vector. N-terminal Nano luciferase (Nluc) labelled rat adenosine $A_{2A}$ and $A_{2B}$ receptor constructs were generated incorporating a 5-HT3A membrane localisation signal sequence in pcDNA3.1 (Soave et al., 2016).

### 2.2.3.2.2 Human NLuc-$A_{2A}$ and NLuc-$A_{2B}$ Receptors

Constructs were kindly donated for use by Dr Laura Kilpatrick (University of Nottingham). These constructs were created using the same technique as previously detailed (**2.2.3.2.1**). In brief, human $A_{2A}$ and $A_{2B}$ receptor cDNA was cloned into a pcDNA3.1 expression vector. N-terminal Nluc- labelled human adenosine $A_{2A}$ and $A_{2B}$ receptor constructs were generated incorporating a 5-HT3A membrane localisation signal sequence in pcDNA3.1 (**Figure 14**).

### 2.2.3.2.3 Human NLuc-VEGFR2

The construct was kindly donated for use by Dr Laura Kilpatrick (University of Nottingham). The creation of this construct was described previously (Kilpatrick et al., 2017). In brief, human VEGFR2 cDNA was cloned in a pF-sNnK CMV/neo expression vector. Full-length N-terminal NLuc- labelled human VEGFR2 receptor constructs were generated incorporating an IL-6 membrane localisation signal sequence in pF-sNnK CMV/neo plasmid cDNA (**Figure 14**) (Kilpatrick et al., 2017).

#### 2.2.3.2.4 Human HiBiT-VEGFR2

NanoLuc can be split into a major protein fragment (LgBiT; 156 amino acids) and a small receptor tag (HiBiT) (**7.1.2.1**) (Dixon et al., 2016). The HiBiT construct was kindly created and donated by Dr Chloe Peach (University of Nottingham). The creation of this construct was described previously (Peach et al., 2021). In brief, human VEGFR2 cDNA was cloned in a pF-sNnK CMV/neo expression vector. N-terminal HiBiT- labelled human VEGFR2 receptor constructs were generated incorporating an IL-6 membrane localisation signal sequence in pF-sNnK CMV/neo plasmid cDNA (**Figure 14**) (Peach et al., 2021).

#### 2.2.3.2.5 Fluorescent Tagged Receptors

Specific receptors were tagged while being expressed in HEK 293 cell lines using cell impermanent fluorophores with distinct excitation/emission spectrums; this was made possible due to specific enzyme moieties encoding the SNAP-Tag binding domain, which was genetically fused onto the N-terminus of the target receptors' DNA. Substrates to these enzymes are conjugated to a fluorophore, such as the green fluorescent dye AlexaFluor488, which has seen extensive use in adenosine receptor research (Kozma et al., 2013). Conjugated substrates impermeable to the membrane only bind to receptors successfully trafficked to the plasma membrane. SNAP-tag® is a 20 kDa modified version of the human DNA repair protein $O^6$-alkylguanine-DNA alkyltransferase, designed by New England Biolabs, which forms covalent bonds with a benzylguanine moiety found in its substrate (Keppler et al., 2003, Keppler et al., 2004).

#### 2.2.3.2.6 Human SNAP-$A_{2A}$ and SNAP-$A_{2B}$ Receptors

Constructs were kindly donated for use by Dr Mark Soave (University of Nottingham). These constructs were created using a similar technique as detailed previously (**2.2.3.2.1**). In brief, human $A_{2A}$ and $A_{2B}$ receptor cDNA was cloned into a pcDNA3.1 expression vector. N-terminal SNAP-tag labelled human adenosine $A_{2A}$ and $A_{2B}$ receptor constructs were generated incorporating a 5-HT3A membrane localisation signal sequence in pcDNA3.1.

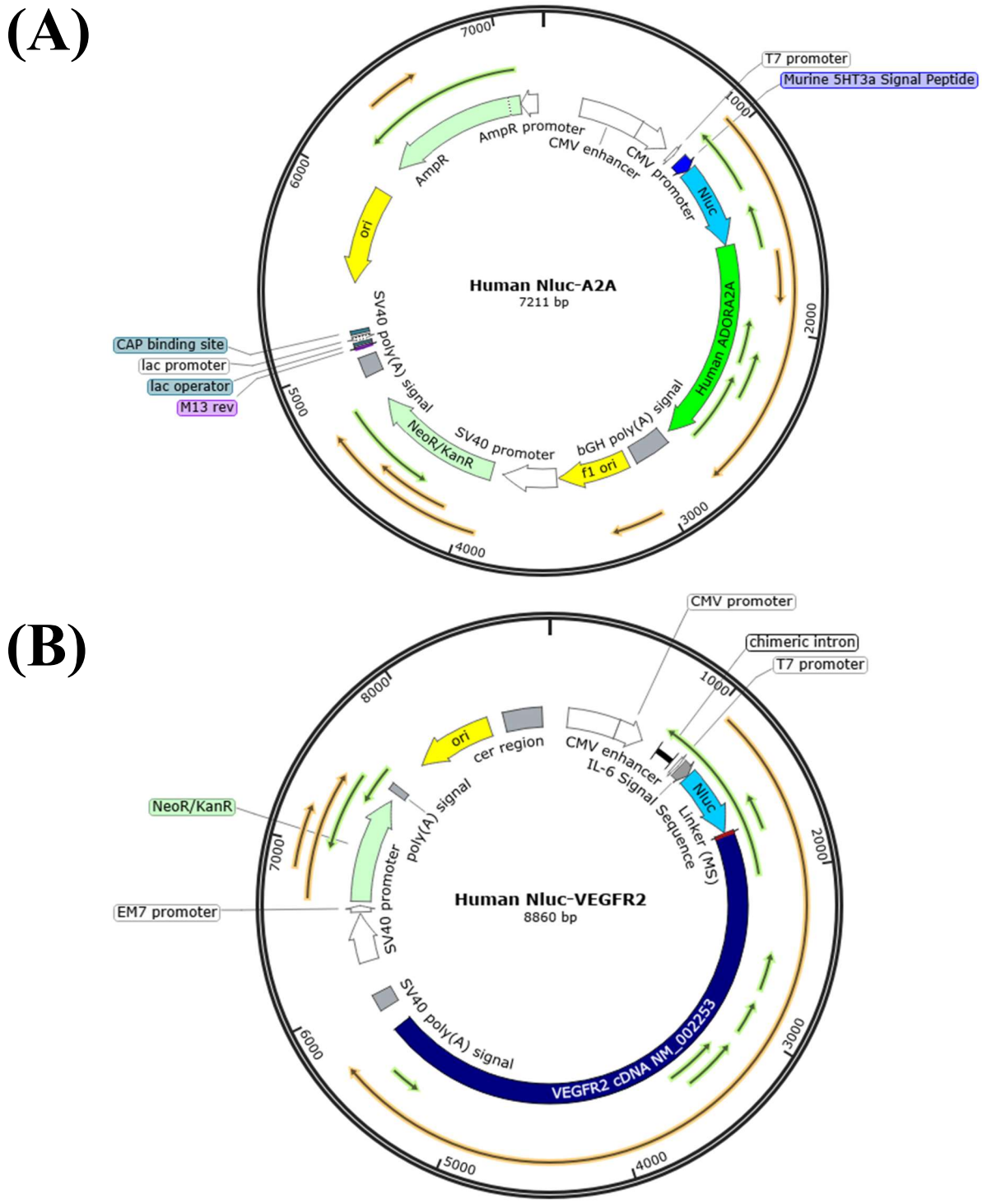


**Figure 14 Example Vector Maps of Nanoluciferase Tagged Receptors. A)** Human NLuc-$A_{2A}$ receptor **B)** Human NLuc-VEGFR2. Both receptors have the human cytomegalovirus (CMV) promoter, which enhances transcription, an SV40 polyadenylation sequence tail to protect the generated mRNA from degradation, and a Kozak consensus sequence motif to initiate translation of the plasmid cDNA. The export of the translated protein to the plasma membrane was enhanced using a signal sequence inserted just before the N-terminal tag on each receptor. This signal sequence was either derived from the interleukin 6 (IL-6) gene for VEGFR2 constructs **(A)** or the murine serotonin 5-hydroxytryptamine 3A (5-HT3A) signal sequence for adenosine receptor constructs **(B)**. *Figure created with SnapGene.*

### 2.2.3.3 Molecular Biology: DNA Amplification

Plasmid cDNA was bulked up for use in transfections from an initial plasmid cDNA sample by transformation into competent *Escherichia coli* (*E. coli*) cells. Sterile Luria Broth (Lennox) [LB (Lennox)] was created before the cDNA purification/amplification process using 20 g/L of powder containing tryptone (10 g/L), yeast extract (5 g/L) and sodium chloride (5 g/L) for optimal bacterial growth, dissolved in double distilled water (2% solution), and autoclaved. Additionally, before cDNA purification/amplification, Petri dishes (92x16 mm) were filled with 20 mL sterile LB broth with Agar (Lennox) which was created using 35 g/L of powder dissolved in double distilled water (3.5% solution), autoclaved, and then either 30 ng/mL kanamycin sulphate or 50 ng/mL ampicillin added. The antibiotic was added while the solution was still warm from the autoclaving process, and the plates poured before the agar completely cooled and solidified. Each plasmid was originally designed to encode an antibiotic resistance gene to either kanamycin or ampicillin. Therefore, Agar plates with kanamycin were used to amplify plasmids containing a kanamycin resistance gene, and ampicillin plates were used to amplify plasmids containing the ampicillin resistance gene.

For each plasmid, 25 µL Subcloning Efficiency DH5α competent *E. coli* cells, at the concentration provided by Thermo-Fisher Scientific, were transferred into sterile 0.5 mL Eppendorf tubes, one per transformation reaction. 1.0 µL of the construct template cDNA was added to the DH5α cells. Tubes were mixed by flicking and then left on ice for 30 minutes to enable the incorporation of the plasmid cDNA with the outer membrane of the bacteria. To facilitate the uptake of plasmid cDNA into the cytoplasm the bacteria were heat-shocked at 42°C for 30 seconds using a heat block before being cooled on ice for a further 2 min. Next, 250 µL LB Lennox was added to each Eppendorf tube, and cells incubated and shaken for 60 minutes at 37°C/225 rpm (SI600 Stuart Large Shaking Incubator, Cole-Parmer, UK) to start bacterial replication to increase the number of bacteria exponentially. After this initial incubation, 100 µL of this bacterial growth mixture was spread across an agar plate (pretreated with the appropriate antibiotic for the plasmid as described above) using a sterile plastic L-shaped spreader, before being incubated overnight at 37°C with the plates positioned upside down to prevent a buildup of condensation on the surface of the dish. Overnight, the bacteria susceptible to the antibiotic were either prevented from growing or killed. In contrast, the bacteria that had taken in the plasmid were resistant and replicated, forming bacterial colonies

on the dish, grown from a single resistant bacteria, making all of the bacteria in a colony genetic clones.

The following morning, a single colony was picked using a pipette tip to establish a starter culture. The pipette tip was placed in 5 mL LB broth containing the appropriate antibiotic (30 µg/mL kanamycin or 50 µg/mL ampicillin) and shaken in a temperature-controlled orbital shaker (Stuart SI600) at 37°C/225 rpm for 8 hours to stimulate bacterial growth. After the incubation, the starter cultures were transferred into a 500 mL conical flask containing 120 ml LB broth with the appropriate antibiotic (30 µg/mL kanamycin or 50 µg/mL ampicillin). These were further shaken overnight in a temperature-controlled orbital shaker at 37°C/225 rpm to stimulate logarithmic exponential bacterial growth to bulk up the number of plasmid copies. Bacteria that lost the plasmid were killed by the antibiotic, thus selecting for plasmid-growing bacteria.

The following morning, cDNA was extracted from the bacteria and purified using Promega's Pureyield™ Plasmid Maxiprep System. The bacterial contents of the conical flask incubated overnight were transferred to 250 mL plastic bottles and were pelleted by spinning at 4,000 *g* for 10 min at 4°C (Eppendorf Centrifuge 5810R). As per the Maxiprep instructions, the supernatant was discarded, and the pellet resuspended by vortexing in 12 mL Cell Resuspension Solution (50 mM Tris-HCl, 10 mM EDTA, 100µg/ml RNase A), followed by lysis of the bacterial cells by the addition of 12 mL Cell Lysis Solution (0.2 M NaOH, 1% sodium dodecyl sulfate-polyacrylamide (SDS)) and after a 3 minute incubation, neutralisation of the solution by 12 mL Neutralization Solution (4.09 M guanidine hydrochloride, 759 mM potassium acetate, 2.12 M glacial acetic acid).

The cell lysate was then transferred into bullet tube containers for centrifugation at 14,000 g for 20 minutes at room temperature in a superspeed centrifuge (Sigma 3K30). This step separated the plasmid cDNA into the supernatant layer, and the pellet was discarded. Using a vacuum pump manifold (Vac-Man, A7231; Promega Corporation, USA), the supernatant containing the plasmid cDNA was eluted through two sequential columns: the PureYield™ Clearing Column (on top) and Maxibinding column (below), with the cDNA adhering to the Maxibinding column.

The Clearing Column was removed before 5 mL isopropanol-based Endotoxin Removal Wash was added to the Maxi Binding Column. Further contaminants were removed by running 20 mL of ethanol-based Column Wash (60% ethanol, 60 mM potassium acetate, 8.3 mM Tris-HCl and 0.04 mM EDTA) through the column. The vacuum was applied for an additional 5 minutes to dry the binding column before the column was placed in a plastic elution chamber (Eluator™ Vacuum Elution Device) with a sterile 1.5 mL Eppendorf positioned beneath the column for collection of the cDNA. The elution chamber was placed onto the vacuum manifold, and the plasmid cDNA was eluted by running 1.0 mL Nuclease-Free Water through the vacuum. Approximately 700 µL of cDNA solution was recovered, at a concentration typically around 500 ng/µL, as measured using a spectrophotometer (**2.2.3.4**). cDNA samples were further aliquoted for future use into Eppendorf tubes and stored at -20°C.

### 2.2.3.4 Molecular Biology: DNA Quantification

The concentration of DNA in samples was quantified using a NanoDrop 2000 Spectrophotometer (Thermo Fisher Scientific). DNA absorbs light at 260 nm; the NanoDrop can estimate the DNA concentration of a 1.0 µL sample by measuring the absorbance at 260 nm, which allows an approximate quantification of the amount of DNA present (Cavaluzzi and Borer, 2004). Blank readings to calibrate the system were made using the buffer used in the cDNA extraction process, which for cDNA samples in this thesis made using the Maxiprep DNA amplification system was nuclease-free water (**2.2.3.3**).

Additionally, the purity of the sample was assessed using the ratio between readings at 260 nm and 280 nm, with ~1.8 being reported as pure DNA. Contaminants such as protein can cause lower 260 nm/280 nm ratios, whereas a ratio >2.0 suggests that RNA could be present in appreciable quantities (Koetsier and Cantor, 2019). The ratios between 260 nm and 230 nm absorption were also assessed, with ~2.2 reported as pure DNA. Low 260 nm/230 nm ratios can signify phenol or carbohydrate contamination, whereas overly high readings can be caused by an inappropriate buffer being used for the blank or dirt on the NanoDrop reading pedestal (Koetsier and Cantor, 2019).

## 2.2.4 *In Vitro* Methods: Experimental Preparations

### 2.2.4.1 Experimental Preparations: Transient Transfections

Plasmid cDNA can be transiently transfected into HEK 293 cell lines, subsequently transcribed into mRNA and translated, leading to expression in the cell of the proteins encoded within the plasmid. Unlike stable transfections in which the cDNA is incorporated into the genome and is thus permanent, transient transfections do not integrate the cDNA into the genome and are thus only suitable for single experimental replicates, with each 'n' number of the experiment requiring a new transient transfection of plasmid cDNA into a new passage of HEK 293 cells. Transient transfections into HEK 293 cell lines were performed using Promega's FuGENE® HD reagent to deliver the plasmid cDNA into the cytoplasm for replication.

HEK 293 cells were seeded into dishes or T25 flask 24 hours before transient transfection, as previously described (**2.2.2.5**). On the day of transfection, the plasmids to be translated were diluted to 0.020 µg/µL in Opti-MEM® reduced serum medium; the cDNA samples were then carefully mixed by shaking with FuGENE® HD at a reagent to cDNA ratio of 3 µL: of FuGENE per 1 µg of cDNA. Transfection solutions were incubated for 10 min at room temperature as per the manufacturers' instructions. An appropriate volume of transfection mixture containing 6.0 µg of the appropriate cDNA stock was added into 10 mL of cell culture media for transfection of a T25 or 11 mL of cell culture media for transfection of a corning TC dish. The media on the cells was aspirated off and replaced with the new transfection media. Alternatively, if no transfection was required for the experiment, and the native HEK cells were to be experimented on, the cell culture media on the cells was aspirated off and replaced with fresh cell culture media. Cells were then incubated for 24h at 37°C / 5% $CO_2$ before being seeded into 96-cell plates (**2.2.4.2**).

### 2.2.4.2 Experimental Preparations: Seeding of HEK 293 Cells into 96-well Plates

White 96-well plates were coated with polymers of D-lysine to encourage strong cell attachment to the bottom of the plate, thus allowing media to be removed multiple times during an assay without dislodging the cells. A polymer of D-lysine is a synthetic chain of positively charged amino acids that can interact with negatively charged ions found on the cell membrane, helping maintain cell adhesion to the plate surface via electrostatic interactions (Harnett et al., 2007).

Poly-D-lysine (PDL) hydrobromide was diluted with PBS to make 40 µL, 5 mg/mL aliquot stocks, which were stored at -20°C. On the day of use, a PDL aliquot was diluted in 20 mL PBS to a total concentration of 10 µg/mL before being filter sterilised using a sterile syringe filter (0.2 µm pores). 50 µL of the PDL mixture was pipetted into each well of a white 96-well plate and incubated at room temperature for 30 min to allow adherence to the bottom of each well. The PDL solution was then aspirated off, and each well rinsed with 100 µL PBS. The PBS solution was subsequently removed, and the plate stored at room temperature for up to one week before use.

HEK 293 cells were transfected as described previously (**2.2.4.1**). 24 h following transfection, the cells were washed, detached from the flask, resuspended, and centrifuged as described previously (**2.2.2.2**). The supernatant was discarded, and the cell pellet was resuspended in 10 mL cell culture media (DMEM/FBS, as previously described (**2.2.2.2**). The cell density of the sample was determined using the average cell count calculated with a haemocytometer (BRAND® counting chamber, BLAUBRAND® Neubauer improved, BR717805, Sigma-Aldrich, UK) averaged over two independent readings. Cells were diluted in a total of 10 mL culture medium at the required density, unique to each experiment, and seeded 100 µL per well into the PDL-coated 96-well plate at either 15,000 or 30,000 cells per well.

### 2.2.4.3 Experimental Preparations: HEPES Buffered Saline Solution (HBSS)

For all experiments, the cell culture media (**2.2.2.2**) was replaced with a colourless HEPES ((4-(2-hydroxyethyl)-1-piperazineethanesulfonic acid)) Buffered Saline Solution (HBSS), which does not interfere with experimental luminescence or fluorescence readings, no more than 2.5 h before the start of the experiment. This buffer provides cells with physiological levels of inorganic ions to maintain their osmotic balance and D-glucose to provide metabolic fuel. HEPES is a sulfonic acid zwitterionic buffer that does not require $CO_2$, in contrast to the $CO_2$-bicarbonate buffering system used in conjunction with DMEM (Wouters et al., 1996). This HBSS buffer consisted of 145 mM NaCl, 5.0 mM KCl, 1.3 mM $CaCl_2$, 1.0 mM $MgSO_4$, 10 mM HEPES, 2.0 mM sodium pyruvate, 1.5 mM $NaHCO_3$, and 10 mM D-glucose, made up in double-distilled water and pH adjusted with concentrated HCl or 3 M NaOH to 7.45.

A 10x stock of the HBSS solution without glucose was made, autoclaved, and stored at 4°C. On the day of the experiments, the 10x stock was diluted 10x in double distilled water, and the glucose added.

### 2.2.4.4 Experimental Preparations: Ligand Stocks

$10^{-2}$ M aliquots of the small molecule drugs used *in vitro* were created from powdered stocks using DMSO as the solvent, aliquoted into Eppendorf tubes, and stored at -20°C until use.

Recombinant human $VEGF_{165}$a was purchased from R&D systems as a lyophilised powder containing Bovine Serum Albumin (BSA) as a carrier. $10^{-9}$ M stocks of recombinant human VEGF-$A_{165}$a were created by resuspending the protein in PBS with 0.1% protease-free BSA (as per the manufacturer's instructions to prevent interactions with the plasticware), aliquoted into Eppendorf tubes, and stored at -20°C until use.

## 2.2.5 *In Vitro* Methods: Measuring Receptor-Ligand Binding Affinity

### 2.2.5.1 An Introduction to Förster Resonance Energy Transfer

Resonance Energy Transfer (RET) is a process in which the excess energy of an excited atom or molecule (the donor) is transferred to a different atom or molecule (the acceptor) via a non-radiative electronic transfer of energy (Cario and Franck, 1922, Jones and Bradshaw, 2019). In RET, the involved atoms or molecules' electrons remain bound to their receptive molecules' nuclei during the transfer process, moving between different electronic states within the molecules (Jones and Bradshaw, 2019). As the electron relaxes to a lower energy state in the donor, the excess energy is transported to the acceptor as a virtual photon facilitated by dipole-dipole couplings between the molecules (**Figure 15**) (Jones and Bradshaw, 2019). In the 1940s, Theodor Förster theoretically explained RET between a donor fluorophore and an acceptor fluorophore, which was subsequently named after him; Förster resonance energy transfer (FRET) (Förster, 1948, Sahoo, 2011).

*It is important to note that* Förster resonance energy transfer *is not exclusively between two fluorophores and describes the overall physical phenomena observed.* Förster resonance energy transfer *between two fluorophores is known as fluorescence resonance energy transfer. In the literature, the acronym FRET is commonly interchangeably used to describe both* Förster resonance energy transfer and *fluorescence resonance energy transfer, which can confuse. In this thesis,* Förster Resonance Energy Transfer is referred to as FRET, whereas *fluorescence resonance energy transfer is referred to as fluorescent donor FRET.*

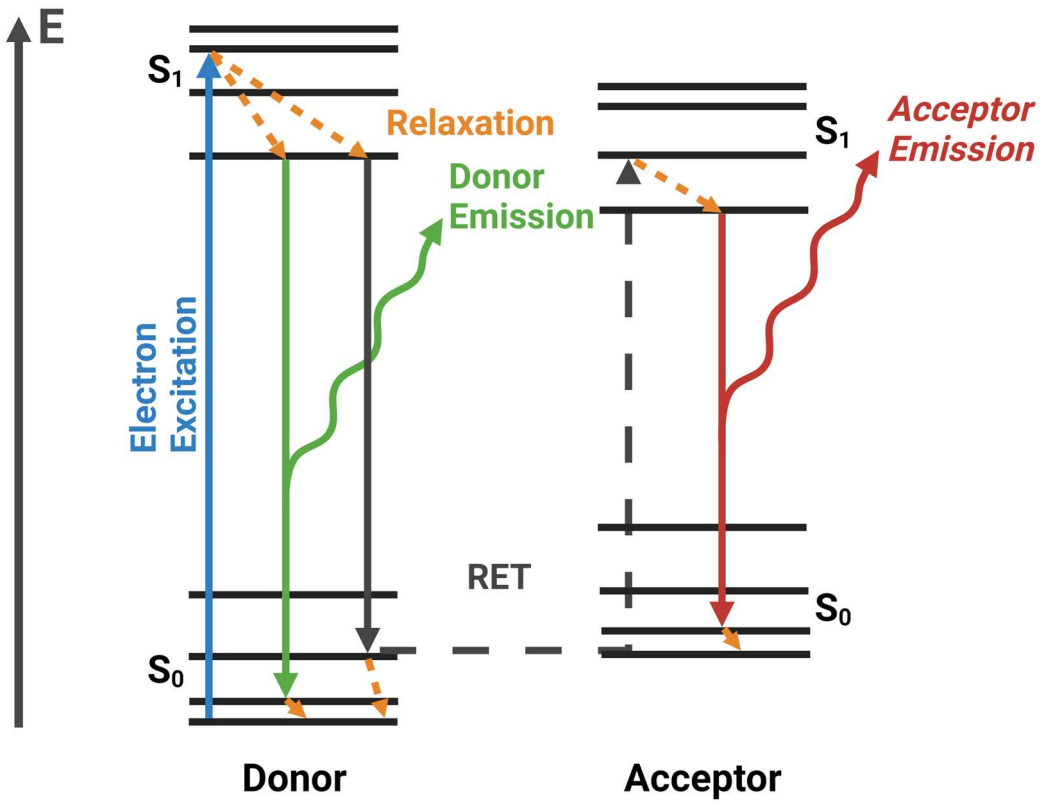


**Figure 15 Jabłoński Diagram Detailing Fluorescent Donor Förster Resonance Energy Transfer (FRET).** Excitation of an electron (blue), which in fluorescence is caused by absorption of a photon, causes an electron to move from its ground state ($S_0$) to a higher energy orbital ($S_1$). The electron relaxes quickly to the lowest possible excited sublevel of $S_1$ due to intramolecular non-radiative energy conversions such as internal conversion and vibrational relaxation (orange). After residing in $S_1$, the electron falls back down to $S_0$, and as a consequence, the excess energy is emitted as a photon (green) with a lower wavelength than the original excitation photon. During FRET, the energy released from the relaxation of an electronically excited donor (solid grey line) is coupled to a suitable acceptor fluorophore in close proximity, leading to the excitation of one of its electrons via the exchange of a virtual photon (dashed grey line), subsequently followed by fluorescent emission of a photon by the acceptor fluorophore.

#### 2.2.5.1.1 FRET Efficiency

The efficiency of FRET between donor and acceptor is the fraction of energy transfer events occurring per donor excitation event. FRET efficiency depends on two essential quantities of the donor/acceptor pair: the spectral overlap and intermolecular distance (Förster, 1946, Förster, 1948). The crossover of the donor's emission spectrum and the absorption spectrum of the acceptor allows the energy lost from the excited donor falling to the ground state to excite the acceptor fluorophore (**Figure 15**). Thus, the greater the overlap integral [J(λ)] of these spectra, the more potential a donor has to transfer energy to the acceptor fluorophore via FRET (**Figure 16A**). If there is no overlap between the donor emission and acceptor absorption, then FRET cannot occur. The efficiency of FRET transfer is inversely proportional to the sixth power ($R^6$) of the distance between the donor and the acceptor (Förster, 1948, Latt et al., 1965). Because of this critical restraint, FRET typically only occurs at any appreciable level when the donor and acceptor are within 10 nm of each other (**Figure 16B**) (Stryer and Haugland, 1967, Ayoub and Pfleger, 2010, Sahoo, 2011).

A third critical factor that allows FRET to occur is the orientation of the donor's emission transition dipole and the acceptor's absorption dipole. When these dipoles are parallel, maximum FRET can occur, but no FRET can occur when they are perpendicular (Khrenova et al., 2015). This factor has particular importance to FRET pairs where the donor and acceptor cannot freely rotate. For example, biologically formed protein fluorophores such as green fluorescent protein (GFP) and its variants are comprised of a stable β-can barrel structure that traps and protects the chromophore inside it but also prevents the fluorophore from rotating (Remington, 2011). This structural restriction has an important consequence for FRET-based biological assays using GFP-based fluorophore pairs because if they are fixed in the wrong orientation, FRET will not be observed between the pair, even if the other conditions for FRET are met (**Figure 16C**) (Khrenova et al., 2015).

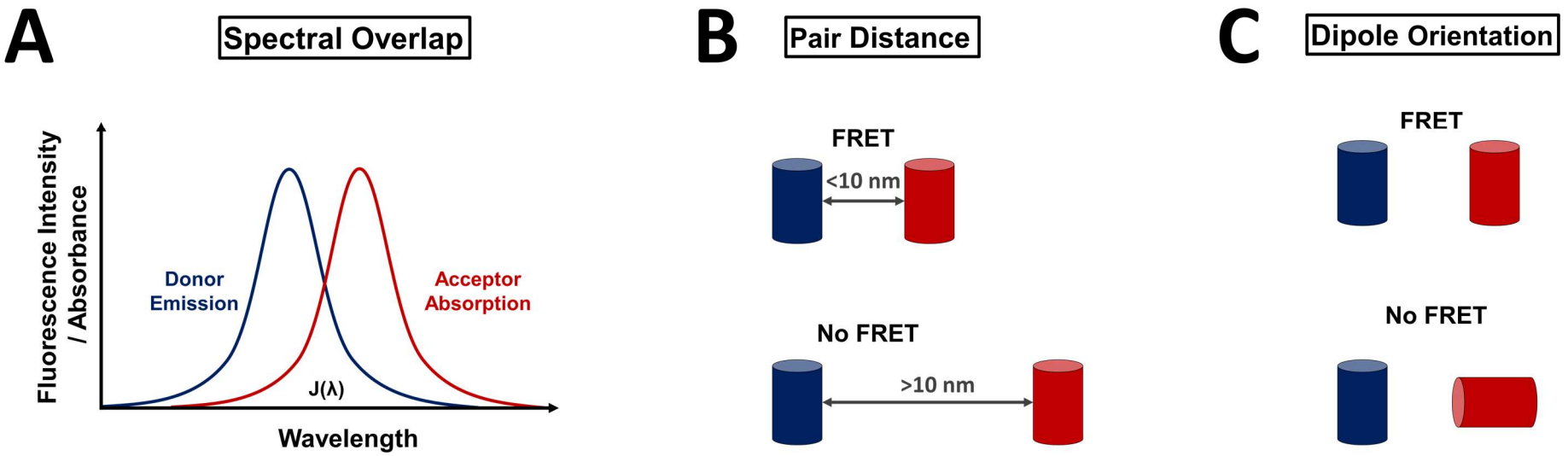


**Figure 16 Major Factors Influencing Förster Resonance Energy Transfer (FRET) Efficiency. A**) Graphical representation of spectral overlap [J(λ)] between donor emission spectra (blue) and acceptor absorption spectra (red) for a theoretical FRET pair. **B**) Graphical representation of the effect on FRET by the distance between donor and acceptor fluorophores. **C**) FRET depends on the orientation of the donor's emission transition dipole and the acceptor's absorption dipole.

#### 2.2.5.2 Bioluminescence Resonance Energy Transfer

Bioluminescence Resonance Energy Transfer (BRET) is a dipole-dipole non-radiative resonance energy transfer (a FRET) between a bioluminescent donor and a fluorescent acceptor. The difference between fluorescent donor FRET and BRET is the donor: in the case of fluorescent donor FRET, a fluorophore acts as a donor of energy, but in BRET, the donor is bioluminescent, meaning that the excitation of an electron from its ground state is driven by a chemical reaction instead of by photon absorption (**Figure 15**). Typically in BRET, the donor is an enzyme that gives off bioluminescent light after oxidation of a luminescent substrate. For the same reasons discussed previously (**2.2.5.1.1**), this non-radiative energy transfer only happens when the involved transfer donor/acceptor pair is in nanometre proximity, which means that this phenomenon will only be observed when the bioluminescent donor and the fluorescent acceptor are close by (Stryer and Haugland, 1967, Dacres et al., 2012).

#### 2.2.5.2.1 BRET Proximity Assays

The $R^6$ distance-dependence of RET means that the phenomenon is extremely sensitive to small changes in distance and, because of this, has been utilised as a 'spectroscopic ruler' to provide information on the proximity of donor and acceptor fluorophores (Stryer and Haugland, 1967, Ayoub and Pfleger, 2010, Sahoo, 2011). Fluorescent donor FRET-based biosensors have been utilised in the quantitative analysis of molecular dynamics in molecular biology, allowing the monitoring of protein-protein interactions, protein conformational changes, and cellular dynamics in real-time (Wiedenmann et al., 2009, Zadran et al., 2012). The first BRET biosensor was described in 1999 as an alternative method to fluorescent donor FRET to detect the interaction of cyanobacterial circadian clock proteins. (Xu et al., 1999, Ciruela, 2008).

Just as with fluorescent donor FRET, BRET proximity assays rely on the principle that if the luciferase donor and acceptor fluorophore are not nearby (>10 nm), no energy transfer occurs, and there is limited stimulated emission from the fluorophore. Alternatively, if the donor luciferase and acceptor fluorophore are nearby (<10 nm), BRET can occur, reducing the donor photon emission and resulting in light emission from the acceptor (Dacres et al., 2012). The distance at which BRET occurs is comparable with the size of most biological macromolecules and their interactions, such as engaging in complex formation or conformational changes (Drinovec et al., 2012). For example, the diameter of a transmembrane core of a GPCR is approximately 4-5 nm, based on the crystal structures of β receptors and rhodopsin, and the distance between rhodopsin monomers in a homodimer is approximately 4.5 nm (Palczewski et al., 2000, Mercier et al., 2002, Fotiadis et al., 2004).

Genetic tags comprising of a bioluminescent protein donor and a fluorescent acceptor can be fused to small molecules or proteins, with BRET effects indicating the proximity of the tagged proteins or small molecules. This technique can be utilised for a diverse range of applications to probe dynamic protein-protein interactions in living cells (Pfleger et al., 2006, Pfleger and Eidne, 2006, Stoddart et al., 2018a). BRET assays have been used to observe many biological functions, including ligand binding, intracellular signalling, receptor-receptor proximity, and intracellular receptor trafficking (Dale et al., 2019).

BRET-based assays do not require an external light source to excite the donor, so they involve low background radiation and do not suffer from common issues associated with FRET-based assays, such as autofluorescence, light scattering, or photobleaching (Dale et al., 2019). The observed BRET signal can be calculated by taking the observed acceptor emission over the observed donor emission. This BRET ratio is a ratiometric measurement independent of the amount of luminescence generated, which helps produce precise results in assays in which the bioluminescent protein expression or cell number may naturally fluctuate.

#### 2.2.5.2.2 Measuring Receptor-Ligand Binding Affinity Using BRET

Until recently, the characterisation of ligand-receptor binding has been investigated primarily by performing radioligand binding experiments (Zwier et al., 2010). Despite high sensitivity, using radiolabelled substances has serious drawbacks due to the complex management required to safely use radioactive sources (Zwier et al., 2010). New techniques based on fluorescence measurements are excellent alternatives to these traditional radioactive assays; these methods are less hazardous, exhibit good sensitivity, and are capable of having a low non-specific binding, which is often a drawback of using radiolabelled ligands (Cottet et al., 2011, Christiansen et al., 2016, Stoddart et al., 2018a). Novel techniques based on BRET have been applied to quantify fundamental aspects of ligand-receptor interactions such as binding kinetics, ligand affinity, and allosteric regulation (Stoddart et al., 2018a).

Assays utilising BRET have recently been developed based on fluorescently labelled ligands alongside receptors tagged with NLuc, a genetically engineered bioluminescent luciferase (**2.2.5.2.3**) (Hall et al., 2012, Stoddart et al., 2015, Stoddart et al., 2016). The utility of this newly developed technique, referred to as NanoBRET, has been demonstrated using a variety of fluorescent ligands for tagged GPCRs, including all four histamine receptors (Mocking et al., 2018, Stoddart et al., 2018b, Gratz et al., 2020), the $\beta_2$ adrenoceptor (Stoddart et al., 2015) and adenosine $A_1$, $A_{2A}$ and $A_3$ receptors (Stoddart et al., 2015, Comeo et al., 2019).

#### 2.2.5.2.3 Assessing Receptor Affinity Using NanoBRET

NLuc is a novel luciferase optimised from the blue-shifted luciferase OLuc, which was initially engineered from a luciferase isolated from the deep-sea shrimp *Oplophorus gracilirostris* (Inouye et al., 2000, Hall et al., 2012). NLuc produces bioluminescence far superior to the previous generation of luciferases derived from either the American firefly (FLuc, *Photinus pyralis*) or the sea pansy (RLuc, *Renilla reniformis*), with NLuc being significantly brighter and having the ability to produce a more sustained luminescent signal over-time (Hall et al., 2012). Additionally, NLuc is much smaller (19 kDa) than previous generations of luciferases (FLuc-61 kDa; RLuc-38 kDa), making it more suitable for use as an N-terminal receptor tag and less likely to affect ligand-receptor binding due to steric hindrance caused by the presence of the luciferase (Hall et al., 2012).

The substrate for NLuc is furimazine, an imidazopyrazinone that has been further engineered from coelenterazine, the original substrate utilised by *O. gracilirostris* (Hall et al., 2012). For NLuc, furimazine results in a luminescent signal ~30-fold brighter than coelenterazine (Hall et al., 2012). The greater brightness of NLuc allows the tag detection at low levels comparable to endogenous physiological protein expression (El Khamlichi et al., 2019, White et al., 2019).

NanoBRET receptor binding assays are BRET-based assays (**2.2.5.2**) utilising NLuc (Hall et al., 2012). NLuc is fused to the N-terminus of the receptor of interest (Stoddart et al., 2015). In the presence of furimazine, substrate oxidation occurs, which produces energy in the form of blue light (460 nm) (Hall et al., 2012). Therefore, the fluorescent ligand has the potential to fluoresce due to RET when binding a suitable fluorescent ligand to the tagged receptor, but only if specific criteria are met; this RET transfer can only occur when there is spectral overlap between the NLuc donor and the fluorescent ligand acceptor when the donor and fluorescent ligand are in the correct orientation, and when the ligand is close to the bioluminescent donor (<10 nm), which helps bolster the specificity of the technique (**2.2.5.1**, **Figure 15**, **Figure 16**, **Figure 17**) (Stoddart et al., 2015, Christiansen et al., 2016, Stoddart et al., 2018a).

.

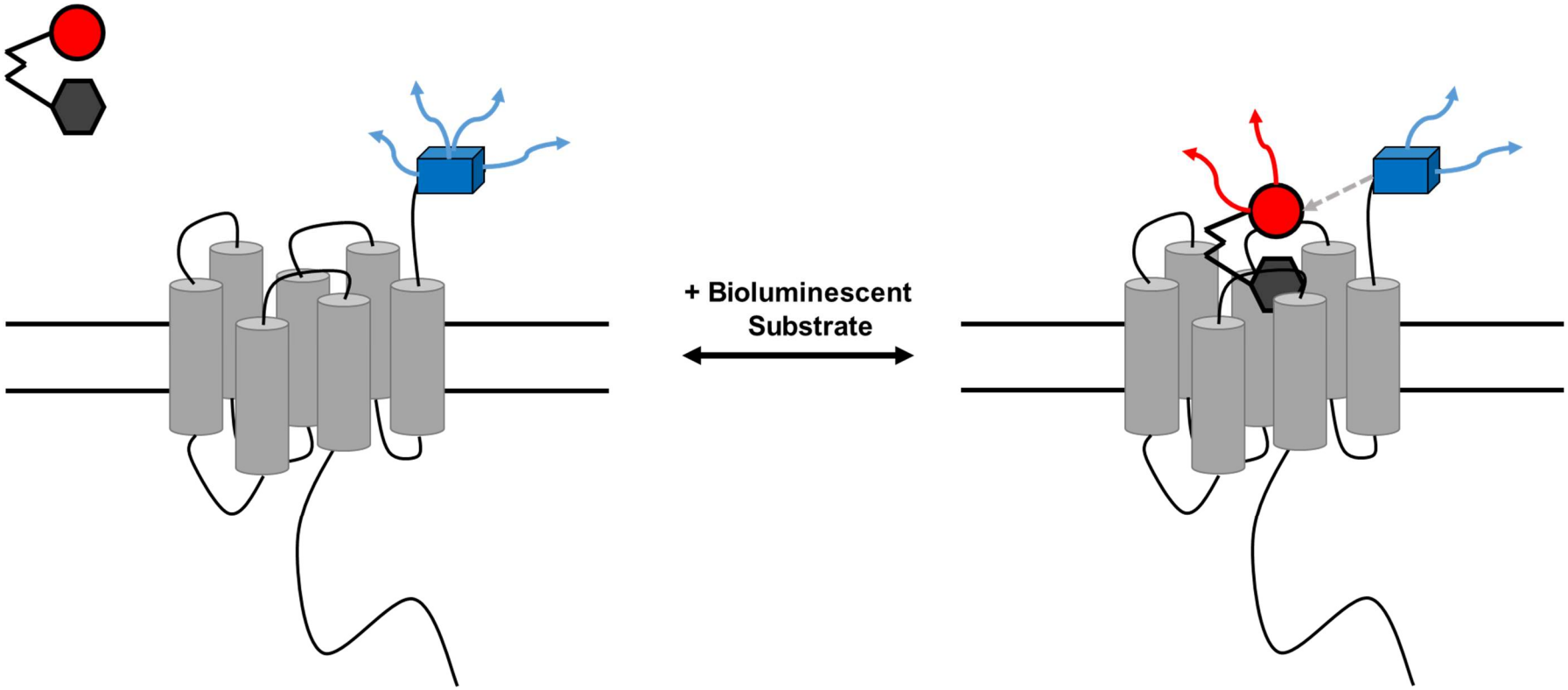


**Figure 17 Schematic Illustrating Bioluminescence Resonance Energy Transfer (BRET) Between a Bioluminescent-Tagged Receptor and Fluorescent Ligand.** The luciferase (*blue rectangular cuboid*) is fused to the N-terminus of the receptor of interest. In the presence of the luciferases' bioluminescent substrate, substrate oxidation occurs, which causes the generation of bioluminescent light. When exposed to a fluorescently labelled ligand to the target receptor (*red circle attached to a grey hexagon*), the ligand binds to the receptor, bringing it in close proximity to the luciferase tag. The close proximity of the bioluminescent donor and fluorescent ligand (<10 nm) facilitates the transfer of energy to excite the acceptor fluorophore via BRET transfer.

#### 2.2.5.2.4 NanoBRET Ligand Binding Experiments

To characterise the binding of a fluorescently labelled ligand to an N-terminal NLuc receptor of interest saturation-binding experiments were employed using increasing concentrations of the labelled ligand (**2.2.5.2.3**, **Figure 17**) in the presence or absence of a high concentration of an unlabelled competitor ligand. The presence of a high concentration of an unlabelled competitor produces a functionally insurmountable blockade of the receptor's active site, which allows the calculation of non-specific binding of a given concentration of the fluorescently labelled ligand to the receptor. The non-specific binding component can then be accounted for to allow the calculation of a labelled ligand's specific binding affinity for the receptor active site (Stoddart et al., 2015, Christiansen et al., 2016, Stoddart et al., 2018a).

The ability to measure the binding affinity of a fluorescent ligand to a receptor via BRET allows the affinity of unlabelled compounds to be calculated via the displacement of a known concentration of the fluorescent ligand in competition binding experiments. This approach, used for the experiments detailed in this thesis, has been successfully applied to measure the affinity of a variety of unlabelled ligands at a range of different receptors, with the $pK_i$ (-log dissociation constant) values obtained for unlabelled ligands being comparable to those obtained using radiolabelled assays (Stoddart et al., 2015, Christiansen et al., 2016, Soave et al., 2016, Hansen et al., 2017).

#### 2.2.5.2.5 Fluorescent Ligands for Adenosine Receptor NanoBRET Experiments

A variety of selective and non-selective fluorescent ligands have been designed to target adenosine receptors, and experiments involving nanoBRET ligand binding assays on $A_1$, $A_{2A}$ and $A_3$ receptors have been published (Kecskés et al., 2010, Vernall et al., 2012, Stoddart et al., 2015, Comeo et al., 2019).

Xanthine-based antagonists have been functionalised as fluorescent ligands and are generally not selective between the adenosine receptor subtypes (Briddon et al., 2004, Baker et al., 2010). The fluorescent ligand used during the experiments detailed in this thesis is CA200645, which is structurally based on the non-specific adenosine receptor antagonist xanthine amine congener (XAC), connected to the

BY630 fluorophore via a polyamide linker (β-alanine, β-alanine) (**Figure 18**) (Stoddart et al., 2012, Bouzo-Lorenzo et al., 2019). CA200645 has an excitation peak of 630 nm, an emission peak of 650 nm, and has previously been demonstrated to be a good BRET partner for NLuc (Stoddart et al., 2015).

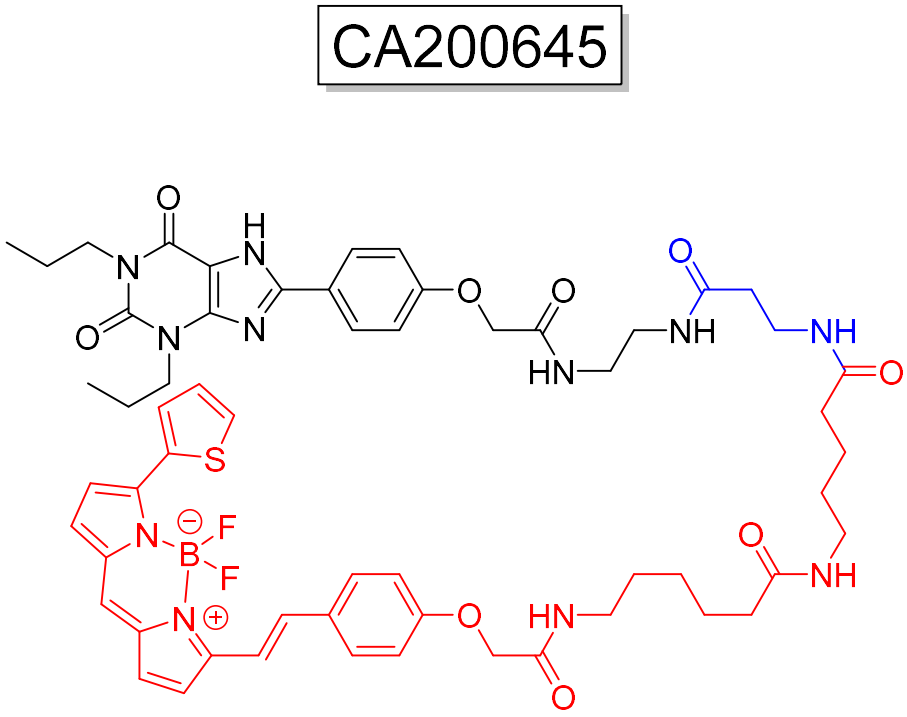


**Figure 18 Chemical Structure of CA200645.** CA200645 is comprised of xanthine amine congener (XAC) (**black**) fused to the fluorophore BY630 (red) via a polyamide linker unit (blue). *Structure as published in (Stoddart et al., 2012).*

## 2.2.5.3 Methodology: NanoBRET Ligand-Binding Assays

### 2.2.5.3.1 NanoBRET Ligand Binding Assays: Experimental Technique

Fluorescent antagonist saturation and competition-binding assays were performed on HEK 293T cells transiently transfected to express NLuc tagged rat receptors (**2.2.3.2.1**) and plated into white 96 well plates, as previously described (**2.2.4.1**, **2.2.4.2**). 24 h after the seeding into the 96-well plates, the cell media was aspirated off and replaced with 100 µL HBSS (**2.2.4.3**) supplemented with 0.1% BSA, and the required concentrations of fluorescent ligand (CA200645) (**2.2.5.2.5, Figure 18**) and competing ligands for the experiment. For saturation binding assays, concentrations of 0–500 nM of CA200645 were used in the presence or absence of a receptor-selective antagonist (for rat $A_{2A}$ receptor: 10 µM of SCH 58261 and rat $A_{2B}$ receptor: 10 µM of PSB 603). For competition binding assays, 50 nM of CA200645 was used in the presence of increasing concentrations of up to $10^{-4}$ M of unlabelled ligand. The concentration of 50 nM ($10^{-7.3}$ M) CA200645 was selected for these experiments because it was in the region of the calculated $pK_D$ for CA200645 for both of the rat receptors studied in this thesis (**Table 15**, **3.3.2.1.1**); allowing adequate receptor-CA200645 binding to produce a clear BRET signal, whilst also allowing relatively easy displacement of the fluorescent ligand by the competitor ligand to remove the BRET signal on competitor-receptor binding. The DMSO concentration in all experimental wells was equalised to a final in-well concentration of 1%. The cells were then incubated for 2 h at 37°C. Next, furimazine (Promega) (**2.2.5.2.3**) was added to each well to give a final in-well concentration of 10 µM. Finally, the cells were incubated for 5 min at 37°C. A PHERAstar FS plate reader (BMG Labtech) was used to measure the resulting BRET using filtered light emissions at 460 nm (80 nm bandpass) and >610 nm (longpass) at 37°C. The ratio between >610 nm emission and 460 nm emission provided the raw BRET data for each experiment.

#### 2.2.5.3.2 NanoBRET Ligand Binding Assays: Data Analysis

Data were recorded on Mars PHERAstar software (version 3.32), collected in Microsoft Excel 2016 (Microsoft Corporation, USA), and analysis and calculations performed using GraphPad Prism (Version 9.2.0, San Diego, CA, USA) to quantify data and generate graphs. Each 'n' number represents a single independent experiment completed with a unique cell line passage. ‘n’ separate experiments were completed, with each experimental condition carried out with triplicate well repeats. All results shown are the average mean of the constituent 'n' numbers for each experiment. All graphs are expressed with error bars representing ± the Standard Error of the Mean (SEM).

A value of $p<0.05$ was considered statistically significant. Therefore, if a value of $p<0.05$ was achieved, it is denoted by a single symbol specific to the statistical test conducted.

**Calculating the Equilibrium Dissociation Constant ($K_D$) of a Fluorescent Ligand to an NLuc Tagged Receptor**

The following equation was used to simultaneously obtain the total and non-specific binding components of nanoBRET saturation curves. $B_{max}$ is the maximum level of specific binding of the fluorescent ligand. [B] is the concentration of the fluorescent ligand. $K_D$ is the equilibrium dissociation constant. M is the linear slope of the non-specific binding component. C is the y-axis intercept of the linear non-specific binding component.

$$BRET\ ratio = \frac{B_{max} \times [B]}{[B] + K_D} + \big((M \times [B]) + C\big)$$

### Calculating the $IC_{50}$ and $K_i$ of Non-labeled Ligands at a Nanoluciferase Tagged Receptor

The half-maximal inhibitory concentration of a non-labelled ligand competing against a fixed concentration of fluorescent ligand was calculated using competition-binding curves fitted to the following equation. [A] is the concentration of the competing drug. $IC_{50}$ is the concentration (M) of ligand required for 50% inhibition of the specific binding of concentration [L] of the fluorescent ligand.

$$\%\ inhibition\ of\ specific\ binding = \frac{100\ \times [A]}{[A] + IC_{50}}$$

The $IC_{50}$ values calculated from the competition-binding curves were then used to determine the inhibitory binding affinity ($K_i$) of the unlabeled ligands using the Cheng–Prusoff equation. [L] is the concentration of the fluorescent ligand mentioned previously. $K_D$ is the equilibrium dissociation constant of the fluorescent ligand at the receptor calculated from the saturation binding experiments detailed above.

$$K_i = \frac{IC_{50}}{1 + \frac{[L]}{K_D}}$$

### 2.2.6 *In Vitro* Methods: BRET Saturation Assays

The use of saturation assays to provide evidence for protein-protein interactions was originally put forward by Mercier *et al.* (Mercier et al., 2002). BRET technology has been utilised as a powerful method to study the formation of receptor complexes of both GPCRs, RTKs and even receptor-receptor interaction between the two (Borroto-Escuela et al., 2013, Kilpatrick et al., 2019).

BRET saturation assays can be utilised to give a measure receptor-receptor proximity (**2.2.5.2.1**, **Figure 19**). To perform this technique, one receptor is fused with the luciferase donor (in this thesis, NLuc), and the other receptor is fused with a fluorescent tag (in this thesis, a SNAP-tag). In this thesis, a cell line is transiently transfected with a constant amount of cDNA per well encoding the luciferase-tagged receptor, while the amount of cDNA of the fluorescently tagged protein is varied across the plate from none up to an amount far exceeding the amount of cDNA encoding the luciferase to produce transfections across the plate with increasing acceptor-to-donor ratios.

Theoretically, in a scenario where the amount of transfected donor is held constant while the amount of acceptor is linearly increasing, if there is a specific receptor-receptor interaction, the BRET ratio signal will increase in a hyperbolic manner, before reaching an asymptote plateau, representing a complete saturation of all donors with acceptor molecules (**Figure 20**). By contrast, in a situation where there is no specific receptor-receptor interaction, then only a small non-specific signal (bystander BRET) will result from the receptors randomly being in close proximity, and the signal will increase approximately linearly with increasing amounts of the acceptor (**Figure 20**) (Marullo and Bouvier, 2007).

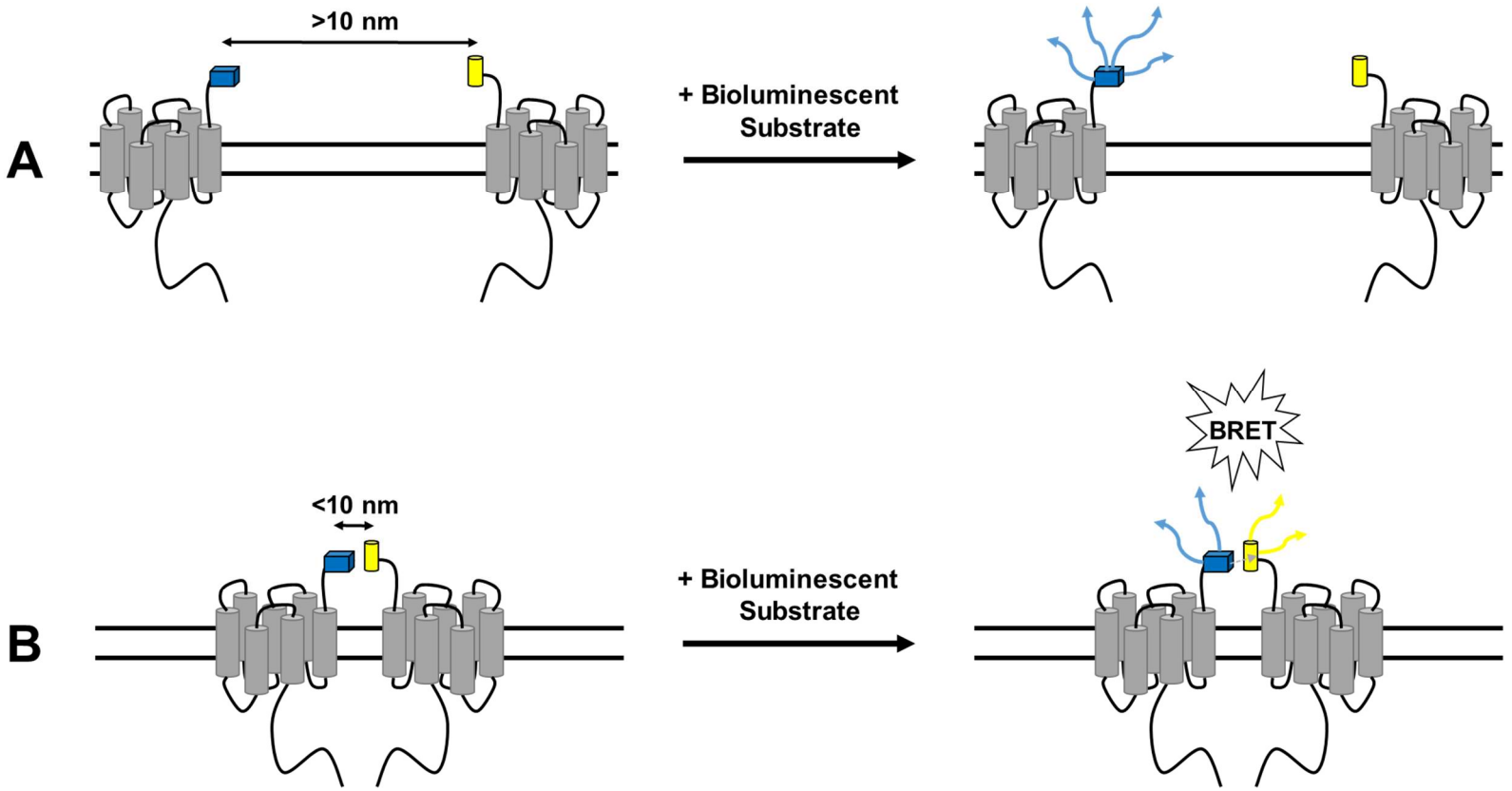


**Figure 19 Schematic Illustrating the Principles of Utilising Bioluminescence Resonance Energy Transfer (BRET) to Detect Receptor Colocalisation. A)** If there is no receptor-receptor colocalisation between bioluminescent (blue rectangular cuboid) and fluorescent-tagged (yellow cylinder) proteins, and the BRET pair tags are apart (>10 nm), then BRET will not occur between the tags in the presence of the bioluminescent protein's substrate. **B)** If there is receptor-receptor colocalisation between bioluminescent and fluorescent-tagged proteins with the BRET pair tags in close proximity (<10 nm), and if all the other physical requirements for BRET are fulfilled (**2.2.5.1**), then BRET will occur between the tags in the presence of the bioluminescent protein's substrate.

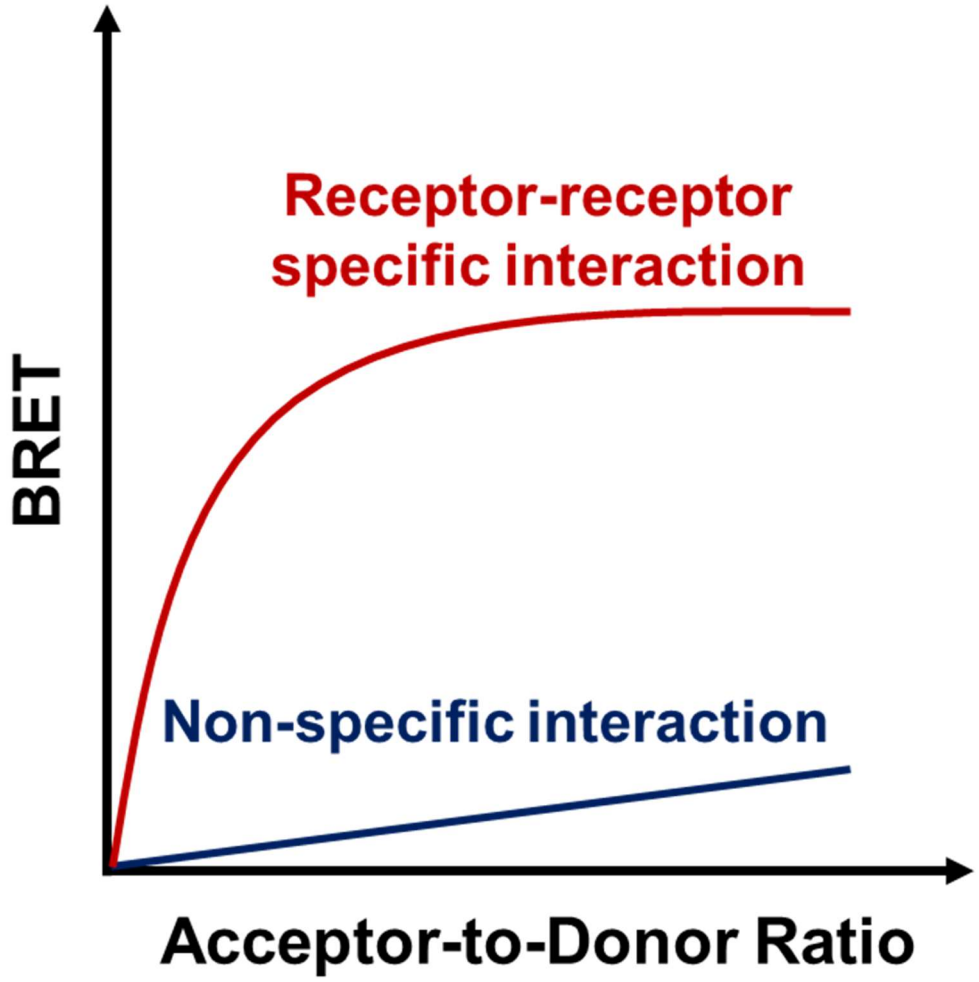


**Figure 20 Representative Graph Illustrating the Principles of Utilising Bioluminescence Resonance Energy Transfer (BRET) Saturation Assays to Detect Receptor-Receptor Colocalisation.** Theoretically, in a saturation assay where there is a constant expression of luciferase-tagged donor receptors, and an increasing expression of fluorescently-tagged acceptor receptors, as the expression of fluorescently-tagged receptors increases: if there is a specific interaction, then BRET (acceptor emission/donor emission) will increase in a hyperbolic manner, but reach an asymptotic plateau, representing a saturation of all donor receptors with acceptor receptors. If there is no interaction, then, by contrast, only a small signal will be detected, increasing approximately linearly with increasing amounts of the acceptor due to bystander BRET.

#### 2.2.6.1 BRET Saturation Assays: Exploring Receptor Colocalisations with NanoBRET Saturation Assays

##### 2.2.6.1.1 NanoBRET Saturation Assays: Experimental Technique

HEK 293T cells were seeded onto poly-D-lysine coated flat bottom white 96-well plates at a density of 15,000 cells/well, and incubated for 16h at 37°C/5% $CO_2$. 16 h after seeding, the cells were transiently cotransfected with an NLuc N-terminal tagged receptor (10 ng/well), alongside increasing concentrations of an N-terminal tagged SNAP-Tag labelled receptor (0-40 ng/well using FuGENE HD (Promega) in Opti-MEM (Promega) at a 3:1 ratio between reagent to cDNA. Additionally, empty p3.1zeo vector was added (0-40 ng/well) to ensure total cDNA concentrations were consistent across wells (50 ng/well).

After transfection, cells grew for a further 24 h at 37°C/5% $CO_2$. On the assay day, cells were incubated for 30 min at 37°C/5% $CO_2$ with 0.2 µM SNAP-Tag Alexa Fluor 488 (New England Biolabs) membrane-impermeable substrate, prepared in serum-free DMEM. After incubation, cells were washed three times with HBSS supplemented with 0.1% BSA, which also served as the experiment's incubation medium. Furimazine was added to each well to a final in-well concentration of 10 µM, and the cells incubated for an additional 5 min at room temperature. The plates were read at room temperature using a PHERAstar FS plate reader. Sequential luminescence and fluorescence emission measurements were taken utilising the BRET 1 plus optic module, measuring filtered light emissions at 475 nm (30 nm bandpass) and 535 nm (30 nm bandpass). The experimental results were represented by raw BRET values, which were calculated by taking the ratio of the 535 nm fluorescence emission (acceptor) over the luminescence 475 nm emission (donor).

#### 2.2.6.1.2 NanoBRET Saturation Assays: Data Analysis

A line of best fit was fitted to a non-linear regression- one site total binding equation. In addition, a one-way analysis of variance (ANOVA) was conducted for all experiments to determine whether there was a significant change with increasing doses of transfected SNAP-receptor, with the significance highlighted for each experiment on each graph.

## 2.2.7 *In Vitro* Methods: Dynamic Detection of Cellular cAMP

### 2.2.7.1 Dynamic Detection of Cellular cAMP: Background

#### 2.2.7.1.1 cAMP Signalling and Detection Techniques

Earl W. Sutherland discovered cAMP in 1958; it was the first, second messenger to be identified (Sutherland and Rall, 1958, Kresge et al., 2005). Intracellular levels of cAMP are regulated by two enzymes, AC, which generates it, and cyclic nucleotide phosphodiesterases (PDEs), which break it down (Sassone-Corsi, 2012). cAMP is an important intracellular second messenger in GPCR signal transduction. Agonist activation of GPCRs that couple to $G_{\alpha s}$ leads to increased intracellular cAMP levels, as the α subunit of the $G_s$ protein binds to and activates AC (Sassone-Corsi, 2012). On the other hand, agonist activation of GPCRs that couple to the $G_{\alpha i}$ protein leads to reduced intracellular cAMP production as the α subunit of the $G_i$ protein binds to and deactivates AC (Sassone-Corsi, 2012).

Historically, one of the most widely used techniques to measure cAMP levels involved radioimmunoassays based upon competition of the cyclic nucleotide with radiolabelled cAMP derivatives for binding sites on specific antibodies (Steiner et al., 1972). More modern immunological techniques have emerged based on the use of antibodies that specifically recognise both intracellular cAMP and a non-radiolabelled cAMP conjugate detected by various techniques, including enzymatic reactions or FRET (Tardieu, 2008, Wang et al., 2017). A drawback to these biochemical assays is that they typically require cAMP liberation from the cells via lysis, so they only provide a single snapshot measurement of cellular cAMP concentrations (Hill et al., 2010, Paramonov et al., 2015).

More recently, direct biosensors have been developed that detect cAMP by the presence of a native or modified cyclic nucleotide-binding domain (CNBD) incorporated into their structure (Willoughby and Cooper, 2007). Typically, these direct biosensors are conformationally flexible multi-domain proteins that undergo a structural change once a cAMP molecule binds to the CNBD, which is associated with a change in the signalling intensity of the sensor, which gives a readout of the concentration of cAMP (Paramonov et al., 2015).

#### 2.2.7.1.2 The GloSensor™ cAMP Assay

In this thesis, experiments measuring dynamic cellular cAMP levels were conducted using Promega's live-cell bioluminescent based GloSensor™ assay. This assay can monitor the activation of endogenous or overexpressed $G_s$- or $G_i$-coupled GPCRs, which act via AC to increase or decrease cellular cAMP production (Promega, 2019).

The assay employs a genetically encoded reversible biosensor, comprised of a semi-split luciferase, based on a mutant of firefly luciferase (*Photinus pyralis*) fused to a cAMP sensor which is comprised of the cAMP-binding domain B from the PKA regulatory subunit type IIβ (Fan et al., 2008). When the cAMP sensor binds cAMP, a conformational change in the protein encourages the split luciferase to reassemble and become functional, and if in the presence of its luciferase substrate, GloSensor™ cAMP Reagent, it generates bioluminescent light (**Figure 21**) (Wang et al., 2017). When expressed in HEK 293 cells, the biosensor is also reported to be able to mediate a 25-fold increase from baseline in the luminescent signal on the addition of 10 mM forskolin, a direct activator of AC, within 3.5 min (Fan et al., 2008).

Promega has produced two variants of the biosensor, encoded in plasmids that can be transfected into cell lines. The sequence for each variant differs, giving biosensors with differing affinities for cAMP. For the experiments in this thesis, a HEK 293G line was acquired from Promega, stability expressing the pGloSensor™-20F (lower affinity) cAMP plasmid, which performs better than the pGloSensor™-22F (higher affinity) variant in HEK 293 cells at 37°C (Promega, 2010).

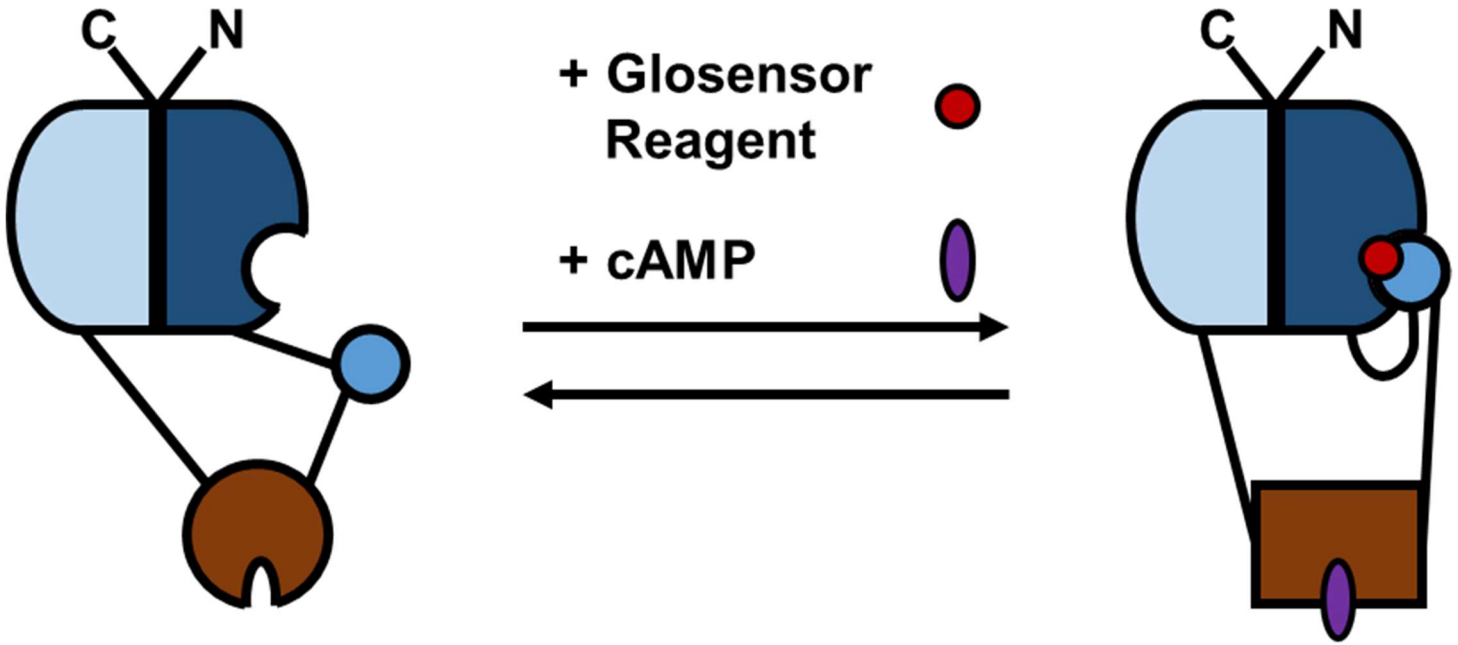


**Figure 21 Schematic of the GloSensor™ Cyclic Adenosine Monophosphate (cAMP) Assay (Promega).** The cAMP sensor is made from a mutant split of firefly luciferase (*Photinus pyralis*) (blue) fused to a cAMP sensor which contains the cAMP-binding domain B from the protein kinase A regulatory subunit type IIβ (brown). In the presence of cAMP (purple), a conformational change occurs, allowing the split luciferase to reassemble, become functional, and if in the presence of its luciferase substrate (Glosensor™ cAMP reagent) (red), generate bioluminescent light.

## 2.2.7.2 Dynamic Detection of cAMP: Sensing Cellular cAMP with the GloSensor™ Assay

### 2.2.7.2.1 GloSensor™ Experimental Technique

GloSensor assays were performed on native HEK 293G cells (**2.2.7.1.2**), or HEK 293G cells transiently transfected to express NLuc (**2.2.3.2.1**) tagged receptors and plated into white 96 cell plates, as previously described (**2.2.4.1**, **2.2.4.2**). 24 h after the seeding into the 96-well plate, the cell media was aspirated off, a BackSeal plate back was attached to the plate, and cells incubated in 50 µL HBSS (**2.2.4.3**) supplemented with 0.1% BSA and 3% GloSensor cAMP reagent (Promega) for 2 h at 37°C. After a baseline read, luminescence was measured on the PHERAstar FS plate reader (BMG Labtech) continuously over 60 min, averaging 1 read per well every 1.0 min, following the addition of 50 µL HBSS in the presence or absence of a ligand in isolation or in combination with another ligand, with the DMSO concentration in all wells equalised to a final in-well DMSO concentration of 1%. For some experiments, antagonists were added to some wells 2 h prior to the other ligands during the addition of the Glosensor cAMP reagent. Where this was the case, the wells were equalised at this stage to a final in-well DMSO concentration matching the DMSO concentration in the wells containing the antagonists. Data analysis for these experiments was completed as was previously described for nanoBRET ligand binding experiments (**2.2.5.3.2**).

# 3 Chapter 3: Haemodynamic Responses to Adenosine $A_2$ Receptor Agonism and Antagonism

# 3.1 Haemodynamic Responses to Adenosine $A_2$ Receptor Agonism: Chapter Introduction

Adenosine is a nucleoside present in all cells that plays a protective and regenerative role in the heart and vasculature (**1.1**) (Fredholm et al., 2011, Borea et al., 2018, Jacobson et al., 2019). The adenosine $A_{2A}$ and $A_{2B}$ receptors are two of four identified adenosine receptor subtypes (**1.1.2**) (Fredholm et al., 2011). $A_{2A}$ and $A_{2B}$ receptors both couple to stimulatory $G_s$ proteins and cause activation of adenylyl cyclase that generates cAMP leading to its intracellular accumulation (**1.1.3**) (Fredholm et al., 2011, Borea et al., 2018).

The $A_{2A}$ receptor has a high sensitivity to adenosine and is widely distributed in the central nervous system, heart, lung, and vasculature, with additional expression across cells of the immune system (**1.1.4**) (Headrick et al., 2013, Borea et al., 2018). The $A_{2B}$ receptor has a lower affinity for adenosine than the $A_{2A}$ receptor and is ubiquitously distributed across the body (Borea et al., 2018). Specifically, in the cardiovascular system, high levels of $A_{2B}$ expression are found throughout the vasculature, both in smooth muscle and endothelial cells, with the $A_{2B}$ receptor demonstrated to be extensively distributed throughout the vasculature of most organs, including the heart, lung, brain, kidney and large intestine (Dixon et al., 1996, Yang et al., 2006, St Hilaire et al., 2008, Maas et al., 2010, Teng et al., 2013).

$A_{2A}$ and $A_{2B}$ receptors are known to be involved in blood pressure regulation by mediating pulmonary and systemic vasodilation (**1.1.5**) (Sheth et al., 2014, Alencar et al., 2017, Bahreyni et al., 2019, Paganelli et al., 2021). Furthermore, in the kidney, activation of $A_{2A}$ and $A_{2B}$ receptors in response to hypoxic or ischaemic stress has been shown to have a role in preventing kidney necrosis by promoting perfusion of renal vascular beds (Yap and Lee, 2012, Borea et al., 2018). As a result of these physiological roles, $A_2$ receptors have been suggested to be potential targets for treating hypertension, as well as potentially helping in an assortment of cardiovascular and renal pathological conditions (**1.1.6**) (Jacobson and Gao, 2006, Jamwal et al., 2019).

In the literature, systemic administration of non-selective adenosine $A_2$ receptor agonists has been shown in rodents to produce hypotension, which is believed to be a result of peripheral vasodilatations induced by $A_{2A}$ and $A_{2B}$ receptor activation,

and additionally due to an $A_2$ receptor mediated increase in renal blood flow and consequential natriuresis, that results in a reduction in blood volume (Evoniuk et al., 1987, Mathôt et al., 1995, Lai et al., 2006, Feng and Navar, 2010). Individually, the $A_{2A}$ receptor has been demonstrated to induce hypotension and a marked increase in HR that is thought to be caused by an increase in sympathetic nervous activity in the rat, associated with an increase in catecholamine stimulation of β adrenoceptors on the heart (Alberti et al., 1997, Dhalla et al., 2006). However, less is known about the contribution of the $A_{2B}$ receptor, although it has been shown to cause vasodilation in *ex vivo* models (Feng and Navar, 2010, Sanjani et al., 2011) and hypotension in anaesthetised rats, associated with no change in HR (Maas et al., 2010).

Previously, in conscious rats, it has been shown that adenosine can cause vasodilation in the renal, mesenteric and hindquarters vascular beds that are not mediated by adenosine $A_1$ receptors and are thus likely to be caused by $A_2$ receptor activation (Cooper et al., 2020). However, the relative extent to which each of the $A_2$ receptors contributes to the vasodilatory effects observed in these vascular beds due to adenosine administration has not yet been investigated.

In the following chapter, to elucidate the cardiovascular effects of $A_{2A}$ and $A_{2B}$ receptors, the haemodynamic effects of adenosine and selective $A_{2A}$ (CGS 21680) and $A_{2B}$ (BAY 60-6583) receptor agonists (Hinz et al., 2014, Goulding et al., 2018) were investigated in the presence or absence of $A_{2A}$ and $A_{2B}$ receptor antagonists, in conscious, freely moving rats. The VC in three different vascular beds (renal, mesenteric and hindquarters) was simultaneously calculated alongside blood pressure and HR to provide systemic haemodynamic measurements and information on changes in the regional vascular beds induced by these ligands.

To complement these experiments, *in vitro* nanoBRET competition binding assays (**2.2.5.3**) were completed using the fluorescent ligand CA200645 (**Figure 18**) to confirm the selectivity of the ligands used *in vivo* to rat NLuc-tagged $A_{2A}$ or $A_{2B}$ receptors (**2.2.5.2.4**) (Stoddart et al., 2012, Bouzo-Lorenzo et al., 2019). Following the results of the ligand binding assays, cAMP Glosensor assays were conducted to assess the ability of the agonists used to produce a cAMP accumulation response *in vitro* (**2.1.7**).

# 3.2 Haemodynamic Responses to Adenosine $A_2$ Receptor Agonism: Chapter Methodology

## 3.2.1 Chapter 3 Methodology: *In Vivo*

### 3.2.1.1 Animals and Surgery

Experiments were carried out on Male Sprague-Dawley rats with approval from the UK Home Office and the University of Nottingham, as previously described (**2.1.5**). Full details of the two surgeries conducted for these experiments can be found in the general methodology (**2.1.5.1**, **2.1.5.2**). In brief, fifty-one rats (350-450 g) were used during the studies detailed in this chapter. The first surgery was conducted to implant miniature pulsed Doppler flow probes around the superior mesenteric and left renal arteries and the descending abdominal aorta to allow haemodynamic measurements that give information regarding the flow of blood to downstream regional vascular beds (**2.1.3.2**). A second surgery was carried out a minimum of 10 days after the implantation of the vascular probes. During this second surgery, a catheter was implanted via the caudal artery into the distal abdominal aorta to measure arterial blood pressure and allow the calculation of heart rate (Gardiner et al., 1980). In addition, three catheter lines were implanted into the right jugular vein to allow i.v. administration of compounds. The probe wires and catheters were protected inside a metal spring secured to a harness that went around the rat's torso, with the spring connected to a counterbalanced pivot system that allowed free movement of the rat (**Figure 12**). Experiments began 24 h after the second surgery, with the rats conscious and unrestrained, singly housed in home cages with access to food and water.

#### 3.2.1.2 Cardiovascular Recordings & Data Analysis

Detailed information on the cardiovascular recordings and data analysis can be found in the general methodology (**2.1.6**, **2.1.7**, **2.1.8**). In brief, rats were indirectly connected to the data acquisition programme (IdeeQ) during the monitoring periods via a tether system (**2.1.3**). Recordings were made for at least 30 min prior to the administration of any interventions and continuously for a minimum of 4 h thereafter. HR, MAP, renal, mesenteric and hindquarters Doppler shifts were measured (**2.1.3.1**, **2.1.3.2**), and changes in VC in the renal, mesenteric, and hindquarter vascular beds were calculated from the changes in MAP and Doppler shift (**2.1.3.3**). For all studies, time-averaged data are shown as variation from baseline [HR (beats.min$^{-1}$); MAP (mmHg); VC (%)].

A Friedman test was used for within-group comparisons compared to the baseline to ascertain if there was a significant difference between the timepoint and the baseline recording at rest (time=0). In addition, a Wilcoxon signed-rank matched-pairs test was conducted for within-group comparisons between different dosing treatment regimens at each specified time point to ascertain if there was a significant difference between the two different treatment conditions at each individual time point. Additionally, when appropriate, a Wilcoxon rank-sum test for integrated area under the curve analysis was used to compare groups. For the statistical analyses of individual studies, a $p<0.05$ was considered significant. For the statistical analyses of a combination of study results, a $p<0.01$ was considered significant.

#### 3.2.1.3 Experimental Protocols

Experiments were run in six studies, with each lasting three days (**2.1.8**). Within each study was a coincident vehicle control (vehicle buffer: 5 % propylene glycol, 2 % Tween 80 in sterile saline). Experiments were run with treatment groups of 8-10 rats.

Animals were randomly allocated based on a study independent identification number assigned to the rat on entry into the animal unit to an antagonist or vehicle group on experimental day one, and the alternative treatment given on experimental day three, allowing each rat to act as its own control.

On the second ('wash-out') day, the rats received no experimental treatment, although the arterial line was flushed with heparinised saline (40 I.U. /mL, ~0.2 mL) for two hours to maintain line patency. This break between experimental days allowed ligands to be metabolised and excreted following the first experimental day's treatment before the start of the experiments on experimental day three.

The $A_{2B}$ receptor antagonist PSB 603 would not go into solution in the required vehicle buffer, so the more water-soluble PSB 1115 was used for *in vivo* experiments.

#### 3.2.1.4 The Haemodynamic Effects of CGS 21680

##### 3.2.1.4.1 Study 1: CGS 21680 in the Presence or Absence of SCH 58261

Eight animals were used to assess the cardiovascular responses to CGS 21680 in the presence or absence of SCH 58261. Rats were randomised into two groups before the start of the experiment. After a period of baseline recording, **group 1** received a vehicle bolus (0.1 ml, i.v.) on day 1 and an SCH 58261 bolus (1.0 mg/kg, 0.1 mL, i.v.) on day 3. **Group 2** received an SCH 58261 bolus (1.0 mg/kg, 0.1 mL, i.v.) on day 1 and a vehicle bolus (0.1 mL, i.v.) on day 3. Approximately 10 min after the initial bolus of either vehicle or SCH 58261 on both day 1 and day 3, all groups received three infusions (0.1 mL/min, i.v.) in continuous succession of CGS 21680 (0.1 [low], 0.3 [mid], and 1.0 [high] µg/kg/min). Each dose was infused for 3 min, starting from the lowest dose. Haemodynamic recordings were made for a subsequent 4-hour period following the completion of the CGS 21680 infusion.

##### 3.2.1.4.2 Study 2: CGS 21680 in the Presence or Absence of PSB 1115

Eight animals were used to assess the cardiovascular responses to CGS 21680 in the presence or absence of PSB 1115. Rats were randomised into two groups before the start of the experiment. After a period of baseline recording, **group 1** received a vehicle bolus (0.1 mL, i.v.) on day 1 and a PSB 1115 bolus (10.0 mg/kg, 0.1 mL, i.v.) on day 3. **Group 2** received a PSB 1115 bolus (10.0 mg/kg, 0.1 mL, i.v.) on day 1 and a vehicle bolus (0.1 mL, i.v.) on day 3. Approximately 10 min after the initial bolus of either vehicle or PSB 1115 on both day 1 and day 3, all groups received three infusions (0.1 mL/min, i.v.) in continuous succession of CGS 21680 (0.1 [low], 0.3 [mid], and 1.0 [high] µg/kg/min). Each dose was infused for 3 min, starting from the lowest dose. Haemodynamic recordings were made for a subsequent 4-hour period following the completion of the CGS 21680 infusion.

# 3.2.1.5 The Haemodynamic Effects of BAY 60-6583

## 3.2.1.5.1 Study 3: BAY 60-6583 in the Presence or Absence of PSB 1115

Eight animals were used to assess the cardiovascular responses to BAY 60-6583 in the presence or absence of PSB 1115. Rats were randomised into two groups before the start of the experiment. After a period of baseline recording, **group 1** received a vehicle bolus (0.1 mL, i.v.) on day 1 and a PSB 1115 bolus (10.0 mg/kg, 0.1 mL, i.v.) on day 3. **Group 2** received a PSB 1115 bolus (10.0 mg/kg, 0.1 mL, i.v.) on day 1 and a vehicle bolus (0.1 mL, i.v.) on day 3. Approximately 10 min after the initial bolus of either vehicle or PSB 1115 on both day 1 and day 3, all groups received three infusions (0.1 mL/min, i.v.) in continuous succession of BAY 60-6583 (4.0 [low], 13 [mid], and 40 [high] µg/kg/min). Each dose was infused for 3 min, starting from the lowest dose. Haemodynamic recordings were made for a subsequent 4-hour period following the completion of the BAY 60-6583 infusion.

## 3.2.1.5.2 Study 4: BAY 60-6583 in the Presence or Absence of SCH 58261

Nine animals were used to assess the cardiovascular responses to BAY 60-6583 in the presence or absence of SCH 58261. Rats were randomised into two groups before the start of the experiment. After a period of baseline recording, **group 1** received a vehicle bolus (0.1 mL, i.v.) on day 1 and an SCH 58261 bolus (1.0 mg/kg, 0.1 mL, i.v.) on day 3. **Group 2** received an SCH 58261 bolus (1.0 mg/kg, 0.1 mL, i.v.) on day 1 and a vehicle bolus (0.1 mL, i.v.) on day 3. Approximately 10 min after the initial bolus of either vehicle or SCH 58261 on both day 1 and day 3, all groups received three infusions (0.1 mL/min, i.v.) in continuous succession of BAY 60-6583 (4.0 [low], 13 [mid], and 40 [high] µg/kg/min). Each dose was infused for 3 min, starting from the lowest dose. Haemodynamic recordings were made for a subsequent 4-hour period following the completion of the BAY 60-6583 infusion.

## 3.2.1.6 The Haemodynamic Effects of Adenosine

### 3.2.1.6.1 Study 5: Adenosine in the Presence or Absence of SCH 58261

Eight animals were used to assess the cardiovascular responses to adenosine in the presence or absence of SCH 58261. Rats were randomised into two groups before the start of the experiment. After a period of baseline recording, **group 1** received a vehicle bolus (0.1 mL, i.v.) on day 1 and an SCH 58261 bolus (1.0 mg/kg, 0.1 mL, i.v.) on day 3. **Group 2** received an SCH 58261 bolus (1.0 mg/kg, 0.1 ml, i.v.) on day 1 and a vehicle bolus (0.1 mL, i.v.) on day 3. Approximately 10 min after the initial bolus of either vehicle or SCH 58261 on both day 1 and day 3, all groups received three infusions (0.1 mL/min, i.v.) in continuous succession of adenosine (30 [low], 100 [mid], and 300 [high] µg/kg/min). Each dose was infused for 3 min, starting from the lowest dose. Haemodynamic recordings were made for a subsequent 4-hour period following the completion of the adenosine infusion. *This experiment was completed by Dr Sam Cooper.*

### 3.2.1.6.2 Study 6: Adenosine in the Presence or Absence of PSB 1115

Ten animals were used to assess the cardiovascular responses to adenosine in the presence or absence of PSB 1115. Rats were randomised into two groups before the start of the experiment. After a period of baseline recording, **group 1** received a vehicle bolus (0.1 mL, i.v.) on day 1 and a PSB 1115 bolus (10 mg/kg, 0.1 mL, i.v.) on day 3. **Group 2** received a PSB 1115 bolus (10 mg/kg, 0.1 mL, i.v.) on day 1 and a vehicle bolus (0.1 mL, i.v.) on day 3. Approximately 10 min after the initial bolus of either vehicle or PSB 1115 on both day 1 and day 3, all groups received three infusions (0.1 mL/min, i.v.) in continuous succession of adenosine (30 [low], 100 [mid], and 300 [high] µg/kg/min). Each dose was infused for 3 min, starting from the lowest dose. Haemodynamic recordings were made for a subsequent 4-hour period following the completion of the adenosine infusion.

## 3.2.2 Chapter 3 Methodology: *In Vitro*

### 3.2.2.1 NanoBRET Ligand Binding Studies

Fluorescent saturation and competition-binding assays were completed on transiently transfected HEK 293T cells expressing rat NLuc-tagged adenosine $A_{2A}$ or $A_{2B}$ receptors that were plated into 96-well plates at 30,000 cells per well (**2.2.5.3**). 24 h after cell plating, the cell media was replaced with 50 µL HBSS buffer supplemented with 0.1% BSA at pH 7.45 (**2.2.4.3**) and the required concentration of the fluorescent ligand CA200645 and non-fluorescent competitive ligands.

For fluorescent ligand saturation binding assays, concentrations of CA200645 (0-500 nM) in the presence or absence of an appropriate receptor selective antagonist ($A_{2A}$ receptor: SCH 58261 (10 µM), $A_{2B}$ receptor: PSB 603 (10 µM)) were used. For competition binding assays, CA200645 (50 nM) binding was monitored in the absence and presence of increasing concentrations of unlabelled ligand. For rat $A_{2A}$ receptor experiments, increasing concentrations of adenosine (0.1 nM–1.0 mM), PSB 603 (0.1 nM–100 µM), CGS 216880 (0.1 nM–100 µM), SCH 58261 (0.01 nM–10 µM), BAY 60-6583 (0.1 nM–100 µM), PSB 1115 (0.1 nM-100 µM) were used, and for rat $A_{2B}$ receptor experiments, increasing concentrations of adenosine (0.1 nM–1.0 mM), PSB 603 (0.01 nM–10 µM), CGS 216880 (0.1 nM–100 µM), SCH 58261 (0.1 nM–100 µM), BAY 60-6583 (0.1 nM–100 µM), PSB 1115 (0.1 nM-100 µM) were used. The DMSO concentration in all wells was equalised to a final concentration of 1%. Cells were incubated with ligands for 2 h at 37ºC, as suggested by previous data from the lab, to allow ligands to equilibrate to the receptor to negate the effects of ligand-receptor kinetics on the final result. Furimazine was then added to each well to a final in-well concentration of 10 µM, and the cells incubated for an additional 5 min at 37°C. The plates were read at 37ºC using a PHERAstar FS plate reader (BMGLabtech), measuring filtered light emissions at 460 nm (80 nm bandpass) and >610 nm (longpass). The experimental results were represented by raw BRET values, which were calculated by taking the ratio of the >610 nm emission over the 460 nm emission.

### 3.2.2.2 GloSensor Cyclic AMP Assay

GloSensor assays were carried out as previously described (**2.2.7.2**). Briefly, HEK 293G cells expressing native human receptors (including $A_{2A}$ and $A_{2B}$ receptors) or the same cell line transiently transfected to also express rat NLuc-$A_{2A}$ receptors (**2.2.4.1**) were plated into 96-well plates at 30,000 cells per well (**2.2.4.2**). The following day, the cell media was replaced with 50 µL of HBSS supplemented with 0.1% BSA (**2.2.4.3**) containing 3% GloSensor cAMP reagent (Promega) and incubated for 2 h at 37°C. A baseline luminescence recording was measured on a PHERAstar FS plate reader before 50 µL HBSS with or without the presence of forskolin (100 µM), CGS 21680 (0.1 nM–100 µM), BAY 60-6583 (0.1 nM–100 µM), SCH 58261 (10 µM) or formoterol (10 µM) was added to the well, with each ligand either in isolation or combination. Following the addition of ligands, luminescence read continuously over 60 min, with 1 read per well every minute. The DMSO concentration in all wells was equalised to a final concentration of 1%. When used, PSB 603 (100 nM) was incubated alongside the Glosensor cAMP reagent for 2 h before the addition of the other ligands.

# 3.3 Haemodynamic Responses to Adenosine $A_2$ Receptor Agonism: Chapter Results

## 3.3.1 Chapter 3 Results: *In Vivo*

### 3.3.1.1 In Vivo Results: Baseline Cardiovascular Recordings

For each study, baseline measurements were taken before the administration of the adenosine receptor antagonists SCH 58261 or PSB 1115, or corresponding vehicle control, and then again before administration of an agonist, with these values corresponding to the baselines at time=0 for each study in **Figures 24-29**; these values can be found in **Tables 12-14. Table 11** is a summation of baseline results from the individual studies prior to the adenosine receptor antagonists. These values correspond to the baselines at time=0 found in **Figure 22** and **Figure 23**.

## 3.3.1.2 In Vivo Results: $A_2$ Receptor Antagonists

### 3.3.1.2.1 The Effect of SCH 58261 and PSB 1115 on Baseline Cardiovascular Responses

Prior to the administration of agonists, a bolus of the $A_{2A}$ receptor antagonist SCH 58261 (combination of results from studies 1 (**3.2.1.4.1**), 4 (**3.2.1.5.2**) and 5 (**3.2.1.6.1**) (**Figure 22**), the $A_{2B}$ receptor antagonist PSB 1115 (combination of results from studies 2 (**3.2.1.4.2**), 3 (**3.2.1.5.1**) and 6 (**3.2.1.6.2**) (**Figure 23**), or respective vehicle control was administered, and cardiovascular effects observed for 10 min.

The $A_{2A}$ receptor antagonist, SCH 58261 (1.0 mg/kg), caused significant ($p<0.01$) differences in area under the curve analysis for HR and hindquarters VC, although these were not associated with a significant change from baseline and were very small in magnitude. There was also a significant difference ($p<0.01$) in the area under the curve analysis for mesenteric VC, with significant ($p<0.01$) decreases in both the vehicle and drug groups from baseline. However, these were not associated with any significant differences at any of the individual timepoints between the two groups (**Figure 22**).

The $A_{2B}$ receptor antagonist, PSB 1115 (10 mg/kg), caused a sustained and significant ($p<0.01$) increase in MAP, accompanied by significant ($p<0.01$) decreases in VC in both the renal and mesenteric vascular beds. These effects may result from the antagonism of an $A_{2B}$ receptor-mediated vasodilatory tone produced by endogenous adenosine in the rat. There was also a significant initial spike in HR and hindquarters VC observed; however, this increase was transient and returned to baseline after 3-5 min, and so is most likely due to temporary effects caused by drug administration (**Figure 23**).

| | Combination of Studies 1 & 4 & 5 | | | | Combination of Studies 2 & 3 & 6 | | | |
|---|---|---|---|---|---|---|---|---|
| | Vehicle | | SCH 58261 | | Vehicle | | PSB 1115 | |
| | Mean ± SEM | n | Mean ± SEM | n | Mean ± SEM | n | Mean ± SEM | n |
| **Cardiovascular Variable** | **Baseline T=0** | | | | | | | |
| **Heart rate (beats·min$^{-1}$)** | 340± 4 | 25 | 352± 5 | 25 | 346 ± 5 | 26 | 351 ± 5 | 26 |
| **Mean BP (mmHg)** | 103 ± 2 | 25 | 103± 2 | 25 | 103 ± 1 | 26 | 102 ± 1 | 26 |
| **Renal VC (U)** | 80 ± 5 | 21 | 83± 6 | 21 | 86 ± 5 | 23 | 90 ± 6 | 23 |
| **Mesenteric VC (U)** | 80± 5 | 22 | 83 ± 5 | 22 | 94 ± 6 | 24 | 97 ± 6 | 24 |
| **Hindquarters VC (U)** | 47 ± 3 | 22 | 47 ± 3 | 22 | 50 ± 3 | 26 | 48 ± 3 | 26 |

**Table 11 Cardiovascular Variables Before Administration of Adenosine $A_2$ Receptor Antagonists.** Values are mean ± SEM; n=21-26 per combined group. Units (U) of vascular conductance (VC) are kHz. mmHg$^{-1}$ x $10^3$. A Wilcoxon signed-rank test was conducted between the antagonist and its corresponding vehicle control group (* = $p<0.01$ significance, no significance was observed in this table). Readings correspond to the baseline recordings (zero values) for the graphs in **Figure 22** and **Figure 23**. Abbreviations: U, units; VC, vascular conductance.

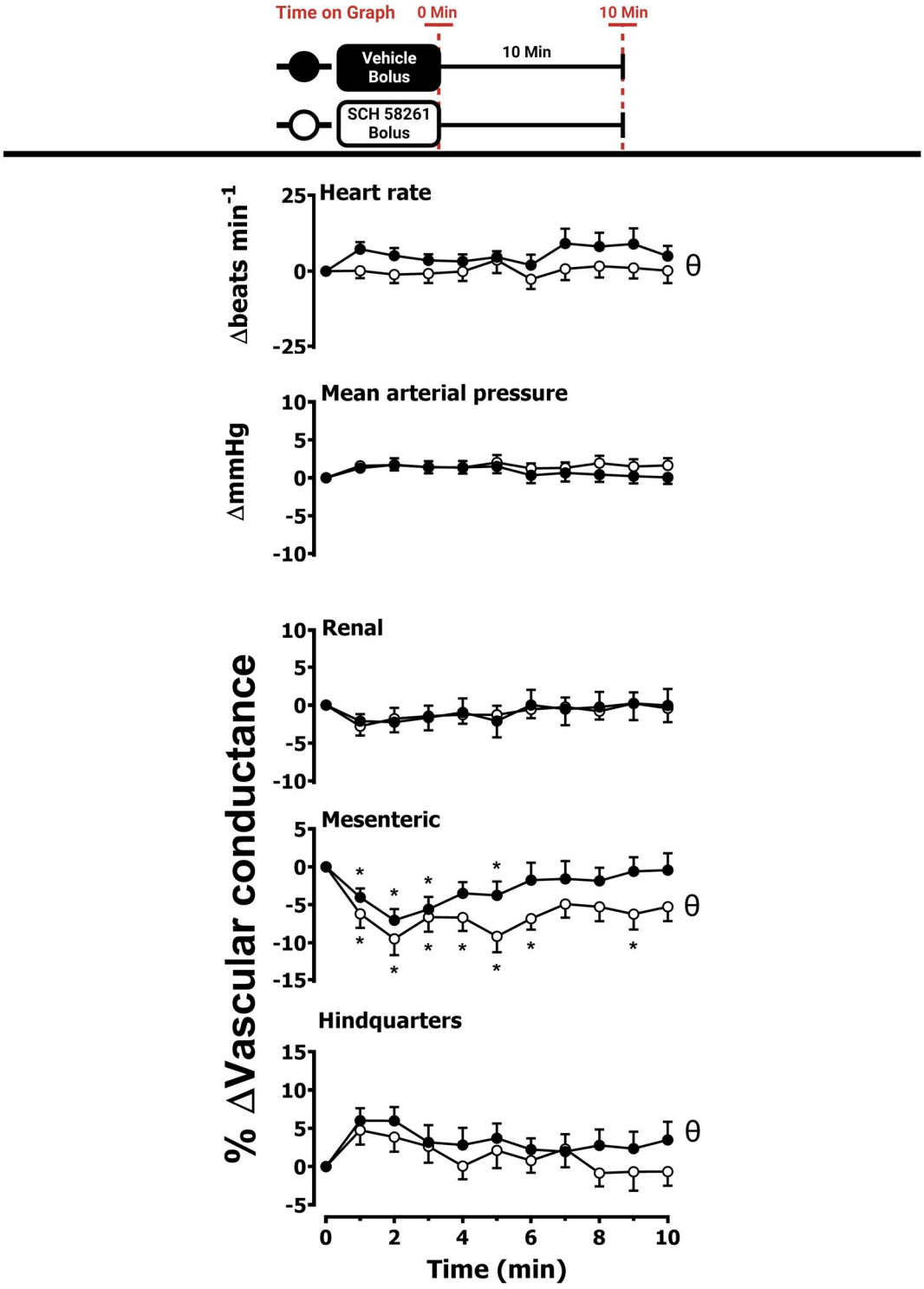


**Figure 22 Cardiovascular Responses to SCH 58261 in Conscious, Freely Moving Rats.** Conscious, freely moving rats were dosed with SCH 58261 (0.1 mL bolus of 1.0 mg/kg i.v., n=25) or vehicle (0.1 mL bolus of 5 % propylene glycol, 2 % Tween 80 in sterile saline, n=25) as described in the chapter methodology (**3.2.1.3**). The graphs show responses over a 10 min period post-dosing. Data points are mean + or - SEM. A Friedman test was conducted for each data point of each group and the group's corresponding baseline (T=0) (***** = p<0.01 significance). A Wilcoxon signed-rank test was conducted between the SCH 58261 and vehicle control groups for a comparison of the area under the curve (**θ** = p<0.01 significance), and additionally to determine differences at each time point (Wilcoxon T-test equivalent) (**#** = p<0.01 significance). Results are a combination of studies 1, 4 & 5. Baseline recordings for this figure can be found in **Table 11**.

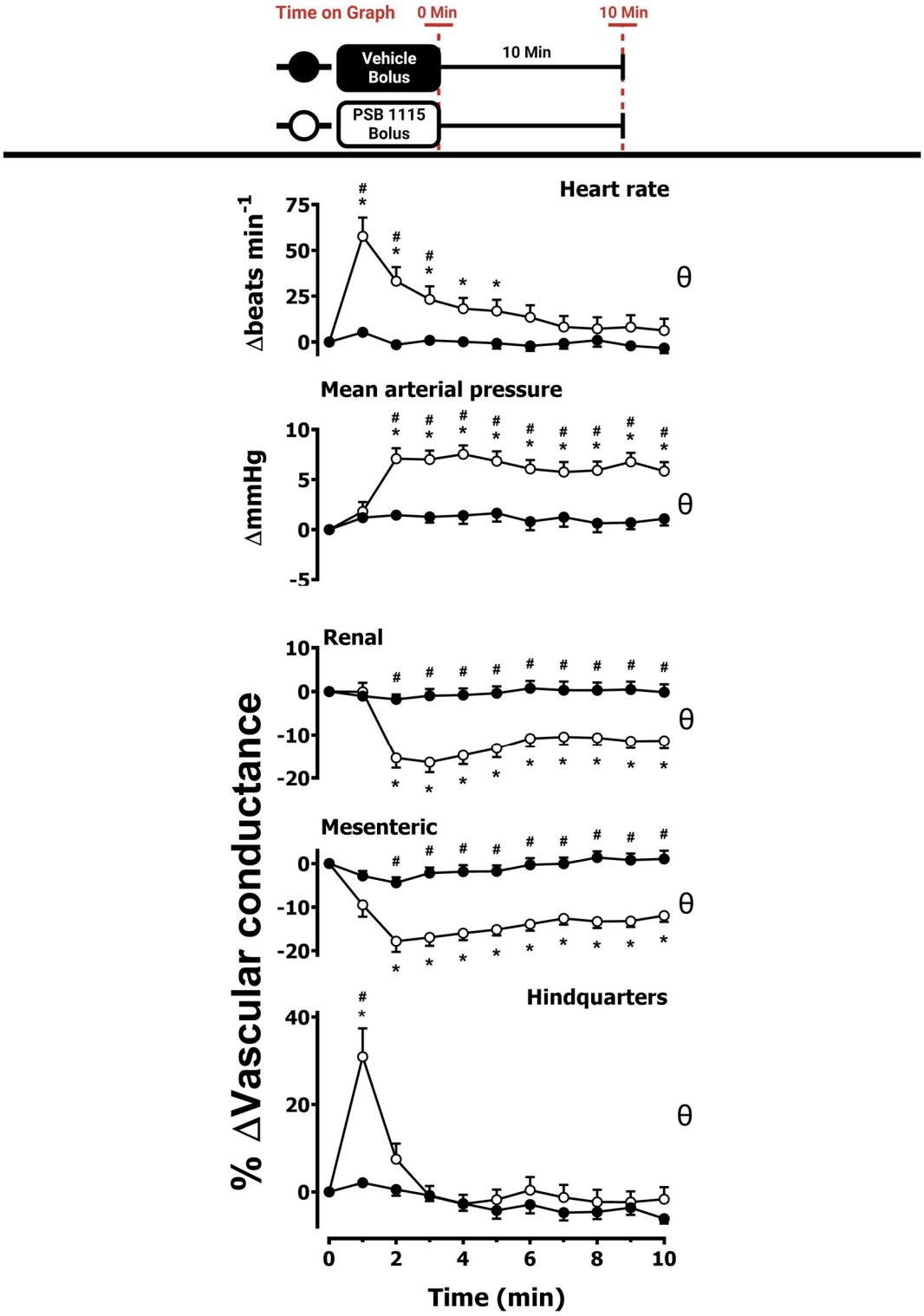


**Figure 23 Cardiovascular Responses to PSB 1115.** Conscious, freely moving rats were dosed with PSB 1115 (0.1 mL bolus of 10 mg/kg i.v., n=26) or vehicle (0.1 mL bolus of 5 % propylene glycol, 2 % Tween 80 in sterile saline, n=26) as described in the chapter methodology (**3.2.1.3**). The graphs show responses over a 10 min period post-dosing. Data points are mean + or - SEM. A Friedman test was conducted for each data point of each group and the group's corresponding baseline (T=0) (***** = p<0.01 significance). A Wilcoxon signed-rank test was conducted between the PSB 1115 and vehicle control groups for a comparison of the area under the curve (**θ** = p<0.01 significance), and additionally to determine differences at each time point (Wilcoxon T-test equivalent) (**#** = p<0.01 significance). Results are a combination of studies 2, 3 & 6. Baseline recordings for this figure can be found in **Table 11.**

## 3.3.1.3 In Vivo Results: $A_{2A}$ Receptor Agonist

### 3.3.1.3.1 Effect of the $A_{2A}$ Receptor Agonist CGS 21680

Rats received an infusion of increasing concentrations of the $A_{2A}$ receptor agonist CGS 21680 (0.1, 0.3 and 1.0 μg/kg/min; 3 min i.v. infusions of each dose). CGS 21680 produced a dose-dependent large and significant ($p<0.05$) increases in HR and hindquarters VC, indicative of vasodilatations in this vascular bed, but only minor, not significant increases in VC in the renal and mesenteric vascular beds (**Figure 24A-B**, **Figure 25A-B**). These effects were accompanied by a significant ($p<0.05$) decrease in MAP (**Figure 24A-B**, **Figure 25A-B**). Cardiovascular recordings returned to baseline levels around 30 min after the final dose of CGS 21680 was administered (**Figure 24B**, **Figure 25B**).

The effect of the $A_{2A}$ receptor antagonist SCH 58261 (1.0 mg/kg) on the cardiovascular response to CGS 21680 was investigated (**Figure 24A-B**). SCH 58261 (1.0 mg/kg) significantly attenuated the vasodilator response to CGS 21680 in the hindquarters, totally preventing the administration of CGS 21680 from causing a significant increase in the VC at this bed. In addition, SCH 58261 (1.0 mg/kg) also attenuated the increase in HR due to CGS 21680 administration and completely attenuated the associated fall in MAP (**Figure 24A-B**).

To investigate any possible involvement of $A_{2B}$ receptors in the cardiovascular responses to CGS 21680, the effect of the $A_{2B}$ receptor antagonist PSB 1115 (10 mg/kg) on the cardiovascular response to CGS 21680 was investigated (**Figure 25A-B**). PSB 1115 (10 mg/kg) caused a significant ($p<0.05$), but minor, attenuation of the HR, MAP, and hindquarters VC responses observed with CGS 21680 administration, which was very likely due to the poor selectivity of PSB 1115, causing the antagonism of $A_{2A}$ receptor responses (**Figure 31F**, **Table 15**, **3.3.2.1.2**).

| | Study 1: CGS 21680 +- SCH 58261 | | | | Study 2: CGS 21680 +- PSB 1115 | | | |
|---|---|---|---|---|---|---|---|---|
| | Vehicle | | SCH 58261 | | Vehicle | | PSB 1115 | |
| | Mean ± SEM | n | Mean ± SEM | n | Mean ± SEM | n | Mean ± SEM | n |
| **Cardiovascular Variable** | **Baseline (T= 0)** | | | | | | | |
| **Heart rate (beats·min$^{-1}$)** | 345 ± 7 | 8 | 356 ± 9 | 8 | 342 ± 11 | 8 | 353 ± 7 | 8 |
| **Mean BP (mmHg)** | 96 ± 1 | 8 | 97 ± 2 | 8 | 101 ± 2 | 8 | 100 ± 3 | 8 |
| **Renal VC (U)** | 72 ± 8 | 6 | 70 ± 9 | 6 | 98 ± 7 | 6 | 113 ± 15 | 6 |
| **Mesenteric VC (U)** | 74 ± 15 | 6 | 88 ± 10 | 6 | 95 ± 15 | 7 | 104 ± 15 | 7 |
| **Hindquarters VC (U)** | 48 ± 7 | 7 | 46 ± 4 | 7 | 45 ± 4 | 8 | 46 ± 5 | 8 |
| **Cardiovascular Variable** | **Prior to Infusion (T = 10 min†)** | | | | | | | |
| **Heart rate (beats·min$^{-1}$)** | 346 ± 8 | 8 | 356 ± 8 | 8 | 338 ± 11 | 8 | 359 ± 20 | 8 |
| **Mean BP (mmHg)** | 96 ± 1 | 8 | 99 ± 2 | 8 | 101 ± 2 | 8 | 106 ± 4 | 8 |
| **Renal VC (U)** | 71 ± 8 | 6 | 71 ± 10 | 6 | 102 ± 11 | 6 | 99 ± 15 | 6 |
| **Mesenteric VC (U)** | 73 ± 13 | 6 | 83 ± 9 | 6 | 100 ± 18 | 7 | 95 ± 14 | 7 |
| **Hindquarters VC (U)** | 51 ± 6 | 7 | 50 ± 6 | 7 | 42 ± 4 | 8 | 44 ± 4 | 8 |

**Table 12 Cardiovascular Variables Before Administration of Adenosine $A_2$ Receptor Antagonists and Before the Subsequent Administration of the $A_{2A}$ Receptor Agonist CGS 21680.** Values are mean ± SEM; n=6-8 per group. Units (U) of vascular conductance (VC) are kHz. mmHg$^{-1}$ x $10^3$. A Wilcoxon signed-rank test was conducted between the antagonist group and its corresponding vehicle control group (* = $p<0.05$ significance). Readings correspond to the baseline recordings (zero values) for the graphs in **Figure 24** and **Figure 25**. †In some instances, agonist administration was delayed past 10 min in the case of movement to allow the rat to settle. Abbreviations: U, units; VC, vascular conductance.

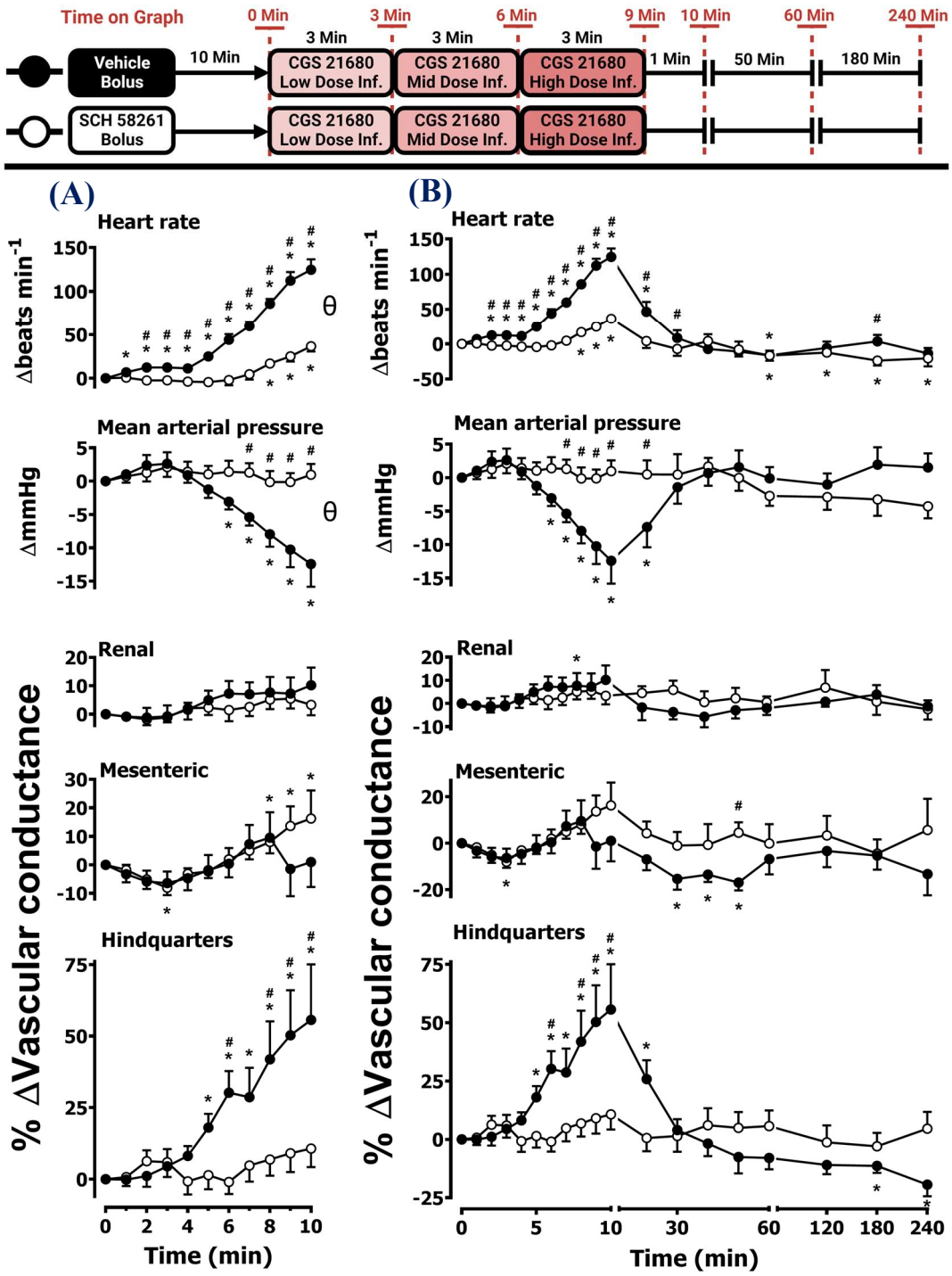


**Figure 24 Cardiovascular Responses to CGS 21680 in the Presence or Absence of SCH 58261.** Conscious, freely moving rats were dosed with SCH 58261 (0.1 mL bolus; 1.0 mg/kg i.v.; n=8) or vehicle (0.1 mL bolus; 5 % propylene glycol, 2 % Tween 80 in sterile saline; n=8) as described in the chapter methodology (**3.2.1**). Approximately 10 min after the bolus, all animals received an infusion of a consecutive low, medium and high dose of CGS 21680 (0.1, 0.3 and 1.0 µg/kg/min, i.v.), with each dose run for 3 min. The graphs show **(A)** the CGS 21680 treatment period, plus a minute, and **(B)** the treatment period and recording period of 4 h. Data points are mean + or - SEM. A Friedman test was conducted for each data point of each group and the group's corresponding baseline (T=0) (***** = $p<0.05$ significance) [**(A)** & **(B)**]. A Wilcoxon signed-rank test was conducted between the two groups for a comparison of the area under the curve (**θ** = $p<0.05$ significance) [**(A)**], and additionally to determine differences at each time point (Wilcoxon T-test equivalent) (**#** = $p<0.05$ significance) [**(A)** & **(B)**]. Results are from study 1. Baseline recordings can be found in **Table 12**.

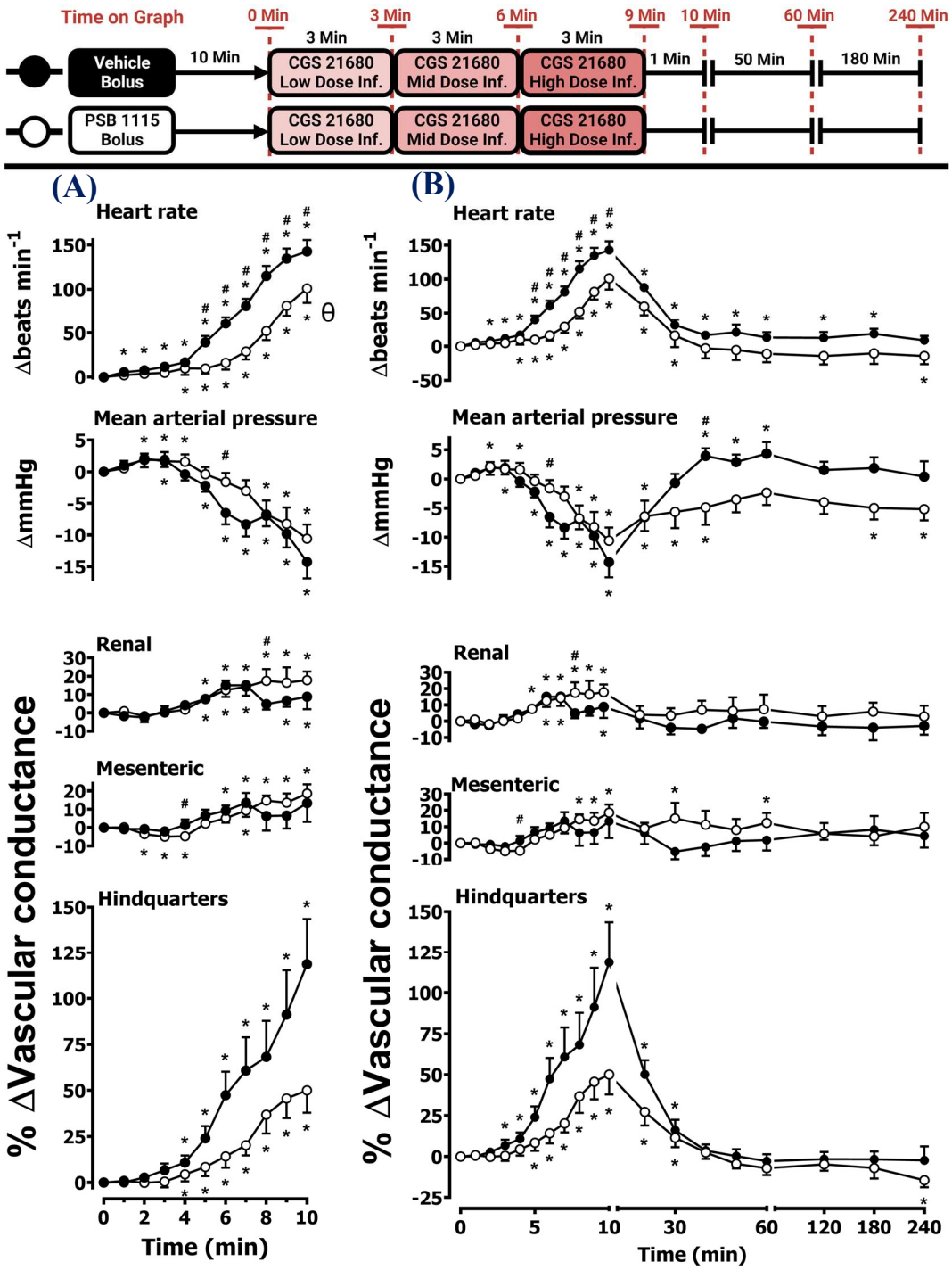


**Figure 25 Cardiovascular Responses to CGS 21680 in the Presence or Absence of PSB 1115.** Conscious, freely moving rats were dosed with PSB 1115 (0.1 mL bolus; 10 mg/kg i.v.; n=8) or vehicle (0.1 mL bolus; 5 % propylene glycol, 2 % Tween 80 in sterile saline; n=8) as described in the chapter methodology (**3.2.1**). Approximately 10 min after the bolus, all animals received an infusion of a consecutive low, medium and high dose of CGS 21680 (0.1, 0.3 and 1.0 µg/kg/min, i.v.), with each dose run for 3 min. The graphs show **(A)** the CGS 21680 treatment period, plus a minute, and **(B)** the treatment period and recording period of 4 h. Data points are mean + or - SEM. A Friedman test was conducted for each data point of each group and the group's corresponding baseline (T=0) (***** = $p<0.05$ significance) [**(A)** & **(B)**]. A Wilcoxon signed-rank test was conducted between the two groups for a comparison of the area under the curve (**θ** = $p<0.05$ significance) [**(A)**], and additionally to determine differences at each time point (Wilcoxon T-test equivalent) (**#** = $p<0.05$ significance) [**(A)** & **(B)**]. Results are from study 2. Baseline recordings can be found in **Table 12**.

## 3.3.1.4 In Vivo Results: $A_{2B}$ Receptor Agonist

### 3.3.1.4.1 Effect of the $A_{2B}$ Receptor Agonist BAY 60-6583

Rats received an infusion of increasing concentrations of the $A_{2B}$ receptor agonist BAY 60-6583 (4.0, 13.3, and 40.0 µg/kg/min, i.v.). BAY 60-6583 produced a dose-dependent significant ($p<0.05$) increases in HR and the VC in both the renal and mesenteric vascular beds (**Figure 26A-B**, **Figure 27A-B**). However, no consistent or significant changes to MAP or hindquarters VC were observed due to BAY 60-6583 administration (**Figure 26A-B**, **Figure 27A-B**). In general, most cardiovascular recordings had returned to baseline levels by 110 min after BAY 60-6583 dosing cessation (**Figure 26B**, **Figure 27B**).

The effect of the $A_{2B}$ receptor antagonist PSB 1115 (10 mg/kg) on the cardiovascular response to BAY 60-6583 was investigated (**Figure 26A-B**). PSB 1115 strongly and significantly ($p<0.05$) attenuated the BAY 60-6583 induced increases in HR and also VC in both the renal and mesenteric vascular beds.

To investigate any possible involvement of $A_{2A}$ receptors in the cardiovascular responses to BAY 60-6583, the effect of the $A_{2A}$ receptor antagonist SCH 58261 (1.0 mg/kg) on the cardiovascular response to BAY 60-6583 was investigated (**Figure 27A-B**). SCH 58261 (1.0 mg/kg) caused little effect on the increase in HR and the increases in VC observed in the renal and mesenteric vascular beds (**Figure 27A-B**).

| | Study 3: BAY 60-6583 +- PSB 1115 | | | | Study 4: BAY 60-6583 +- SCH 58261 | | | |
|---|---|---|---|---|---|---|---|---|
| | Vehicle | | PSB 1115 | | Vehicle | | SCH 58261 | |
| | Mean ± SEM | n | Mean ± SEM | n | Mean ± SEM | n | Mean ± SEM | n |
| **Cardiovascular Variable** | **Baseline (T=0)** | | | | | | | |
| **Heart rate (beats·min$^{-1}$)** | 350 ± 8 | 8 | 362 ± 12 | 8 | 343 ± 6 | 9 | 357 ± 10 | 9 |
| **Mean BP (mmHg)** | 105 ± 3 | 8 | 105 ± 3 | 8 | 105 ± 2 | 9 | 108 ± 2 | 9 |
| **Renal VC (U)** | 74 ± 10 | 7 | 80 ± 9 | 7 | 85 ± 7 | 9 | 89 ± 10 | 9 |
| **Mesenteric VC (U)** | 91 ± 8 | 8 | 89 ± 11 | 8 | 72 ± 4 | 8 | 78 ± 7 | 8 |
| **Hindquarters VC (U)** | 46 ± 5 | 8 | 48 ± 7 | 8 | 44 ± 4 | 8 | 42 ± 6 | 8 |
| **Cardiovascular Variable** | **Prior to infusion (T = 10 min†)** | | | | | | | |
| **Heart rate (beats·min$^{-1}$)** | 350 ± 9 | 8 | 352 ± 13 | 8 | 353 ± 9 | 9 | 349 ± 9 | 9 |
| **Mean BP (mmHg)** | 105 ± 2 | 8 | **110 ± 3*** | 8 | 105 ± 2 | 9 | 106 ± 1 | 9 |
| **Renal VC (U)** | 74 ± 10 | 7 | 74 ± 8 | 7 | 86 ± 8 | 9 | 90 ± 10 | 9 |
| **Mesenteric VC (U)** | 90 ± 8 | 8 | 79 ± 8 | 8 | 69 ± 5 | 8 | 77 ± 7 | 8 |
| **Hindquarters VC (U)** | 45 ± 6 | 8 | 47 ± 6 | 8 | 47 ± 5 | 8 | 39 ± 5 | 8 |

**Table 13 Cardiovascular Variables Before Administration of Adenosine $A_2$ Receptor Antagonists and Before the Subsequent Administration of the $A_{2B}$ Receptor Agonist BAY 60-6583.** Values are mean ± SEM; n=7-9 per group. Abbreviations: U, units; VC, vascular conductance. Units (U) of vascular conductance (VC) are kHz. mmHg$^{-1}$ x $10^3$. A Wilcoxon signed-rank test was conducted between the antagonist group and its corresponding vehicle control group (* = $p<0.05$ significance). Readings correspond to the baseline recordings (zero values) for the graphs. †In some instances, agonist administration was delayed past 10 min in the case of movement to allow the rat to settle.

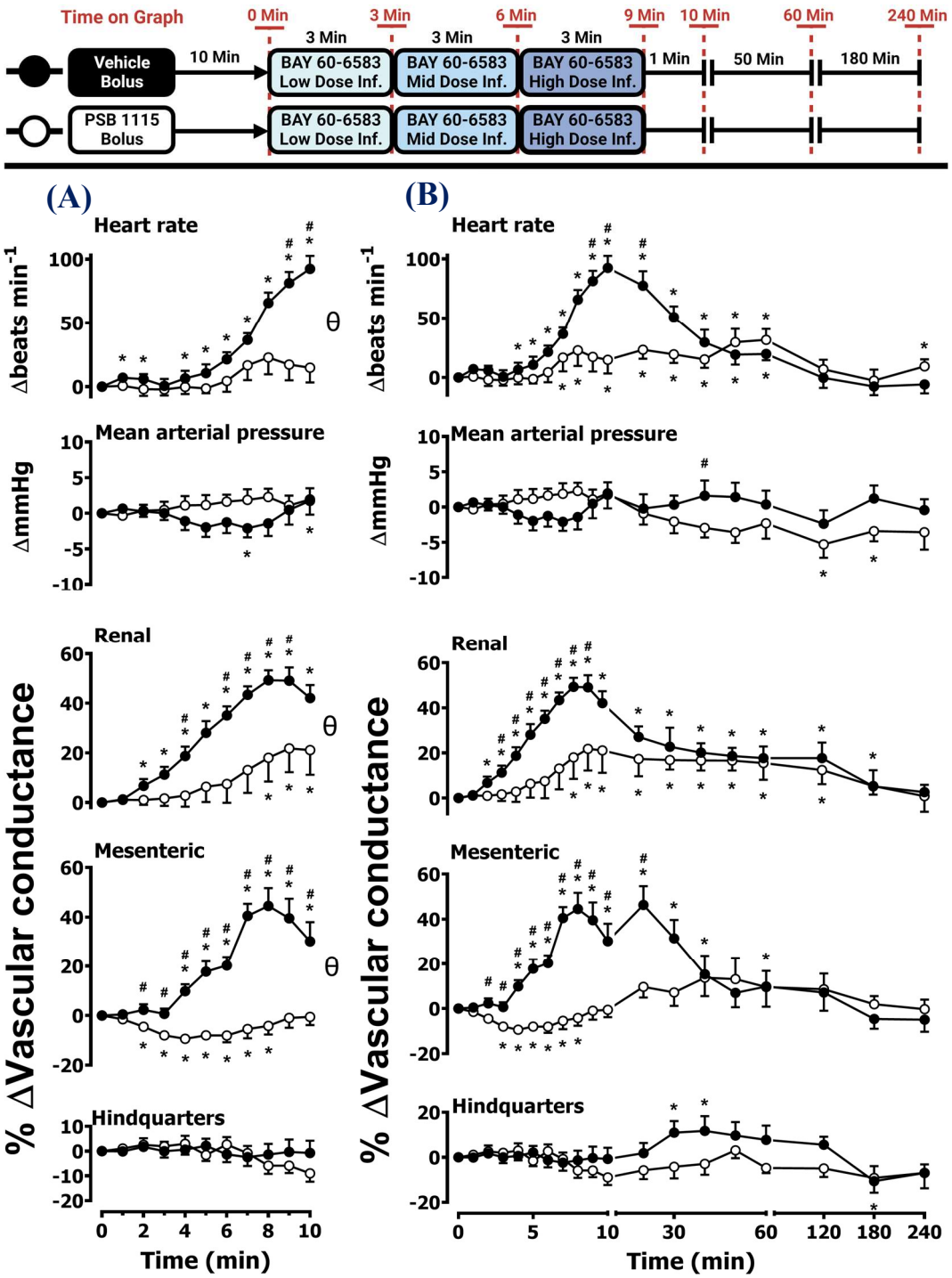


**Figure 26 Cardiovascular Responses to BAY 60-6583 in the Presence or Absence of PSB 1115.** Conscious, freely moving rats were dosed with PSB 1115 (0.1 mL bolus; 10 mg/kg i.v.; n=8) or vehicle (0.1 mL bolus; 5 % propylene glycol, 2 % Tween 80 in sterile saline; n=8) as described in the chapter methodology (**3.2.1**). Approximately 10 min after the bolus, all animals received an infusion of a consecutive low, medium and high dose of BAY 60-6583 (4.0, 13.3, and 40.0 µg/kg/min, i.v.), with each dose run for 3 min. The graphs show **(A)** the BAY 60-6583 treatment period, plus a minute, and **(B)** the treatment period and recording period of 4 h. Data points are mean + or - SEM. A Friedman test was conducted for each data point of each group and the group's corresponding baseline (T=0) (***** = $p<0.05$ significance) [**(A)** & **(B)**]. A Wilcoxon signed-rank test was conducted between the two groups for a comparison of the area under the curve (**θ** = $p<0.05$ significance) [**(A)**], and additionally to determine differences at each time point (Wilcoxon T-test equivalent) (**#** = $p<0.05$ significance) [**(A)** & **(B)**]. Results are from study 3. Baseline recordings can be found in **Table 13**.

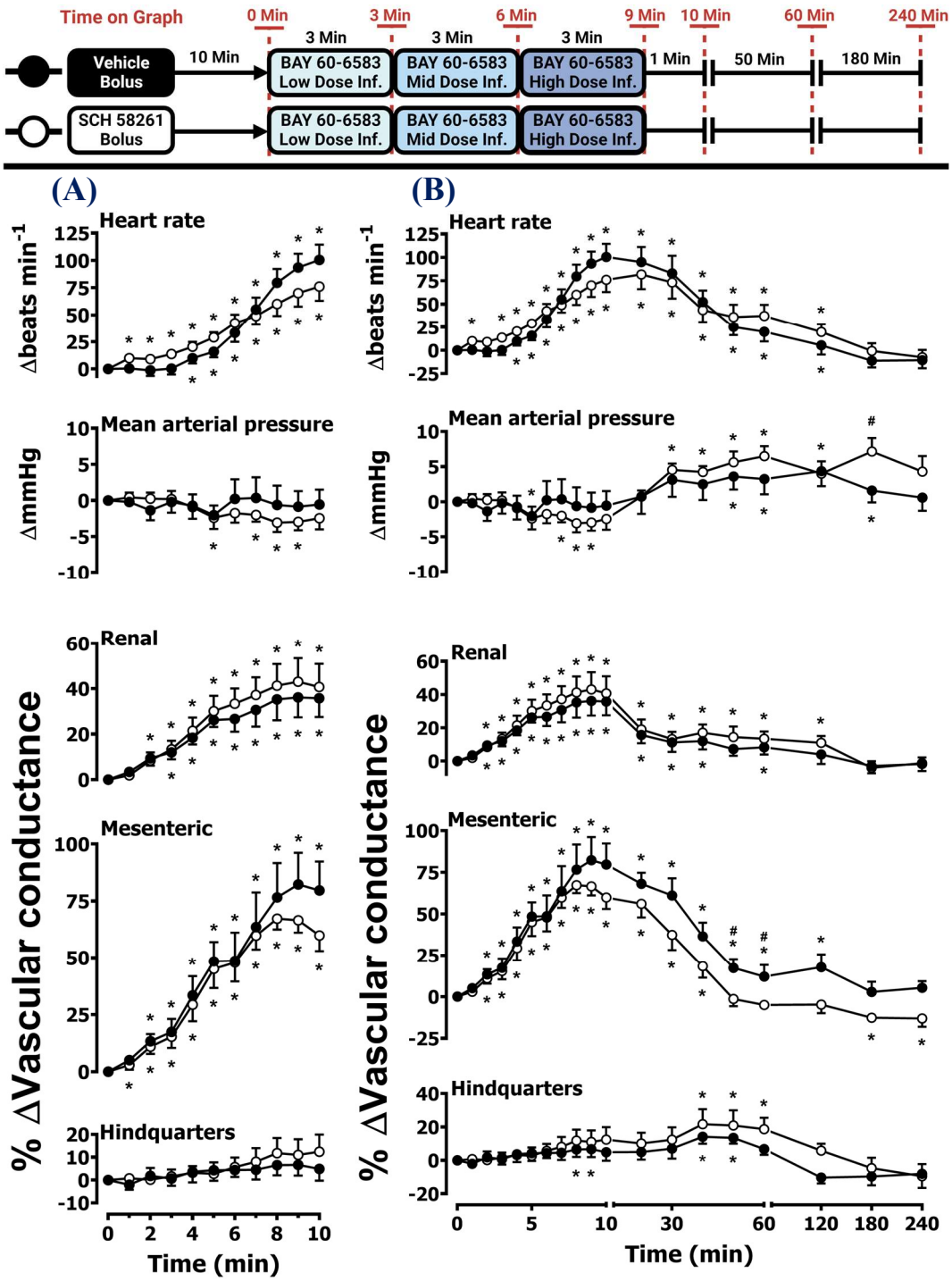


**Figure 27 Cardiovascular Responses to BAY 60-6583 in the Presence or Absence of SCH 58261.** Conscious, freely moving rats were dosed with SCH 58261 (0.1 mL bolus; 1.0 mg/kg i.v.; n=9) or vehicle (0.1 mL bolus; 5 % propylene glycol, 2 % Tween 80 in sterile saline; n=9) as described in the chapter methodology (**3.2.1**). Approximately 10 min after the bolus, all animals received an infusion of a consecutive low, medium and high dose of BAY 60-6583 (4.0, 13.3, and 40.0 µg/kg/min, i.v.), with each dose run for 3 min. The graphs show **(A)** the BAY 60-6583 treatment period, plus a minute, and **(B)** the treatment period and recording period of 4 h. Data points are mean + or - SEM. A Friedman test was conducted for each data point of each group and the group's corresponding baseline (T=0) (***** = $p<0.05$ significance) [**(A)** & **(B)**]. A Wilcoxon signed-rank test was conducted between the two groups for a comparison of the area under the curve (**θ** = $p<0.05$ significance) [**(A)**], and additionally to determine differences at each time point (Wilcoxon T-test equivalent) (**#** = $p<0.05$ significance) [**(A)** & **(B)**]. Results are from study 4. Baseline recordings can be found in **Table 13**.

# 3.3.1.5 In Vivo Results: Adenosine

## 3.3.1.5.1 Effect of Adenosine

Rats received an infusion of increasing concentrations of adenosine (30, 100, and 300 µg/kg/min, i.v.). Adenosine produced a dose-dependent significant ($p<0.05$) increase in HR and renal, mesenteric and hindquarters VC, indicative of vasodilatations in these vascular beds (**Figure 28A-B**, **Figure 29A-B**). These effects were accompanied by a significant ($p<0.05$) decrease in MAP (**Figure 28A-B**, **Figure 29A-B**). All Cardiovascular recordings rapidly returned to baseline levels, with a sharp decrease seen after only 1 minute following dosing cessation (**Figure 28A-B**, **Figure 29A-B**).

The effect of the $A_{2A}$ receptor antagonist SCH 58261 (1.0 mg/kg) on the cardiovascular response to adenosine was investigated (**Figure 28A-B**). SCH 58261 (1.0 mg/kg) produced an attenuation of the vasodilator response to CGS 21680 in the hindquarters that was significant ($p<0.05$) for the majority of the highest dose of adenosine. In addition, SCH 58261 (1.0 mg/kg) significantly attenuated the increase in HR due to adenosine administration. However, SCH 58261 did not cause a significant effect on MAP, or affect the cardiovascular response of adenosine in the renal and mesenteric vascular beds.

The effect of the $A_{2B}$ receptor antagonist PSB 1115 (10 mg/kg) on the cardiovascular response to adenosine was investigated (**Figure 29A-B**). PSB 1115 strongly and significantly ($p<0.05$) attenuated the adenosine-induced fall in MAP at the highest dose of adenosine and also completely attenuated ($p<0.05$) the increase in VC caused by adenosine in the mesenteric vascular bed (**Figure 29A-B**). PSB 1115 partially attenuated the adenosine-induced increase in VC in the renal vascular bed, although significance ($p<0.05$) was only achieved in the minute after the cessation of dosing (**Figure 29A-B**). PSB 1115 (10 mg/kg) did not significantly affect adenosine's cardiovascular response in the hindquarters vascular bed (**Figure 29A-B**).

| | Study 5: Adenosine +- SCH 58261 | | | | Study 6: Adenosine +- PSB 1115 | | | |
|---|---|---|---|---|---|---|---|---|
| | Vehicle | | SCH 58261 | | Vehicle | | PSB 1115 | |
| | Mean ± SEM | n | Mean ± SEM | n | Mean ± SEM | n | Mean ± SEM | n |
| **Cardiovascular Variable** | **Baseline T=0** | | | | | | | |
| **Heart rate (beats·min$^{-1}$)** | 334± 7 | 8 | 341± 9 | 8 | 347± 9 | 10 | 342± 4 | 10 |
| **Mean BP (mmHg)** | 107 ± 4 | 8 | 104± 4 | 8 | 102 ± 2 | 10 | 102± 2 | 10 |
| **Renal VC (U)** | 80± 10 | 6 | 86± 15 | 6 | 88 ± 8 | 10 | 83± 5 | 10 |
| **Mesenteric VC (U)** | 91 ± 7 | 8 | 85 ± 10 | 8 | 96± 11 | 9 | 99± 9 | 9 |
| **Hindquarters VC (U)** | 49± 3 | 7 | 54± 6 | 7 | 56 ± 5 | 10 | 49± 5 | 10 |
| **Cardiovascular Variable** | **Prior to Infusion (T = 10 min†)** | | | | | | | |
| **Heart rate (beats·min$^{-1}$)** | 330± 6 | 8 | 335± 7 | 8 | 346± 8 | 10 | 353± 6 | 10 |
| **Mean BP (mmHg)** | 105± 3 | 8 | 106 ± 3 | 8 | 105 ± 2 | 10 | 110± 2 | 10 |
| **Renal VC (U)** | 82 ± 9 | 6 | 87±17 | 6 | 85± 7 | 10 | 74 ± 5 | 10 |
| **Mesenteric VC (U)** | 91± 9 | 8 | 86 ± 9 | 8 | 95± 12 | 9 | 86 ± 8 | 9 |
| **Hindquarters VC (U)** | 49± 3 | 7 | 54 ± 6 | 7 | 51 ± 4 | 10 | 47 ± 4 | 10 |

**Table 14 Cardiovascular Variables Before Administration of Adenosine $A_2$ receptor Antagonists and Before the Subsequent Administration of Adenosine.** Values are mean ± SEM; n=6-10 per group. Units (U) of vascular conductance (VC) are kHz. mmHg$^{-1}$ x $10^3$. A Wilcoxon signed-rank test was conducted between the antagonist group and its corresponding vehicle control group (* = $p<0.05$ significance). Readings correspond to the baseline recordings (zero values) for the graphs. †In some instances, agonist administration was delayed past 10 min in the case of movement to allow the rat to settle. Abbreviations: U, units; VC, vascular conductance.

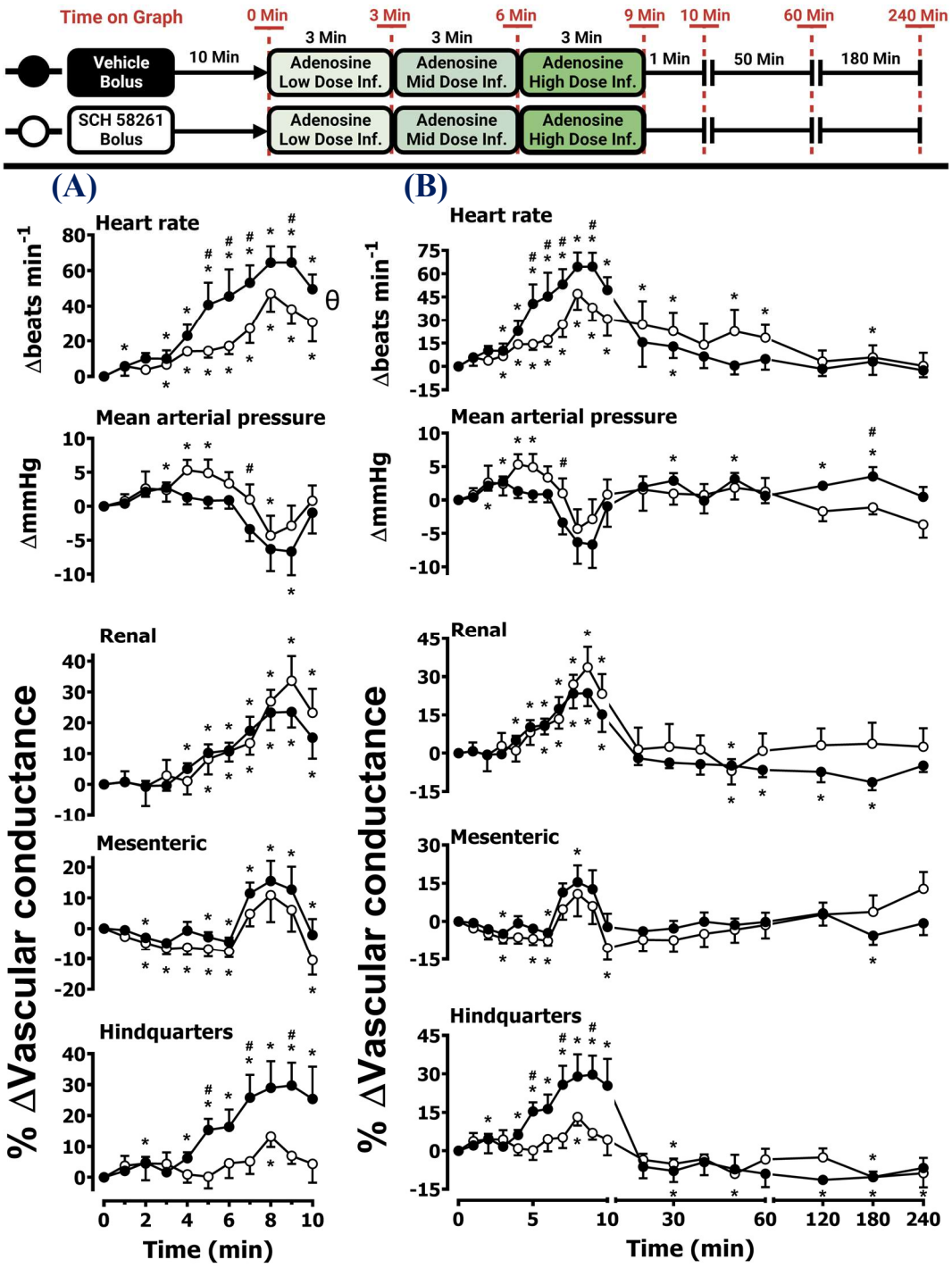


**Figure 28 Cardiovascular Responses to Adenosine in the Presence or Absence of SCH 58261.** Conscious, freely moving rats were dosed with SCH 58261 (0.1 mL bolus; 1.0 mg/kg i.v.; n=8) or vehicle (0.1 mL bolus; 5 % propylene glycol, 2 % Tween 80 in sterile saline; n=8) as described in the chapter methodology (**3.2.1**). Approximately 10 min after the bolus, all animals received an infusion of a consecutive low, medium and high dose of adenosine (30, 100, and 300 µg/kg/min, i.v.), with each dose run for 3 min. The graphs show **(A)** the adenosine treatment period, plus a minute, and **(B)** the treatment period and recording period of 4 h. Data points are mean + or - SEM. A Friedman test was conducted for each data point of each group and the group's corresponding baseline (T=0) (* = p<0.05 significance) [**(A)** & **(B)**]. A Wilcoxon signed-rank test was conducted between the two groups for a comparison of the area under the curve (**θ** = p<0.05 significance) [**(A)**], and additionally to determine differences at each time point (Wilcoxon T-test equivalent) (**#** = p<0.05 significance) [**(A)** & **(B)**]. Experiments were completed by Dr Sam Cooper and are from study 5. Baseline recordings for this figure can be found in **Table 14**.

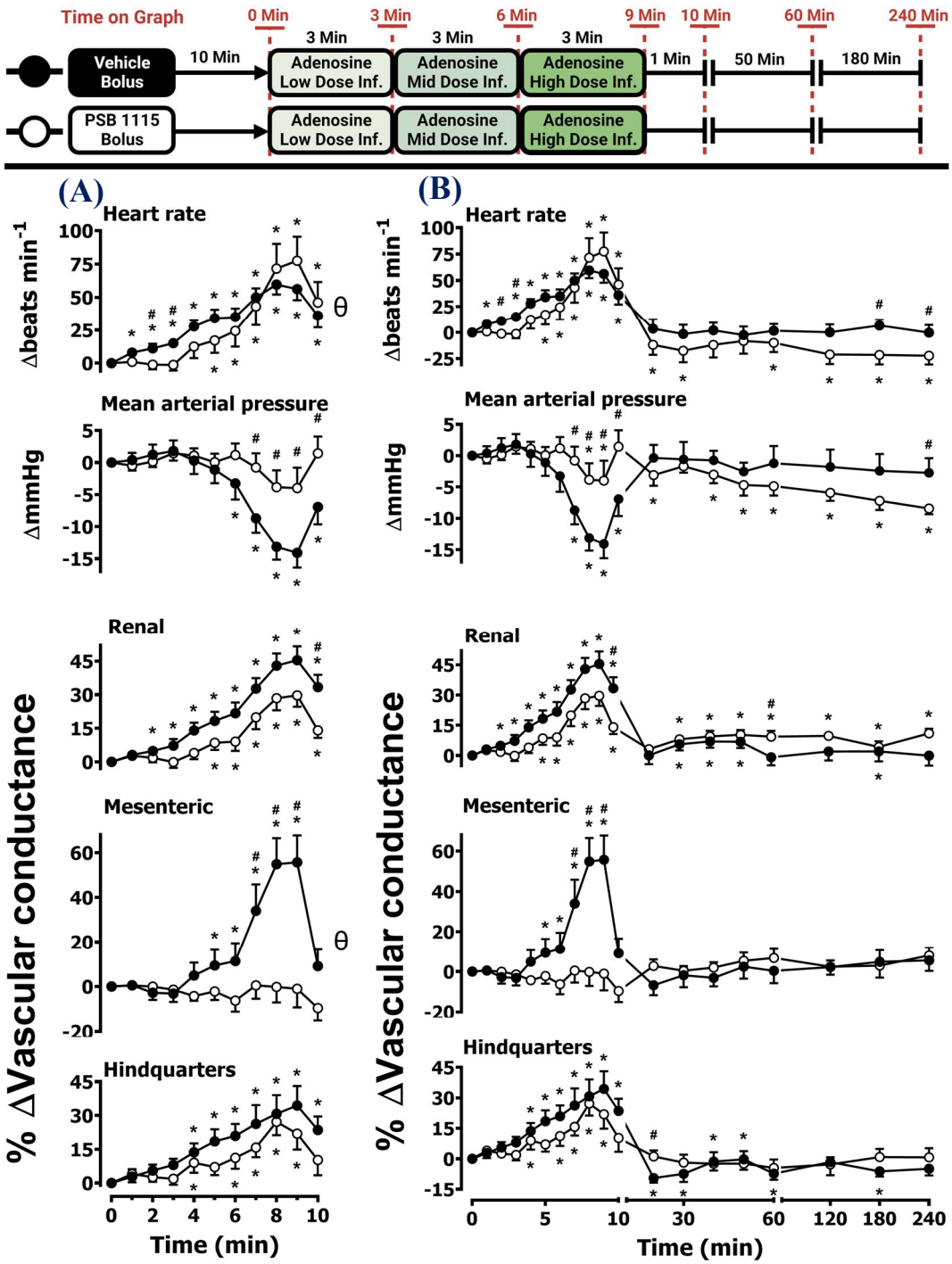


**Figure 29 Cardiovascular Responses to Adenosine in the Presence or Absence of PSB 1115.** Conscious, freely moving rats were dosed with PSB 1115 (0.1 mL bolus; 10 mg/kg i.v.; n=10) or vehicle (0.1 mL bolus; 5 % propylene glycol, 2 % Tween 80 in sterile saline; n=10) as described in the chapter methodology (**3.2.1**). Approximately 10 min after the bolus, all animals received an infusion of a consecutive low, medium and high dose of adenosine (30, 100, and 300 µg/kg/min, i.v.), with each dose run for 3 min. The graphs show **(A)** the adenosine treatment period, plus a minute, and **(B)** the treatment period and recording period of 4 h. Data points are mean + or - SEM. A Friedman test was conducted for each data point of each group and the group's corresponding baseline (T=0) (* = $p<0.05$ significance) [**(A)** & **(B)**]. A Wilcoxon signed-rank test was conducted between the two groups for a comparison of the area under the curve (**θ** = $p<0.05$ significance) [**(A)**], and additionally to determine differences at each time point (Wilcoxon T-test equivalent) (**#** = $p<0.05$ significance) [**(A)** & **(B)**]. Results are from study 6. Baseline recordings for this figure can be found in **Table 14**.

## 3.3.2 Chapter 3 Results: *In Vitro*

### 3.3.2.1 Study α (Part 1): Rat $A_2$ Receptor Ligand Affinity

#### 3.3.2.1.1 The Measurement of the Specific Binding of CA200645 to Rat $A_{2A}$ and $A_{2B}$ Receptors

Saturation binding analysis using increasing concentrations of the fluorescent ligand CA200645 showed specific binding to the NLuc-tagged rat $A_{2A}$ receptor and $A_{2B}$ receptor ($pK_D$ for CA200645: rat NLuc-$A_{2A}$ receptor = 7.02 ± 0.03; rat NLuc-$A_{2B}$ receptor = 7.43 ± 0.03) (**Figure 30A-B**, **Table 15**). The levels of non-specific binding observed (across the range of concentrations of CA200645 used) in the presence of a robust blockade of the tagged receptor by SCH 58261 ($10^{-5}$ M) for NLuc-$A_{2A}$ receptor and PSB 603 ($10^{-5}$ M) for NLuc-$A_{2B}$ receptor were low, confirming that the BRET effects observed for these experiments were explicitly caused by binding to the NLuc-tagged receptor under investigation (**2.2.5.3**).

#### 3.3.2.1.2 Competitive Inhibition of CA200645 at Rat $A_{2A}$ and $A_{2B}$ Receptors.

The binding affinities to rat NLuc-$A_{2A}$ or NLuc-$A_{2B}$ receptors were determined for non-fluorescent ligands by competitive inhibition of the specific binding of 50 nM CA200645 to the receptor by increasing concentrations of six ligands: Adenosine, PSB 603, CGS 21680, SCH 58261, BAY 60-6583 and PSB 1115 (**Figure 31A-F**). The use of the previously calculated $pK_D$ values for CA200645 at each receptor (**Table 15**, **3.3.2.1.1**), the CA200645 concentration of 50 nM and the $IC_{50}$ values obtained from these experiments allowed the calculation of $pK_i$ values for these ligands at the tagged receptors using the Cheng-Prusoff equation (**Table 15, 2.2.5.3.2**).

The results from these studies indicated that CGS 21680 was selective for the rat NLuc-$A_{2A}$ receptor over the NLuc-$A_{2B}$ receptor up to the maximum concentration investigated ($10^{-4}$ M) (**Figure 31C**, **Table 15**). BAY 60-6583 was selective for the rat NLuc-$A_{2B}$ receptor at concentrations up to $10^{-5}$ M; however, at $10^{-4}$ M BAY 60-6583, there was an attenuation of binding to the NLuc-$A_{2A}$ receptor (**Figure 31E**). Adenosine, PSB 603, SCH 58261 and PSB 1115 all displaced specific CA200645 binding at both rat $A_2$ receptors (**Figure 31A,B,D,F**). As anticipated, adenosine had a moderately higher affinity for the NLuc-$A_{2A}$ receptor than the NLuc-$A_{2B}$ receptor (**Figure 31A**, **Table 15**). Also, as expected, SCH 58261 had a much higher affinity for the NLuc-$A_{2A}$ receptor than the NLuc-$A_{2B}$ receptor, and the reverse was true for PSB 603 (**Figure 31B**, **Table 15**). PSB 1115 had a much lower affinity for the NLuc-$A_{2B}$ receptor than PSB 603 but still demonstrated some selectivity for the NLuc-$A_{2B}$ receptor over the NLuc-$A_{2A}$ receptor (**Figure 31F**, **Table 15**).

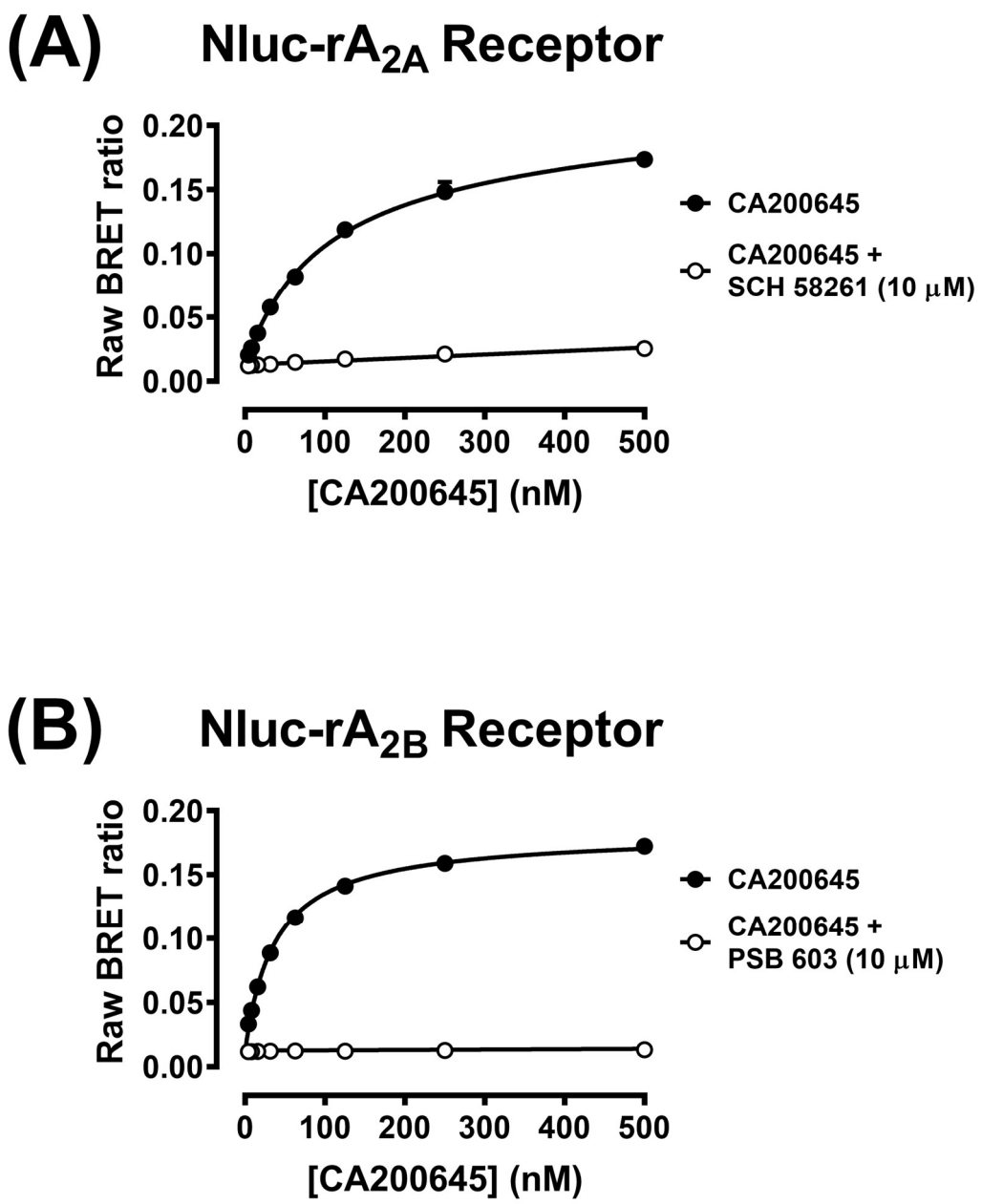


**Figure 30 Saturation Binding of Increasing Concentrations of CA200645.** HEK 293T cells were transiently transfected with **(A)** rat NLuc-$A_{2A}$ receptor or **(B)** rat NLuc-$A_{2B}$ receptor, in the absence (black circles) or presence (white circles) of the adenosine receptor antagonists **(A)** SCH 58261 (10 µM) or **(B)** PSB 603 (10 µM) to define non-specific binding for each transfected receptor. All ligands were added simultaneously to triplicate well replicates and incubated for 120 min at 37°C. Data are presented as raw BRET ratios. Graphical values represent mean ± SEM of five independent experiments (n=5). Calculated $pK_D$ values from these experiments are shown in **Table 15**.

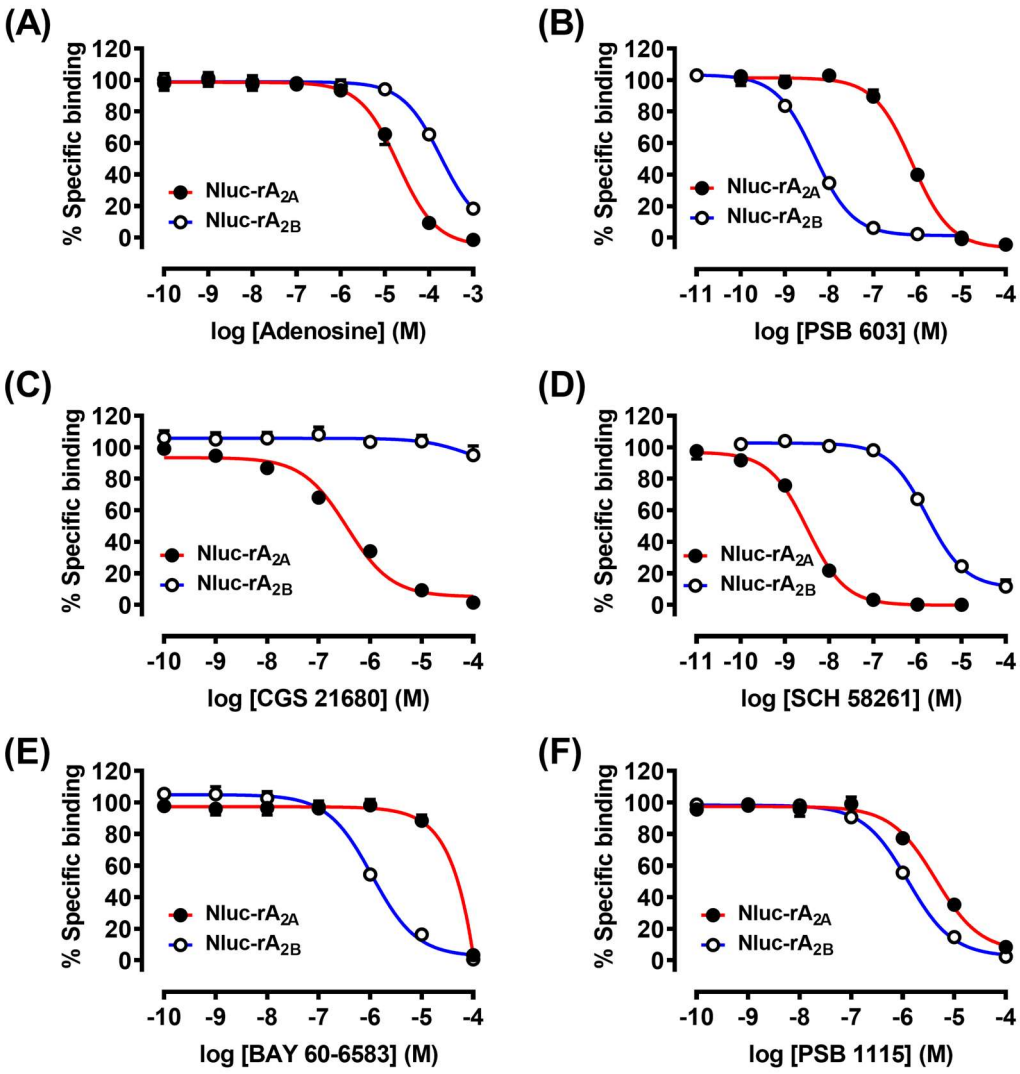


**Figure 31 Inhibition of the Binding of CA200645 (50 nM) to NanoLuc-tagged Rat-$A_{2A}$ or Rat $A_{2B}$ Receptors by Increasing Concentrations of Competitor Ligands.** Rat NLuc-$A_{2A}$ or NLuc-$A_{2B}$ receptors were transiently transfected into HEK 293T cells. CA200645 and inhibitors were added simultaneously to triplicate well replicates and incubated for 120 min at 37°C. Graphical values represent mean ± SEM of five independent experiments. Data are expressed as a percentage of the specific binding of 50 nM CA200645 obtained in each experiment. Calculated $pK_i$ values from these experiments are shown in **Table 15**.

| Ligand | NLuc-rat $A_{2A}$ receptor ($pK_D$ or $pK_i$) | n | NLuc-rat $A_{2B}$ receptor ($pK_D$ or $pK_i$) | n |
|---|---|---|---|---|
| **CA200645** | 7.02 ± 0.03 | 5 | 7.43 ± 0.03 | 5 |
| **Adenosine** | 4.88 ± 0.10 | 5 | 4.08 ± 0.07 | 5 |
| **PSB 603** | 6.31 ± 0.07 | 5 | 8.70 ± 0.03 | 5 |
| **CGS 21680** | 6.63 ± 0.04 | 5 | n/a | 5 |
| **SCH 58261** | 8.67 ± 0.08 | 5 | 6.15 ± 0.05 | 5 |
| **BAY 60-6583** | n/a | 5 | 6.33 ± 0.03 | 5 |
| **PSB 1115** | 5.54 ± 0.03 | 5 | 6.27 ± 0.04 | 5 |

**Table 15 Calculated Binding Affinities of Six Competing Ligands as Determined by Inhibition of the Specific Binding of 50 nM CA200645 at the Rat NLuc-$A_{2A}$ and NLuc-$A_{2B}$ Receptors Expressed in HEK 293T Cells.** Data are expressed as mean ± SEM from five separate experiments (n=5) performed with triplicate well repeats. $pK_D$ values for CA200645 were determined from saturation binding experiments. $pK_i$ values were determined from $IC_{50}$ values using the Cheng-Prusoff equation.

## 3.3.2.2 Study β: cAMP Accumulation Assays

### 3.3.2.2.1 BAY 60-6583 Affects Functional Responses to CGS 21680 and Formoterol

The results of the binding affinity experiments showed that BAY 60-6583 was selective for the NLuc-$A_{2B}$ receptor at concentrations up to $10^{-5}$ M; however, at $10^{-4}$ M, there was binding to the NLuc-$A_{2A}$ receptor (**3.3.2.1.2**). Therefore, to further investigate the actions of BAY 60-6583 at high concentrations, its effect on agonist responses to $A_{2A}$ receptors, $A_{2B}$ receptors and $\beta_2$ adrenoceptors in HEK 293 cells expressing the Glosensor cAMP biosensor (HEK 293G) were studied (**2.2.7.2**). It has been previously shown that CGS 21680 and BAY 60-6583 cause cAMP responses that are selectively mediated via endogenous human $A_{2A}$ and $A_{2B}$ receptors, respectively, in HEK 293G cells (Goulding et al., 2018). Therefore, experiments were run exploring the effect of an increasing dose of CGS 21680 and BAY 60-6583 in native HEK 293G cells and those transfected with the NLuc-rat $A_{2A}$ receptors to have both endogenous human adenosine receptors and overexpressed rat NLuc-$A_{2A}$ receptors (**Figure 32**). A similar cAMP response was observed in both the native and rat NLuc-$A_{2A}$ receptor transfected HEK 293G cells, and this response was similar to results reported previously in native HEK 293G cells in the literature (**Figure 32A-B**) (Goulding et al., 2018). In the native cell line, CGS 21680 had a $pEC_{50}$=6.7, and BAY 60-6583 had a $pEC_{50}$=6.9 (**Figure 32B**). In the rat NLuc-$A_{2A}$ receptor transfected HEK 293G cells, CGS 21680 had a $pEC_{50}$= 7.5, and BAY 60-6583 had a $pEC_{50}$=7.4 (**Figure 32A**).

However, it was notable that at $10^{-4}$ M BAY 60-6583, there was a marked drop in response to this agonist in both the native and rat NLuc-$A_{2A}$ receptor transfected HEK 293G cells (**Figure 32A-B**).

As a similar effect was observed in both transfected and non-transfected cells, and because there was the presence of raised basal levels of the cAMP signal in the rat NLuc-$A_{2A}$ receptor expressing HEK G cells, likely due to constitutive activation of this receptor in this cell line (**Figure 32B**), further experiments were carried out exclusively on the native HEK 293G cell line.

With 2 h pretreatment of the $A_{2B}$ receptor-selective antagonist PSB 603 ($10^{-7}$ M), the response to an $A_{2A}$ receptor mediated CGS 21680 response was attenuated by simultaneous treatment with either BAY 60-6583 ($10^{-4}$ M) or the $A_{2A}$ receptor antagonist SCH 58261 ($10^{-5}$ M), suggesting BAY 60-6583 was acting as an $A_{2A}$ receptor antagonist (**Figure 32C**). However, the inhibitory effect of BAY 60-6583 ($10^{-4}$ M) was shown to be non-specific as BAY 60-6583 ($10^{-4}$ M) similarly affected cAMP responses to the $\beta_2$ receptor agonist formoterol (**Figure 32D-E**), but this was not the case with the $A_{2A}$ receptor antagonist SCH 58261 ($10^{-5}$ M), which had no significant effect on the response to formoterol (**Figure 32F**).

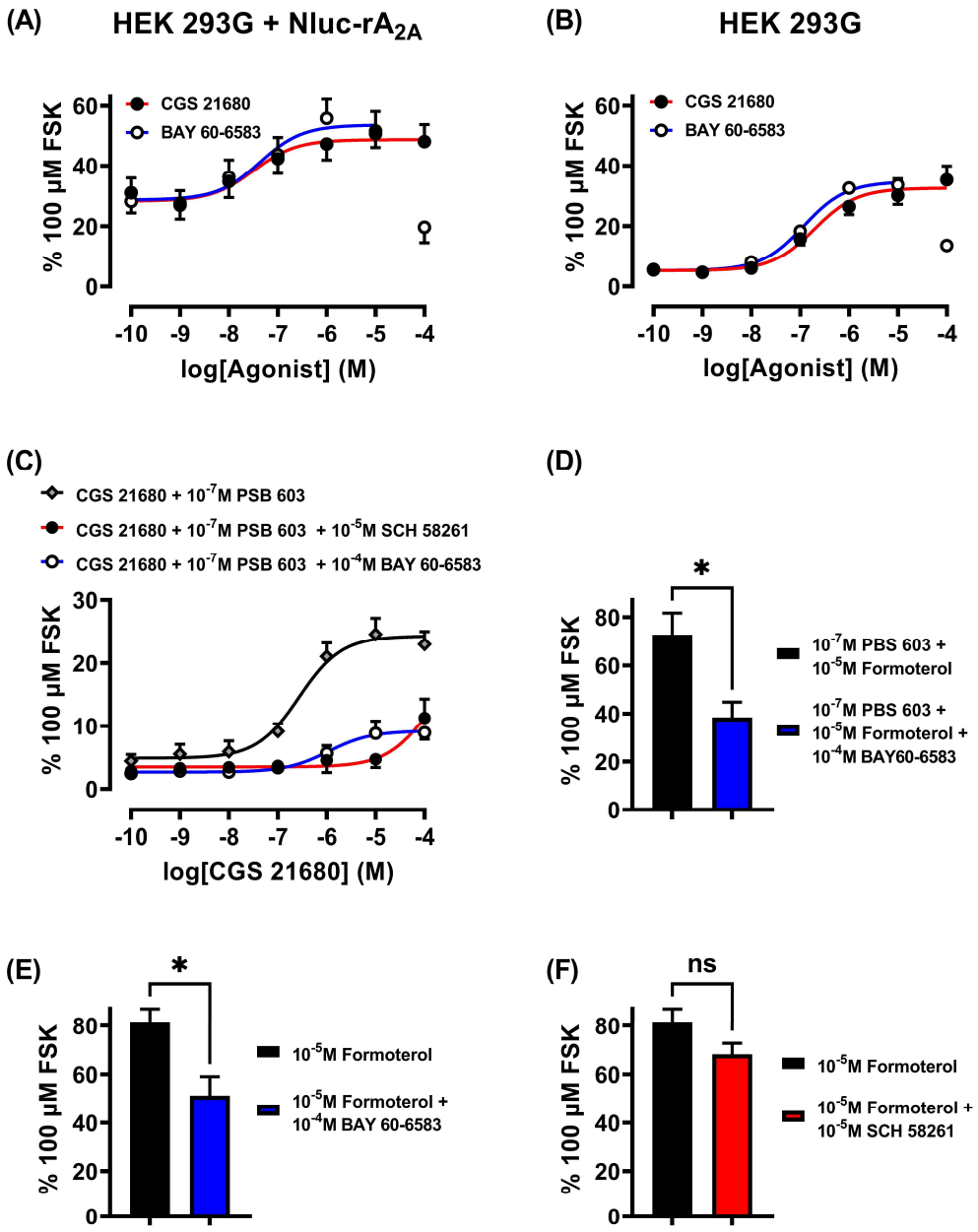


**Figure 32 Glosensor cyclic AMP Responses to CGS 21680 and BAY 60-6583 in HEK 293G Cells.** [**(A)**,**(B)**] concentration-response curves for agonist-stimulated Glosensor cAMP luminescence responses in **(A)** HEK 293G cells transfected with the NLuc-rat $A_{2A}$ receptor and **(B)** HEK 293G cells, in response to CGS 21680 and BAY 60-6583. **(C)** The effect of simultaneous addition of BAY 60-6583 ($10^{-4}$ M) or SCH 58261 ($10^{-5}$ M) on the concentration-response curve to CGS 21680, following 2 h pretreatment with PSB 603 ($10^{-7}$ M) in HEK 293G cells. [**(D)**,**(E)**] The effect of simultaneous addition of BAY 60-6583 ($10^{-4}$M) on the response to formoterol ($10^{-5}$ M) in the presence **(D)** or absence **(E)** of a 2 h pretreatment with PSB 603 ($10^{-7}$ M). **(F)** The effect of simultaneous addition of SCH 58261 ($10^{-5}$ M) on the response to 10 µM formoterol. Data represent mean + or - SEM of the peak luminescence response from 5 separate experiments (n=5), each carried out in triplicate well repeats, with data normalised as a percentage of the peak luminescence response obtained with 100 µM forskolin (FSK) control response in the absence of other agents, measured on the same experimental plate. [**(D),(E),(F)**] an unpaired T-test was performed between groups (* = $p<0.05$ significance).

# 3.4 Haemodynamic Responses to Adenosine $A_2$ Receptor Agonism: Chapter Discussion

In this chapter, the haemodynamic consequences of activating adenosine $A_{2A}$ and $A_{2B}$ receptors on vascular conductance in renal, mesenteric and hindquarter vascular beds were investigated in conscious, freely moving rats.

In competition binding studies, CGS 21680 was shown to have affinity for the rat NLuc-$A_{2A}$ receptor ($pK_i$ 6.63), whereas CGS 21680 did not directly bind to rat NLuc-$A_{2B}$ receptors, even at high concentrations of the ligand up to 100 µM, confirming its selectivity for the rat $A_{2A}$ receptor. Previous radioligand studies have reported a similar $pK_i$ for CGS 21680 in the rat striatum ($pK_i$ 6.95) (Zocchi et al., 1996). Additionally, CGS 21680 was confirmed to produce a dose-dependent cAMP response in both native HEK 293T cells and those additionally expressing the rat NLuc-$A_{2A}$ receptor. Together, these *in vitro* results confirm that CGS 21680 is a rat $A_{2A}$ receptor-selective agonist, as previously demonstrated in the literature (Alnouri et al., 2015). Also, the antagonist SCH 58261 was confirmed to be selective for the rat NLuc-$A_{2A}$ receptor over the rat NLuc-$A_{2B}$ receptor ($pK_i$ $A_{2A}$ receptor: 8.67; $pK_i$ $A_{2B}$ receptor: 6.15); a similar $pK_i$ value was reported for the $A_{2A}$ receptors found in the rat striatum ($pK_i$ 8.96) (Zocchi et al., 1996).

It is of note that for the competition binding studies, a 2 h incubation time was used to allow ligands to equilibrate to the receptor to negate the effects of ligand-receptor kinetics on the final result. However, this long incubation time might have effected the results, as receptor signalling may have caused dynamic changes to the receptor throughout the incubation, especially in response to agonists, which may cause receptor phosphorylation via PKA, or internalisation via β-Arrestins (Klaasse et al., 2008).

CGS 21680 produced large and significant increases in HR and hindquarters VC, indicative of vasodilatations in this vascular bed, but only minor increases in VC in the renal and mesenteric vascular beds. A significant decrease in MAP accompanied these effects. The effects of CGS 21680 on HR, hindquarters VC and MAP were entirely attenuated by the $A_{2A}$ receptor antagonist SCH 58261. The effects of CGS 21680 were also investigated in the presence of the $A_{2B}$ receptor antagonist PSB 1115. PSB 1115 partially inhibited the HR and hindquarters response produced by CGS 21680. However, in competition binding studies, PSB 1115 was shown to have only limited selectivity for the rat NLuc-$A_{2B}$ receptor over the rat NLuc-$A_{2A}$ receptor ($pK_i$ $A_{2B}$ receptor: 6.13; $pK_i$ $A_{2A}$ receptor: 5.54), this is similar to results seen previously for rat $A_2$ receptors in a radioligand binding study ($pK_i$ $A_{2A}$ receptor: 4.61; $pK_i$ $A_{2B}$ receptor: 5.50) (Alnouri et al., 2015). Because of this result, it is likely that the attenuation caused by PSB 1115 on the CGS 21680 response was due to the antagonism of $A_{2A}$ receptors by PSB 1115. Unfortunately, solubility issues prevented the use of the highly selective $A_{2B}$ receptor antagonist PSB 603 in these *in vivo* experiments (Borrmann et al., 2009, Alnouri et al., 2015). For future *in vivo* experiments, novel selective $A_{2B}$ receptor antagonists with subnanomolar or even picomolar potency (that were not available when these experiments were undertaken), such as PSB 1901, could potentially be utilised to provide selective antagonism of the $A_{2B}$ receptor (Jiang et al., 2019, Prieto-Díaz et al., 2023).

The results of this chapter are in agreement with other *in vivo* studies showing that $A_{2A}$ receptor activation in rats causes a reduction in MAP (Alberti et al., 1997, Dhalla et al., 2006) and studies involving $A_{2A}$ receptor knock-out mice, which are known to be hypertensive, demonstrating an important role for the $A_{2A}$ receptor in blood pressure regulation (Ledent et al., 1997). In addition, this current research on the effects of CGS 21680 also agrees with a previous *in vivo* study demonstrating that the $A_{2A}$ receptor can cause vasodilation in the hindquarter vascular beds (Bryan and Marshall, 1999).

In competition binding studies, BAY 60-6583 was shown to have an affinity for the rat NLuc-$A_{2B}$ receptor (pKi 6.33) and did not affect NLuc-$A_{2A}$ receptor binding of the fluorescent antagonist CA200645 (50 nM) up to 10 μM. This result was also the case in a ligand binding study in the literature, which showed no binding to rat $A_{2A}$ receptors up to 10 μM, and an $A_{2B}$ receptor binding of $pK_i$ 7.0 (Alnouri et al., 2015). However, at the highest concentration of 100 μM, the binding of CA200645 to the rat $A_{2A}$ receptor was entirely attenuated by BAY 60-6583. To interrogate this result, Glosensor assays were conducted to assess the cAMP response in both native HEK 293T cells and those expressing the rat NLuc-$A_{2A}$ receptor, where it was demonstrated that 100 μM BAY 60-6583 causes a decrease in the cAMP response compared to 10 μM BAY 60-6583, and the higher dose was capable of blocking a dose-dependent cAMP response to CGS 21680. This effect was likely due to a non-specific effect on the cells; however, since 100 μM BAY 60-6583 additionally attenuated the cAMP response to the $\beta_2$ agonist formoterol.

BAY 60-6583 significantly increased HR as well as renal and mesenteric VC but caused no change to hindquarters VC. BAY 60-6583 caused little change to MAP. The cardiovascular responses caused by BAY 60-6583 were attenuated by the $A_{2B}$ receptor antagonist PSB 1115 but were not affected by the $A_{2A}$ receptor selective antagonist SCH 58261. These results confirm that $A_{2B}$ receptors mediated the effects of BAY 60-6583 and not $A_{2A}$ receptors.

These results indicate that the regulation of vascular tone by $A_{2A}$ and $A_{2B}$ receptors is regionally selective to the vascular beds in which each receptor exerts its effect. It has been shown that $A_{2A}$ receptors, and not the $A_{2B}$ receptor, mediate vasodilatation in the hindquarters, but the $A_{2B}$ receptor has a much more significant role in mediating VC in renal and mesenteric vascular beds than the $A_{2A}$ receptor.

In this chapter, adenosine produced a dose-dependent increase in HR, alongside increases in renal, mesenteric and hindquarters VC that were accompanied by a significant decrease in MAP. This cardiovascular response was the same as what was found previously by Cooper *et al.* (Cooper et al., 2020).

In the presence of the $A_{2A}$ receptor antagonist SCH 58261, the vasodilatory response to adenosine in the hindquarters was almost entirely attenuated, suggesting that the hindquarters vasodilation caused as a result of adenosine administration was almost entirely due by $A_{2A}$ receptor activation. In addition, SCH 58261 also moderately attenuated the increase in HR due to adenosine administration and slightly attenuated the fall in MAP associated with adenosine, consistent with $A_{2A}$ receptor activation influencing both of these cardiovascular responses. However, SCH 58261 did not affect the adenosine-induced cardiovascular response in the renal and mesenteric vascular beds, showing that the $A_{2A}$ receptor was not responsible for the increase in VC in these beds; with this result fitting in with the results seen previously for CGS 21680.

The effect of the $A_{2B}$ receptor antagonist PSB 1115 on the cardiovascular response to adenosine was also investigated at a dose previously demonstrated to also partially block the $A_{2A}$ receptor. PSB 1115 completely attenuated the adenosine-induced increase in VC in the mesenteric vascular bed, which along with the lack of attenuation at this bed by SCH 58261, is evidence that the $A_{2B}$ receptor causes the increase in mesenteric VC. Evidence of the low-affinity $A_{2B}$ receptor's role at the mesenteric bed is that increases in VC are only seen at the highest dose of adenosine; when, in contrast, increases in the hindquarters VC, which are the high-affinity $A_{2A}$ receptor-mediated, are observed much earlier.

PSB 1115 only slightly attenuated adenosine's cardiovascular response in the hindquarters vascular bed, indicating a minor $A_{2A}$ receptor blockade by this dose of PSB 1115. Interestingly, PSB 1115 only partially attenuated the adenosine-induced increase in VC in the renal vascular bed, demonstrating only partial involvement of the $A_{2B}$ receptor in this response. It has been demonstrated that the increase in VC in the renal vascular bed due to adenosine administration is thus not due to $A_1$ (Cooper et al., 2020) or $A_{2A}$ receptor activation and is only partially related to $A_{2B}$ receptor agonism. Another interesting result is that PSB 1115 strongly and significantly attenuated the adenosine-induced fall in MAP, whereas the $A_{2B}$ receptor agonist BAY 60-6583 was shown not to cause a decrease in MAP on its own.

Overall, the result of this chapter shows that activation of $A_{2A}$ or $A_{2B}$ receptors both cause an increase in HR, but only activation of the $A_{2A}$ receptor causes a fall in MAP. In addition, adenosine administration also caused a tachycardic response that was partially blocked by $A_{2A}$ receptor antagonism. Previously in the literature,

it has been demonstrated that the tachycardia in the heart following $A_{2A}$ receptor agonism is due to the stimulation of the sympathetic nervous system and appears to have components caused directly by the instigation of homeostatic reflexes activated by a dip in blood pressure caused by the vasodilatory effects of the $A_{2A}$ receptor (Alberti et al., 1997, Nekooeian and Tabrizchi, 1998, Dhalla et al., 2006). It has also been shown that the activation of $A_{2A}$ receptors in the central nervous system directly stimulate these responses, causing the release of catecholamines leading to a tachycardic response in the heart (Alberti et al., 1997, Nekooeian and Tabrizchi, 1998, Dhalla et al., 2006). Additionally, adenosine has been demonstrated to activate afferent nerve terminals in the heart and kidney, which lead to sympathetic activity (Katholi et al., 1984, Cox et al., 1989).

The $A_{2A}$ receptor response seen in this chapter causes an increase in HR and a fall in MAP, which is directly proportional to the $A_{2A}$ receptor-mediated vasodilation response in the hindquarters vascular bed, suggesting that indirect activation of the sympathetic nervous system might be the cause of the rise in HR due to a drop in MAP. On the other hand, the increases in renal and mesenteric VC induced by $A_{2B}$ receptor activation were not accompanied by a change in MAP, which could suggest that the increase in HR caused by $A_{2B}$ receptor activation could be a result of direct activation of the sympathetic nervous system. Investigations into the role of sympathetic activation on the cardiovascular responses to $A_{2A}$ and $A_{2B}$ receptor activation are conducted in the next chapter of this thesis (**4.1**).

In the literature, adenosine has been shown to cause increases in superior mesenteric arterial conductance in anesthetised cats using electromagnetic flowmetry (**2.1.1.2.1**) (Zhang et al., 1991), and $A_{2A}$ receptor activation has been demonstrated to cause vasodilation in isolated rat mesenteric arterial beds (Hiley et al., 1995). $A_{2B}$ receptor activation has also been reported to cause vasodilation in the arteries comprising the mesenteric arterial bed (Rubino et al., 1995, Tabrizchi and Lupichuk, 1995, Teng et al., 2013). It has been demonstrated that rat *in vivo* mesenteric vascular flow is increased by the administration of adenosine and the non-selective adenosine receptor agonist NECA (Gardiner et al., 1991, Jolly et al., 2008, Cooper et al., 2020). From the results of this chapter, it has been demonstrated that the $A_{2B}$ receptor is responsible for the $A_2$ receptor increase previously observed in the mesentery, with the $A_{2A}$ receptor only having a minor role.

In the literature, adenosine has been observed to cause vasodilation in renal vascular beds (Arend et al., 1985, Spielman and Arend, 1991, Cooper et al., 2020). In addition, the activation of $A_2$ receptors in renal vasculature are known to cause vasodilation (Tang et al., 1999). $A_{2B}$ receptor activation has previously been demonstrated to be the primary driver of this $A_2$ receptor vasodilation in the afferent arterioles, with $A_{2A}$ receptors shown to be present but only having a minor role in the functional vasodilatory response (Martin and Potts, 1994, Feng and Navar, 2010, El-Gowelli et al., 2013). In addition, the $A_{2B}$ receptor has been shown to increase renal blood flow, which can protect the kidney from ischaemic reperfusion injury (Grenz et al., 2008, Rabadi and Lee, 2015). The results from this chapter agree with the previous literature, suggesting that the $A_{2B}$ receptor has a major role in regulating renal vascular flow, but the $A_{2A}$ receptor only has a minor role.

Alongside renovascular dilation, $A_2$ receptors are known to cause increased renin secretion, which will subsequently lead to vasoconstrictor effects caused by angiotensin II release (Holz and Steinhausen, 1987, Churchill and Bidani, 1987, Rabadi and Lee, 2015); this may counteract decreases in MAP caused by $A_2$ receptor activation, which alongside an increase in HR, might explain why $A_{2B}$ receptor activation did not lead to a decrease in MAP.

The results of this study confirm that $A_{2A}$ receptors agonists are good candidates for treating hypertension, especially hypertension associated with vasoconstrictions in hindquarter vascular beds, which is discussed further in chapter 5 (**5.1**) (Jacobson and Gao, 2006, Jamwal et al., 2019). In addition, the results of this research also add to evidence that the development of $A_{2B}$ receptor agonists could provide an excellent therapeutic approach for treating mesenteric ischemia and acute kidney injury (Hart et al., 2009, Rabadi and Lee, 2015). The potential implications of this chapter's research are discussed further in the thesis discussion (**6.1**).

# 4 Chapter 4: β adrenoceptor Influence on the Haemodynamic Responses to Adenosine $A_{2A}$ and $A_{2B}$ Receptor Agonists

# 4.1 β-adrenoceptor Influence on $A_{2A}$ & $A_{2B}$ Receptor Agonist Responses: Introduction

$A_{2A}$ and $A_{2B}$ receptors in the cardiovascular system are important in regulating the heart and modulating blood pressure as they have a crucial role in regulating the vascular tone of the coronary and systemic vasculature (Lewis et al., 1994, Shryock et al., 1998, Leal et al., 2008, Mustafa et al., 2009, Berwick et al., 2010). As previously discussed, targeting $A_{2A}$ and $A_{2B}$ receptors has potential therapeutic benefits for many cardiovascular diseases, including acute kidney injury and hypertension (**1.1.6.2**) (Yap and Lee, 2012, Borea et al., 2018, Jamwal et al., 2019).

In **chapter 3**, *in vivo* evaluation of the cardiovascular effects of the selective $A_{2A}$ receptor agonist CGS 21680 and the selective $A_{2B}$ receptor agonist BAY 60-6583 in conscious, freely moving rats showed that $A_{2A}$ and $A_{2B}$ receptors exert selective control of VC in different regions of the body. $A_{2A}$ receptor stimulation was shown to cause profound increases in VC in the hindquarters vascular bed but have minimal impact on the renal and mesenteric vasculature beds, whereas $A_{2B}$ receptor stimulation was shown to increase renal and mesenteric VC but have no effect on the VC of the hindquarters vascular bed.

Additionally, in these *in vivo* studies, the activation of either the $A_{2A}$ (**3.3.1.3.1**) or $A_{2B}$ (**3.3.1.4.1**) receptor resulted in tachycardia. It has been shown that $A_{2A}$ receptor activation in Langendorff rat heart preparations does not cause a change in HR (Hutchison et al., 1989). Similarly, evidence from *ex vivo* studies and anesthetised rats show that activation of $A_{2B}$ receptors appears to cause minimal direct physiological effects to HR (Liu et al., 2010, Maas et al., 2010), suggesting that $A_2$ receptors on the heart are not the direct cause of the observed increase in HR due to the administration of CGS 21680 or BAY 60-6583.

It is known from research in both conscious and anaesthetised rats that $A_{2A}$ receptor-induced tachycardia is caused by stimulation of the sympathetic nervous system associated with noradrenaline release, which can be blocked by ganglionic inhibition, indicative of the involvement of the autonomic nervous system in mediating this response (Nekooeian and Tabrizchi, 1996, Alberti et al., 1997, Dhalla et al., 2006).

The baroreflex is an autonomic reflex mechanism that has a critical role in modulating blood pressure (**1.2**) (Kougias et al., 2010). The continuous sensation of pressure by tonic arterial baroreceptors in the carotid sinus and the aortic arch allows the baroreflex to exert a rapid influence on blood pressure by inducing changes in HR and peripheral vascular resistance (**1.2**) (Kougias et al., 2010). The neural control of the baroreflex is conducted by the NTS, a region in the brainstem that processes cardiovascular afferent inputs (**1.2**). An acute fall in blood pressure will cause an increase in sympathetic activity via the baroreflex (**1.2**). The physiological cardiovascular responses to sympathetic activation are a consequence of the interaction between catecholamines (principally noradrenaline and adrenaline) and adrenoceptors (principally $\beta_1$ and $\beta_2$ adrenoceptors) (**1.2.1**).

As detailed above, a fall in blood pressure can activate the sympathetic nervous system. Alternatively, it can also be influenced by direct activation of the NTS or indirectly by influencing other neuronal regions that regulate the NTS (**1.2**). Regarding $A_{2A}$ and $A_{2B}$ receptors, there is evidence of $A_{2A}$ receptor involvement in the control of baroreflex activity by direct modulation of the output of the NTS by these receptors (El-Mas et al., 2011), as well as $A_{2B}$ receptor involvement in regulating the posterior hypothalamus, which is a region that influences the NTS (**1.2.2**) (Lee and Koh, 2009).

Although it is known through studies using non-specific β receptor antagonists that $A_{2A}$ receptor activation causes tachycardia via indirect β receptor activation (Alberti et al., 1997, Dhalla et al., 2006), currently, it is unknown what the specific influence of the separate $\beta_1$ and $\beta_2$ receptors have on this response. Also, it is yet to be determined if the tachycardia observed as a consequence of $A_{2B}$ receptor activation is a result of a similar physiological response to that observed with $A_{2A}$ receptor activation or if this tachycardia is due to a different, unrelated physiological process. Finally, it is unknown what influence the release of catecholamines via an increase in reflex-mediated sympathetic activity has on the cardiovascular response observed in regional vascular beds by either $A_{2A}$ or $A_{2B}$ receptor activation.

To investigate the contribution of $\beta_1$ and $\beta_2$ adrenoceptors to the cardiovascular response induced by selective $A_{2A}$ and $A_{2B}$ receptor agonism, a $\beta_1$-selective antagonist (CGP 20712A) (Baker et al., 2011, Baker et al., 2017), a $\beta_2$-selective antagonist (ICI 118,551) (Baker et al., 2011, Baker et al., 2017) and a non-selective β antagonist (propranolol) (Gardiner and Bennett, 1988, Janssen et al., 1991) were used to assess the extent to which the positive chronotropic and vasodilatory effects induced by CGS 21680 and BAY 60-6583 resulted from an increase in β receptor-mediated sympathetic activity. To complement these experiments, *in vitro* NanoBRET competition binding assays were completed using the fluorescent ligand CA200645 to confirm that the β antagonists used do not directly bind to rat $A_{2A}$ or $A_{2B}$ receptors, and thus any changes to the cardiovascular profile of the $A_{2A}$ or $A_{2B}$ receptor agonists was due to secondary activation of β receptors and not due to off-target binding of these compounds to $A_{2A}$ or $A_{2B}$ receptors.

# 4.2 β-adrenoceptor Influence on $A_{2A}$ & $A_{2B}$ Receptor Agonist Responses: Methodology

## 4.2.1 Chapter 4 Methodology: *In Vivo*

### 4.2.1.1 Animals and Surgery

Experiments were carried out on Male Sprague-Dawley rats with approval from the UK Home Office and the University of Nottingham, as previously described (**2.1.5**). Full details of the two surgeries conducted for these experiments can be found in the general methodology (**2.1.5.1**, **2.1.5.2**). In brief, fifty-three rats (350-450 g) were used during the studies detailed in this chapter. The first surgery was conducted to implant miniature pulsed Doppler flow probes around the superior mesenteric and left renal arteries and the descending abdominal aorta to allow haemodynamic measurements that give information regarding the flow of blood to downstream regional vascular beds (**2.1.3.2**). A second surgery was carried out a minimum of 10 days after the implantation of the vascular probes. During this second surgery, a catheter was implanted via the caudal artery into the distal abdominal aorta to measure arterial blood pressure and allow the calculation of heart rate (Gardiner et al., 1980). In addition, three catheter lines were implanted into the right jugular vein to allow i.v. administration of compounds. The probe wires and catheters were protected inside a metal spring secured to a harness that went around the rat's torso, with the spring connected to a counterbalanced pivot system that allowed free movement of the rat (**Figure 12**). Experiments began 24 h after the second surgery, with the rats conscious and unrestrained, singly housed in home cages with access to food and water.

#### 4.2.1.2 Cardiovascular Recordings & Data Analysis

Detailed information on the cardiovascular recordings and data analysis can be found in the general methodology (**2.1.6**, **2.1.7**, **2.1.8**). In brief, rats were indirectly connected to the data acquisition programme (IdeeQ) during the monitoring periods via a tether system (**2.1.3**). Recordings were made for at least 30 min prior to the administration of any interventions and continuously for a minimum of 4 h thereafter. HR, MAP, renal, mesenteric and hindquarters Doppler shifts were measured (**2.1.3.1**, **2.1.3.2**), and changes in VC in the renal, mesenteric, and hindquarter vascular beds were calculated from the changes in MAP and Doppler shift (**2.1.3.3**). For all studies, time-averaged data are shown as variation from baseline [HR (beats.min$^{-1}$); MAP (mmHg); VC (%)].

A Friedman test was used for within-group comparisons compared to the baseline to ascertain if there was a significant difference between the timepoint and the baseline recording at rest (time=0). In addition, a Wilcoxon signed-rank matched-pairs test was conducted for within-group comparisons between different dosing treatment regimens at each specified time point to ascertain if there was a significant difference between the two different treatment conditions at each individual time point. Additionally, when appropriate, a Wilcoxon rank-sum test for integrated area under the curve analysis was used to compare groups. For the statistical analyses of individual studies, a $p<0.05$ was considered significant. For the statistical analyses of a combination of study results, a $p<0.01$ was considered significant.

#### 4.2.1.3 Drug Dose Selection

The doses of the $A_{2A}$ and $A_{2B}$ receptor agonists CGS 21680 and BAY 60-6583 were the same as those used previously in **chapter 3**, which have been shown to produce dose-dependent physiological responses to these ligands (**3.3.1.3**, **3.3.1.4**).

The dosage regimen used for CGP 20712A and ICI 118,551 was specifically chosen based on previous studies in rats, indicating that the doses produce highly selective antagonism *in vivo* of $\beta_1$ and $\beta_2$ receptor cardiovascular responses, respectively (Baker et al., 2011, Baker et al., 2017). In addition, the dose of propranolol was based on previous studies that have shown that the chosen dose can cause a blockade of both $\beta_1$ and $\beta_2$ receptor-mediated cardiovascular responses in conscious rats (Gardiner and Bennett, 1988, Janssen et al., 1991, Woolard et al., 2004).

#### 4.2.1.4 Experimental Protocols

Experiments were run in six studies, with each lasting three days (**2.1.8**). Within each study was a coincident vehicle control (vehicle buffer: 5 % propylene glycol, 2 % Tween 80 in sterile saline). Experiments were run with treatment groups of 8-10 rats.

Animals were randomly allocated based on a study independent identification number assigned to the rat on entry into the animal unit to an antagonist or vehicle group on experimental day one, and the alternative treatment given on experimental day three, allowing each rat to act as its own control.

On the second ('wash-out') day, the rats received no experimental treatment, although the arterial line was flushed with heparinised saline (40 I.U. /mL, ~0.2 mL) for two hours to maintain line patency. This break between experimental days allowed ligands to be metabolised and excreted following the first experimental day's treatment before the start of the experiments on experimental day three.

#### 4.2.1.5 The Haemodynamic Effects of CGS 21680

##### 4.2.1.5.1 Study 7: The Effect of CGP 20712A on the Haemodynamic Profile of CGS 21680

Eight animals were used to assess the cardiovascular responses to CGS 21680 in the presence or absence of CGP 20712A. Rats were randomised into two groups before the start of the experiment. After a period of baseline recording, **group 1** received a vehicle bolus (0.1 mL, i.v.) and an immediate infusion of vehicle (0.4 mL/hr, 90 min, i.v.) on day 1 and a CGP 20712A bolus (200 µg/kg, 0.1 mL, i.v.) and an immediate infusion of CGP 20712A (100 µg/kg/hr, 0.4 mL/hr, 90 min, i.v.) on day 3. **Group 2** received a CGP 20712A bolus (200 µg/kg, 0.1 mL, i.v.) and an immediate infusion of CGP 20712A (100 µg/kg/hr, 0.4 mL/hr, 90 min, i.v.) on day 1 and a vehicle bolus (0.1 mL, i.v.) and an immediate infusion of vehicle (0.4 mL/hr, 90 min, i.v.) on day 3. Approximately 90 min after the initial bolus of either vehicle or CGP 20712A on both day 1 and day 3, all groups received three infusions (0.1 mL/min, i.v.) in continuous succession of CGS 21680 (0.1 [low], 0.3 [mid], and 1.0 [high] µg/kg/min). Each dose was infused for 3 min, starting from the lowest dose. Haemodynamic recordings were made for a subsequent 4-hour period following the completion of the CGS 21680 infusion.

#### 4.2.1.5.2 Study 8: The Effect of ICI 118,551 on the Haemodynamic Profile of CGS 21680

Nine animals were used to assess the cardiovascular responses to CGS 21680 in the presence or absence of ICI 118,551. Rats were randomised into two groups before the start of the experiment. After a period of baseline recording, **group 1** received a vehicle bolus (0.1 mL, i.v.) and an immediate infusion of vehicle (0.4 mL/hr, 90 min, i.v.) on day 1 and an ICI 118,551 bolus (2.0 mg/kg, 0.1 mL, i.v.) and an immediate infusion of ICI 118,551 (1.0 mg/kg/hr, 0.4 mL/hr, 90 min, i.v.) on day 3. **Group 2** received an ICI 118,551 bolus (2.0 mg/kg, 0.1 mL, i.v.) and an immediate infusion of ICI 118,551 (1.0 mg/kg/hr, 0.4 mL/hr, 90 min, i.v.) on day 1 and a vehicle bolus (0.1 mL, i.v.) and an immediate infusion of vehicle (0.4 mL/hr, 90 min, i.v.) on day 3. Approximately 90 min after the initial bolus of either vehicle or ICI 118,551 on both day 1 and day 3, all groups received three infusions (0.1 mL/min, i.v.) in continuous succession of CGS 21680 (0.1 [low], 0.3 [mid], and 1.0 [high] μg/kg/min). Each dose was infused for 3 min, starting from the lowest dose. Haemodynamic recordings were made for a subsequent 4-hour period following the completion of the CGS 21680 infusion. *This experiment was completed by Patrizia Pannucci*.

#### 4.2.1.5.3 Study 9: The Effect of Propranolol on the Haemodynamic Profile of CGS 21680

Ten animals were used to assess the cardiovascular responses to CGS 21680 in the presence or absence of propranolol. Rats were randomised into two groups before the start of the experiment. After a period of baseline recording, **group 1** received a vehicle bolus (0.1 mL, i.v.) and an immediate infusion of vehicle (0.4 mL/hr, 90 min, i.v.) on day 1 and a propranolol bolus (1.0 mg/kg, 0.1 mL, i.v.) and an immediate infusion of propranolol (0.5 mg/kg/hr, 0.4 mL/hr, 90 min, i.v.) on day 3. **Group 2** received a propranolol bolus (1.0 mg/kg, 0.1 mL, i.v.) and an immediate infusion of propranolol (0.5 mg/kg/hr, 0.4 ml/hr, 90 min, i.v.) on day 1 and a vehicle bolus (0.1 mL, i.v.) and an immediate infusion of vehicle (0.4 ml/hr, 90 min, i.v.) on day 3. Approximately 90 min after the initial bolus of either vehicle or propranolol on both day 1 and day 3, all groups received three infusions (0.1 mL/min, i.v.) in continuous succession of CGS 21680 (0.1 [low], 0.3 [mid], and 1.0 [high] µg/kg/min). Each dose was infused for 3 min, starting from the lowest dose. Haemodynamic recordings were made for a subsequent 4-hour period following the completion of the CGS 21680 infusion.

#### 4.2.1.6 The Haemodynamic Effects of BAY 60-6583

##### 4.2.1.6.1 Study 10: The Effect of CGP 20712A on the Haemodynamic Profile of BAY 60-6583

Eight animals were used to assess the cardiovascular responses to BAY 60-6583 in the presence or absence of CGP 20712A. Rats were randomised into two groups before the start of the experiment. After a period of baseline recording, **group 1** received a vehicle bolus (0.1 mL, i.v.) and an immediate infusion of vehicle (0.4 mL/hr, 90 min, i.v.) on day 1 and a CGP 20712A bolus (200 µg/kg, 0.1 mL, i.v.) and an immediate infusion of CGP 20712A (100 µg/kg/hr, 0.4 mL/hr, 90 min, i.v.) on day 3. **Group 2** received a CGP 20712A bolus (200 µg/kg, 0.1 mL, i.v.) and an immediate infusion of CGP 20712A (100 µg/kg/hr, 0.4 mL/hr, 90 min, i.v.) on day 1 and a vehicle bolus (0.1 ml, i.v.) and an immediate infusion of vehicle (0.4 mL/hr, 90 min, i.v.) on day 3. Approximately 90 min after the initial bolus of either vehicle or CGP 20712A on both day 1 and day 3, all groups received three infusions (0.1 mL/min, i.v.) in continuous succession of BAY 60-6583 (4.0 [low], 13 [mid], and 40 [high] µg/kg/min). Each dose was infused for 3 min, starting from the lowest dose. Haemodynamic recordings were made for a subsequent 4-hour period following the completion of the BAY 60-6583 infusion.

#### 4.2.1.6.2 Study 11: The Effect of ICI 118,551 on the Haemodynamic Profile of BAY 60-6583

Eight animals were used to assess the cardiovascular responses to BAY 60-6583 in the presence or absence of ICI 118,551. Rats were randomised into two groups before the start of the experiment. After a period of baseline recording, **group 1** received a vehicle bolus (0.1 mL, i.v.) and an immediate infusion of vehicle (0.4 mL/hr, 90 min, i.v.) on day 1 and an ICI 118,551 bolus (2.0 mg/kg, 0.1 mL, i.v.) and an immediate infusion of ICI 118,551 (1.0 mg/kg/hr, 0.4 mL/hr, 90 min, i.v.) on day 3. **Group 2** received an ICI 118,551 bolus (2.0 mg/kg, 0.1 mL, i.v.) and an immediate infusion of ICI 118,551 (1.0 mg/kg/hr, 0.4 ml/hr, 90 min, i.v.) on day 1 and a vehicle bolus (0.1 mL, i.v.) and an immediate infusion of vehicle (0.4 mL/hr, 90 min, i.v.) on day 3. Approximately 90 min after the initial bolus of either vehicle or ICI 118,551 on both day 1 and day 3, all groups received three infusions (0.1 mL/min, i.v.) in continuous succession of BAY 60-6583 (4.0 [low], 13 [mid], and 40 [high] µg/kg/min). Each dose was infused for 3 min, starting from the lowest dose. Haemodynamic recordings were made for a subsequent 4-hour period following the completion of the BAY 60-6583 infusion. *This experiment was completed by Patrizia Pannucci*.

#### 4.2.1.6.3 Study 12: The Effect of Propranolol on the Haemodynamic profile of BAY 60-6583

Ten animals were used to assess the cardiovascular responses to BAY 60-6583 in the presence or absence of propranolol. Rats were randomised into two groups before the start of the experiment. After a period of baseline recording, **group 1** received a vehicle bolus (0.1 mL, i.v.) and an immediate infusion of vehicle (0.4 mL/hr, 90 min. i.v.) on day 1 and a propranolol bolus (1.0 mg/kg, 0.1 mL, i.v.) and an immediate infusion of propranolol (0.5 mg/kg/hr, 0.4 mL/hr, 90 min, i.v.) on day 3. **Group 2** received a propranolol bolus (1.0 mg/kg, 0.1 mL, i.v.) and an immediate infusion of propranolol (0.5 mg/kg/hr, 0.4 mL/hr, 90 min, i.v.) on day 1 and a vehicle bolus (0.1 mL, i.v.) and an immediate infusion of vehicle (0.4 mL/hr, 90 min, i.v.) on day 3. Approximately 90 min after the initial bolus of either vehicle or propranolol on both day 1 and day 3, all groups received three infusions (0.1 mL/min, i.v.) in continuous succession of BAY 60-6583 (4.0 [low], 13 [mid], and 40 [high] µg/kg/min). Each dose was infused for 3 min, starting from the lowest dose. Haemodynamic recordings were made for a subsequent 4-hour period following the completion of the BAY 60-6583 infusion.

## 4.2.2 Chapter 4 Methodology: *In Vitro*

### 4.2.2.1 Study α (Part 2): NanoBRET Ligand Binding Studies

The binding of β adrenoceptor antagonists to rat NLuc-tagged adenosine $A_{2A}$ and $A_{2B}$ receptors transiently transfected and expressed in HEK 293T cells were conducted as described previously in chapter 3 (**3.2.2.1**). In short, competition binding experiments were performed with 50 nM CA200645 in the presence or absence of increasing concentrations (0.1 nM-100 μM) of CGP 20712A, ICI 118,551, or propranolol in HBSS buffer supplemented with 0.1% BSA at pH 7.45 (**2.2.4.3**). Cells were incubated with ligands for 2 h at 37°C to allow ligands to equilibrate to the receptor. Furimazine was then added to each well to a final in-well concentration of 10 μM, and the cells incubated for an additional 5 min at 37°C. The plates were read at 37°C using a PHERAstar FS plate reader (BMGLabtech), measuring filtered light emissions at 460 nm (80 nm bandpass) and >610 nm (longpass). The experiment results were represented by raw BRET values, calculated by taking the ratio of the >610 nm emission and the 460 nm emission.

# 4.3 β-adrenoceptor Influence on $A_{2A}$ & $A_{2B}$ Receptor Agonist Responses: Chapter Results

## 4.3.1 Chapter 4 Results: *In Vivo*

### 4.3.1.1 Baseline Cardiovascular Recordings

For each study, baseline measurements were taken before the administration of the adrenergic β receptor antagonists CGP 20712A, ICI 118,511, propranolol, or corresponding vehicle control, and then again before administration of an adenosine $A_2$ receptor agonist, with these values corresponding to the baselines at time=0 for each study in **Figures 36-41**. These values can be found in **Tables 17-18. Table 16** is a summation of baseline results from the individual studies prior to the administration of the β receptor antagonists. These values correspond to the baselines at time=0 found in **Figures 33-35.**

#### 4.3.1.2 The Effect of the β Receptor Antagonists CGP 20712A, ICI 118,551 and Propranolol on Baseline Cardiovascular Responses

Prior to the administration of $A_2$ receptor agonists, a bolus and subsequent 90 min infusion of the $\beta_1$ adrenoceptor antagonist CGP 20712A (**Figure 33**), the $\beta_2$ adrenoceptor antagonist ICI 118,551 (**Figure 34**), the non-specific β antagonist propranolol (**Figure 35**), or respective vehicle control was administered, and cardiovascular effects observed for the 90 min dosing period.

The selective $\beta_1$ adrenoceptor antagonist CGP 20712A (200 µg/kg bolus, followed by a 90 min 100 µg/kg/hr infusion) caused a significant ($p<0.01$) decrease in HR, indicative of a basal sympathetic tone involving $\beta_1$ adrenoceptors in HR maintenance at rest (**Figure 33**). CGP 20712A also caused an initial small but significant ($p<0.01$) decrease in MAP for a few minutes after bolus administration and again at around 30 min onwards (**Figure 33**). Additionally, CGP 20712A caused a modest increase in renal VC and a transient increase in hindquarters VC for the first five minutes following the bolus dose; however, the antagonist caused no change to mesenteric VC (**Figure 33**).

The selective $\beta_2$ adrenoceptor antagonist ICI 118,551 (2.0 mg/kg bolus, followed by a 90 min 1.0 µg/kg/hr infusion) produced a significant ($p<0.01$) but short-lived transient decrease in HR. In addition, ICI 118,551 also caused a modest significant increase in MAP from baseline and small decreases in vascular conductance in the renal and mesenteric vascular beds (**Figure 34**).

The selective β adrenoceptor antagonist propranolol (1.0 mg/kg bolus, followed by a 90 min 0.5 mg/kg/hr infusion) produced effects that were consistent with a combination of $\beta_1$ and $\beta_2$ adrenoceptor antagonism (**Figure 35**). Propranolol caused a significant ($p<0.01$) reduction in HR and small decreases in mesenteric and hindquarter VC (**Figure 35**). Propranolol caused limited changes to renal VC and a transient increase in MAP, which returned to baseline 70 min after the beginning of the propranolol infusion (**Figure 35**).

| | Combination of Studies 7 & 10 | | | | Combination of Studies 8 & 11 | | | | Combination of Studies 9 & 12 | | | |
|---|---|---|---|---|---|---|---|---|---|---|---|---|
| | Vehicle | | CGP 20712A | | Vehicle | | ICI 118,551 | | Vehicle | | Propranolol | |
| | Mean ± SEM | n | Mean ± SEM | n | Mean ± SEM | n | Mean ± SEM | n | Mean ± SEM | n | Mean ± SEM | n |
| **Cardiovascular Variable** | **Baseline T=0** | | | | | | | | | | | |
| **Heart rate (beats·min$^{-1}$)** | 333 ± 5 | 16 | 338 ± 8 | 16 | 330 ± 6 | 17 | 332 ± 7 | 17 | 348 ± 5 | 20 | 344 ± 5 | 20 |
| **Mean BP (mmHg)** | 102 ± 2 | 16 | 104 ± 2 | 16 | 104 ± 3 | 17 | 103 ± 2 | 17 | 104 ± 1 | 20 | 103 ± 2 | 20 |
| **Renal VC (U)** | 81 ± 7 | 15 | 73 ± 5 | 15 | 93 ± 8 | 16 | 89 ± 7 | 16 | 83 ± 7 | 16 | 85 ± 5 | 16 |
| **Mesenteric VC (U)** | 82 ± 7 | 14 | 75 ± 8 | 14 | 87 ± 7 | 17 | 83 ± 5 | 17 | 93 ± 7 | 18 | 102 ± 7 | 18 |
| **Hindquarters VC (U)** | 44 ± 5 | 14 | 42 ± 4 | 14 | 44 ± 4 | 16 | 43 ± 4 | 16 | 54 ± 5 | 19 | 54 ± 5 | 19 |

**Table 16 Cardiovascular Variables Before Administration of β receptor Antagonists.** Values are mean ± SEM; n=14-20 per group. Abbreviations: U, units; VC, vascular conductance. Units (U) of vascular conductance (VC) are kHz. $mmHg^{-1}$ x $10^3$. A Wilcoxon signed-rank test was conducted between the antagonist group and its corresponding vehicle control group (* = $p<0.01$ significance, no significance was observed in this table). Readings correspond to the baseline recordings (zero values) for the graphs in **Figures 33-35**.

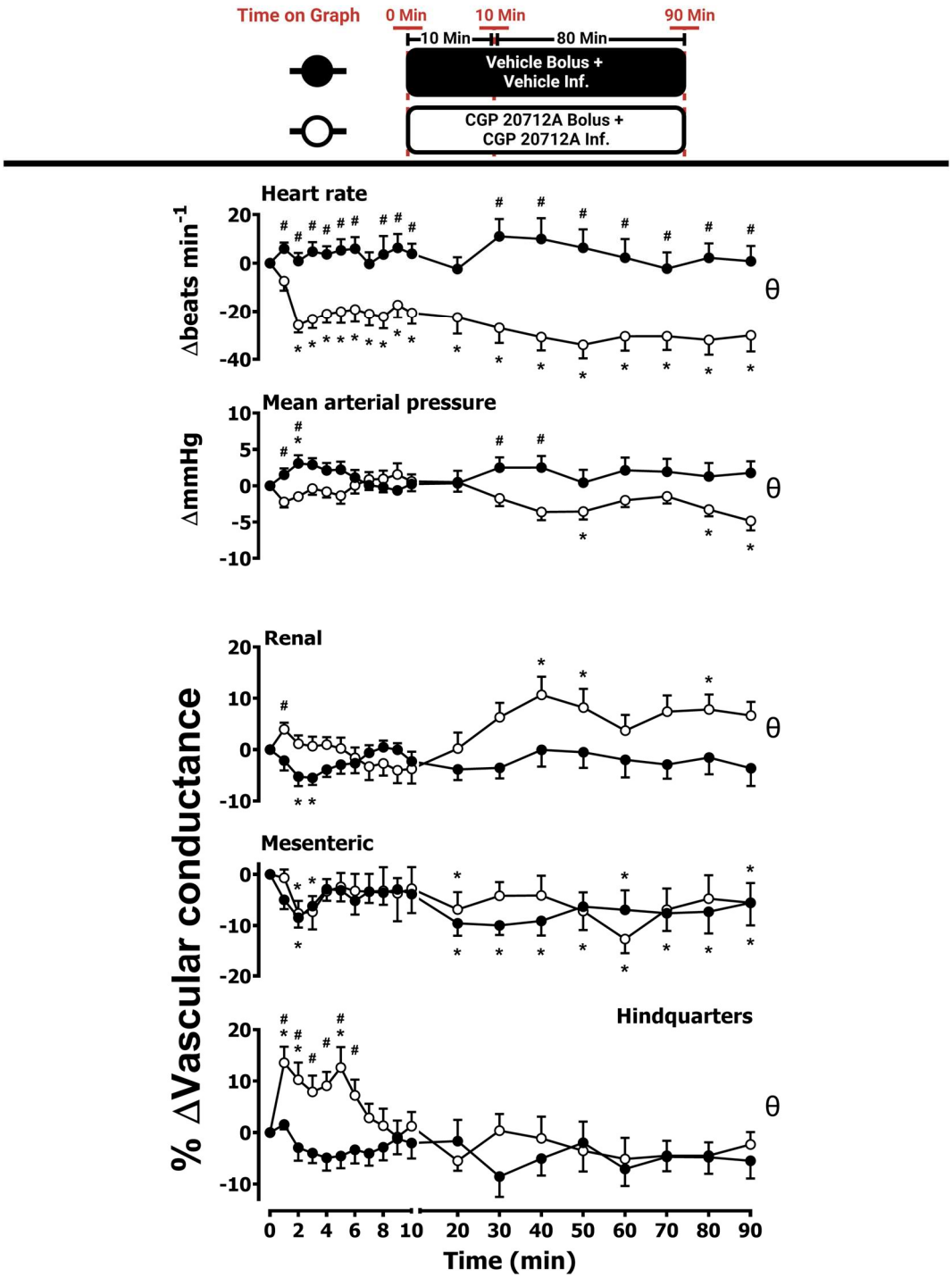


**Figure 33 Cardiovascular Responses to CGP 20712A.** Conscious, freely moving rats were dosed with CGP 20712A (0.1 mL bolus of 200 µg/kg, 0.1 mL, i.v.) and an immediate subsequent infusion of CGP 20712A (100 µg/kg/hr, 0.4 mL/hr, 90 min, i.v., n=16) or vehicle (0.1 mL bolus of 5 % propylene glycol, 2 % Tween 80 in sterile saline) and an immediate subsequent infusion of vehicle (0.4 mL/hr, 90 min, i.v., n=16) as described in the chapter methodology (**4.2.1**). The graphs show the responses over the 90 min dosing period. Data points are mean + or - SEM. A Friedman test was conducted for each data point of each group and the group's corresponding baseline (T=0) (* = p<0.01 significance). A Wilcoxon signed-rank test was conducted between the CGP 20712A and vehicle control groups for a comparison of the area under the curve (**θ** = p<0.01 significance), and additionally to determine differences at each time point (Wilcoxon T-test equivalent) (**#** = p<0.01 significance). Results are a combination of Studies 7 & 10. Baseline recordings for this figure can be found in **Table 16**.

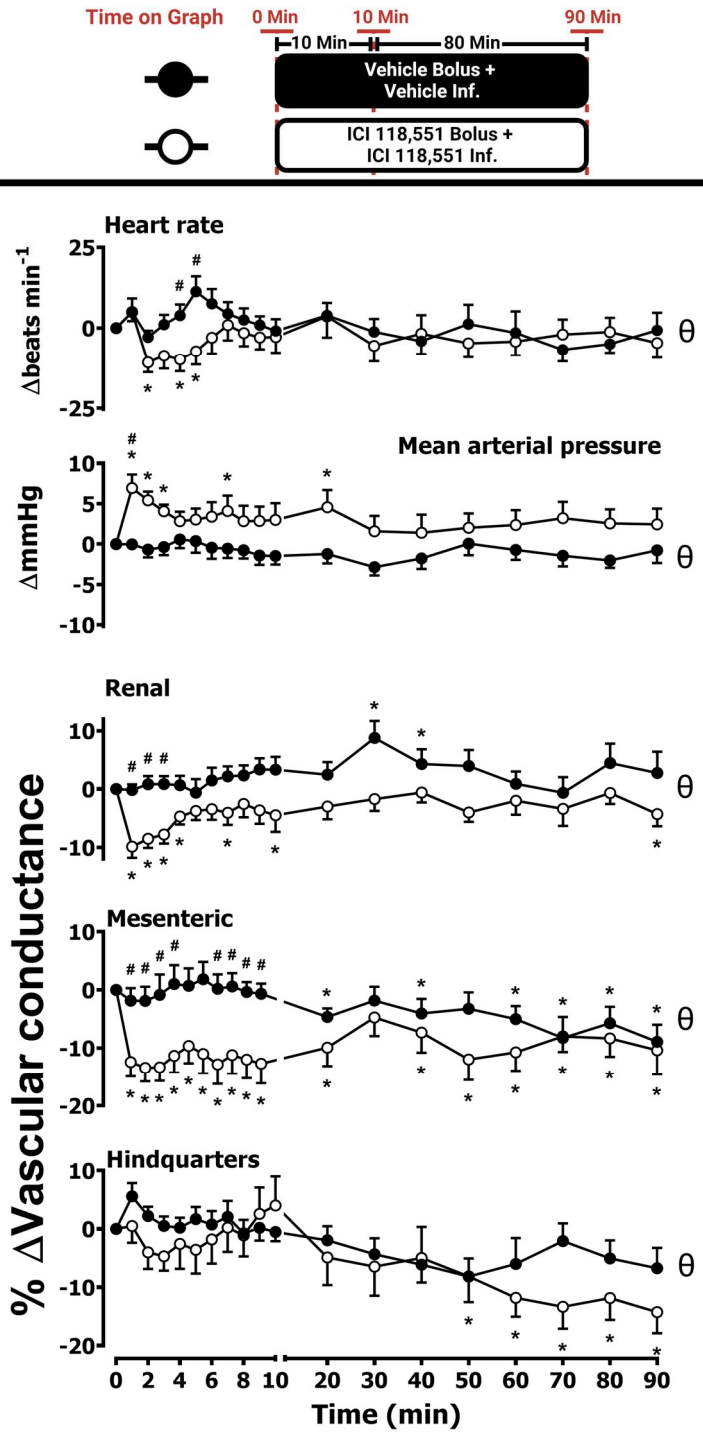


**Figure 34 Cardiovascular Responses to ICI 118,551.** Conscious, freely moving rats were dosed with ICI 118,511 (0.1 mL bolus of 2.0 mg/kg, 0.1 mL, i.v.,) and an immediate subsequent infusion of ICI 118,551 (1.0 mg/kg/hr, 0.4 mL/hr, 90 min, i.v., n=17) or vehicle (0.1 mL bolus of 5 % propylene glycol, 2 % Tween 80 in sterile saline) and an immediate subsequent infusion of vehicle (0.4 mL/hr, 90 min, i.v., n=17) as described in the chapter methodology (**4.2.1**). The graphs show the responses over the 90 min dosing period. Data points are mean + or - SEM. A Friedman test was conducted for each data point of each group and the group's corresponding baseline (T=0) (***** = p<0.01 significance). A Wilcoxon signed-rank test was conducted between the ICI 118,551 and vehicle control groups for a comparison of the area under the curve (**θ** = p<0.01 significance), and additionally to determine differences at each time point (Wilcoxon T-test equivalent) (**#** = p<0.01 significance). Results are a combination of Studies 8 & 11 completed by Patrizia Pannucci. Baseline recordings for this figure can be found in **Table 16**.

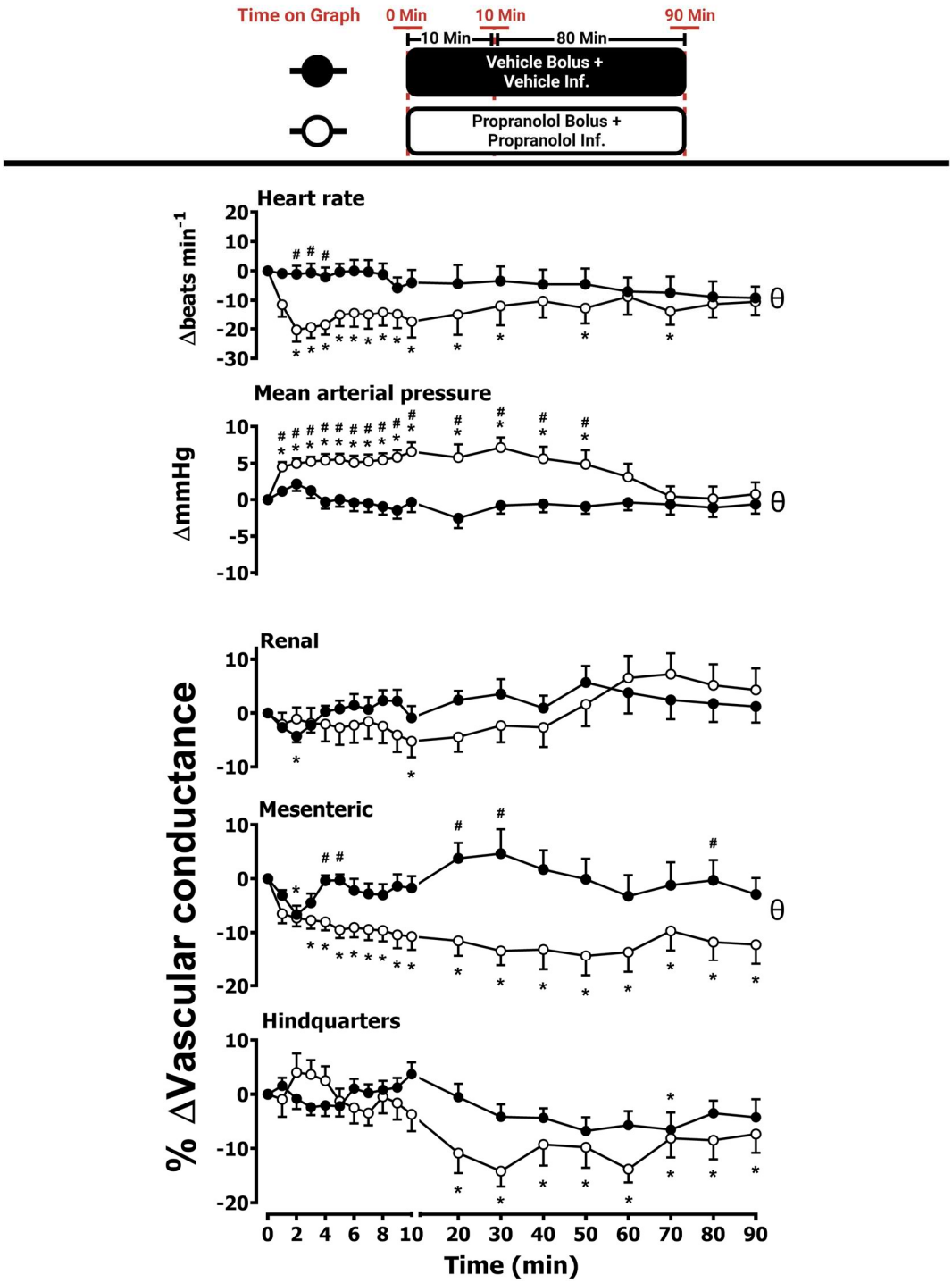


**Figure 35 Cardiovascular Responses to Propranolol.** Conscious, freely moving rats were dosed with propranolol (0.1 mL bolus of 1.0 mg/kg, i.v.,) and an immediate subsequent infusion of propranolol (0.5 mg/kg/hr, 0.4 mL/hr, 90 min, i.v, n=20) or vehicle (0.1 mL bolus of 5 % propylene glycol, 2 % Tween 80 in sterile saline) and an immediate subsequent infusion of vehicle (0.4 mL/hr, 90 min, i.v, n=20) as described in the chapter methodology (**4.2.1**). The graphs show the responses over the 90 min dosing period. Data points are mean + or - SEM. A Friedman test was conducted for each data point of each group and the group's corresponding baseline (T=0) (* = p<0.01 significance). A Wilcoxon signed-rank test was conducted between the propranolol and vehicle control groups for a comparison of the area under the curve (**θ** = p<0.01 significance), and additionally to determine differences at each time point (Wilcoxon T-test equivalent) (**#** = p<0.01 significance). Results are a combination of Studies 9 & 12. Baseline recordings for this figure can be found in **Table 16**.

#### 4.3.1.3 Effect of β Adrenoceptor Antagonists on the Haemodynamic Consequences of Administration with the $A_{2A}$ Receptor Agonist CGS 21680

Consistent with the results from the previous chapter (**3.3.1.3.1**), the selective $A_{2A}$ receptor agonist CGS 21680 (0.1, 0.3 and 1.0 μg/kg/min; 3 min i.v. infusions of each dose) produced dose-dependent large and significant ($p<0.05$) increases in HR and hindquarters VC, indicative of vasodilatations in this vascular bed, but only minor increases in VC in the renal and mesenteric vascular beds that were rarely significant ($p<0.05$) versus baseline (**Figures 36-38**). In addition, these effects were accompanied by a significant ($p<0.05$) decrease in MAP.

The effect of pretreatment with the $\beta_1$ adrenoceptor-selective antagonist, CGP 20712A (200 μg/kg bolus, followed by a 90 min 100 μg/kg/hr infusion) on the cardiovascular response to CGS 21680 was investigated (**Figure 36**). CGP 20712A significantly ($p<0.05$) attenuated the $A_{2A}$ receptor agonist-induced increase in HR (**Figure 36**). However, no significant ($p<0.05$) difference was observed in renal, mesenteric, or hindquarters VC, or MAP between CGP 20712A pretreated rats and the corresponding vehicle control (**Figure 36**).

The effect of pretreatment with the $\beta_2$ adrenoceptor-selective antagonist, ICI 118,511 (2.0 mg/kg bolus, followed by a 90 min 1.0 mg/kg/hr infusion) on the cardiovascular response to CGS 21680 was also investigated (**Figure 37**). ICI 118,551 caused no significant ($p<0.05$) difference observed in all cardiovascular parameters between ICI 118,551 pretreated rats and the corresponding vehicle control, apart from the hindquarters vascular bed, in which there was a small but significant under the curve difference observed in the first ten minutes (**Figure 37**).

The effect of pretreatment with the non-selective β adrenoceptor-selective antagonist propranolol (1.0 mg/kg bolus, followed by a 90 min 0.5 mg/kg/hr infusion) on the cardiovascular response to CGS 21680 was also investigated (**Figure 37**). Propranolol caused a significant ($p<0.05$) decrease in HR but no significant change in MAP (**Figure 38**). However, propranolol did produce a small but significant reduction ($p<0.05$) in the hindquarters VC in propranolol pretreated rats versus the corresponding vehicle control (**Figure 38**).

| | Study 7: CGS 21680 +- CGP 20712A | | | | Study 8: CGS 21680 +- ICI 118,551 | | | | Study 9: CGS 21680 +- Propranolol | | | |
|---|---|---|---|---|---|---|---|---|---|---|---|---|
| | Vehicle | | CGP 20712A | | Vehicle | | ICI 118,551 | | Vehicle | | Propranolol | |
| | Mean ± SEM | n | Mean ± SEM | n | Mean ± SEM | n | Mean ± SEM | n | Mean ± SEM | n | Mean ± SEM | n |
| **Cardiovascular Variable** | **Baseline (T= 0)** | | | | | | | | | | | |
| **Heart rate (beats·min$^{-1}$)** | 337 ± 8 | 8 | 328 ± 11 | 8 | 320 ± 5 | 9 | 320 ± 8 | 9 | 350 ± 7 | 10 | 344 ± 7 | 10 |
| **Mean BP (mmHg)** | 101 ± 2 | 8 | 107 ± 3 | 8 | 101 ± 3 | 9 | 97 ± 2 | 9 | 105 ± 3 | 10 | 104 ± 3 | 10 |
| **Renal VC (U)** | 83 ± 10 | 7 | **69 ± 8*** | 7 | 88 ± 9 | 9 | 92 ± 8 | 9 | 85 ± 7 | 10 | 86 ± 7 | 10 |
| **Mesenteric VC (U)** | 84 ± 7 | 7 | 73 ± 7 | 7 | 97 ± 10 | 9 | 89 ± 8 | 9 | 80 ± 7 | 9 | 103 ± 8 | 9 |
| **Hindquarters VC (U)** | 36 ± 7 | 7 | 32 ± 5 | 7 | 48 ± 3 | 9 | 48 ± 4 | 9 | 51 ± 5 | 10 | 53 ± 7 | 10 |
| **Cardiovascular Variable** | **Prior to Infusion (T = 90 min†)** | | | | | | | | | | | |
| **Heart rate (beats·min$^{-1}$)** | 329 ± 9 | 8 | **303 ± 9*** | 8 | 312 ± 5 | 9 | 316 ± 8 | 9 | 341 ± 7 | 10 | 333 ± 8 | 10 |
| **Mean BP (mmHg)** | 103 ± 1 | 8 | 99 ± 3 | 8 | 99 ± 2 | 9 | 100 ± 3 | 9 | 104 ± 2 | 10 | 101 ± 3 | 10 |
| **Renal VC (U)** | 82 ± 10 | 7 | 81 ± 11 | 7 | 88 ± 8 | 9 | 87 ± 8 | 9 | 85 ± 7 | 10 | 89 ± 8 | 10 |
| **Mesenteric VC (U)** | 78 ± 4 | 7 | 71 ± 6 | 7 | 86 ± 9 | 9 | 82 ± 9 | 9 | 81 ± 8 | 9 | 99 ± 11 | 9 |
| **Hindquarters VC (U)** | 34 ± 6 | 7 | 33 ± 6 | 7 | 47 ± 3 | 9 | 43 ± 5 | 9 | 51 ± 5 | 10 | 47 ± 4 | 10 |

**Table 17 Cardiovascular Variables Before Administration of β receptor Antagonists and Before the Subsequent Administration of the $A_{2A}$ Receptor Agonist CGS 21680.** Values are mean ± SEM; n=7-10 per group. Abbreviations: U, units; VC, vascular conductance. Units (U) of vascular conductance (VC) are kHz. mmHg$^{-1}$ x $10^3$. A Wilcoxon signed-rank test was conducted between the antagonist group and its corresponding vehicle control group (* = $p<0.05$ significance). Readings correspond to the baseline recordings (zero values) for the graphs in **Figure 36-8**. †In some instances, agonist administration was delayed past 90 min in the case of movement to allow the rat to settle.

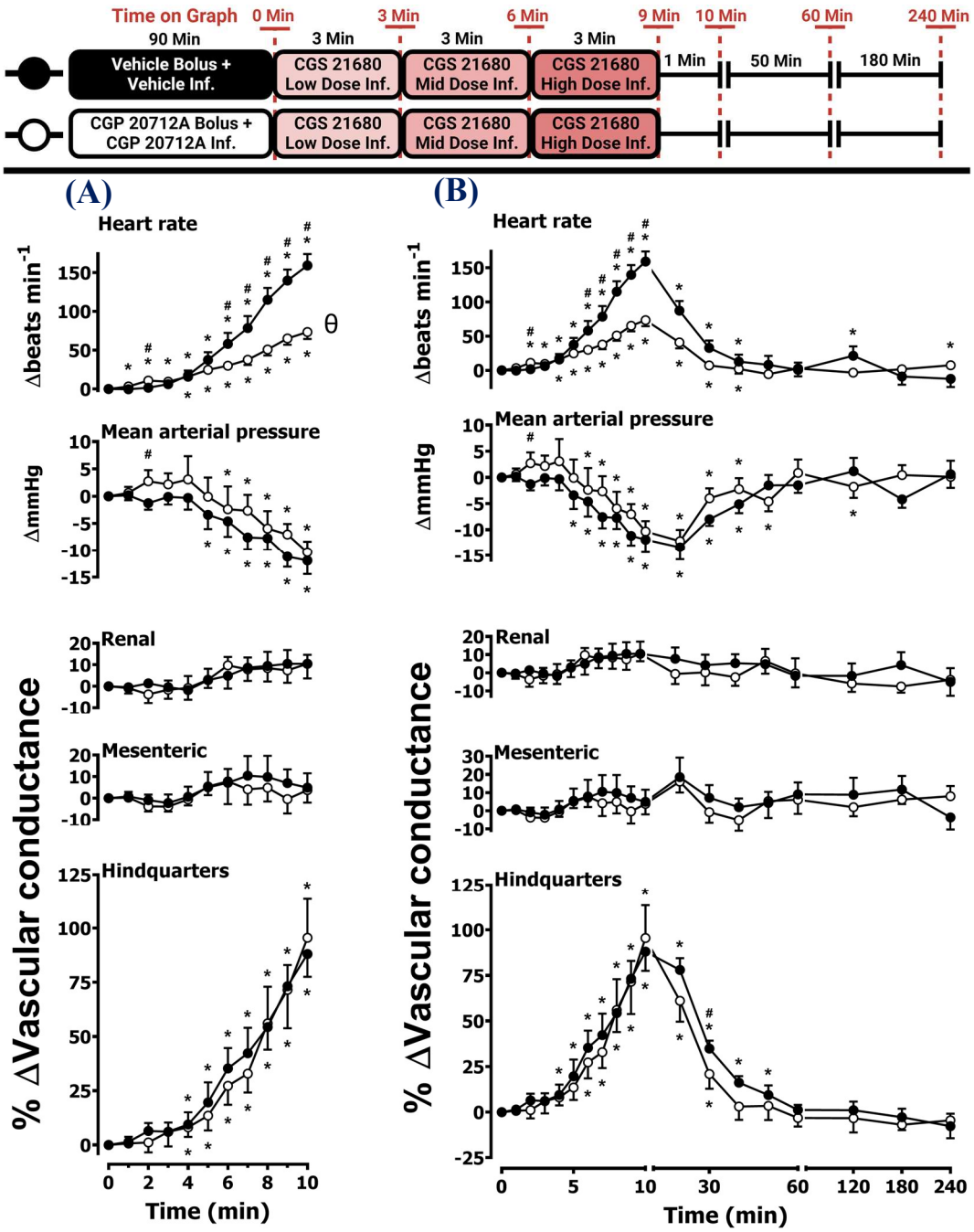


**Figure 36 Cardiovascular Responses to CGS 21680 in the Presence or Absence of CGP 20712A.** Conscious, freely moving rats were dosed with CGP 20712A (0.1 mL bolus of 200 µg/kg, 0.1 mL, i.v.) and an immediate subsequent infusion of CGP 20712A (100 µg/kg/hr, 0.4 mL/hr, 90 min, i.v., n=8) or vehicle (0.1 mL bolus of 5 % propylene glycol, 2 % Tween 80 in sterile saline) and an immediate subsequent infusion of vehicle (0.4 mL/hr, 90 min, i.v. n=8) as described in the chapter methodology (**4.2.1**). On completion of the 90 min infusion, all animals received an infusion of a consecutive low, medium and high dose of CGS 21680 (0.1, 0.3 and 1.0 µg/kg/min, i.v.), with each dose run for 3 min. The graphs show **(A)** the CGS 21680 treatment period, plus an additional minute, and **(B)** the treatment period and recording period of 4 h. Data points are mean + or - SEM. A Friedman test was conducted for each data point of each group and the group's corresponding baseline (T=0) (***** = $p<0.05$ significance) [**(A)** & **(B)**]. A Wilcoxon signed-rank test was conducted between the two groups for a comparison of the area under the curve (**θ** = $p<0.05$ significance) [**(A)**], and additionally to determine differences at each time point (Wilcoxon T-test equivalent) (**#** = $p<0.05$ significance) [**(A)** & **(B)**]. Results are from study 7. Baseline recordings can be found in **Table 17**.

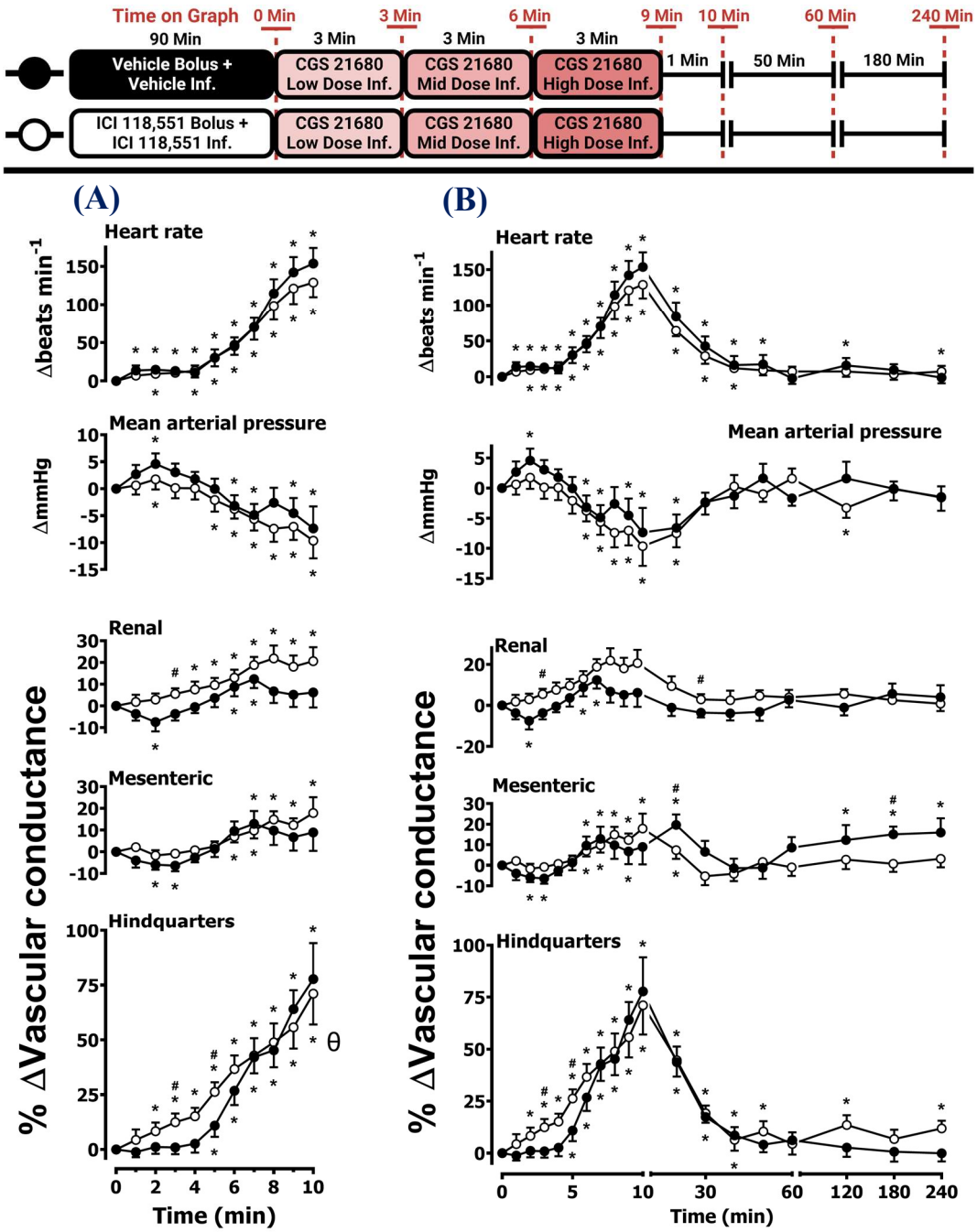


**Figure 37 Cardiovascular Responses to CGS 21680 in the Presence or Absence of ICI 188,551.** Conscious, freely moving rats were dosed with ICI 118,511 (0.1 mL bolus of 2.0 mg/kg, 0.1 mL, i.v.,) and an immediate subsequent infusion of ICI 118,551 (1.0 mg/kg/hr, 0.4 mL/hr, 90 min, i.v., n=9) or vehicle (0.1 mL bolus of 5 % propylene glycol, 2 % Tween 80 in sterile saline) and an immediate subsequent infusion of vehicle (0.4 mL/hr, 90 min, i.v., n=9) as described in the chapter methodology (**4.2.1**). On completion of the 90 min infusion, all animals received an infusion of a consecutive low, medium and high dose of CGS 21680 (0.1, 0.3 and 1.0 µg/kg/min, i.v.), with each dose run for 3 min. The graphs show **(A)** the CGS 21680 treatment period, plus an additional minute, and **(B)** the treatment period and recording period of 4 h. Data points are mean + or - SEM. A Friedman test was conducted for each data point of each group and the group's corresponding baseline (T=0) (* = $p<0.05$ significance) [**(A)** & **(B)**]. A Wilcoxon signed-rank test was conducted between the two groups for a comparison of the area under the curve (**θ** = $p<0.05$ significance) [**(A)**], and additionally to determine differences at each time point (Wilcoxon T-test equivalent) (**#** = $p<0.05$ significance) [**(A)** & **(B)**]. Experiments were completed by Patrizia Pannucci and are from study 8. Baseline recordings can be found in **Table 17**.

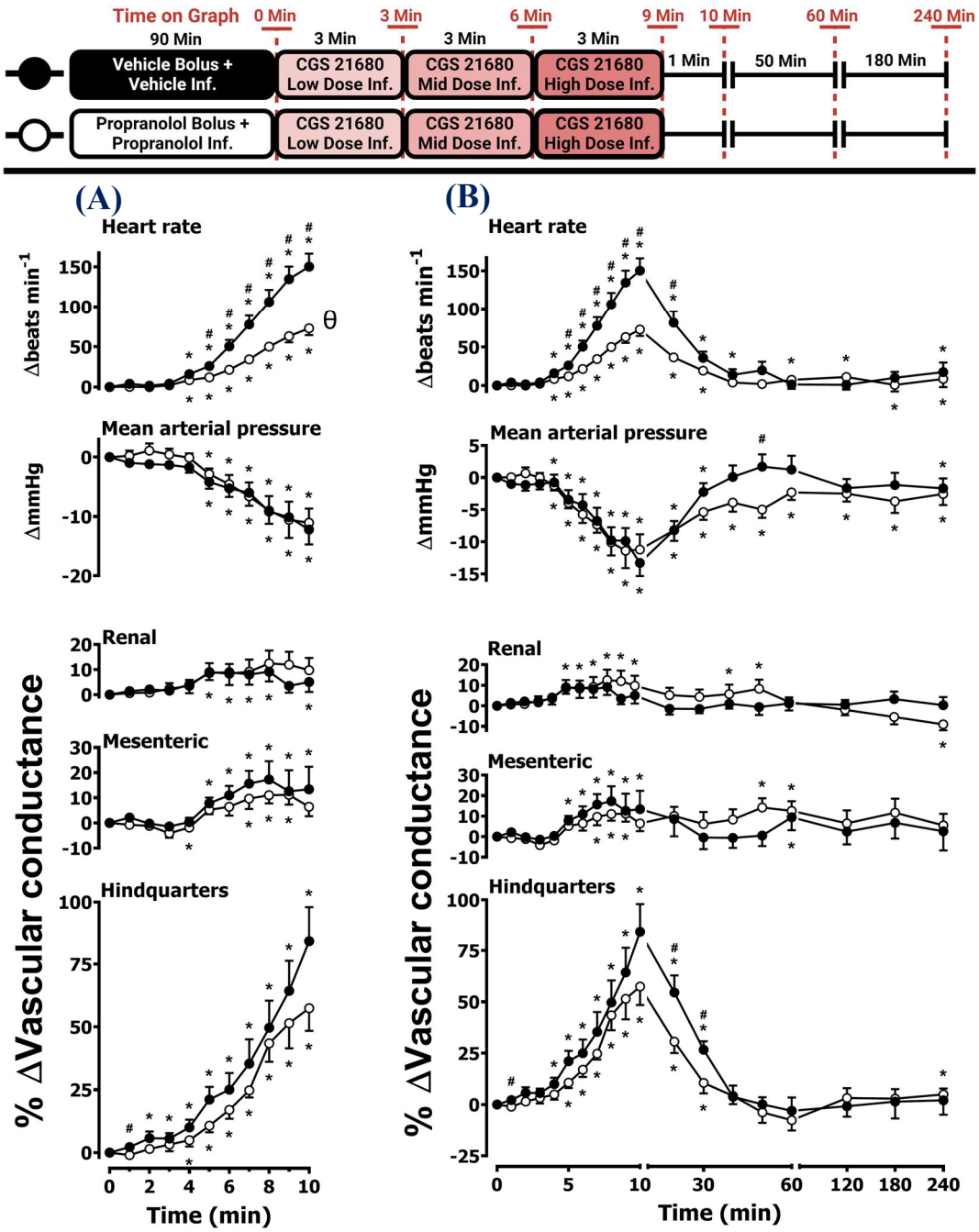


**Figure 38 Cardiovascular Responses to CGS 21680 in the Presence or Absence of Propranolol.** Conscious, freely moving rats were dosed with propranolol (0.1 mL bolus of 1.0 mg/kg, 0.1 mL, i.v.,) and an immediate subsequent infusion of propranolol (0.5 mg/kg/hr, 0.4 mL/hr, 90 min, i.v., n=10) or vehicle (0.1 mL bolus of 5 % propylene glycol, 2 % Tween 80 in sterile saline) and an immediate subsequent infusion of vehicle (0.4 mL/hr, 90 min, i.v., n=10) as described in the chapter methodology (**4.2.1**). On completion of the 90 min infusion, all animals received an infusion of a consecutive low, medium and high dose of CGS 21680 (0.1, 0.3 and 1.0 µg/kg/min, i.v.), with each dose run for 3 min. The graphs show **(A)** the CGS 21680 treatment period, plus an additional minute, and **(B)** the treatment period and recording period of 4 h. Data points are mean + or - SEM. A Friedman's test was conducted for each data point of each group and the group's corresponding baseline (T=0) (* = $p<0.05$ significance) [**(A)** & **(B)**]. A Wilcoxon signed-rank test was conducted between the two groups for a comparison of the area under the curve (**θ** = $p<0.05$ significance) [**(A)**], and additionally to determine differences at each time point (Wilcoxon T-test equivalent) (**#** = $p<0.05$ significance) [**(A)** & **(B)**]. Results are from study 9. Baseline recordings for this figure can be found in **Table 17**.

#### 4.3.1.4 Effect of β Adrenoceptor Antagonists on the Haemodynamic Consequences of Administration with the $A_{2B}$ Receptor Agonist BAY 60-6583

Consistent with the results from the previous chapter (**3.3.1.4.1**), the selective $A_{2B}$ receptor agonist BAY 60-6583 (4, 13.3 and 40 μg/kg/min; 3 min i.v. infusions of each dose) produced a large increase in HR, alongside significant ($p<0.05$) increases in renal and mesenteric VC but caused no significant effect on MAP or hindquarters VC (**Figures 39-41**).

The effect of pretreatment with the $\beta_1$ adrenoceptor-selective antagonist, CGP 20712A (200 μg/kg bolus, followed by a 90 min 100 μg/kg/hr infusion) on the cardiovascular response to BAY 60-6583 was investigated (**Figure 39**). CGP 20712A significantly ($p<0.05$) attenuated the $A_{2B}$ receptor agonist-induced increase in HR (**Figure 39**). However, no significant difference was observed in renal, mesenteric, or hindquarters VC, or MAP between CGP 20712A pretreated rats and the corresponding vehicle control (**Figure 39**).

The effect of pretreatment with the $\beta_2$ adrenoceptor-selective antagonist, ICI 118,511 (2.0 mg/kg bolus, followed by a 90 min 1.0 mg/kg/hr infusion) on the cardiovascular response to BAY 60-6583 was also investigated (**Figure 40**). ICI 118,551 significantly ($p<0.05$) increased the HR, as well as the renal and mesenteric responses induced by BAY 60-6583 and additionally led to a decrease in MAP that was not found when BAY 60-6583 was administered alone (**Figure 40**).

The effect of pretreatment with the non-selective β adrenoceptor-selective antagonist propranolol (1.0 mg/kg bolus, followed by a 90 min 0.5 mg/kg/hr infusion) on the cardiovascular response to BAY 60-6583 was also investigated (**Figure 41**). Antagonism of $\beta_1$ and $\beta_2$ adrenoceptors produced a marked significant ($p<0.05$) decrease in the HR response to BAY 60-6583 and additionally led to a small decrease in MAP that was not found when BAY 60-6583 was administered alone (**Figure 41**). Propranolol did not, however, attenuate or enhance the increases in renal and mesenteric VC induced by the selective $A_{2B}$ receptor agonist (**Figure 41**).

| | Study 10: BAY 60-6583 +- CGP 20712A | | | | Study 11: BAY 60-6583 +- ICI 118,551 | | | | Study 12: BAY 60-6583 +- Propranolol | | | |
|---|---|---|---|---|---|---|---|---|---|---|---|---|
| | Vehicle | | CGP 20712A | | Vehicle | | ICI 118,551 | | Vehicle | | Propranolol | |
| | Mean ± SEM | n | Mean ± SEM | n | Mean ± SEM | n | Mean ± SEM | n | Mean ± SEM | n | Mean ± SEM | n |
| **Cardiovascular Variable** | **Baseline (T= 0)** | | | | | | | | | | | |
| **Heart rate (beats·min$^{-1}$)** | 329 ± 7 | 8 | 348 ± 12 | 8 | 341 ± 12 | 8 | 346 ± 9 | 8 | 346 ± 6 | 10 | 343 ± 7 | 10 |
| **Mean BP (mmHg)** | 102 ± 3 | 8 | 102 ± 1 | 8 | 109 ± 5 | 8 | 110 ± 3 | 8 | 103 ± 1 | 10 | 102 ± 3 | 10 |
| **Renal VC (U)** | 79 ± 9 | 8 | 78 ± 6 | 8 | 100 ± 16 | 7 | 86 ± 12 | 7 | 83 ± 12 | 6 | 84 ± 7 | 6 |
| **Mesenteric VC (U)** | 80 ± 13 | 7 | 78 ± 15 | 7 | 76 ± 8 | 8 | 76 ± 6 | 8 | 106 ± 11 | 9 | 102 ± 12 | 9 |
| **Hindquarters VC (U)** | 53 ± 6 | 7 | 52 ± 5 | 7 | 39 ± 7 | 7 | 37 ± 7 | 7 | 55 ± 8 | 9 | 55 ± 8 | 9 |
| **Cardiovascular Variable** | **Prior to Infusion (T = 90 min†)** | | | | | | | | | | | |
| **Heart rate (beats·min$^{-1}$)** | 331 ± 10 | 8 | 309 ± 8 | 8 | 340 ± 11 | 8 | 334 ± 11 | 8 | 336 ± 8 | 10 | 332 ± 8 | 10 |
| **Mean BP (mmHg)** | 103 ± 2 | 8 | 99 ± 2 | 8 | 107 ± 5 | 8 | 110 ± 2 | 8 | 100 ± 2 | 10 | **107 ± 3*** | 10 |
| **Renal VC (U)** | 76 ± 8 | 8 | 79 ± 6 | 8 | 103 ± 16 | 7 | **83 ± 12*** | 7 | 81 ± 12 | 6 | 85 ± 7 | 6 |
| **Mesenteric VC (U)** | 74 ± 11 | 7 | 71 ± 13 | 7 | 71 ± 6 | 8 | 67 ± 8 | 8 | 101 ± 12 | 9 | 82 ± 11 | 9 |
| **Hindquarters VC (U)** | 49 ± 5 | 7 | 49 ± 4 | 7 | 35 ± 7 | 7 | 31 ± 6 | 7 | 54 ± 9 | 9 | 47 ± 7 | 9 |

**Table 18 Cardiovascular Variables Before Administration of β Receptor Antagonists and Before the Subsequent Administration of the $A_{2B}$ Receptor Agonist BAY 60-6583.** Values are mean ± SEM; n=6-10 per group. Abbreviations: U, units; VC, vascular conductance. Units (U) of vascular conductance (VC) are kHz. mmHg$^{-1}$ x $10^3$. A Wilcoxon signed-rank test was conducted between the antagonist group and its corresponding vehicle control group (* = $p<0.05$ significance). Readings correspond to the baseline recordings (zero values) for the graphs in **Figure 39-41**. †In some instances, agonist administration was delayed past 90 min in the case of movement to allow the rat to settle.

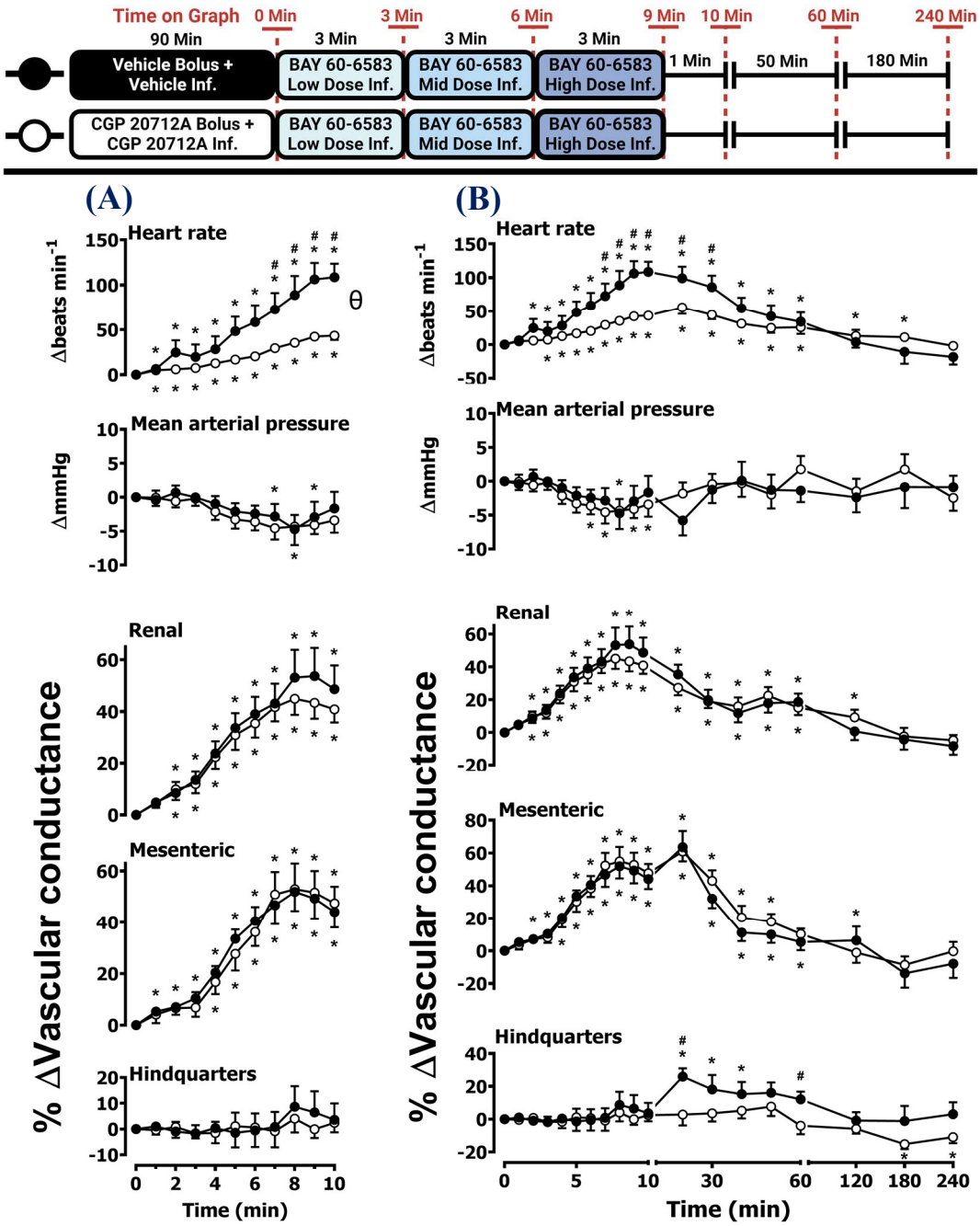


**Figure 39 Cardiovascular Responses to BAY 60-6583 in the Presence or Absence of CGP 20712A.** Conscious, freely moving rats were dosed with CGP 20712A (0.1 mL bolus of 200 µg/kg, 0.1 mL, i.v.) and an immediate subsequent infusion of CGP 20712A (100 µg/kg/hr, 0.4 mL/hr, 90 min, i.v., n=8) or vehicle (0.1 mL bolus of 5 % propylene glycol, 2 % Tween 80 in sterile saline) and an immediate subsequent infusion of vehicle (0.4 mL/hr, 90 min, i.v. n=8) as described in the chapter methodology (**4.2.1**). On completion of the 90 min infusion, all animals received an infusion of a consecutive low, medium and high dose of BAY 60-6583 (4.0, 13.3, and 40.0 µg/kg/min, i.v.), with each dose run for 3 min. The graphs show **(A)** the BAY 60-6583 treatment period, plus an additional minute, and **(B)** the treatment period and recording period of 4 h. Data points are mean + or - SEM. A Friedman test was conducted for each data point of each group and the group's corresponding baseline (T=0) (* = $p<0.05$ significance) [**(A)** & **(B)**]. A Wilcoxon signed-rank test was conducted between the two groups for a comparison of the area under the curve (**θ** = $p<0.05$ significance) [**(A)**], and additionally to determine differences at each time point (Wilcoxon T-test equivalent) (**#** = $p<0.05$ significance) [**(A)** & **(B)**]. Results are from study 10. Baseline recordings for this figure can be found in **Table 18**.

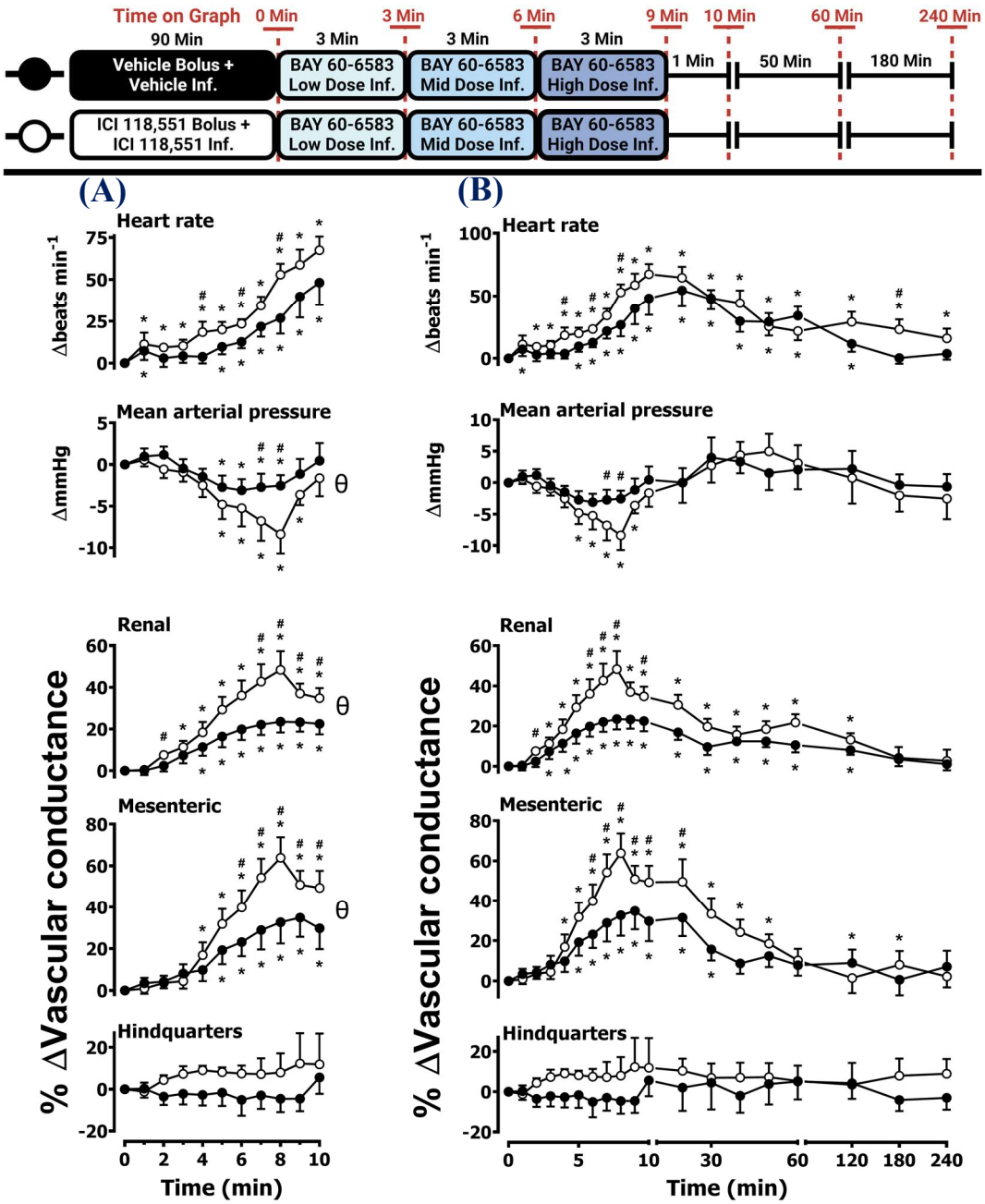


**Figure 40 Cardiovascular Responses to BAY 60-6583 in the Presence or Absence of ICI 118,551.** Conscious, freely moving rats were dosed with ICI 118,511 (0.1 mL bolus of 2.0 mg/kg, 0.1 mL, i.v.,) and an immediate subsequent infusion of ICI 118,551 (1.0 mg/kg/hr, 0.4 mL/hr, 90 min, i.v., n=8) or vehicle (0.1 mL bolus of 5 % propylene glycol, 2 % Tween 80 in sterile saline) and an immediate subsequent infusion of vehicle (0.4 mL/hr, 90 min, i.v., n=8) as described in the chapter methodology (**4.2.1**). On completion of the 90 min infusion, all animals received an infusion of a consecutive low, medium and high dose of BAY 60-6583 (4.0, 13.3, and 40.0 µg/kg/min, i.v.), with each dose run for 3 min. The graphs show **(A)** the BAY 60-6583 treatment period, plus an additional minute, and **(B)** the treatment period and recording period of 4 h. Data points are mean + or - SEM. A Friedman test was conducted for each data point of each group and the group's corresponding baseline (T=0) (***** = p<0.05 significance) [**(A)** & **(B)**]. A Wilcoxon signed-rank test was conducted between the two groups for a comparison of the area under the curve (**θ** = p<0.05 significance) [**(A)**], and additionally to determine differences at each time point (Wilcoxon T-test equivalent) (**#** = p<0.05 significance) [**(A)** & **(B)**]. Experiments were completed by Patrizia Pannucci and are from study 11. Baseline recordings for this figure can be found in **Table 18**.

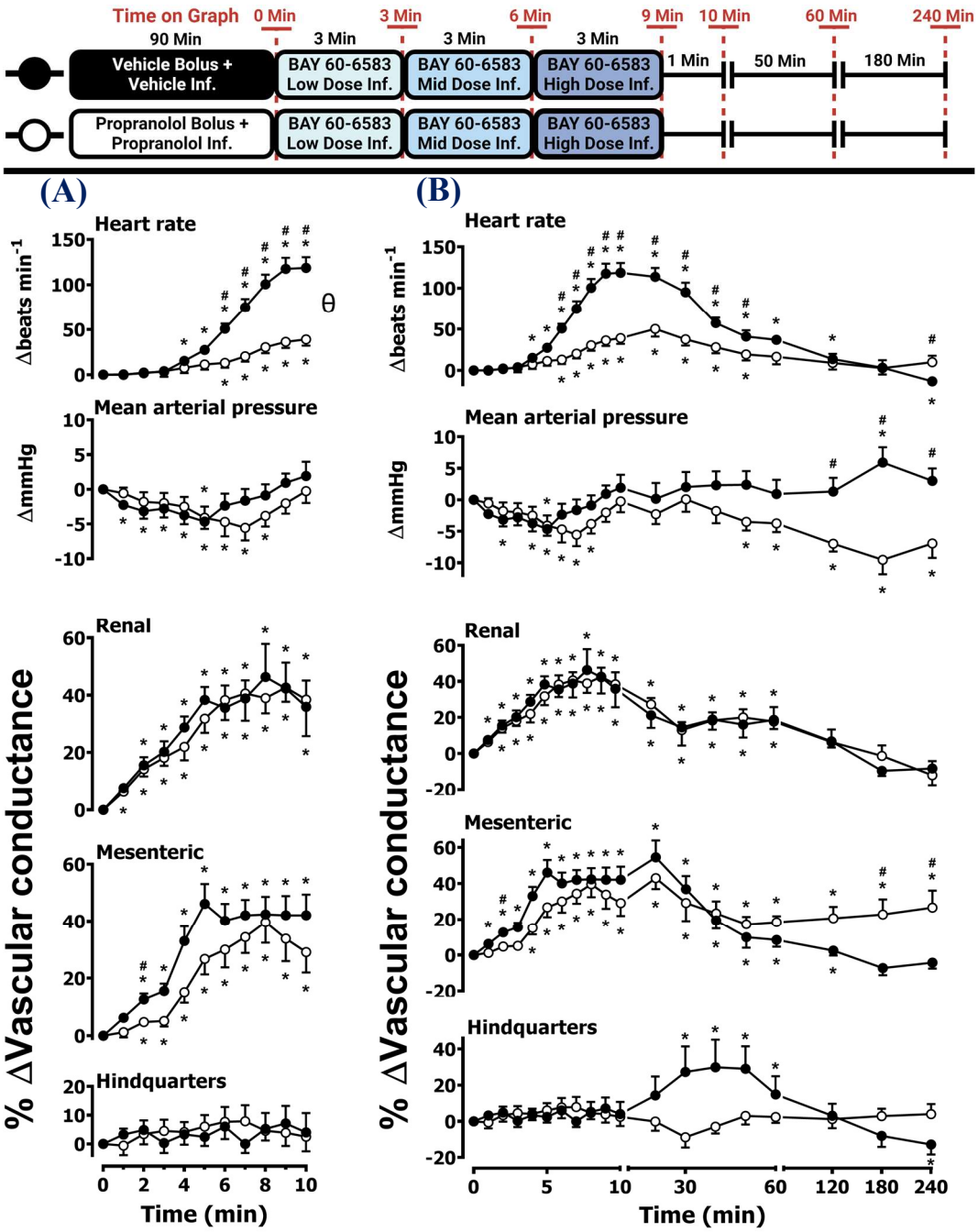


**Figure 41 Cardiovascular Responses to BAY 60-6583 in the Presence or Absence of Propranolol.** Conscious, freely moving rats were dosed with propranolol (0.1 mL bolus of 1.0 mg/kg, 0.1 mL, i.v.,) and an immediate subsequent infusion of propranolol (0.5 mg/kg/hr, 0.4 mL/hr, 90 min, i.v., n=10) or vehicle (0.1 mL bolus of 5 % propylene glycol, 2 % Tween 80 in sterile saline) and an immediate subsequent infusion of vehicle (0.4 mL/hr, 90 min, i.v., n=10) as described in the chapter methodology (**4.2.1**). On completion of the 90 min infusion, all animals received an infusion of a consecutive low, medium and high dose of BAY 60-6583 (4.0, 13.3, and 40.0 µg/kg/min, i.v.), with each dose run for 3 min. The graphs show **(A)** the BAY 60-6583 treatment period, plus an additional minute, and **(B)** the treatment period and recording period of 4 h. Data points are mean + or - SEM. A Friedman test was conducted for each data point of each group and the group's corresponding baseline (T=0) (* = $p<0.05$ significance) [**(A)** & **(B)**]. A Wilcoxon signed-rank test was conducted between the two groups for a comparison of the area under the curve (**θ** = $p<0.05$ significance) [**(A)**], and additionally to determine differences at each time point (Wilcoxon T-test equivalent) (**#** = $p<0.05$ significance) [**(A)** & **(B)**]. Results are from study 12. Baseline recordings for this figure can be found in **Table 18**.

## 4.3.2 Chapter 4 Results: *In Vitro*

### 4.3.2.1 Binding of CA200645 at Rat $A_{2A}$ and $A_{2B}$ Receptors

As previously described, saturation binding analysis using increasing concentrations of the fluorescent ligand CA200645 confirmed specific binding to NLuc-tagged rat $A_{2A}$ and $A_{2B}$ receptors expressed in HEK 293T cells (**3.2.2.1**). Binding to rat NLuc-$A_{2A}$ or NLuc-$A_{2B}$ receptors were investigated for non-fluorescent ligands by competitive inhibition of the specific binding of 50 nM CA200645 to the receptor by increasing concentrations of three β-antagonists: CGP 20712A, ICI 118,551 and propranolol (**Figure 42A-C**).

CGP 20712A, ICI 118,551 and propranolol did not affect the specific binding of 50 nM CA200645 to either rat adenosine $A_2$ receptor (n=5) at concentrations up to 100 μM, suggesting that these ligands do not directly bind to either of the rat $A_2$ receptors, even at high concentrations.

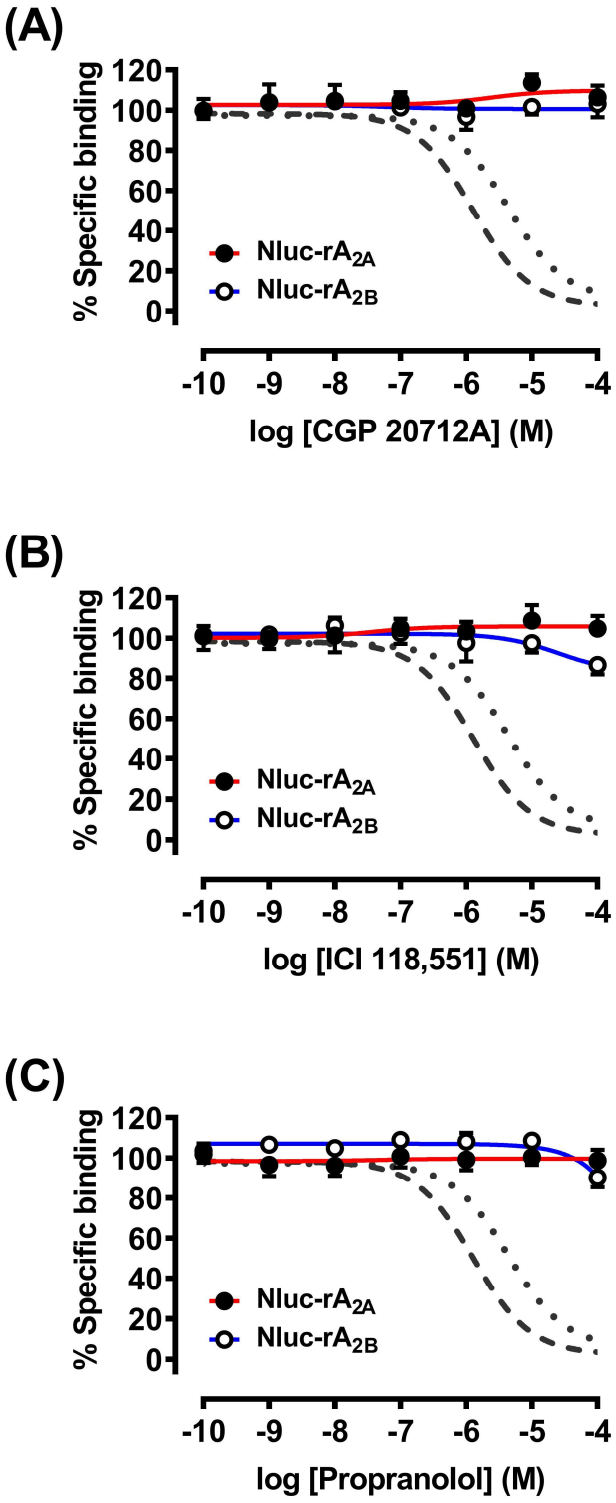


**Figure 42 Inhibition of the Binding of 50 nM CA200645 to NanoLuc-tagged Rat $A_{2A}$ or Rat $A_{2B}$ Receptors by Increasing Concentrations of Competitor Ligands.** NanoLuc-tagged rat-$A_{2A}$ or rat $A_{2B}$ receptors were transfected into HEK 293T cells. CA200645 and inhibitors were added simultaneously to triplicate well replicates and incubated for 120 min at 37°C. Graphical values represent mean ± SEM of five independent experiments. Data are expressed as a percentage of the specific binding of 50 nM CA200645 obtained in each experiment. Specific binding was calculated as previously described (**3.3.2.1.1**). Grey curves represent PSB 1115 binding (dotted Nluc-r$A_{2A}$ receptor, dashed Nluc-r$A_{2B}$ receptor), as presented in **Figure 31** and **Table 15**, to serve as a positive control.

# 4.4 β-adrenoceptor Influence on $A_{2A}$ & $A_{2B}$ Receptor Agonist Responses: Chapter Discussion

In this chapter, the effect of $\beta_1$ and $\beta_2$ receptor antagonism on the different cardiovascular responses to the $A_{2A}$ receptor-selective agonist CGS 21680 and the $A_{2B}$ receptor-selective agonist BAY 60-6583 was investigated to determine the extent to which the cardiovascular response to $A_{2A}$ and $A_{2B}$ receptor agonism is secondary to sympathetic excitation in conscious, freely moving rats.

*In vitro* binding studies show that the β-antagonists CGP 20712A, ICI 118,551 and propranolol do not directly bind the rat $A_{2A}$ or $A_{2B}$ receptors, even at high concentrations of the ligand up to 100 μM. As a result, it can be concluded that the effects seen when using these β-antagonists *in vivo* are due to direct actions on β receptors and not off-target binding to the $A_{2A}$ and $A_{2B}$ receptors.

Consistent with the results of **chapter 3** (**3.3.1.3.1**), the selective $A_{2A}$ receptor agonist CGS 21680 produced an increase in HR and a fall in MAP. Both the selective $\beta_1$ adrenoceptor antagonist CGP 20712A and the non-selective β-blocker propranolol significantly attenuated the HR response to CGS 21680 without modifying the fall in MAP, the presence of the $\beta_2$ adrenoceptor antagonist ICI 118,551 did not cause a change to the observed HR or MAP. A similar effect in rats was observed in a study with the $A_{2A}$ receptor agonist regadenoson (Dhalla et al., 2006). This study found that the increase in HR was attenuated by the non-specific β-blocker metoprolol (Dhalla et al., 2006). The results from the present experiments agree with this earlier study and add to what is known about the response by showing that the rise in HR is mediated explicitly by the $\beta_1$ receptor.

Neither CGP 20712A nor ICI 118,551 affected the regionally selective increase in hindquarters VC observed with CGS 21680 administration. However, propranolol did slightly attenuate the hindquarters response, but this could be due to off-target actions on other receptors. Propranolol has been demonstrated to have affinity to 5-hydroxytryptamine (5-HT) receptors, such as the 5-$HT_{1B}$ receptor, which is known to have vasodilatory effects in the rat hindquarters vasculature and could imply that 5-HT receptors have a role to play in the vasodilation caused by $A_{2A}$ receptor activation (Pauwels and Palmier, 1994, Calama et al., 2002).

When taken together, these results suggest a similar conclusion to that proposed by Dhalla *et al.*, that a baroreflex-mediated increase in HR caused as a direct result of a decrease in blood pressure is not the sole reason for the tachycardia observed with CGS 21680, and that a direct $A_{2A}$ receptor mediated stimulation of the sympathetic nervous system may be involved since the HR response was found to be decoupled from the fall in MAP when in the presence of $\beta_1$ blockade (Dhalla et al., 2006).

Consistent with the results of chapter 3 (**3.3.1.4.1**), the selective $A_{2B}$ receptor agonist BAY 60-6583 produced a large increase in HR that was not accompanied by a decrease in MAP. This result could either be due to the tachycardic response being either a direct effect of $A_{2B}$ receptor activation in the heart or due to a similar stimulation of the sympathetic nervous system as described above for the $A_{2A}$ receptor.

In these *in vivo* studies in conscious rats, CGP 20712A and propranolol significantly attenuated the HR response to BAY 60-6583, which suggests that the increase in HR is due to a stimulation of the sympathetic nervous system and not due to direct activation of the heart. This result aligns with evidence from studies involving Langendorff heart preparations and anaesthetised rodents that activation of $A_{2B}$ receptors appear to cause minimal direct effects on heart rate when isolated from reflex activity (Liu et al., 2010, Maas et al., 2010).

In contrast to $A_{2A}$ receptor stimulation, $A_{2B}$ receptor activation produced increases in renal and mesenteric VC but no change to hindquarters VC (**3.3.1.4.1**). The presence of CGP 20712A did not modify these results. Of interest is that the response to BAY 60-6583 in renal and mesenteric VC was increased by treatment with ICI 118,551, which was also associated with a small but significant increase in the HR response. Notably, ICI 118,551 administration alone produced a transient fall in HR and a more prolonged decrease in both renal and mesenteric VC, suggesting the presence of a $\beta_2$-mediated sympathetic tone under basal conditions blocked by ICI 118,551. It could thus be the case that the enhanced effects of BAY 60-6583 in the presence of ICI 118,551 are a consequence of the $A_{2B}$ receptor responses being able to achieve a maximum response from a lower baseline signal which thus brings about a more considerable change. Evidence for this can also be seen in the response of CGS 21680 on the renal VC, wherein the presence of ICI 118,551, a small but significant increase in VC occurs that otherwise would not be present (**3.3.1.3.1**). However, this enhancement was not observed with BAY 60-6583 in the presence of propranolol, which also causes $\beta_2$-

antagonism. In study 11, the BAY 60-6583 response in the absence of ICI 118, 551 (**4.2.1.6.1, Figure 40**) produced notably smaller vasodilatory effects at the renal and mesenteric beds than that seen in study 12 for the same dose of BAY 60-6583 in the absence of propranolol (**4.2.1.6.3**, **Figure 41**), which could explain the differences between the results of these two studies, and could be due to differences in the batch of rats used for each of the experiments, or that different experimenters did these experiments, or that different aliquots of BAY 60-6583 were used. Because of these differing results, further investigations are required to confirm if $\beta_2$-antagonism enhances the effects of BAY 60-6583.

To conclude, the findings from this chapter suggest that the regionally selective effects of both $A_{2A}$ and $A_{2B}$ receptor agonism on VC are the result of the activation of receptors in specific regional vascular beds and that these effects are not caused or influenced by secondary activation of the sympathetic nervous system acting at β receptors. In contrast, the tachycardia induced by both $A_{2A}$ and $A_{2B}$ receptor agonism has been shown to involve a component of sympathetic activation that leads to stimulation of $\beta_1$ adrenoceptors in the heart. However, in the presence of CGP 20712A, both $A_{2A}$ and $A_{2B}$ receptor agonists still caused a slight increase in HR, which could indicate that some of the effects might be due to chronotropic effects on the heart not involving β adrenoceptors.

Overall, data from this chapter suggest that the conjoint use of an $A_{2A}$ or $A_{2B}$ receptor selective agonist and a β-blocker might be an effective way to achieve the beneficial therapeutic effects of $A_{2A}$ and $A_{2B}$ receptor agonism while reducing the tachycardia associated with targeting these receptors, this will be discussed in detail in the discussion section of this thesis (**6.2**).

**Chapters 3** & **4** show that $A_{2A}$ receptor agonism produces a direct vasodilatory effect in the hindquarters, which is not due to β receptor reflex activity, and is associated with decreases in MAP. The next chapter will investigate the ability of $A_{2A}$ receptor agonism to relieve RTKI-induced hypertension associated with hindquarters vasoconstrictions (**5.1**).

# 5 Chapter 5: Potential for Adenosine $A_{2A}$ Receptor Agonists to Address the Haemodynamic Consequences of Sunitinib Treatment

# 5.1 Haemodynamic Responses to Sunitinib with $A_{2A}$ Receptor Activation: Chapter Introduction

RTKIs block the catalytic function of RTKs, preventing ATP-dependent phosphorylation (Davis et al., 2011). Most small molecule RTKIs are multi-targeted and inhibit numerous kinases; many of these are associated with cell growth, and thus RTKIs are effective anti-cancer agents (**1.3.1.1**) (Davis et al., 2011).

Sunitinib is an RTKI that has both antiangiogenic and antitumour activities against a broad range of malignancies; it has seen longstanding clinical use and is approved for treating advanced renal cell carcinomas, gastrointestinal stromal tumours and pancreatic neuroendocrine tumours (**1.3.3**) (Goodman et al., 2007, Motzer et al., 2017, Vivanet et al., 2022). Sunitinib has been demonstrated to inhibit a selection of RTKs that are important to cell division and angiogenesis, including VEGFRs1-3 and PDGFR α & β (**1.3.3**) (Abrams et al., 2003, Mendel et al., 2003, Faivre et al., 2007).

Unfortunately, treatment with sunitinib is known to cause a large number of cardiovascular side effects, including high blood pressure in 30% of patients treated with this drug, with over a third of those developing severe grade 3-4 hypertension; other side effects of sunitinib include renal damage associated with proteinuria (**1.3.3**) (Motzer et al., 2009, Aparicio-Gallego et al., 2011, Lankhorst et al., 2014, Ollero and Sahali, 2014). Many of these side effects are due to the on-target blockade of VEGF signalling at VEGFR2 (**1.3.2.2**) (León-Mateos et al., 2015).

It has been shown that VEGFR2 inhibition decreases the production of the vasodilatory second messengers NO and prostacyclin, leading to vasoconstrictions and vascular rarefaction (a reduction in microvasculature surface area) in vascular beds, causing an elevation in peripheral vascular resistance and, as a result, hypertension (Taraseviciene-Stewart et al., 2001, Facemire et al., 2009). In addition, there is growing evidence that anti-VEGF therapies, including sunitinib, cause an increase in ET-1, a vasoconstrictor that has been demonstrated to be involved in anti-VEGF induced renal injury and contributes to the rise in blood pressure caused by these therapies (Bhargava, 2009, Lankhorst et al., 2014, León-Mateos et al., 2015). VEGF-targeting therapies can cause hypertension that is

resistant to standard antihypertensive medication (Robinson et al., 2010b, Carter et al., 2017). If unsuccessfully treated, long-term clinical hypertension can increase the risk of ischaemic vascular events, left ventricular dysfunction and heart failure (Katsi et al., 2014, Abi Aad et al., 2015). Antihypertensive medications commonly used to treat therapy-induced hypertension include vasodilatory treatments to counter the vasoconstrictive effects of RTKIs, such as angiotensin-converting enzyme inhibitors (ACEIs), $Ca^{2+}$ channel blockers and angiotensin II blockers (Maitland et al., 2010, de Jesus-Gonzalez et al., 2012, León-Mateos et al., 2015).

In the rat, it has been demonstrated that sunitinib causes hypertension associated with ET-1 release and suppression of the renin-angiotensin system by decreasing the functional responses to bradykinin and angiotensin II (Kappers et al., 2010, Blasi et al., 2012). The block of VEGF-induced production of prostacyclin and NO causes a subsequent increase in ET-1, which is involved in causing sunitinib-induced kidney damage and inducing proteinuria (Lankhorst et al., 2014, Baek Moller et al., 2019, Mirabito Colafella et al., 2020). Rat studies have demonstrated that ET-1 receptor blockade can reduce sunitinib-induced hypertension and proteinuria (Lankhorst et al., 2014, Mirabito Colafella et al., 2020). Although it is known that sunitinib causes hypertension associated with renal dysfunction and vasoconstriction, the extent to which regional vascular beds are affected remains unknown. Previously, a study of four multitargeted RTKIs (cediranib, sorafenib, pazopanib, or vandetanib) has shown that these RTKIs cause significant increases in MAP accompanied by decreases in mesenteric and hindquarters VC but not generally significant decreases in renal VC (Carter et al., 2017). In this chapter, the haemodynamic effects of sunitinib will be investigated, observing the regional effects of the drug at the renal, mesenteric and hindquarters vascular beds to determine if the hypertension induced by sunitinib has a profile similar to that observed for the other RTKIs investigated.

Both $A_{2A}$ and $A_{2B}$ receptors promote NO-induced vasodilatation, and, as a result, $A_{2A}$ and $A_{2B}$ receptors are potential targets for the treatment of hypertension (**1.1.6.2**) (Jacobson and Gao, 2006, Borea et al., 2018, Jamwal et al., 2019). Furthermore, in the kidney, activation of $A_{2A}$ and $A_{2B}$ receptors in response to hypoxic or ischaemic stress has been shown to have a role in preventing kidney necrosis by promoting perfusion of renal vascular beds (Yap and Lee, 2012, Borea et al., 2018). As a result of these physiological roles, $A_2$ receptors could be potential targets for treating both RTKI-induced hypertension and RTKI-induced kidney dysfunction (**6.2.1**, **6.2.2**).

Studies completed in **chapter 3** demonstrated that although the $A_{2B}$ receptor agonist BAY 60-6583 caused an increase in renal and mesenteric VC, it was not associated with a decrease in MAP (**3.3.1.4.1**). Conversely, the $A_{2A}$ receptor agonist CGS 21680 caused a reduction in MAP alongside increased hindquarters VC (**3.3.1.3.1**). In this chapter, because of the ability of $A_{2A}$ receptor agonism to cause a reduction in MAP, CGS 21680 was taken forward; investigations were thus undertaken to assess the ability of $A_{2A}$ receptor activation to temporarily reverse sunitinib-induced hypertension and decrease VC in regional vascular beds.

It is known that adenosine and VEGF receptors both promote cell growth, survival, and proliferation, angiogenesis, and tumour metastasis, but little is known about the potential synergism between adenosine and VEGF signalling in regulating haemodynamics (Adair, 2005, Escudero et al., 2014). In this chapter, to investigate the link between $A_2$ receptors and VEGFR2, exploratory *in vitro* studies were conducted to assess if a relationship between the cellular signalling of these receptors could be found. Adenosine $A_{2A}$ receptors cause vasodilation via cAMP-mediated NO release (Ray and Marshall, 2006, El-Gowelli et al., 2013). To investigate if VEGFR2 signalling could influence the cAMP response caused by $A_{2A}$ receptor activation, Glosensor cAMP assays were completed in HEK 293G cells transiently transfected with HiBiT-VEGFR2 to show if the presence of VEGF-$A_{165}$a, with or without sunitinib, influenced cAMP accumulation caused by treatment with CGS 21680.

One way receptors have been shown to exert influence on the signalling of other receptors is by receptor-receptor oligomerisation (Rozenfeld and Devi, 2010). For example, adenosine $A_2$ receptors are known to form functional oligomeric complexes (**1.4.1.1**) (Gahbauer and Bockmann, 2016). Furthermore, VEGFR2 has been shown to form both homodimers and heterodimers with other VEGFRs (**1.4.1.2**) (Nilsson et al., 2010, Sarabipour et al., 2016, Cai et al., 2017). Additionally, oligomeric complexes involving VEGFR2 and the $\beta_2$ adrenoceptor have been reported (Kilpatrick et al., 2019). This chapter investigated the possibility that VEGFR2 might colocalise with either $A_{2A}$ or $A_{2B}$ receptors using BRET saturation assays (Mercier et al., 2002), which were completed with NLuc- and SNAP-tagged versions of VEGFR2 and the $A_{2A}$ and $A_{2B}$ receptors (**2.2.6**).

# 5.2 Haemodynamic Responses to Sunitinib with $A_{2A}$ Receptor Activation: Chapter Methodology

## 5.2.1 Chapter 5 Methodology: *In Vivo*

### 5.2.1.1 Animals and Surgery

Experiments were carried out on Male Sprague-Dawley rats with approval from the UK Home Office and the University of Nottingham, as previously described (**2.1.5**). Full details of the two surgeries conducted for these experiments can be found in the general methodology (**2.1.5.1**, **2.1.5.2**). In brief, twenty-three rats (350-450 g) were used during the studies detailed in this chapter. The first surgery was conducted to implant miniature pulsed Doppler flow probes around the superior mesenteric and left renal arteries and the descending abdominal aorta to allow haemodynamic measurements that give information regarding the flow of blood to downstream regional vascular beds (**2.1.3.2**). A second surgery was carried out a minimum of 10 days after the implantation of the vascular probes. During this second surgery, a catheter was implanted via the caudal artery into the distal abdominal aorta to measure arterial blood pressure and allow the calculation of heart rate (Gardiner et al., 1980). In addition, three catheter lines were implanted into the right jugular vein to allow i.v. administration of compounds. The probe wires and catheters were protected inside a metal spring secured to a harness that went around the rat's torso, with the spring connected to a counterbalanced pivot system that allowed free movement of the rat (**Figure 12**). Experiments began 24 h after the second surgery, with the rats conscious and unrestrained, singly housed in home cages with access to food and water.

#### 5.2.1.2 Cardiovascular Recordings & Data Analysis

Detailed information on the cardiovascular recordings and data analysis can be found in the general methodology (**2.1.6**, **2.1.7**, **2.1.8**). In brief, rats were indirectly connected to the data acquisition programme (IdeeQ) during the monitoring periods via a tether system (**2.1.3**). Daily recordings were made for at least 30 min prior to the administration of any interventions and continuously for a minimum of 4 h thereafter. HR, MAP, renal, mesenteric and hindquarters Doppler shifts were measured (**2.1.3.1**, **2.1.3.2**), and changes in VC in the renal, mesenteric, and hindquarter vascular beds were calculated from the changes in MAP and Doppler shift (**2.1.3.3**). For both studies found in this chapter, time-averaged data are shown as variation from day 1 baseline [HR (beats.min$^{-1}$); MAP (mmHg); VC (%)]. The day 1 baseline was taken when the rat was at rest before the administration of any interventions.

A Friedman test was used for within-group comparisons compared to the day 1 baseline to ascertain if there was a significant difference between the timepoint and the day 1 baseline. Additionally, a Mann-Whitney test was also conducted for between-group comparisons concerning different dosing treatment regimens at each time point. For all statistical analyses, $p<0.05$ was considered significant.

Statistical tests were not performed on the results of the experiments detailed in study 13 (**5.2.1.3.1**) as these experiments were pilot studies and were purposely underpowered, so they could not provide statistical significance.

## 5.2.1.3 The Haemodynamic Effects of Sunitinib

### 5.2.1.3.1 Study 13 (Pilot Study): Sunitinib Dose Selection

Experiments were run for three days. This pilot study aimed to find a tolerable daily dose of sunitinib that caused the development of hypertension over the course of a 3-day protocol, as previously demonstrated to occur with a range of other RTKIs (Carter et al., 2017). The vehicle buffer used for these experiments was 5 % propylene glycol, 2 % Tween 80 in sterile saline. Because these experiments were pilots to determine hypertension of the dose of Sunitinib, only the HR and MAP are presented in the results of these studies (**Table 19**, **Figure 43**, **Figure 44**). However, complete experimental data for these pilot studies can be found in the appendix (**7.3**, **Table 23**, **Figure 56**, **Figure 57**).

A single rat was administered with 4.0 mg/kg/day sunitinib (**group 1A**). On completion of this experiment, this dose (4.0 mg/kg/day) of sunitinib failed to produce a sustained hypertensive effect (**Figure 43**), and so a single rat was run with 8.0 mg/kg/day sunitinib (**group 1B**). Upon completion of this second experiment, 8.0 mg/kg/day sunitinib looked to have caused sustained hypertension, so the pilot was expanded to n=3, with an n=3 vehicle control group run alongside this study (**group 2**). Rats were randomly allocated based on a study independent identification number assigned to the rat on entry into the animal unit into the sunitinib group (**group 1B**) or the vehicle control group (**group 2**). Upon completing this pilot study, it became apparent that 8.0 mg/kg/day sunitinib would not likely lead to sustained hypertension between the experimental days if the experiment was expanded to n=8 (**Figure 44**). Because the primary objective to find a dose of sunitinib that caused sustained hypertension over the course of 3-days was not met, no further animals were completed at this dose of sunitinib, as to do so would not be ethical. As a result of this pilot, a higher dose of 16 mg/kg/day was successfully investigated, as discussed in study 14 (**5.2.1.3.2**).

### Group 1A (Pilot Study): Sunitinib (4.0 mg/kg/day) with Additional Vehicle Administration on Day 3

One animal was used to assess the cardiovascular responses to sunitinib over a 3-day administration period, with an additional administration of vehicle on day 3. At the beginning of each of the three days, after a period of baseline recording, a sunitinib bolus (2.0 mg/kg, 0.1 mL, i.v.) and an immediate infusion of sunitinib (2.0 mg/kg/hr, 0.4 mL/hr, 60 min, i.v.) were administered. On day 3, 50 min after the start of the sunitinib infusion, the group received an additional three infusions (0.1 mL/min, i.v.) in continuous succession of the vehicle, with each dose infused for 3 min. Haemodynamic recordings were made for a subsequent 4-hour period following the completion of these vehicle infusions on each day.

### Group 1B (Pilot Study): Sunitinib (8.0 mg/kg/day) with Additional Vehicle Administration on Day 3

Three animals were used to assess the cardiovascular responses to sunitinib over a 3-day administration period, with an additional vehicle administration on day 3. At the beginning of each of the three days, after a period of baseline recording, a sunitinib bolus (4.0 mg/kg, 0.1 mL, i.v.) and an immediate infusion of sunitinib (4.0 mg/kg/hr, 0.4 mL/hr, 60 min, i.v.) were administered. On day 3, 50 min after the start of the sunitinib infusion, the group received an additional three infusions (0.1 mL/min, i.v.) in continuous succession of the vehicle, with each dose infused for 3 min. Haemodynamic recordings were made for a subsequent 4-hour period following the completion of these vehicle infusions on each day.

### Group 2 (Pilot Study): Vehicle Administration with Additional Vehicle Administration on Day 3

Three animals were used to assess the cardiovascular responses to vehicle over a 3-day administration period, with an additional administration of vehicle on day 3. At the beginning of each of the three days, after a period of baseline recording, a vehicle bolus (0.1 mL, i.v.) and an immediate infusion of vehicle (0.4 mL/hr, 60 min, i.v.) were administered. On day 3, 50 min after the start of the vehicle infusion, the group received an additional three infusions (0.1 mL/min, i.v.) in continuous succession of the vehicle, with each dose infused for 3 min. Haemodynamic recordings were made for a subsequent 4-hour period following the completion of these vehicle infusions on each day.

#### 5.2.1.3.2 Study 14: The Haemodynamic Effects of Sunitinib and the Modulation of its Effects by CGS 21680

### Study 14: Experimental Protocol

After 4.0 and 8.0 mg/kg/day doses of sunitinib failed to produce sustained hypertension (**5.2.1.3.1**, **Figure 43**, **Figure 44**), 16.0 mg/kg/day sunitinib was trialled; for this increased dose, the bolus was increased to 0.2 mL as there were solubility issues with the compound at this concentration. A single rat was run with 16.0 mg/kg/day sunitinib with additional doses of CGS 21680 on day 3 to ensure that this dosing regimen was tolerable before expanding this experiment to include other animals (**group 1**). Upon completion, sustained hypertension was observed in this rat and was tolerable for the animal, so the experiment was expanded to n=8 (**group 1**), with an n=8 vehicle control group run alongside this study (**group 2**). Rats were randomly allocated based on a study-independent identification number assigned to the rat on entry into the animal unit into the sunitinib group (**group 1**) or a control vehicle group (**group 2**). The vehicle buffer used for these experiments was 5 % propylene glycol, 2 % Tween 80 in sterile saline.

### Group 1: Sunitinib Administration with Additional CGS 21680 Administration on Day 3

Eight animals were used to assess the cardiovascular responses to sunitinib over a 3-day administration period, with an additional administration of CGS 21680 on day 3. At the beginning of each of the three days, after a period of baseline recording, a sunitinib bolus (8.0 mg/kg, 0.2 mL, i.v.) and an immediate infusion of sunitinib (8.0 mg/kg/hr, 0.4 mL/hr, 60 min, i.v.) were administered. On day 3, 50 min after the start of the sunitinib infusion, the group received an additional three infusions (0.1 mL/min, i.v.) in continuous succession of CGS 21680 (0.1 [low], 0.3 [mid], and 1.0 [high] µg/kg/min), with each dose infused for 3 min, starting from the lowest dose. Haemodynamic recordings were made for a subsequent 4-hour period following the completion of these CGS 21680 infusions each day.

**Group 2: Vehicle Administration with Additional Vehicle Administration on Day 3**

Eight animals were used to assess the cardiovascular responses to the vehicle over a 3-day administration period, with an additional vehicle administration on day 3. At the beginning of each of the three days, after a period of baseline recording, a vehicle bolus (0.2 mL, i.v.) and an immediate infusion of vehicle (0.4 mL/hr, 60 min, i.v.) were administered. On day 3, 50 min after the start of the vehicle infusion, the group received an additional three infusions (0.1 mL/min, i.v.) in continuous succession of vehicle, with each infusion infused for 3 min. Haemodynamic recordings were made for a subsequent 4-hour period following the completion of these vehicle infusions on each day.

## 5.2.2 Chapter 5 Methodology: *In Vitro*

### 5.2.2.1 GloSensor Cyclic AMP Assays

GloSensor cAMP assays were carried out as previously described (**2.2.7.2**). Briefly, HEK G cells were transiently transfected to express human HiBiT-VEGFR2 receptors (**2.2.4.1**), and were seeded onto white 96-well plates at a density of 30,000 cells/well (**2.2.4.2**). The following day, the cell media was replaced with 50 µL of HBSS supplemented with 0.1% BSA (**2.2.4.3**) containing 3% GloSensor cAMP reagent (Promega) and incubated for 2 h at 37°C. A baseline luminescence recording was measured on a PHERAstar FS plate reader set to 37°C before 50 µL HBSS with or without the presence of (10 µM) or CGS 21680 (1.0 µM) was added to the well, and luminescence was read continuously over 60 min, with 1 read per well every minute. When used, VEGF-$A_{165}$a (1.0 nM), sunitinib (10 µM) or a combination of the two was incubated alongside the Glosensor cAMP reagent for 2 h before the addition of the other ligands. The DMSO concentration in all wells was equalised to a final in-well concentration of 0.1%.

#### 5.2.2.2 NanoBRET Saturation Assays

NanoBRET saturation assays were carried out as previously described (**2.2.6.1.1**). Briefly, HEK 293T cells were seeded onto white 96-well plates at a density of 15,000 cells/well and incubated for 16 h at 37°C/5% $CO_2$. Then, 16 h after seeding, the cells were transiently cotransfected with an NLuc N-terminal tagged receptor (either NLuc-$A_{2A}$ receptor, NLuc-$A_{2B}$ receptor or NLuc-VEGFR2 (10 ng/well), alongside increasing concentrations of an N-terminal tagged SNAP-tag labelled receptor (SNAP-$A_{2A}$ receptor or SNAP-$A_{2B}$ receptor (0-40 ng/well) using FuGENE HD (Promega), with empty p3.1zeo vector used to ensure total transfected cDNA concentrations were kept consistent at 50 ng/well across all wells (**2.2.6.1.1**).

After transfection, cells grew for an additional 24 h at 37°C/5% $CO_2$. On the assay day, cells were incubated with 0.2 µM SNAP-Tag AF488 membrane impermeable substrate prepared in FBS-free DMEM for 30 min at 37°C/5% $CO_2$. After incubation, cells were washed three times with HBSS supplemented with 0.1% BSA, which also served as the experiment's incubation medium. Furimazine was added to each well to a final in-well concentration of 10 µM, and the cells incubated for an additional 5 min at room temperature. The plates were read at room temperature using a PHERAstar FS plate reader. Sequential luminescence and fluorescence emission measurements were taken utilising the BRET 1 plus optic module, measuring filtered light emissions at 475 nm (30 nm bandpass) and 535 nm (30 nm bandpass). The experimental results were represented by raw BRET values, which were calculated by taking the ratio of the 535 nm fluorescence emission (acceptor) over the luminescence 475 nm emission (donor).

For all experiments, a line of best fit was fitted to a non-linear regression- one site total binding equation. In addition, a one-way ANOVA was conducted for each experiment to determine whether there was a significant change with increasing doses of transfected SNAP-receptor, with the significance highlighted for each experiment on each graph.

# 5.3 Haemodynamic Responses to Sunitinib with $A_{2A}$ Receptor Activation: Chapter Results

## 5.3.1 Chapter 5 Results: *In Vivo*

### 5.3.1.1 The Cardiovascular Consequences of Sunitinib Administration

Pilot studies were conducted to find a suitable daily dose of sunitinib that was well-tolerated and caused the development of sustained hypertension in the rat over the 3-day experimental protocol (**5.2.1.3**). First, an experiment was conducted on a single rat exploring the effect of 4.0 mg/kg/day sunitinib (**5.2.1.3.1**). 4.0 mg/kg/day caused observable increases in MAP, but these were transient and not sustained between days (**Figure 43**). Following this, 8.0 mg/kg/day was trialled, as previously described (**5.2.1.3.1**). 8.0 mg/kg/day sunitinib did not cause an observable sustained increase in MAP against vehicle control across this pilot study (**Figure 44**). After this result, 16.0 mg/kg/day sunitinib was successfully trialled, and experiments were continued at this dose (n=8) (**5.2.1.3.2**). For the 16.0 mg/kg/day sunitinib experiment, the daily dose of sunitinib comprised of a 0.2 mL bolus (8.0 mg/kg, i.v.), followed by an immediate infusion of sunitinib lasting for 60 min (8.0 mg/kg/hr, 0.4 mL/hr, i.v.).

Sunitinib (16.0 mg/kg/day) infusion caused a significant ($p<0.05$) versus baseline reduction in HR throughout the dosing period on days 1 and 2 that was present from 5 min after the bolus infusion. The reduction in HR caused by sunitinib in the dosing period was significantly ($p<0.05$) different to the vehicle group on day 1 and at sporadic timepoints throughout the dosing period of day 2 (**Figure 45**). The significant ($p<0.05$) fall in HR caused by sunitinib versus both baseline and vehicle control was sustained during the 4 hour monitoring period on day 1, but only versus baseline on day 2, with the significance of the effect wearing off by 4 hours post-dosing (**Figure 46**). The bradycardia caused by sunitinib infusion was transient and not sustained across study days (**Figure 45, Figure 46**).

On study day 1, sunitinib infusion caused a significant ($p<0.05$) versus baseline, but not vehicle, increase in MAP from 5 min after the bolus infusion, with this increase continued throughout the sunitinib dosing period but not sustained during the 4 hour monitoring period on this day. MAP continued to climb throughout the study; the rise in MAP caused by sunitinib was significant ($p<0.05$) versus both baseline and vehicle control before the administration of the drug at the start of day 2; with MAP continuing to increase following sunitinib treatment on this second day (**Figure 46**).

Sunitinib (16.0 mg/kg/day) caused a reduction in renal VC from 3 hours after the dosing period on day 1, which was significant ($p<0.05$) versus both baseline and vehicle control, and that was sustained from this point onwards throughout the study (**Figure 45, Figure 46**). Sunitinib also caused a similar significant ($p<0.05$) reduction in mesenteric VC versus both baseline and vehicle control on day 2 (**Figure 45, Figure 46**); however, in contrast to the renal vascular beds, on day 1, a significant ($p<0.05$) reduction versus both baseline and vehicle control was observed in mesenteric VC during the sunitinib dosing period; mesenteric VC remained significantly ($p<0.05$) decreased versus baseline but not vehicle control throughout the first day across the 4 hour observation period (**Figure 45, Figure 46**). In the hindquarters vascular bed, on day 1, a decrease in VC was observed during the sunitinib dosing period, which was significant ($p<0.05$) versus baseline and sporadically significant ($p<0.05$) versus vehicle control (**Figure 45**). During the post-dosing 4 hour observation period on day 1, hindquarters VC was significantly ($p<0.05$) decreased from both baseline and vehicle control (**Figure 46**). On the second day, before drug administration, hindquarters VC was significantly ($p<0.05$) lower than both baseline and vehicle control (**Figure 45, Figure 46**). However, during the sunitinib dosing period on this second day, hindquarters VC increased compared to the conductance observed before sunitinib administration, and as a result, throughout the second day, hindquarters VC was not significantly different ($p>0.05$) compared to vehicle control, although hindquarters VC throughout day 2 remained significantly ($p<0.05$) lower when compared to the day 1 baseline (**Figure 45, Figure 46**).

On day 3, before drug administration, the group receiving sunitinib (16.0 mg/kg/day) had a significant ($p<0.05$) versus both day 1 baseline and vehicle control group increase in MAP and decrease in the VC of the renal, mesenteric and hindquarters vascular beds. No significant change in HR was present on day 3 before the administration of ligands (**Figure 45, Figure 46**).

Sunitinib (16.0 mg/kg/day) administration on day 3 caused no additional change to VC at any of the three vascular beds across the dosing period (**Figure 45**). A reduction in MAP was observed across the sunitinib dosing period on day 3; MAP 50 min into the sunitinib dosing period was significantly ($p<0.05$, Wilcoxon matched-pairs signed rank test) lower than the MAP before dosing began on the third day. However, for these rats dosed with sunitinib, MAP remained significantly ($p<0.05$) increased compared to both the day 1 baseline and the vehicle control group throughout the day-3 dosing period (**Figure 45**). In addition, sunitinib (16.0 mg/kg/day) administration on day 3 caused a reduction in HR during the dosing period that was significant ($p<0.05$) versus baseline and that was significant ($p<0.05$) versus vehicle from 40 min after the start of the sunitinib infusion (**Figure 45**).

| | Study 13: Sunitinib 4.0 mg/kg/day | | Study 13: Sunitinib 8.0 mg/kg/day | | Study 13: Vehicle | |
|---|---|---|---|---|---|---|
| | Vehicle | | Vehicle | | Vehicle | |
| | Value | n | Mean ± SEM | n | Mean ± SEM | n |
| **Cardiovascular Variable** | **Baseline T=0** | | **Baseline T=0** | | **Baseline T=0** | |
| **Heart rate (beats·min$^{-1}$)** | 318 | 1 | 359 ± 8 | 3 | 333 ± 17 | 3 |
| **Mean BP (mmHg)** | 103 | 1 | 112 ± 7 | 3 | 106 ± 6 | 3 |

**Table 19 Cardiovascular Variables Before Administration of Sunitinib or Vehicle in Study 13.** n=1-3 per group. Values are mean ± SEM when n>1. Readings correspond to the baseline recordings (zero values) for the graphs in **Figure 43** & **Figure 44**.

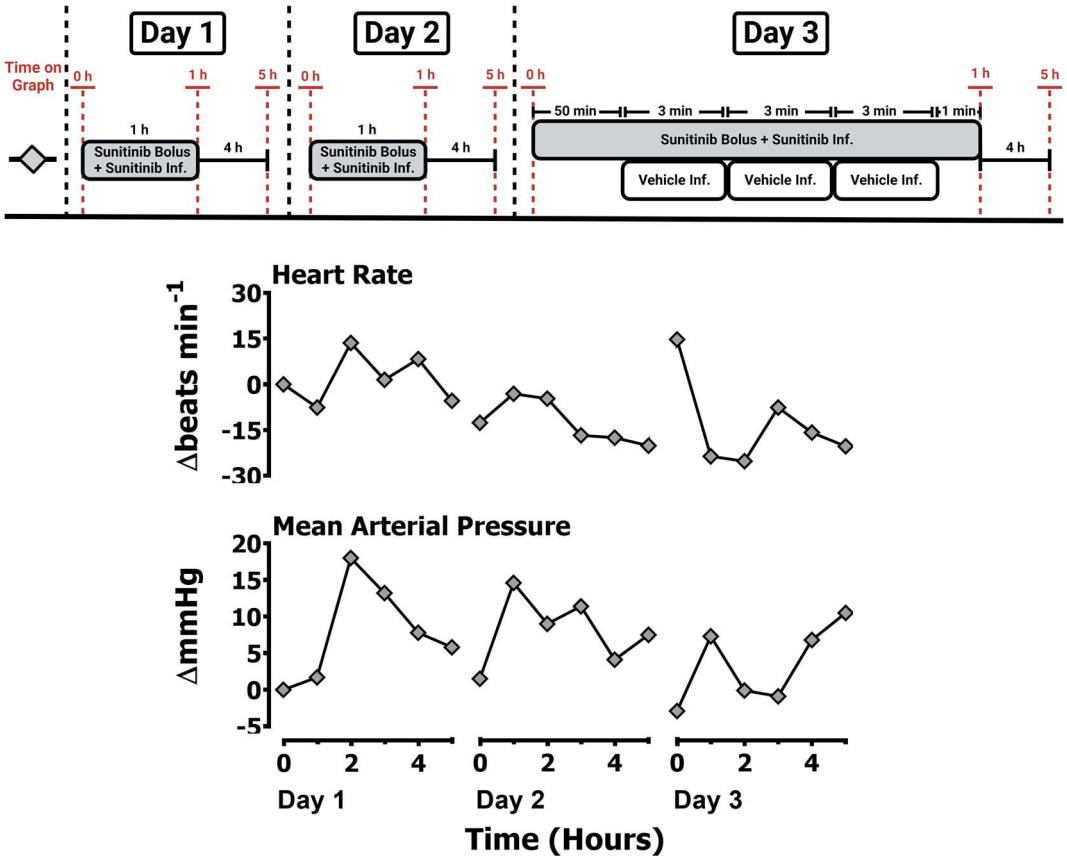


**Figure 43 Cardiovascular Responses to Sunitinib (4.0 mg/kg/day).** A conscious, freely moving rat was dosed daily for three consecutive days at time=0 each day with sunitinib (0.1 mL bolus of 2.0 mg/kg, i.v.) and an immediate subsequent infusion of sunitinib (2.0 mg/kg/hr, 0.4 mL/hr, 60 min, i.v., n=1). On day 3, 50 min after the start of the sunitinib infusion, the group received an additional three infusions (0.1 mL/min, i.v.) in succession of the vehicle, with each dose infused for 3 minutes as described in the chapter methodology (**5.2.1.3.1**). The graphs show the responses 4 hours post-dosing for all 3 experimental days. Data points are single values. Results are from study 13. Baseline recordings for this figure can be found in **Table 19**.

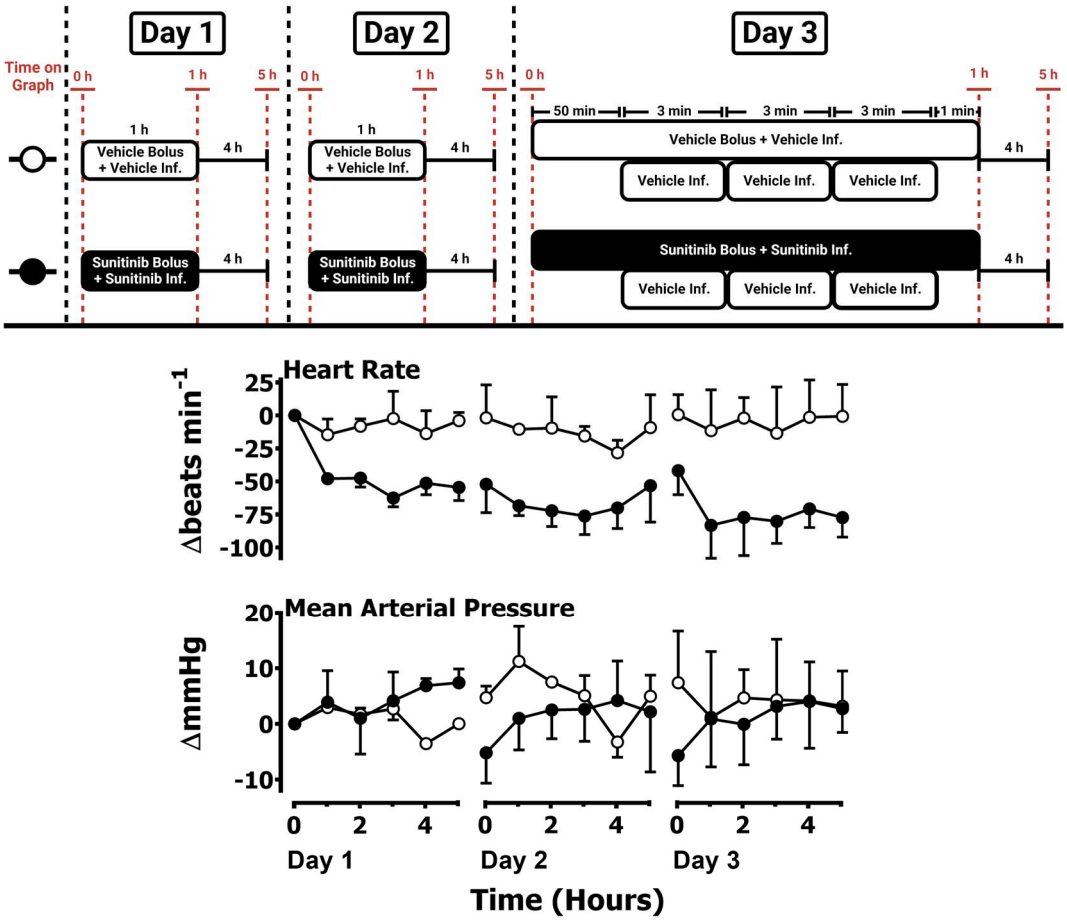


**Figure 44 Cardiovascular Responses to Sunitinib (8.0 mg/kg/day).** Conscious, freely moving rats were dosed daily for three consecutive days at time=0 each day with sunitinib (0.1 mL bolus of 4.0 mg/kg, i.v.) and an immediate subsequent infusion of sunitinib (4.0 mg/kg/hr, 0.4 mL/hr, 60 min, i.v., n=3) or vehicle (0.1 mL bolus of 5 % propylene glycol, 2 % Tween 80 in sterile saline, i.v.) and an immediate subsequent infusion of vehicle (0.4 mL/hr, 90 min, i.v., n=3). On day 3, 50 min after the start of the sunitinib or vehicle infusion, the group received an additional three infusions (0.1 mL/min, i.v.) in succession of the vehicle, with each dose infused for 3 minutes as described in the chapter methodology (**5.2.1.3.1**). The graphs show the responses 4 hours post-dosing for all 3 experimental days. Data points are mean + or - SEM. Results are from study 13. Baseline recordings for this figure can be found in **Table 19**.

| | **Study 14: Sunitinib 16 mg/kg/day + Day 3 CGS 21680** | | **Study 14: Vehicle + Day 3 Vehicle** | |
|---|---|---|---|---|
| | **Vehicle** | | **Vehicle** | |
| | **Mean ± SEM** | **n** | **Mean ± SEM** | **n** |
| **Cardiovascular Variable** | **Baseline T=0** | | **Baseline T=0** | |
| **Heart rate (beats·min$^{-1}$)** | 342 ± 11 | 8 | 340 ± 8 | 8 |
| **Mean BP (mmHg)** | 100 ± 3 | 8 | 106 ± 4 | 8 |
| **Renal VC (U)** | 105 ± 6 | 6 | 96 ± 6 | 7 |
| **Mesenteric VC (U)** | **100 ± 7*** | 8 | 72 ± 9 | 7 |
| **Hindquarters VC (U)** | 41 ± 5 | 8 | 45 ± 6 | 7 |

**Table 20 Cardiovascular Variables Before Administration of Sunitinib or Vehicle in Study 14.** Values are mean ± SEM; n=6-8 per group. Abbreviations: U, units; VC, vascular conductance. Units (U) of vascular conductance (VC) are kHz. mmHg$^{-1}$ x $10^3$. A Mann-Whitney test was conducted between the antagonist group and its corresponding vehicle control group (* = $p<0.05$ significance). Readings correspond to the baseline recordings (zero values) for the graphs in **Figures 45 & 46.**

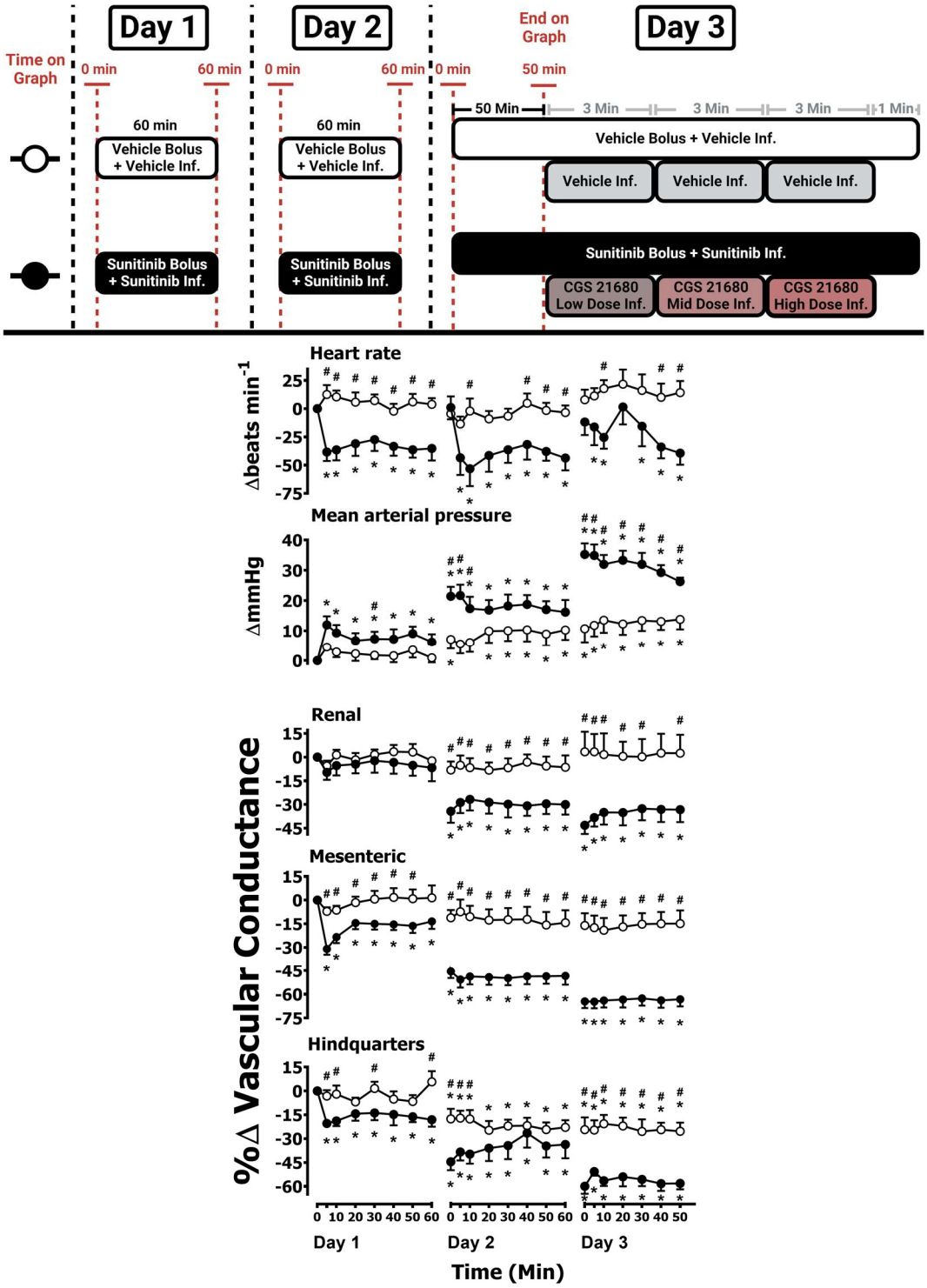


**Figure 45 Cardiovascular Responses to Sunitinib (16.0 mg/kg/day), 10 Min.** Conscious, freely moving rats were dosed daily for three consecutive days at time=0 for each day with sunitinib (0.2 mL bolus of 8.0 mg/kg, i.v.) and an immediate subsequent infusion of sunitinib (8.0 mg/kg/hr, 0.4 mL/hr, 60 min, i.v., n=8) or vehicle (0.2 mL bolus of 5 % propylene glycol, 2 % Tween 80 in sterile saline, i.v.) and an immediate subsequent infusion of vehicle (0.4 mL/hr, 90 min, i.v., n=8) as described in the chapter methodology (**5.2.1.3.2**). The graphs show the cardiovascular responses over the 60 min dosing period for day 1 & day 2 and over 50 min of the dosing period on day 3. Data points are mean + or - SEM. A Friedman test was conducted for each data point of each group and the group's corresponding baseline (time 0 on day 1) (* = $p<0.05$ significance). A Mann-Whitney test was conducted between the sunitinib and vehicle control groups to determine differences at each time point (**#** = $p<0.05$ significance). Results from study 14. Baseline recordings can be found in **Table 20**.

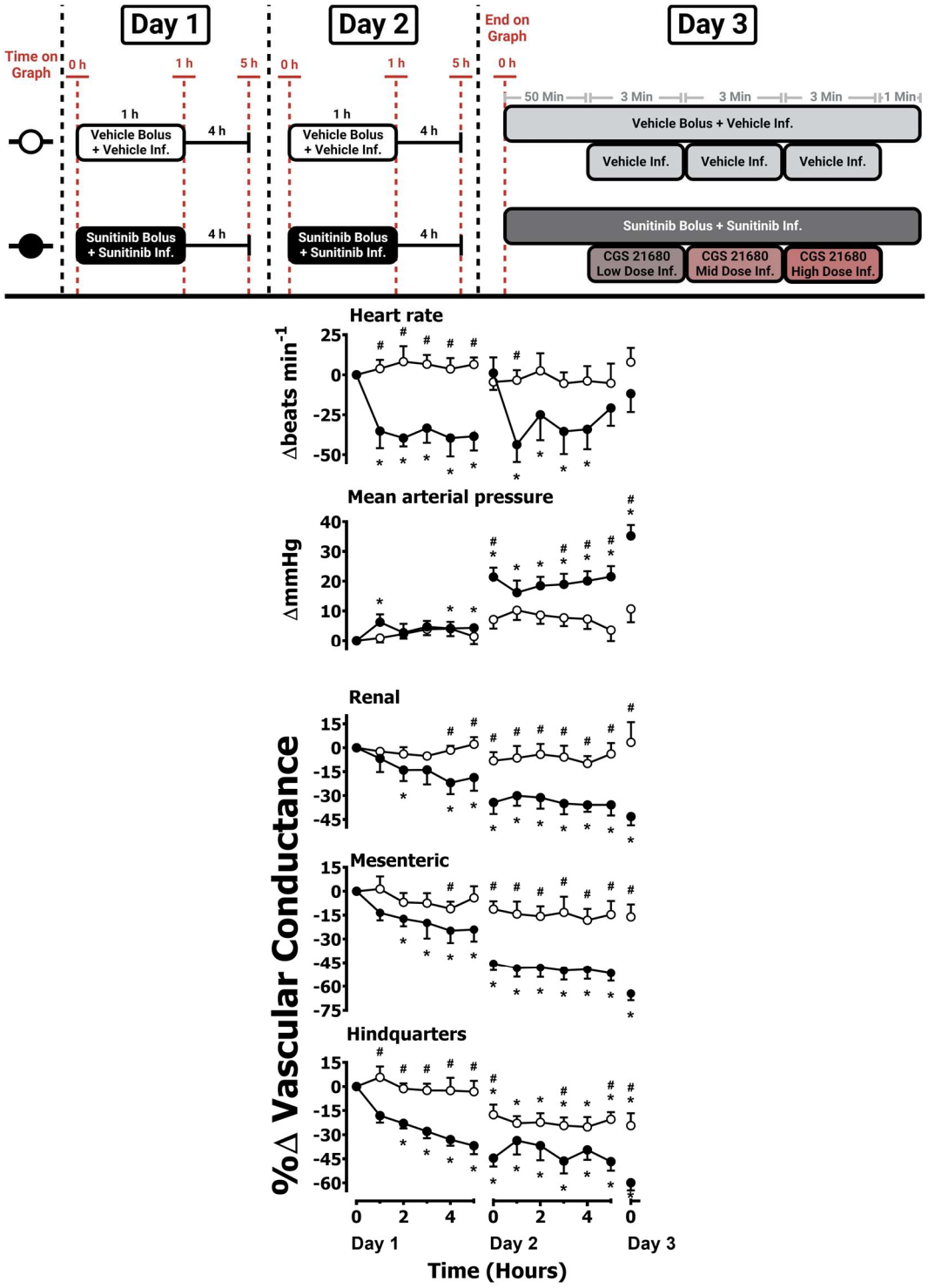


**Figure 46 Cardiovascular Responses to Sunitinib (16.0 mg/kg/day), Hourly.** Conscious, freely moving rats were dosed daily for three consecutive days at time=0 for each day with sunitinib (0.2 mL bolus of 8.0 mg/kg, i.v.) and an immediate subsequent infusion of sunitinib (8.0 mg/kg/hr, 0.4 mL/hr, 60 min, i.v., n=8) or vehicle (0.2 mL bolus of 5 % propylene glycol, 2 % Tween 80 in sterile saline, i.v.) and an immediate subsequent infusion of vehicle (0.4 mL/hr, 90 min, i.v., n=8) as described in the chapter methodology (**5.2.1.3.2**). The graphs show the responses for 4 hours after the dosing period on day 1 & day 2 and the baseline before the dosing period (time 0) on day 3. Data points are mean + or - SEM. A Friedman test was conducted for each data point of each group and the group's corresponding baseline (time 0 on day 1) (* = $p<0.05$ significance). A Mann-Whitney test was conducted between the sunitinib and vehicle control groups to determine differences at each time point (**#** = $p<0.05$ significance). Results from study 14. Baseline recordings can be found in **Table 20**.

#### 5.3.1.2 Cardiovascular Responses to CGS 21680, Following Pretreatment with Sunitinib

Rats were split into two groups and dosed daily for three consecutive days with sunitinib (0.2 mL bolus of 8.0 mg/kg, i.v.) and an immediate subsequent infusion of sunitinib (8.0 mg/kg/hr, 0.4 mL/hr, 60 min, i.v., n=8) or vehicle (0.2 mL bolus of 5 % propylene glycol, 2 % Tween 80 in sterile saline, i.v.) and an immediate subsequent infusion of vehicle (0.4 mL/hr, 90 min, i.v., n=8). On day 3, 50 min into the infusion of either sunitinib or vehicle, the group undergoing sunitinib infusion was additionally administered with an infusion of a consecutive low, medium and high dose of CGS 21680 (0.1, 0.3 and 1.0 µg/kg/min, 0.1 mL/min, i.v.), with each dose run for 3 min, and the vehicle group administered corresponding vehicle control infusions (0.1 mL/min, i.v.) as described in the chapter methodology (**5.2.1.2**).

The haemodynamic effects of the sunitinib infusion have been discussed previously (**5.3.1.1**, **Figure 45, Figure 46**). Just before the administration of CGS 21680 or vehicle control (time=50 min **Figure 45**; time=0 **Figure 47**), the group receiving sunitinib (16.0 mg/kg/day) had a significant ($p<0.05$) versus day 1 baseline and vehicle control group increase in MAP and decrease in the VC of the renal, mesenteric and hindquarters vascular beds (**Figure 45**, **Figure 47**). Additionally, as a result of the ongoing sunitinib administration, the sunitinib treatment group had a significant ($p<0.05$) decrease in HR versus day 1 baseline and vehicle control (**5.3.1.1**; **Figure 45, Figure 46, Figure 47**).

In the group undergoing sunitinib treatment, the administration of consecutive doses of CGS 21680 caused a dose-dependent increase in HR (**Figure 47**). Before CGS 21680 administration, HR was significantly ($p<0.05$) lower than both the day 1 baseline and vehicle control; HR rose to a value similar to the vehicle control approximately after the mid-dose of CGS 21680, and then became significantly ($p<0.05$) higher than both the day 1 baseline and vehicle control during the high dose of CGS 21680 (**Figure 47**).

In the group undergoing sunitinib treatment, the administration of consecutive doses of CGS 21680 caused a dose-dependent decrease in MAP (**Figure 47**). Before CGS 21680 administration, MAP was significantly ($p<0.05$) higher than both the day 1 baseline and vehicle control; MAP fell to a value similar to the vehicle control during the high dose of CGS 21680 (**Figure 47**). Immediately after the completion of the CGS 21680 dosing regimen, MAP was significantly ($p<0.05$) lower than the vehicle control group and was not significantly ($p>0.05$) different from the day 1 baseline (**Figure 47**).

In the group undergoing sunitinib treatment, the administration of consecutive doses of CGS 21680 caused a dose-dependent increase in VC in the renal, mesenteric and hindquarters vascular beds (**Figure 47**). Due to the increase in VC caused by the CGS 21680 dosing regimen, immediately following CGS 21680 administration VC at all three vascular beds was no longer significantly ($p>0.05$) different than either the day 1 baseline or the vehicle control group (**Figure 47**). Notably, the most considerable increase in VC observed by the effects of CGS 21680 was found at the hindquarters vascular bed (**Figure 47**). Significant ($p<0.05$) effects were observed up to 50 min following the completion of the CGS 21680 dosing period (**Figure 47**).

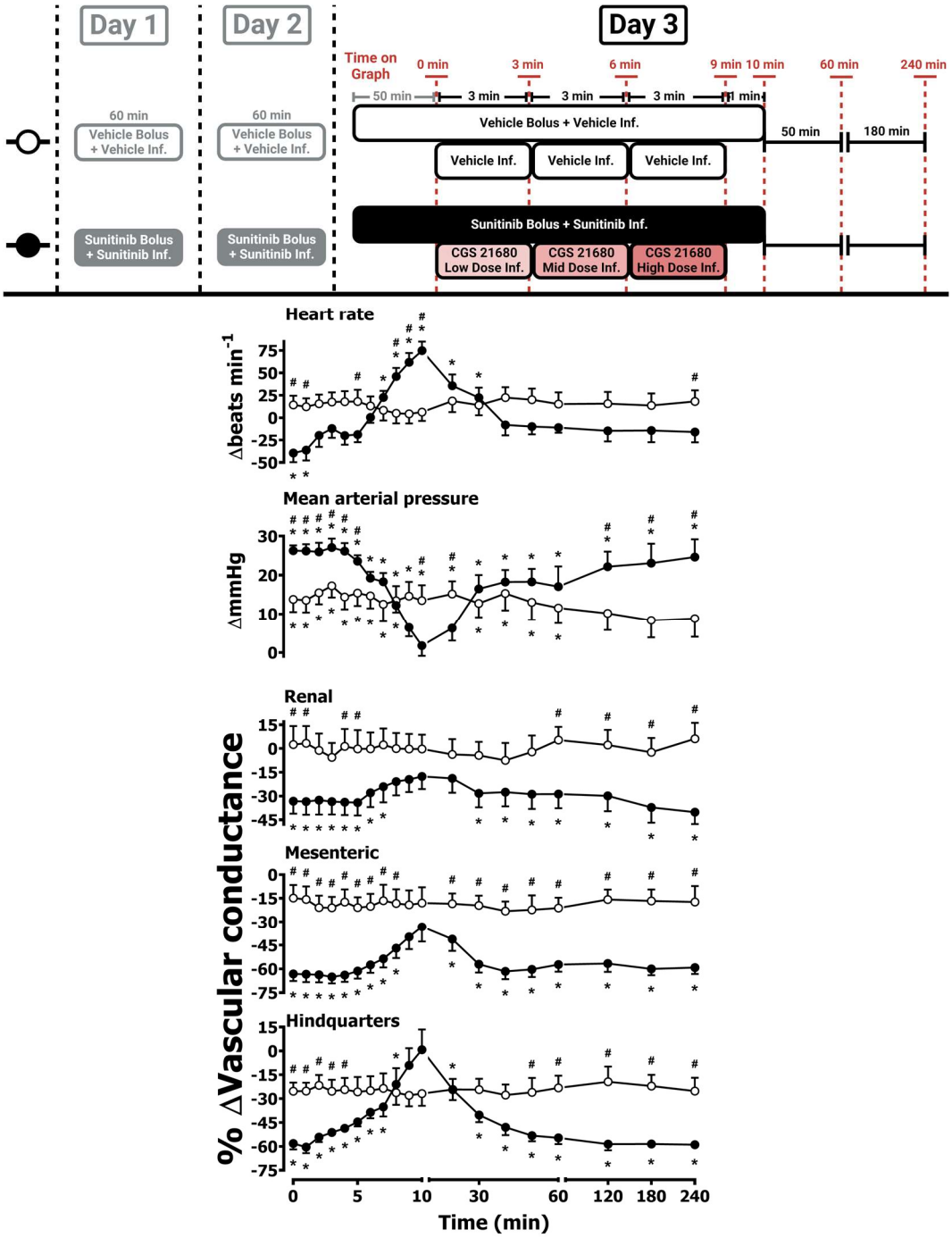


**Figure 47 Cardiovascular Responses to CGS 21680, Following Pretreatment with Sunitinib.** Conscious, freely moving rats were dosed daily for three consecutive days with sunitinib (0.2 mL bolus of 8.0 mg/kg, i.v.) and an immediate subsequent infusion of sunitinib (8.0 mg/kg/hr, 0.4 mL/hr, 60 min, i.v., n=8) or vehicle (0.2 mL bolus of 5 % propylene glycol, 2 % Tween 80 in sterile saline, i.v.) and an immediate subsequent infusion of vehicle (0.4 mL/hr, 90 min, i.v., n=8). On day 3, 50 min into the infusion of either sunitinib or vehicle (Time=0 on this figure), the group undergoing sunitinib infusion was additionally administered with an infusion of a consecutive low, medium and high dose of CGS 21680 (0.1, 0.3 and 1.0 µg/kg/min, 0.1 mL/min, i.v.), with each dose run for 3 min. The vehicle group was administered corresponding vehicle control infusions (0.1 mL/min, i.v.). Dosing as described in the chapter methodology (**5.2.1.3.2**). Data points are mean + or - SEM. A Friedman test was conducted for each data point of each group, and the group's corresponding baseline was taken on day 1 (* = $p<0.05$ significance). A Mann-Whitney test was conducted between the sunitinib and vehicle control groups to determine differences at each time point (**#** = $p<0.05$ significance). Results are from study 14.

## 5.3.2 Chapter 5 Results: *In Vitro*

### 5.3.2.1 Glosensor cAMP Assays

Glosensor assays were carried out as previously described to investigate cyclic AMP responses to CGS 21680 (1.0 μM) in the presence or absence of other ligands (**5.2.2.1**). The CGS 21680 dose was chosen based on previous dose-response cAMP Glosensor experimental results that showed that 1.0 μM CGS 21680 provided a robust but submaximal CGS 21680 response in HEK 293G cells (**Figure 32**).

In HEK 293G cells transiently transfected with human HiBiT-VEGFR2, Glosensor cyclic AMP responses to CGS 21680 in the presence and absence of VEGF-$A_{165}$a were investigated (**Figure 48**). The presence of a 2 h pretreatment of $VEGF_{165}$a (1.0 nM) significantly ($p<0.05$) enhanced the peak cAMP response to CGS 21680 (1.0 μM) (**Figure 48A**). Conversely, a 2 h pretreatment of both VEGF-$A_{165}$a (1.0 nM) and sunitinib (10 μM) did not cause a significant ($p>0.05$) change to the peak cAMP response to CGS 21680 (1.0 μM) when compared to either the response of CGS 21680 in isolation (**Figure 48B**) or CGS 21680 in the presence of a 2 h pretreatment of sunitinib (10 μM) (**Figure 48C**). In addition, the presence or absence of sunitinib did not significantly ($p>0.05$) affect the peak response to CGS 21680 (1.0 μM) (**Figure 48D**).

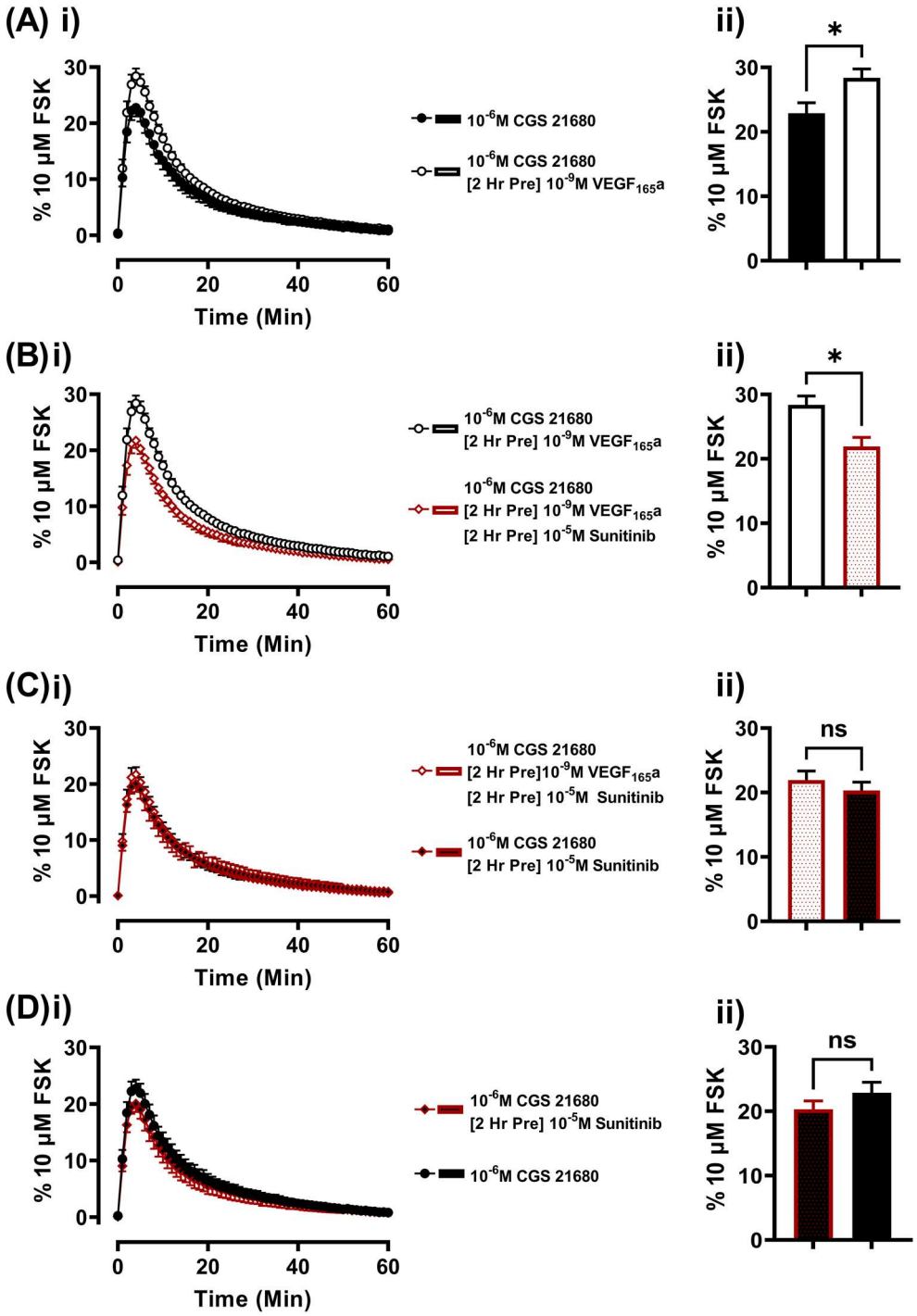


**Figure 48 Glosensor Cyclic AMP Responses to CGS 21680 in the Presence and Absence of VEGF-$A_{165}$a and Sunitinib in HEK 293G cells Transiently Transfected with Human HiBiT-VEGFR2**. Glosensor cAMP accumulation studies were conducted investigating **[(A),(D)]** the response of CGS 21680 (1.0 µM) in the presence and absence of **(A)** a 2 h pretreatment with VEGF-$A_{165}$a (1.0 nM) or (**D**) a 2 h pretreatment with sunitinib (10 µM). **(B)** the response of CGS 21680 (1.0 µM) and a 2 h pretreatment of VEGF-$A_{165}$a in the presence or absence of sunitinib (10 µM). **(C)** the response of CGS 21680 (1.0 µM) and a 2 h pretreatment with sunitinib (10 µM) in the presence or absence of $VEGF_{165}$a (1.0 nM). For each experiment: **i)** response-time curve (60 min), **ii**) peak luminescence response, with an unpaired T-test performed between groups (***** = $p<0.05$ significance). Data represent the mean + or - SEM of the peak response from 5 separate experiments (n=5), each carried out in triplicate well repeats, with data normalised per plate as a percentage of the peak luminescence response obtained to a 10 µM forskolin (FSK) control response in the absence of other agents.

### 5.3.2.2 NanoBRET Saturation Assays

NanoBRET saturation experiments investigated complex formation between adenosine $A_2$ receptors and VEGFR2 (**5.2.2.2**). Experiments were conducted using transient co-transfection of cDNA encoding for the NLuc-$A_{2A}$ receptor (10 ng/well) with the SNAP-$A_{2A}$ receptor (0-40 ng/well), as well as cDNA for the NLuc-$A_{2B}$ receptor (10 ng/well) receptor with the SNAP-$A_{2B}$ receptor (0-40 ng/well). For the $A_{2A}$ receptor pair, saturable BRET was observed alongside a significant ($p<0.0001$) increase in the BRET ratio with increasing doses of the SNAP-$A_{2A}$ receptor (**Figure 49A**), indicative of close proximity (<10 nm) in this receptor-receptor pairing (Mercier et al., 2002). However, this was not found to be the case for the $A_{2B}$ receptor pairing, and thus there is no indication that the NLuc-$A_{2B}$ receptor is in close proximity with the SNAP-$A_{2B}$ receptor as there was not a significant ($p>0.05$) increase in the BRET ratio with increasing doses of the SNAP-tagged $A_{2B}$ receptor (**Figure 49B**).

NanoBRET saturation assays were conducted to investigate a potential $A_{2A}$-$A_{2B}$ receptor-receptor pairing using transient co-transfection of cDNA encoding for the NLuc-$A_{2A}$ receptor (10 ng/well) with the SNAP-$A_{2B}$ receptor (0-40 ng/well), as well as for cDNA for the NLuc-$A_{2B}$ receptor (10 ng/well) with the SNAP-$A_{2A}$ receptor (0-40 ng/well). Saturable BRET was observed for both receptor-receptor pairs, alongside a significant (NLuc-$A_{2A}$ receptor--SNAP-$A_{2B}$ receptor, $p<0.0001$; NLuc-$A_{2A}$ receptor--SNAP-$A_{2B}$ receptor, $p<0.001$) increase in the BRET ratio with increasing dose of SNAP-tagged receptor for both $A_{2A}$-$A_{2B}$ receptor pairings (**Figure 49C-D**), indicative of close proximity in both of these receptor-receptor pairings (Mercier et al., 2002).

Finally, nanoBRET saturation assays were conducted to investigate potential VEGFR2 and $A_{2A}$ or $A_{2B}$ receptor pairing. Transient co-transfections of cDNA encoding for NLuc-VEGFR2 (10 ng/well) with the SNAP-$A_{2A}$ receptor (0-40 ng/well) (**Figure 49E**) or the SNAP-$A_{2B}$ receptor (0-40 ng/well) (**Figure 49F**) were completed. Saturable BRET was not observed for either receptor-receptor pair, as neither pairing resulted in a significant ($p>0.05$) increase in the BRET ratio with increasing doses of the SNAP-tagged $A_2$ receptor, and thus there is no indication that the NLuc-VEGFR2 receptor was in close proximity with either the SNAP-$A_{2A}$ or SNAP-$A_{2B}$ receptor.

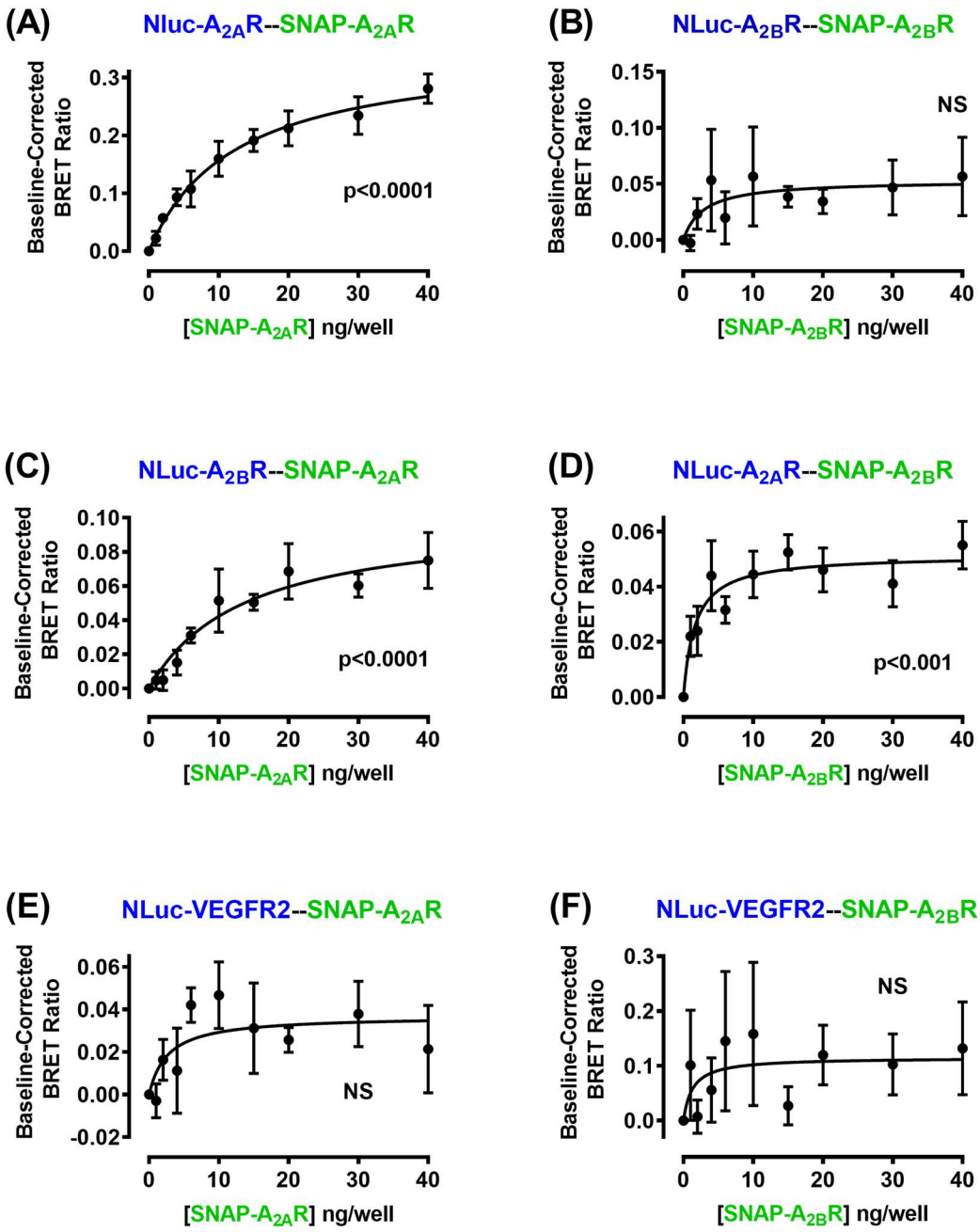


**Figure 49 NanoBRET Saturation Experiments Investigating Complex Formation between Adenosine $A_2$ receptors and VEGF Receptor 2**. Receptor colocation was investigated using simultaneous transient transfection of a constant amount of NanoLuc (NLuc) receptor and a variable amount of SNAP-tagged receptor in HEK 293T cells. **[(A),(D)]** NLuc-$A_{2A}$ receptor cDNA (10 ng/well) and increasing concentrations of **(A)** SNAP-$A_{2A}$ receptor cDNA (0-40 ng/well) or **(D)** SNAP-$A_{2B}$ receptor cDNA (0-40 ng/well). **[(B),(C)]** NLuc-$A_{2B}$ receptor cDNA (10 ng/well) and increasing concentrations of **(B)** SNAP-$A_{2B}$ receptor cDNA (0-40 ng/well) or **(C)** SNAP-$A_{2A}$ receptor cDNA (0-40 ng/well). **[(E),(F)]** NLuc-VEGFR2 cDNA (10 ng/well) and increasing concentrations of **(E)** SNAP-$A_{2A}$ receptor cDNA (0-40 ng/well) or **(F)** SNAP-$A_{2B}$ receptor cDNA (0-40 ng/well). Data are means ± SEM from 5 separate experiments (n=5), each carried out in triplicate well repeats. A one-way ANOVA was conducted for all experiments to determine whether there is a significant change in the BRET ratio with increasing doses of transfected SNAP-receptor, with significance highlighted on each graph.

# 5.4 Haemodynamic Responses to Sunitinib with $A_{2A}$ Receptor Activation: Chapter Discussion

This chapter investigated the cardiovascular effects of sunitinib administration in conscious, freely moving rats. Additionally, investigations into the potential of adenosine $A_{2A}$ receptor agonists to address the haemodynamic consequences of sunitinib treatment were examined.

Sunitinib (16.0 mg/kg/day) over a 3-day study caused a significant transient reduction of HR that returned to baseline between days. Sunitinib infusion caused a transient MAP rise during sunitinib infusion on day 1, with sustained significant increases in MAP from day 2 onwards. In addition, sunitinib caused a significant reduction in renal VC from 3 hours following the day 1 dosing period onwards. Sunitinib also caused a similar significant reduction in mesenteric and hindquarters VC, with VC decreases beginning from the start of the dosing period on day 1 and continuing throughout the study.

The 3-hour delay on day 1 between sunitinib dosing and decreases in renal VC compared to the immediate decreases observed in the mesenteric and hindquarters vascular beds suggests that the VC decrease in the renal vasculature is caused by a different mechanism than those observed in the mesenteric and hindquarter vascular beds. Sunitinib inhibits VEGFR2 and has been reported to have a nanomolar affinity to the receptor (Abrams et al., 2003, Mendel et al., 2003, Faivre et al., 2007). It has been shown that VEGFR2 inhibition decreases the production of the vasodilatory second messengers NO and prostacyclin, causing vasoconstrictions (Taraseviciene-Stewart et al., 2001, Facemire et al., 2009). NO has been demonstrated to play an important role in maintaining the vascular tone of the renal, mesenteric and hindquarters vascular beds, as the administration of $N^G$-nitro-L-arginine methyl ester (L-NAME), which is an antagonist of eNOS, and has been shown to cause a decrease in VC in all three of these vascular beds (Gardiner et al., 2006). Therefore, a reduction in NO and prostacyclin could cause the immediate decreases observed in mesenteric and hindquarters VC due to sunitinib administration. The sunitinib-induced decrease in NO is known to consequentially increase the production of the vasoconstrictor ET-1 (Wiley and Davenport, 2001, Merkus et al., 2006). The kidney is known to be particularly

sensitive compared to other beds to the vasoconstrictive effects of ET-1 (Pernow et al., 1989, Dhaun et al., 2012). The 3-hour delay from the dosing of sunitinib to the observed vasoconstrictions in the renal vascular bed could thus be a secondary effect caused by the upregulation of ET-1, caused by a reduction in NO triggered by sunitinib VEGFR2 blockade. Alternatively, the effects on the renal vasculature could be due to changes in gene transcription, which have been shown *in vitro* to occur with VEGFR2 receptor stimulation within hours (Carter et al., 2015).

The relative contribution of fast-acting vasoconstrictive mechanisms, slower-acting influences on gene expression or more long-term structural changes to the vasculature, such as vascular rarefaction in causing hypertension associated with RTKI inhibition, is not fully understood (Veronese et al., 2006, Mourad et al., 2008, Robinson et al., 2010a). In this study, by 5 min into the dosing period, sunitinib had caused significant decreases in both mesenteric and hindquarters VC, suggesting fast-acting vasoconstrictive mechanisms could cause these effects. Furthermore, increases in MAP were observed that were significant versus baseline by 5 min into the sunitinib dosing period, although this increase was not significant versus the vehicle control. Additionally, a significant decrease in HR was observed after 5 min of sunitinib treatment. Therefore, it could be hypothesised that the decrease in HR due to sunitinib treatment could be caused by a baroreflex-mediated decrease in the sympathetic tone on the heart as a response to an increase in MAP (**1.2**) (Kougias et al., 2010). However, the baroreflex can only deal with acute and transient changes in blood pressure, and if hypertension is sustained, then vascular baroreceptors reset; in the rat, this resetting process happens over the course of 48 hours to acclimatise to a new blood pressure (Krieger, 1988). Thus, it could be hypothesised that the baroreflex resetting between treatment days could explain why at the start of days 2 and 3 HR had returned to baseline in the sunitinib-treated rats.

On day 3, the sunitinib treated group was administered consecutive doses of the $A_{2A}$ receptor agonist CGS 21680, which caused a significant dose-dependent increase in HR, decrease in MAP, and increases in VC across the renal, mesenteric and hindquarters vascular beds, with the most considerable effects of CGS 21680 occurring at the hindquarters. The response to CGS 21680 temporally corrected MAP and VC in all three vascular beds so far as they were not significantly different to the day 1 baseline recording before the administration of sunitinib. The effects of CGS 21680 were broadly similar to those observed in naive rats in experiments completed in earlier chapters of the thesis (**3.3.1.3.1, 3.3.1.4.1**).

Notably, in naive rats, CGS 21680 administration was found to cause minimal increases in renal or mesenteric VC, whereas, in sunitinib-treated rats, CGS 21680 caused a significant increase in both of those vascular beds. The increase observed in the renal and mesenteric vascular beds could be a consequence of the $A_{2A}$ receptor responses being able to achieve a greater maximal response in these beds due to the lower baseline signal caused by the sunitinib administration, allowing $A_{2A}$ receptor agonism to result in a more considerable change. $A_{2A}$ receptor activation causes NO-induced vasodilation, which could directly counter the decrease in NO caused by sunitinib administration, as discussed above (Jacobson and Gao, 2006, Borea et al., 2018, Jamwal et al., 2019). These results show the ability of $A_{2A}$ receptor activation to reverse sunitinib-induced hypertension and decreases in VC, which will be further discussed in the final chapter of this thesis (**6.2.1**).

In this chapter, a Glosensor cAMP assay was conducted to determine if VEGF-$A_{165}$a acting at human VEGFR2 could modify the cAMP response caused by CGS 21680, which is specific for the human $A_{2A}$ receptor, as well as the rat $A_{2A}$ receptor (Hutchison et al., 1989, Müller and Jacobson, 2011, Goulding et al., 2018). VEGF-$A_{165}$a (1.0 nM) was found to significantly enhance the peak cAMP response to CGS 21680 (1.0 μM), an effect that was blocked in the presence of sunitinib (10 μM), but the presence or absence of sunitinib did not significantly affect the baseline response to CGS 21680 (1.0 μM) on its own. The enhancement of the $A_{2A}$ receptor-induced cAMP response by VEGF-$A_{165}$a acting at VEGFR2 could be due to interactions in cellular signalling downstream of the receptors. In the literature, it has been shown that sunitinib can cause the suppression of the functional responses to bradykinin and angiotensin II (Kappers et al., 2010, Blasi et al., 2012). If the results of this experiment translate into an *in vivo* setting, then it could be a possibility that sunitinib, by inhibiting the VEGF-$A_{165}$a response at VEGFR2, could suppress the vasodilatory response of adenosine acting on adenosine $A_{2A}$ receptors in the vasculature; further *ex vivo* and *in vivo* studies are required to explore this.

Another possible explanation for the enhancement of the $A_{2A}$ receptor-induced cAMP response by VEGF-$A_{165}$a acting at VEGFR2 is that VEGF-$A_{165}$a-VEGFR2 signalling could directly influence the $A_{2A}$ receptor due to the formation of VEGFR2-$A_{2A}$ receptor-receptor oligomers. To investigate if there could be a direct receptor-receptor interaction between VEGFR2 and adenosine $A_{2A}$ receptors nanoBRET saturation assays were conducted using transient co-transfection of cDNA encoding for an NLuc-tagged receptor with a SNAP-tagged receptor to assess receptor-receptor proximity of the adenosine $A_2$ receptors and VEGFR2. The results from this study indicated that $A_{2A}$-$A_{2A}$ receptors colocalise, but $A_{2B}$-$A_{2B}$ receptors do not. The results of this study are in line with the literature, where $A_{2A}$-$A_{2A}$ receptor-receptor dimerisation has been demonstrated (Canals et al., 2004, Briddon et al., 2008, Schonenbach et al., 2016), but the presence of an $A_{2B}$ receptor-receptor homodimer pair has not. This experiment also showed that $A_{2A}$-$A_{2B}$ receptors colocalise, which has been recently described in the literature (Hinz et al., 2018). However, the results of this experiment did not find evidence that VEGFR2 and $A_{2A}$ or $A_{2B}$ receptors colocalise. The result of this experiment suggests that the enhancement of the $A_{2A}$ receptor-induced cAMP response by VEGF-$A_{165}$a acting at VEGFR2 is not caused by a direct receptor-receptor link, but is more likely due to interactions in cellular signalling downstream of the receptors. More investigations will be suggested in the general discussion of this thesis to greater explore this result (**6.2.3**, **6.2.4**).

# 6 General Discussion & Conclusions

# 6.1 General Discussion & Conclusions: Research Summary

Adenosine is an important modulator of the cardiovascular system, acting at four GPCRs, known as the adenosine receptors (**1.1.2**). A crucial role of adenosine $A_{2A}$ and $A_{2B}$ receptors is the induction of vasodilation in vascular beds via the coupling of both the $A_2$ receptors to $G_s$ proteins, which leads to the relaxation of the smooth muscle surrounding blood vessels (**1.1.3**, **1.1.5**). Both adenosine $A_2$ receptors can cause vasodilation in small resistance arteries that comprise vascular beds, leading to an increase in the VC of these beds (**1.1.5**). In a model where cardiac output remains constant, a generalised increase in VC will lead to a decrease in blood pressure, and as a result, both $A_2$ receptors have been suggested to have therapeutic potential in treating hypertension (**1.1.6.2**). However, adenosine receptor expression across the vasculature is neither universal nor ubiquitous, and neither are the physiological changes induced by the activation of these receptors; different regions have different sensitivities and responses to adenosine through differences in receptor expression and function across the body (**1.1.4**).

To gain a greater understanding of how $A_{2A}$ and $A_{2B}$ receptors influence the cardiovascular system, this project aimed to investigate the physiological consequences of adenosine $A_{2A}$ and $A_{2B}$ receptor activation on the regional flow of blood in the renal, mesenteric and hindquarter vascular circulations, in conscious, freely moving rats.

**Chapter 3** investigated the response of adenosine $A_{2A}$ and $A_{2B}$ receptor ligands. It was discovered that inhibition of the $A_{2B}$ receptor caused a decrease in VC in both the renal and mesenteric vascular beds, indicative that an $A_{2B}$ receptor-regulated tone influences the conductance of these vascular beds in the rats at rest (**3.3.1.2.1**). $A_{2A}$ receptor activation was shown to cause a significant increase in VC in the hindquarters vascular beds but had limited overall effects on VC in the renal and mesenteric vascular beds (**3.3.1.3.1**). The opposite was found to be the case with the $A_{2B}$ receptor, which caused increases in the VC of renal and mesenteric vascular beds, but not the hindquarters (**3.3.1.4.1**). Adenosine was shown to cause increases in all three vascular beds studied (**3.3.1.5.1**). Both $A_{2A}$ and $A_{2B}$ receptor activation induced tachycardia, but only agonism of the $A_{2A}$ receptor caused a decrease in the MAP in the rats studied (**3.3.1.3.1, 3.3.1.4.1**).

Homeostatic reflexes attempt to avert acute changes to blood pressure that could cause catastrophic damage to the vasculature from an acute pressure spike or loss of tissue perfusion due to a sharp drop in pressure. A key homeostatic reflex that regulates acute changes in blood pressure is the baroreflex, which exerts control over systemic blood pressure by modulating the autonomic nervous system (**1.2**). Sympathetic activity is known to be increased by the baroreflex as a result of an acute decrease in blood pressure, with physiological effects driven by catecholamine stimulation of the heart and vasculature due to activation of adrenergic $\beta_1$ and $\beta_2$ receptors, respectively (**1.2.1**). Adenosine $A_{2A}$ and $A_{2B}$ receptors indirectly influence the baroreflex by causing changes in blood pressure but also directly by modulating the brain regions responsible for the baroreflex response (**1.2.2**).

To better understand how the sympathetic activation of β receptors influences the haemodynamic profile caused by $A_{2A}$ or $A_{2B}$ receptor activation, this project investigated the physiological consequences of adenosine $A_{2A}$ and $A_{2B}$ receptor activation in the presence of β blockade in conscious, freely moving rats.

**Chapter 4** investigated the response of adenosine $A_{2A}$ and $A_{2B}$ receptor agonists in the presence of $\beta_1$, $\beta_2$ or non-specific β blockade. This research showed that the tachycardia induced by both $A_{2A}$ and $A_{2B}$ receptor activation was primarily due to the indirect stimulation of the $\beta_1$ receptor and not a result of direct $A_{2A}$ or $A_{2B}$ receptor activation in the heart (**4.4**). Furthermore, the effects of $A_{2A}$ receptor activation on VC at the three observed vascular beds were not changed due to β blockade, demonstrating that the effects were directly due to $A_{2A}$ receptor activation (**4.3.1.3**). However, antagonism of the $\beta_2$ receptor appeared to enhance the $A_{2B}$ receptor responses in HR and VC in renal and mesenteric vascular beds (**4.3.1.4**).

RTKIs are powerful chemotherapeutic agents but can cause severe clinical hypertension as a side effect (**1.3.1.1**). A key driver of RTKI drug-induced hypertension is VEGFR2 inhibition, which is associated with increased vascular resistance across the body, as endogenous VEGF, via VEGFR2, is known to activate signalling pathways, which cause production of the vasodilatory second messengers NO and prostacyclin (**1.3.2**). The RTKI sunitinib is known to block VEGFR2, can cause severe hypertension, and is additionally known to cause renal injury associated with vasoconstriction of the renal vasculature (**1.3.3**).

To better understand the cardiovascular effects of sunitinib, this project aimed to investigate the change in the regional flow of blood in the renal, mesenteric and hindquarter vascular circulations caused by sunitinib over a three-day protocol in conscious, freely moving rats. Additionally, as work in **chapter 3** demonstrated that $A_{2A}$ receptor activation could lower MAP (**3.3.1.3.1**), an investigation was undertaken to see if $A_{2A}$ receptor activation could relieve the deleterious hypertensive effects of sunitinib by reducing blood pressure and by restoring vascular conductance in regional vascular beds.

**Chapter 5a** showed that sunitinib treatment over a three-day protocol caused sustained hypertension accompanied by decreases in renal, mesenteric and hindquarters VC, associated with vasoconstrictions in the resistance arteries in these regional areas (**5.3.1.1**). $A_{2A}$ receptor agonism was shown to temporarily relieve hypertension and decrease renal, mesenteric and hindquarters VC (**5.3.1.2**). As seen previously in **chapter 3**, $A_{2A}$ receptor activation caused an increase in HR that, as demonstrated in **chapter 4**, was most probably caused by indirect $\beta_1$ receptor activation (**3.3.1.3.1**, **4.4**).

It could be possible that adenosine $A_2$ receptors and VEGFR2 interact to influence cell signalling and, as a result, physiological processes such as vascular tone (**1.4.2**). This interaction could be caused by indirect interactions involving signalling cascades activated or inhibited by these receptors or by direct receptor-receptor interactions (**1.4.2**).

To better understand the interaction between $A_2$ receptors and VEGFR2, the ability of VEGF-$A_{165}$a acting at VEGFR2 to influence a cAMP response caused by $A_{2A}$ receptor activation was investigated in HEK 293 cells expressing a luminescent cAMP biosensor (**2.2.7**). Additionally, receptor colocalisation was assessed by transient transfection of NLuc- and SNAP-tagged receptors transiently transfected into HEK 293T cells, with observed BRET between the two receptor tags indicating their close proximity (**2.2.6**).

**Chapter 5b** showed that VEGF-$A_{165}$a acting at VEGFR2 enhanced an $A_{2A}$ receptor-induced cAMP response and that the RTKI sunitinib could block this effect (**5.3.2.1**). Additionally, this chapter found no evidence of VEGFR2 and $A_{2A}$ or $A_{2B}$ receptor colocalisation in the absence of receptor ligands (**5.3.2.2**).

# 6.2 General Discussion & Conclusions: Future Directions

## 6.2.1 Future Directions: *In Vivo*- Sustained $A_2$ Receptor Activation in the Presence of $\beta_1$ Blockade and Sunitinib

Results of **Chapter 3** highlight the effects of an acute 10 min dosing regimen of the $A_2$ receptor agonists, CGS 21680 and BAY 60-6583, with the effect of both drugs wearing off within an hour (**3.3.1.3.1, 3.3.1.4.1**). Although an acute dosing challenge was utilised to demonstrate the haemodynamic effects of these drugs, an advantage of our group's in vivo model is that drugs can be administered continuously throughout the day via i.v. catheters without disturbing the rats (**2.1.1.2**). A lower, continual dose of these agonists could thus be trialled to see if the haemodynamic effects of activating these $A_2$ receptors are sustained, which would be necessary if targeting these receptors was used to treat conditions such as hypertension. Furthermore, in light of the results of experiments detailed in **Chapter 4**, a potential unwanted side effect of utilising $A_2$ receptor agonists could be their ability to produce unwanted tachycardia via reflex activity driven by the indirect activation of $\beta_1$ receptors (**4.3.1**). Therefore, for the proposed studies involving the sustained administration of $A_2$ receptor agonists, coadministration with the $\beta_1$ antagonist CGP 20712A could be investigated to see if the rise in HR could be prevented throughout the dosing period. Finally, to further probe the ability of $A_{2A}$ receptor ligands to relieve RTKI-induced hypertension, a sustained dose of CGS 21680 in the presence of CGP 20712A could be investigated to see if this could bring about a sustained decrease in MAP and a sustained increase in renal, mesenteric and hindquarters VCs.

### 6.2.2 Future Directions: *In Vivo*- $A_{2B}$ Receptor Activation in Anesthetised Rodents

Mechanical ventilation is life support undertaken when a critically ill patient's breathing is impaired, for example, after a severe stroke or during a life-threatening Coronavirus disease 2019 (COVID-19) infection (Robba et al., 2019, Fogagnolo et al., 2022). Mechanical ventilation is known to cause acute kidney injury, which worsens the patient's prognosis (Hepokoski et al., 2018, Vemuri et al., 2022). Renal injury is the second most frequent type of organ damage caused by COVID-19 infection, and patients with severe COVID-19 requiring mechanical ventilation are susceptible to acute kidney injury, associated with ischemic reperfusion injury and increases in renal vascular resistivity (Schmidt et al., 2021, Fogagnolo et al., 2022). Kidney injury induced by ventilation is believed to occur due to renal perfusion impairment, blood flow reduction, and upregulation of inflammatory mediators (Hepokoski et al., 2018). In a rat model, mechanically ventilated rats had a raised level of renal ET-1, which caused a reduction in blood flow to the kidneys over the course of the 4 hour study (Kuiper et al., 2008).

Clinical trials have been conducted to see if dopaminergic or $\beta_2$ activation could help in acute kidney injury by restoring blood flow; however, the results of these studies were not positive and, at best, inconclusive (Friedrich et al., 2005, Redfors et al., 2011, Bove et al., 2014). Nevertheless, targeting the $A_{2B}$ receptor may succeed where dopaminergic or adrenergic targeting has failed for three reasons. The first is that, as the results have **chapter 3** have demonstrated, the $A_{2B}$ receptor is regionally specific and does not cause dilations in the hindquarters (**3.3.1.4.1**); on the other hand, $\beta_2$ stimulation is known to cause hindquarters dilation (Baker et al., 2017); dilations in the hindquarters could cause to a reduction in blood pressure, which would be detrimental in reperfusion of the kidney. Second, $A_{2B}$ receptor activation is known to be reno-protective and supports the organ via mechanisms unrelated to organ blood flow, such as via kidney ischemic preconditioning (Grenz et al., 2008). Third and finally, $A_{2B}$ receptor activation is immunosuppressive, which, although beyond this thesis's scope, may also help control a detrimental inflammatory response associated with mechanical ventilation-induced acute kidney injury (Vallon and Osswald, 2009). With approval from the relevant regulatory authorities, the *in vivo* technique covered in this thesis

could be repurposed to additionally investigate the regional haemodynamic effects of rats underneath anaesthesia and undergoing mechanical ventilation, as this has already been demonstrated to be a model that mimics the physiological changes that occur in human patients undergoing similar procedures (Kuiper et al., 2008).

### 6.2.3 Future Directions: *In Vitro*- Investigating Receptor Colocalisation

*In vitro* research probing the potential for colocalisation of adenosine $A_2$ receptors and VEGFR2 should be continued; although work in **chapter 5** did not find evidence for receptor colocalisation between VEGFR2 and $A_{2A}$ or $A_{2B}$ receptors (**5.3.2.2**), it could be the case that colocalisation only occurs in the presence of ligands binding to these receptors. Previous work by Kilpatrick *et al*. demonstrated that NLuc-tagged VEGFR2 and SNAP-tagged $\beta_2$ adrenoceptors colocalise with the BRET signal increasing as a response to both VEGF-$A_{165}$a and isoprenaline in a dose-dependent manner (**Figure 50**) (Kilpatrick et al., 2019). BRET proximity assay should thus be conducted with increasing doses of VEGF-$A_{165}$a for VEGFR2, alongside CGS 21680 and BAY 60-6583 for $A_{2A}$ and $A_{2B}$ receptors, respectively.

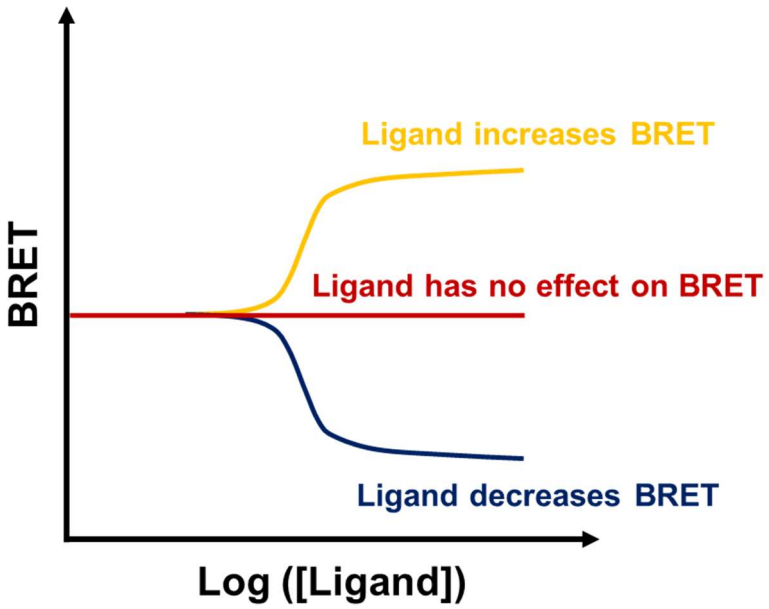


**Figure 50 Representative Graph Illustrating the Principles of Utilising Bioluminescence Resonance Energy Transfer (BRET) to Explore Ligand Promoted Changes to Receptor-Receptor Colocalisation.** A colocalised receptor-receptor pair, with one receptor tagged with a bioluminescent protein and the other tagged with a fluorescent protein, can produce BRET if in close proximity (<10 nm), in the correct orientation to each other and if their spectra overlap. The binding of a ligand to one or both of the receptors in the receptor-receptor pair could have no effect on observed BRET (red line) or alternatively increase (yellow line) or decrease (blue line) BRET. Increases or decreases in observed BRET could be due to an increase or decrease in the number of colocalised receptor pairs or the number of interactions between the two paired receptors. Alternatively, changes in the observed BRET could be caused by changes to the receptor conformation in the receptor pair, changing the donor and acceptor tags' relative positioning.

### 6.2.4 Future Directions: *In Vitro*- Investigating VEGF Enhancement of $A_2$ Receptors

Work investigating the ability of VEGF to enhance the cAMP response due to $A_{2A}$ receptor activation demonstrated in **chapter 5** should be continued (**5.3.2.1**). Studies in this thesis only investigated the effects of a 2-hour pretreatment of VEGF before the administration of CGS 21680; future experiments should be conducted with the VEGF pretreatment closer to the administration of CGS 21680, as the effects of VEGF may have been waning after the 2-hour pretreatment. Furthermore, these experiments should be expanded to see if there is a similar effect for the $A_{2B}$ receptor cAMP response, as this experiment would reveal if the observed enhancement of cAMP accumulation is due to an $A_{2A}$ receptor-specific mechanism or not.

Additionally, assays should be conducted to assess if the presence of an $A_{2A}$ receptor agonist impacts VEGF-$A_{165}$a -- VEGFR2 signalling. VEGFR2 activation is known to cause nuclear translocation of the nuclear factor of activated T-cells (NFAT) transcription factor, which increases the expression of genes which include the NFAT promoter region (Suehiro et al., 2014). VEGFR2 activity can be measured by the expression of an NFAT reporter gene containing the NFAT promoter coupled with the expression of firefly luciferase in specially modified HEK 293T cells, and so experiments could be conducted using this technique (Carter et al., 2015, Kilpatrick et al., 2017, Peach et al., 2021).

# 6.3 General Discussion & Conclusions: Concluding Remarks

This thesis examined the response to adenosine $A_{2A}$ and $A_{2B}$ receptor ligands in conscious, freely moving rats. **First**, the data presented in this thesis identified regionally selective roles for adenosine $A_{2A}$ and $A_{2B}$ receptors in causing vasodilations in the vascular beds that make up the renal, mesenteric and hindquarters (**3.4**). Activating both $A_2$ receptors caused tachycardia, but only $A_{2A}$ receptor activation caused a dose-dependent decrease in MAP (**3.4**).

**Second**, this work demonstrated that the increase in HR caused by both $A_2$ receptor agonists was mainly caused by secondary activation of $\beta_1$ receptors in the heart (**4.4**). Additionally, it was demonstrated that the vasodilatory effects of $A_{2A}$ receptor activation on the hindquarters were not caused by or enhanced by secondary stimulation of $\beta_2$ receptors (**4.4**). In contrast, data in this thesis showed that $\beta_2$ receptor antagonism appeared to enhance the responses to $A_{2B}$ receptor activation, including increases in HR and its effects on regional vascular flows (**4.4**).

**Third**, it was shown that the RTKI sunitinib over a three-day protocol causes hypertension, associated with vasoconstrictions in the vascular beds that make up the renal, mesenteric and hindquarters, but all of these haemodynamic effects could be temporarily reversed by $A_{2A}$ receptor activation, although this lead to an increase in HR in these rats (**5.4**).

**Finally**, explorative *in vitro* studies found that VEGF-$A_{165}$a acting at VEGFR2 enhanced an $A_{2A}$ receptor-induced cAMP response and that sunitinib can block this enhancement (**5.4**). Additionally, no evidence was found that VEGFR2 and $A_{2A}$ or $A_{2B}$ receptors colocalise on the plasma membrane (**5.4**).

The regional specificity demonstrated in the vasodilatory effects of systemic activation of the $A_{2A}$ and $A_{2B}$ receptor results of this thesis imply differing potential uses for $A_{2A}$ and $A_{2B}$ receptor activation (**3.4**). Results from this thesis highlight that any future systemic treatment involving $A_{2A}$ or $A_{2B}$ receptor activation must consider the tachycardic effects of systemic $A_{2A}$ or $A_{2B}$ receptor activation (**4.4**). Experiments in this thesis also demonstrated that simultaneous $\beta_1$ blockade is one way to manage such increases in HR, and thus if the increase in HR is deemed an unwanted, on-target side effect of $A_{2A}$ or $A_{2B}$ receptor activation, additional $\beta_1$ blockade may be required. Results from this thesis suggest that $A_{2A}$ receptor activation could help treat hypertension associated with vasoconstriction in the renal, mesenteric and hindquarters vascular beds, such as RTKI-induced hypertension (**5.4**). As demonstrated in this thesis, the ability of $A_{2B}$ receptor activation to selectively cause vasodilations in the renal and mesenteric vascular beds without an associated fall in MAP means that the selective targeting of $A_{2B}$ receptors could be beneficial in treating conditions known to be associated with deleterious vasoconstrictions in the renal and mesenteric vasculature. For example, RTKI-induced renal damage is associated with vasoconstrictions (**1.3.1.1**), so $A_{2B}$ receptor activation could be beneficial in preventing kidney damage associated with these drugs. Additionally, research from this thesis has suggested that $A_{2B}$ receptor activation could be beneficial in other renal or mesenteric conditions, such as acute kidney injury (**6.2.2**).

*In vitro* research probing the potential for colocalisation of adenosine $A_2$ receptors and VEGFR2 should be continued, with the presence of receptor ligands investigated (**6.2.3**). Additionally, the ability of VEGF to enhance the responses of $A_{2A}$ receptor agonism should be expanded to see if there is a similar effect for $A_{2B}$ receptor responses (**6.2.4**).

Further *in vivo* research could be conducted to assess if the use of $A_{2A}$ and $A_{2B}$ receptor activation could treat conditions associated with vasoconstrictions in renal, mesenteric or hindquarter vascular beds, such as ventilator-induced acute kidney injury (**6.2.2**) or RTKI-induced hypertension (**6.2.1**) to determine the suitability of targeting these receptors as novel treatments for these conditions.

# 7 Appendix

## 7.1 Appendix: Receptor Peptide Sequences

### 7.1.1 Receptor Peptide Sequences: Adenosine Receptors

#### 7.1.1.1 Adenosine Receptor Tags

**5-HT3A/NLuc/*Linker***

**MRLCIPQVLLALFLSMLTGPGEGSRKLL**VFTLEDFVGDWRQTAGYNLDQVLEQ
GGVSSLFQNLGVSVTPIQRIVLSGENGLKIDIHVIIPYEGLSGDQMGQIEKIFKVVY
PVDDHHFKVILHYGTLVIDGVTPNMIDYFGRPYEGIAVFDGKKITVTGTLWNGNK
IIDERLINPDGSLLFRVTINGVTGWRLCERILA***GS***

**5-HT3A/SNAP tag/*Linker***

**MRLCIPQVLLALFLSMLTGPGEGSRKLL**DKDCEMKRTTLDSPLGKLELSGCEQ
GLHEIKLLGKGTSAADAVEVPAPAAVLGGPEPLMQATAWLNAYFHQPEAIEEFP
VPALHHPVFQQESFTRQVLWKLLKVVKFGEVISYQQLAALAGNPAATAAVKTAL
SGNPVPILIPCHRVVSSSGAVGGYEGGLAVKEWLLAHEGHRLGKPGL***GS***

### 7.1.1.2 Adenosine Receptor Sequences

#### Human Adenosine $A_{2A}$ Receptor

LPIMGSSVYITVELAIAVLAILGNVLVCWAVWLNSNLQNVTNYFVVSLAAADIAVG
VLAIPFAITISTGFCAACHGCLFIACFVLVLTQSSIFSLLAIAIDRYIAIRIPLRYNGLV
TGTRAKGIIAICWVLSFAIGLTPMLGWNNCGQPKEGKNHSQGCGEGQVACLFE
DVVPMNYMVYFNFFACVLVPLLLMLGVYLRIFLAARRQLKQMESQPLPGERAR
STLQKEVHAAKSLAIIVGLFALCWLPLHIINCFTFFCPDCSHAPLWLMYLAIVLSHT
NSVVNPFIYAYRIREFRQTFRKIIRSHVLRQQEPFKAAGTSARVLAAHGSDGEQV
SLRLNGHPPGVWANGSAPHPERRPNGYALGLVSGGSAQESQGNTGLPDVELL
SHELKGVCPEPPGLDDPLAQDGAGVS

#### Human Adenosine $A_{2B}$ Receptor

LLLETQDALYVALELVIAALSVAGNVLVCAAVGTANTLQTPTNYFLVSLAAADVA
VGLFAIPFAITISLGFCTDFYGCLFLACFVLVLTQSSIFSLLAVAVDRYLAICVPLRY
KSLVTGTRARGVIAVLWVLAFGIGLTPFLGWNSKDSATNNCTEPWDGTTNESC
CLVKCLFENVVPMSYMVYFNFFGCVLPPLLIMLVIYIKIFLVACRQLQRTELMDHS
RTTLQREIHAAKSLAMIVGIFALCWLPVHAVNCVTLFQPAQGKNKPKWAMNMAI
LLSHANSVVNPIVYAYRNRDFRYTFHKIISRYLLCQADVKSGNGQAGVQPALGV
GL

## Rat Adenosine $A_{2A}$ Receptor

LGSSVYITVELAIAVLAILGNVLVCWAVWINSNLQNVTNFFVVSLAAADIAVGVLAI
PFAITISTGFCAACHGCLFFACFVLVLTQSSIFSLLAIAIDRYIAIRIPLRYNGLVTGV
RAKGIIAICWVLSFAIGLTPMLGWNNCSQKDGNSTKTCGEGRVTCLFEDVVPMN
YMVYYNFFAFVLLPLLLMLAIYLRIFLAARRQLKQMESQPLPGERTRSTLQKEVH
AAKSLAIIVGLFALCWLPLHIINCFTFFCSTCRHAPPWLMYLTIILSHSNSVVNPFIY
AYRIREFRQTFRKIIRTHVLRRQEPFQAGGSSAWALAAHSTEGEQVSLRLNGHP
LGVWANGSATHSGRRPNGYTLGLGGGGSAQGSPRDVELPTQERQEGQEHPG
LRGHLVQARVGASSWSSEFAPS

## Rat Adenosine $A_{2B}$ Receptor

LQLETQDALYVALELVIAALAVAGNVLVCAAVGASSALQTPTNYFLVSLATADVA
VGLFAIPFAITISLGFCTDFHSCLFLACFVLVLTQSSIFSLLAVAVDRYLAIRVPLRY
KGLVTGTRARGIIAVLWVLAFGIGLTPFLGWNSKDRATSNCTEPGDGITNKSCC
PVKCLFENVVPMSYMVYFNFFGCVLPPLLIMMVIYIKIFMVACKQLQHMELMEHS
RTTLQREIHAAKSLAMIVGIFALCWLPVHAINCITLFHPALAKDKPKWVMNVAILL
SHANSVVNPIVYAYRNRDFRYSFHRIISRYVLCQTDTKGGSGQAGGQSTFSLSL

## 7.1.2 Receptor Peptide Sequences: VEGFR2

### 7.1.2.1 VEGFR2 Tags

#### IL-6/NLuc/*Linker*

**MNSFSTSAFGPVAFSLGLLLVLPAAFPAPR**VFTLEDFVGDWRQTAGYNLDQVL
EQGGVSSLFQNLGVSVTPIQRIVLSGENGLKIDIHVIIPYEGLSGDQMGQIEKIFK
VVYPVDDHHFKVILHYGTLVIDGVTPNMIDYFGRPYEGIAVFDGKKITVTGTLWN
GNKIIDERLINPDGSLLFRVTINGVTGWRLCERILA***GSSGAIA***

#### IL-6/HiBiT/*Linker*

**MNSFSTSAFGPVAFSLGLLLVLPAAFPAPR**VSGWRLFKKIS***GSSGGSSGAIA***

### 7.1.2.2 VEGFR2 Sequence

## Human VEGFR2

SVGLPSVSLDLPRLSIQKDILTIKANTTLQITCRGQRDLDWLWPNNQSGSEQRV
EVTECSDGLFCKTLTIPKVIGNDTGAYKCFYRETDLASVIYVYVQDYRSPFIASVS
DQHGVVYITENKNKTVVIPCLGSISNLNVSLCARYPEKRFVPDGNRISWDSKKG
FTIPSYMISYAGMVFCEAKINDESYQSIMYIVVVVGYRIYDVVLSPSHGIELSVGE
KLVLNCTARTELNVGIDFNWEYPSSKHQHKKLVNRDLKTQSGSEMKKFLSTLTI
DGVTRSDQGLYTCAASSGLMTKKNSTFVRVHEKPFVAFGSGMESLVEATVGE
RVRIPAKYLGYPPPEIKWYKNGIPLESNHTIKAGHVLTIMEVSERDTGNYTVILTN
PISKEKQSHVVSLVVYVPPQIGEKSLISPVDSYQYGTTQTLTCTVYAIPPPHHIHW
YWQLEEECANEPSQAVSVTNPYPCEEWRSVEDFQGGNKIEVNKNQFALIEGKN
KTVSTLVIQAANVSALYKCEAVNKVGRGERVISFHVTRGPEITLQPDMQPTEQE
SVSLWCTADRSTFENLTWYKLGPQPLPIHVGELPTPVCKNLDTLWKLNATMFS
NSTNDILIMELKNASLQDQGDYVCLAQDRKTKKRHCVVRQLTVLERVAPTITGN
LENQTTSIGESIEVSCTASGNPPPQIMWFKDNETLVEDSGIVLKDGNRNLTIRRV
RKEDEGLYTCQACSVLGCAKVEAFFIIEGAQEKTNLEIIILVGTAVIAMFFWLLLVII
LRTVKRANGGELKTGYLSIVMDPDELPLDEHCERLPYDASKWEFPRDRLKLGK
PLGRGAFGQVIEADAFGIDKTATCRTVAVKMLKEGATHSEHRALMSELKILIHIG
HHLNVVNLLGACTKPGGPLMVIVEFCKFGNLSTYLRSKRNEFVPYKTKGARFRQ
GKDYVGAIPVDLKRRLDSITSSQSSASSGFVEEKSLSDVEEEEAPEDLYKDFLTL
EHLICYSFQVAKGMEFLASRKCIHRDLAARNILLSEKNVVKICDFGLARDIYKDPD
YVRKGDARLPLKWMAPETIFDRVYTIQSDVWSFGVLLWEIFSLGASPYPGVKID
EEFCRRLKEGTRMRAPDYTTPEMYQTMLDCWHGEPSQRPTFSELVEHLGNLL
QANAQQDGKDYIVLPISETLSMEEDSGLSLPTSPVSCMEEEEVCDPKFHYDNTA
GISQYLQNSKRKSRPVSVKTFEDIPLEEPEVKVIPDDNQTDSGMVLASEELKTLE
DRTKLSPSFGGMVPSKSRESVASEGSNQTSGYQSGYHSDDTDTTVYSSEEAE
LLKLIEIGVQTGSTAQILQPDSGTTLSSPPV

# 7.2 Alternative Data: Combined Antagonist Datasets with Statistical Tests with p<0.05 Threshold

| | Combination of Studies 1 & 4 & 5 | | | | Combination of Studies 2 & 3 & 6 | | | |
|---|---|---|---|---|---|---|---|---|
| | Vehicle | | SCH 58261 | | Vehicle | | PSB 1115 | |
| | Mean ± SEM | n | Mean ± SEM | n | Mean ± SEM | n | Mean ± SEM | n |
| **Cardiovascular Variable** | **Baseline T=0** | | | | | | | |
| **Heart rate (beats·min$^{-1}$)** | 340± 4 | 25 | **352± 5*** | 25 | 346 ± 5 | 26 | 351 ± 5 | 26 |
| **Mean BP (mmHg)** | 103 ± 2 | 25 | 103± 2 | 25 | 103 ± 1 | 26 | 102 ± 1 | 26 |
| **Renal VC (U)** | 80 ± 5 | 21 | 83± 6 | 21 | 86 ± 5 | 23 | 90 ± 6 | 23 |
| **Mesenteric VC (U)** | 80± 5 | 22 | 83 ± 5 | 22 | 94 ± 6 | 24 | 97 ± 6 | 24 |
| **Hindquarters VC (U)** | 47 ± 3 | 22 | 47 ± 3 | 22 | 50 ± 3 | 26 | 48 ± 3 | 26 |

**Table 21 Cardiovascular Variables Before Administration of Adenosine $A_2$ Receptor Antagonists.** Values are mean ± SEM; n=21-26 per combined group. Units (U) of vascular conductance (VC) are kHz. mmHg$^{-1}$ x $10^3$. A Wilcoxon signed-rank test was conducted between the antagonist and its corresponding vehicle control group (* = p<0.05 significance). Readings correspond to the baseline recordings (zero values) for the graphs in **Figure 51** and **Figure 52**. Abbreviations: U, units; VC, vascular conductance.

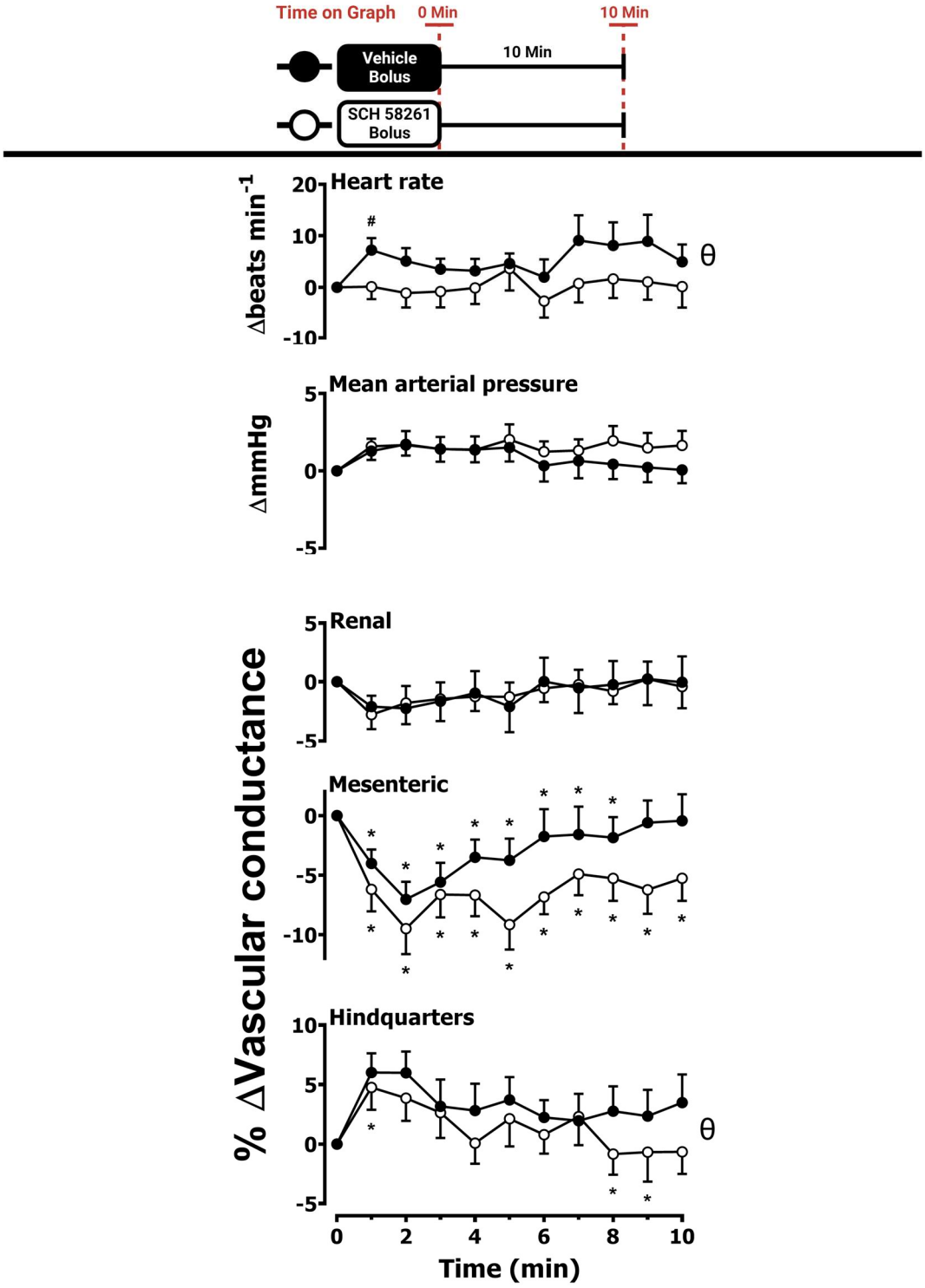


**Figure 51 Cardiovascular Responses to SCH 58261 in Conscious, Freely Moving Rats.** Conscious, freely moving rats were dosed with SCH 58261 (0.1 mL bolus of 1.0 mg/kg i.v., n=25) or vehicle (0.1 mL bolus of 5 % propylene glycol, 2 % Tween 80 in sterile saline, n=25) as described in the chapter 3 methodology (**3.2.1.3**). The graphs show responses over a 10 min period post-dosing. Data points are mean + or - SEM. A Friedman test was conducted for each data point of each group and the group's corresponding baseline (T=0) (* = $p<0.05$ significance). In addition, a Wilcoxon signed-rank test was conducted between the SCH 58261 and vehicle control groups for a comparison of the area under the curve (**θ** = $p<0.05$ significance) and additionally to determine differences at each time point (Wilcoxon T-test equivalent) (**#** = $p<0.05$ significance). Results are a combination of studies 1, 4 & 5. Baseline recordings for this figure can be found in **Table 21**.

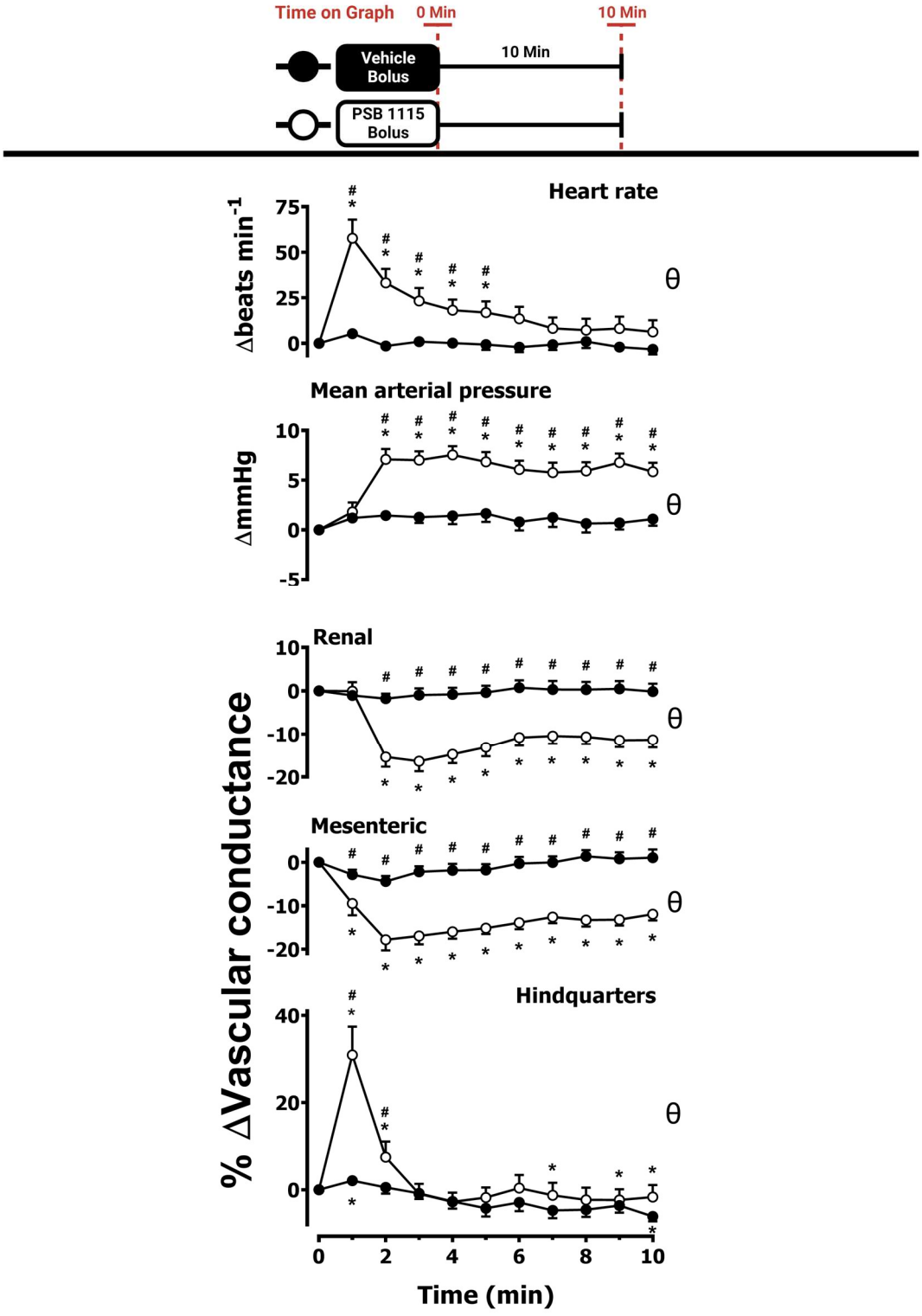


**Figure 52 Cardiovascular Responses to PSB 1115.** Conscious, freely moving rats were dosed with PSB 1115 (0.1 mL bolus of 10 mg/kg i.v., n=26) or vehicle (0.1 mL bolus of 5 % propylene glycol, 2 % Tween 80 in sterile saline, n=26) as described in the chapter 3 methodology (**3.2.1.3**). The graphs show responses over a 10 min period post-dosing. Data points are mean + or - SEM. A Friedman test was conducted for each data point of each group and the group's corresponding baseline (T=0) (* = $p<0.05$ significance). A Wilcoxon signed-rank test was conducted between the PSB 1115 and vehicle control groups for a comparison of the area under the curve (**θ** = $p<0.05$ significance) and additionally to determine differences at each time point (Wilcoxon T-test equivalent) (**#** = $p<0.05$ significance). Results are a combination of studies 2, 3 & 6. Baseline recordings for this figure can be found in **Table 21.**

| | Combination of Studies 7 & 10 | | | | Combination of Studies 8 & 11 | | | | Combination of Studies 9 & 12 | | | |
|---|---|---|---|---|---|---|---|---|---|---|---|---|
| | Vehicle | | CGP 20712A | | Vehicle | | ICI 118,551 | | Vehicle | | Propranolol | |
| | Mean ± SEM | n | Mean ± SEM | n | Mean ± SEM | n | Mean ± SEM | n | Mean ± SEM | n | Mean ± SEM | n |
| **Cardiovascular Variable** | **Baseline T=0** | | | | | | | | | | | |
| **Heart rate (beats·min$^{-1}$)** | 333 ± 5 | 16 | 338 ± 8 | 16 | 330 ± 6 | 17 | 332 ± 7 | 17 | 348 ± 5 | 20 | 344 ± 5 | 20 |
| **Mean BP (mmHg)** | 102 ± 2 | 16 | 104 ± 2 | 16 | 104 ± 3 | 17 | 103 ± 2 | 17 | 104 ± 1 | 20 | 103 ± 2 | 20 |
| **Renal VC (U)** | 81 ± 7 | 15 | 73 ± 5 | 15 | 93 ± 8 | 16 | 89 ± 7 | 16 | 83 ± 7 | 16 | 85 ± 5 | 16 |
| **Mesenteric VC (U)** | 82 ± 7 | 14 | 75 ± 8 | 14 | 87 ± 7 | 17 | 83 ± 5 | 17 | 93 ± 7 | 18 | 102 ± 7 | 18 |
| **Hindquarters VC (U)** | 44 ± 5 | 14 | 42 ± 4 | 14 | 44 ± 4 | 16 | 43 ± 4 | 16 | 54 ± 5 | 19 | 54 ± 5 | 19 |

**Table 22 Cardiovascular Variables Before Administration of β receptor Antagonists.** Values are mean ± SEM; n=14-20 per group. Abbreviations: U, units; VC, vascular conductance. Units (U) of vascular conductance (VC) are kHz. mmHg$^{-1}$ x 10$^{3}$. A Wilcoxon signed-rank test was conducted between the antagonist group and its corresponding vehicle control group (* = $p<0.05$ significance, no significance was observed in this table). Readings correspond to the baseline recordings (zero values) for the graphs in **Figures 52-54**.

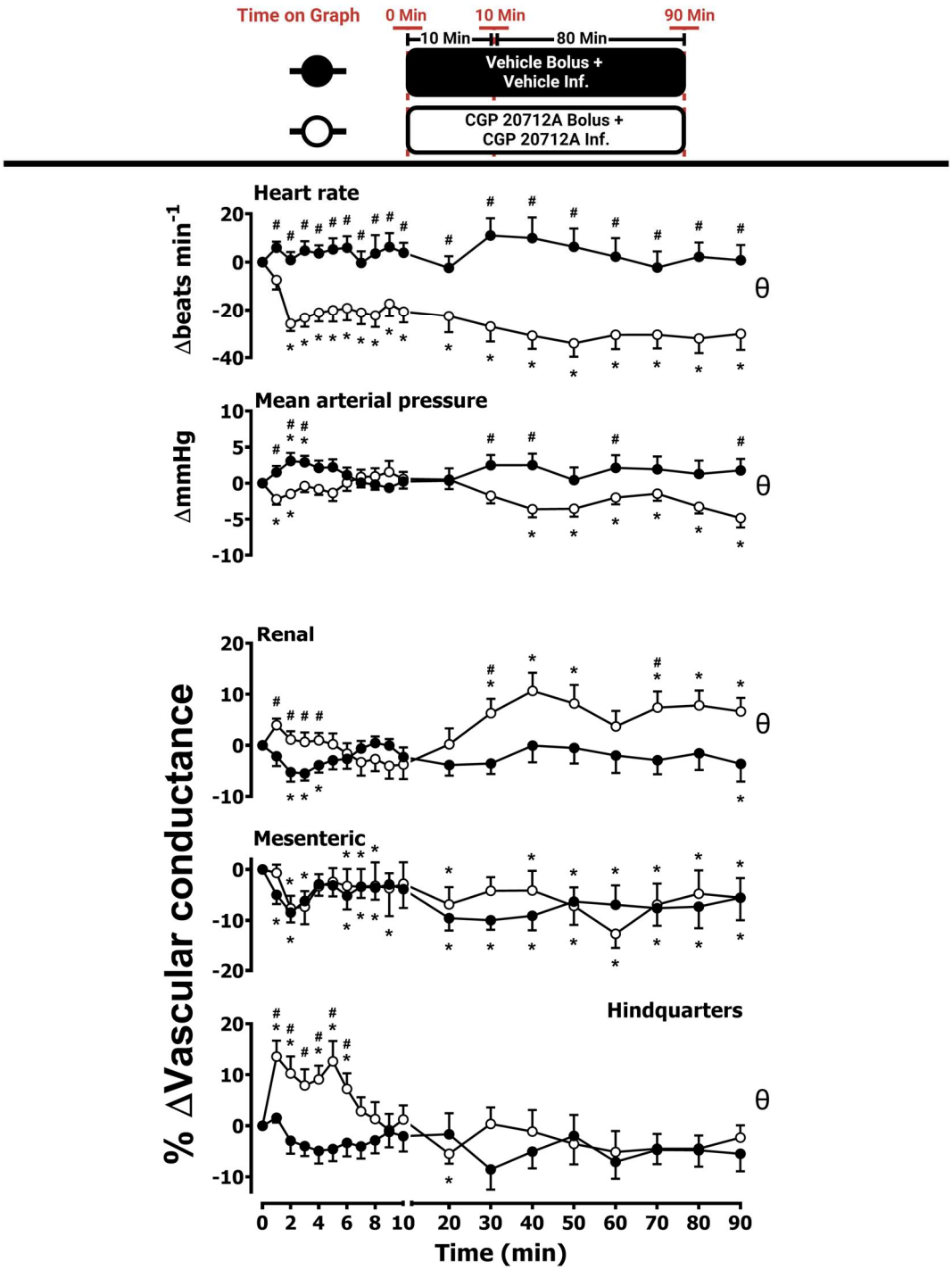


**Figure 53 Cardiovascular Responses to CGP 20712A.** Conscious, freely moving rats were dosed with CGP 20712A (0.1 mL bolus of 200 µg/kg, 0.1 mL, i.v.) and an immediate subsequent infusion of CGP 20712A (100 µg/kg/hr, 0.4 mL/hr, 90 min, i.v., n=16) or vehicle (0.1 mL bolus of 5 % propylene glycol, 2 % Tween 80 in sterile saline) and an immediate subsequent infusion of vehicle (0.4 mL/hr, 90 min, i.v., n=16) as described in the chapter 4 methodology (**4.2.1**). The graphs show the responses over the 90 min dosing period. Data points are mean + or - SEM. A Friedman test was conducted for each data point of each group and the group's corresponding baseline (T=0) (* = p<0.05 significance). In addition, a Wilcoxon signed-rank test was conducted between the CGP 20712A and vehicle control groups for a comparison of the area under the curve (**θ** = p<0.05 significance) and additionally to determine differences at each time point (Wilcoxon T-test equivalent) (**#** = p<0.05 significance). Results are a combination of Studies 7 & 10. Baseline recordings for this figure can be found in **Table 22**.

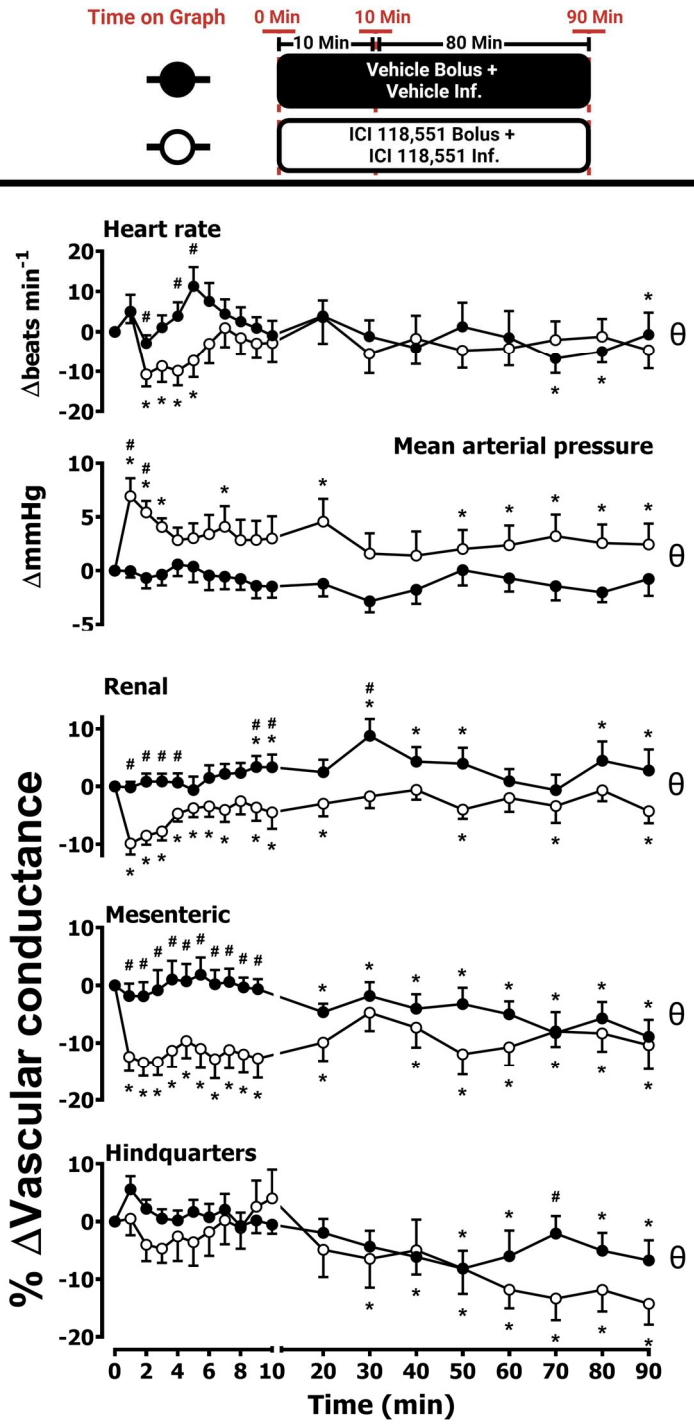


**Figure 54 Cardiovascular Responses to ICI 118,551.** Conscious, freely moving rats were dosed with ICI 118,511 (0.1 mL bolus of 2.0 mg/kg, 0.1 mL, i.v.,) and an immediate subsequent infusion of ICI 118,551 (1.0 mg/kg/hr, 0.4 mL/hr, 90 min, i.v., n=17) or vehicle (0.1 mL bolus of 5 % propylene glycol, 2 % Tween 80 in sterile saline) and an immediate subsequent infusion of vehicle (0.4 mL/hr, 90 min, i.v., n=17) as described in the chapter 4 methodology (**4.2.1**). The graphs show the responses over the 90 min dosing period. Data points are mean + or - SEM. A Friedman test was conducted for each data point of each group and the group's corresponding baseline (T=0) (* = $p<0.05$ significance). A Wilcoxon signed-rank test was conducted between the ICI 118,551 and vehicle control groups for a comparison of the area under the curve (**θ** = $p<0.05$ significance) and additionally to determine differences at each time point (Wilcoxon T-test equivalent) (**#** = $p<0.05$ significance). Results are a combination of Studies 8 & 11 completed by Patrizia Pannucci. Baseline recordings for this figure can be found in **Table 22**.

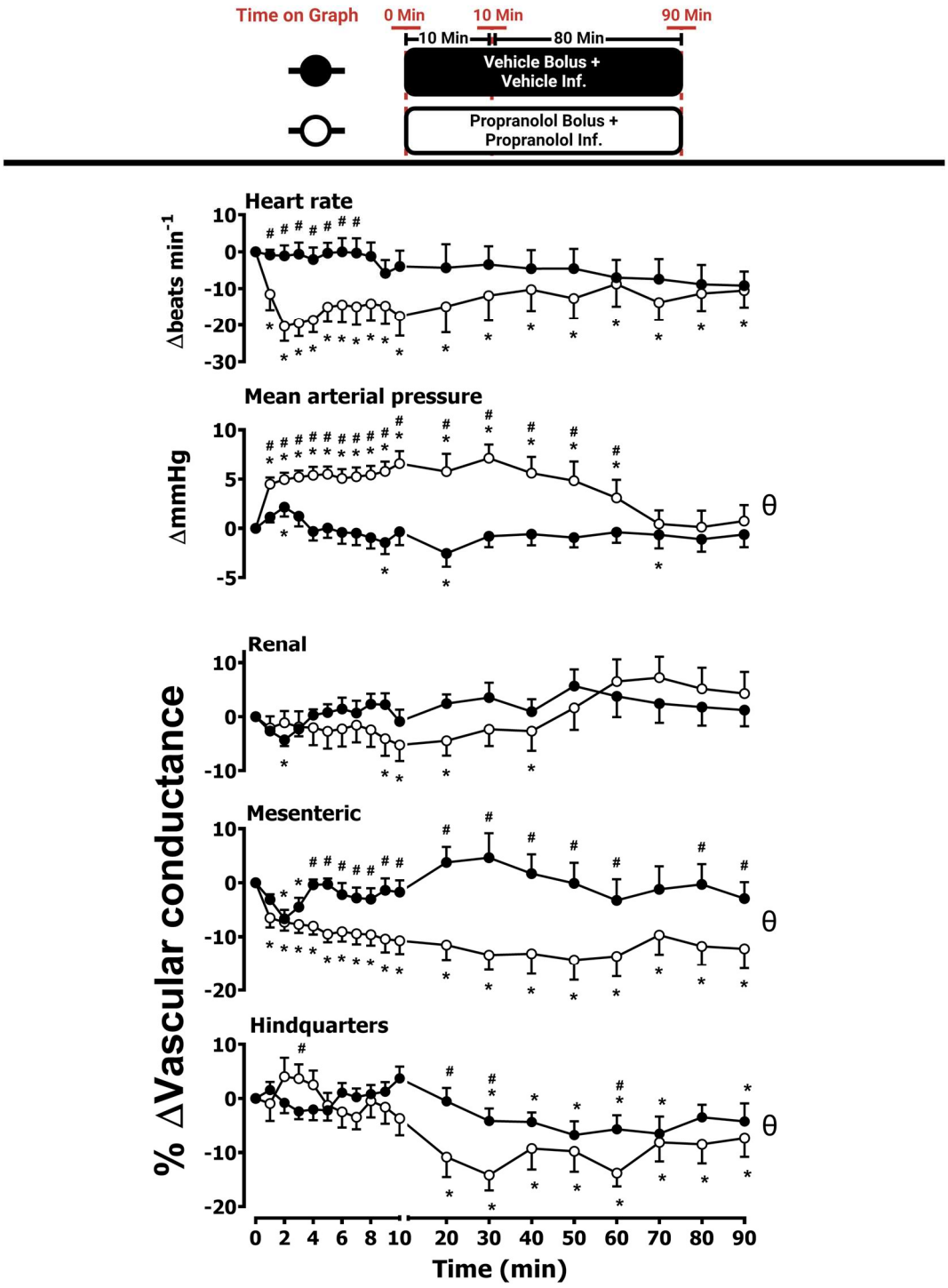


**Figure 55 Cardiovascular Responses to Propranolol.** Conscious, freely moving rats were dosed with propranolol (0.1 mL bolus of 1.0 mg/kg, i.v.,) and an immediate subsequent infusion of propranolol (0.5 mg/kg/hr, 0.4 mL/hr, 90 min, i.v, n=20) or vehicle (0.1 mL bolus of 5 % propylene glycol, 2 % Tween 80 in sterile saline) and an immediate subsequent infusion of vehicle (0.4 mL/hr, 90 min, i.v, n=20) as described in the chapter 4 methodology (**4.2.1**). The graphs show the responses over the 90 min dosing period. Data points are mean + or - SEM. A Friedman test was conducted for each data point of each group and the group's corresponding baseline (T=0) (***** = $p<0.05$ significance). A Wilcoxon signed-rank test was conducted between the propranolol and vehicle control groups for a comparison of the area under the curve (**θ** = $p<0.05$ significance) and additionally to determine differences at each time point (Wilcoxon T-test equivalent) (**#** = $p<0.05$ significance). Results are a combination of Studies 9 & 12. Baseline recordings for this figure can be found in **Table 22**.

# 7.3 Additional Data: Study 13: Sunitinib Dose Selection

| | Study 13: Sunitinib 4.0 mg/kg/day | | Study 13: Sunitinib 8.0 mg/kg/day | | Study 13: Vehicle | |
|---|---|---|---|---|---|---|
| | Vehicle | | Vehicle | | Vehicle | |
| | Value | n | Mean ± SEM | n | Mean ± SEM | n |
| **Cardiovascular Variable** | **Baseline T=0** | | **Baseline T=0** | | **Baseline T=0** | |
| **Heart rate (beats·min$^{-1}$)** | 318 | 1 | 359 ± 8 | 3 | 333 ± 17 | 3 |
| **Mean BP (mmHg)** | 103 | 1 | 112 ± 7 | 3 | 106 ± 6 | 3 |
| **Renal VC (U)** | 111 | 1 | 81 ± 18 | 3 | 67 ± 13 | 2 |
| **Mesenteric VC (U)** | 76 | 1 | 87 ± 27 | 3 | 61 ± 0 | 2 |
| **Hindquarters VC (U)** | 18 | 1 | 49 ± 17 | 3 | 34 ± 16 | 2 |

**Table 23 Cardiovascular Variables Before Administration of Sunitinib or Vehicle in Study 13.** n=1-3 per group. Values are mean ± SEM when n>1; Abbreviations: U, units; VC, vascular conductance. Units (U) of vascular conductance (VC) are kHz. mmHg$^{-1}$ x $10^3$. Readings correspond to the baseline recordings (zero values) for the graphs in **Figure 56** & **Figure 57**.

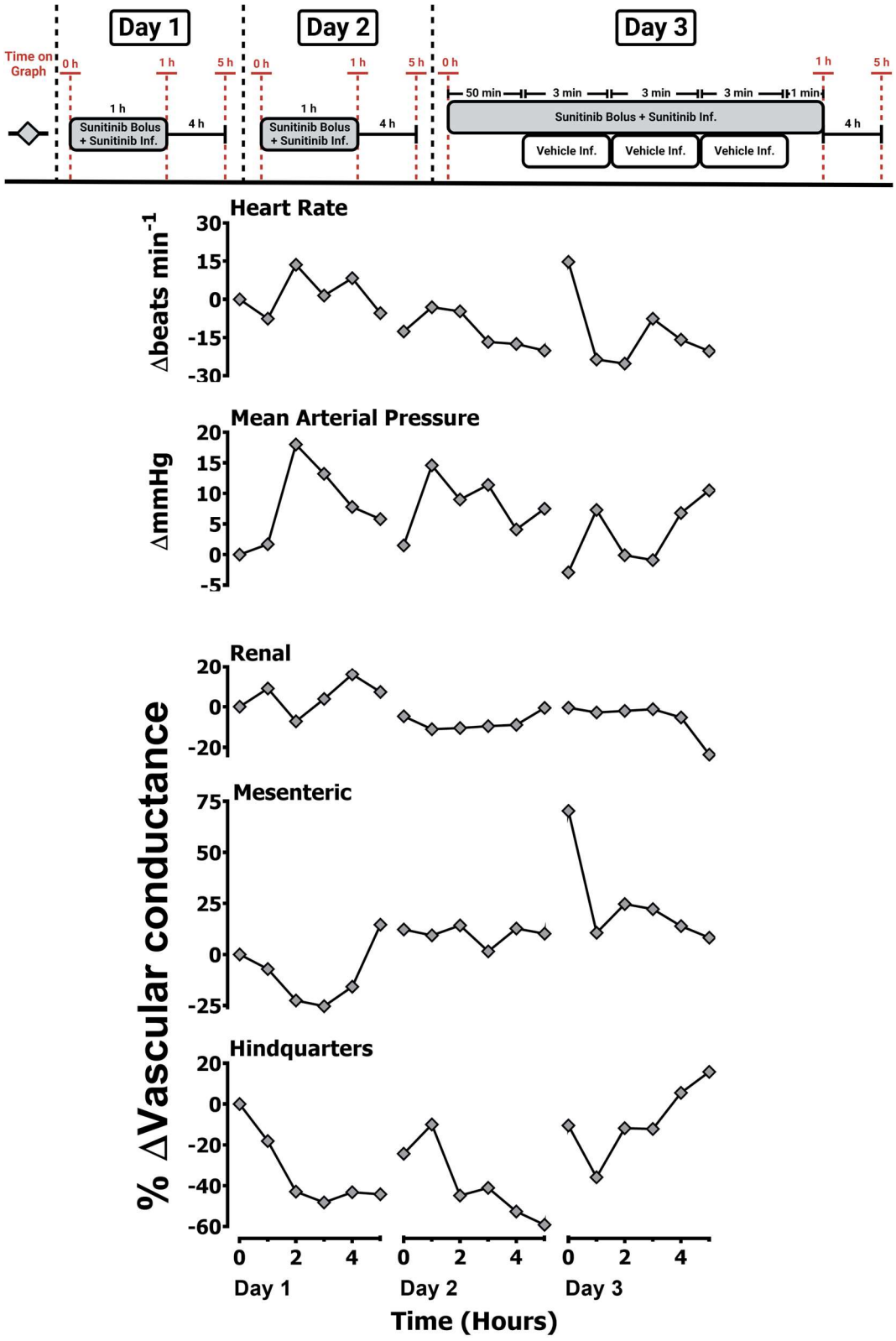


**Figure 56 Cardiovascular Responses to Sunitinib (4.0 mg/kg/day).** A conscious, freely moving rat was dosed daily for three consecutive days at time=0 each day with sunitinib (0.1 mL bolus of 2.0 mg/kg, i.v.) and an immediate subsequent infusion of sunitinib (2.0 mg/kg/hr, 0.4 mL/hr, 60 min, i.v., n=1). On day 3, 50 min after the start of the sunitinib infusion, the group received an additional three infusions (0.1 mL/min, i.v.) in succession of the vehicle, with each dose infused for 3 minutes as described in the chapter 5 methodology (**5.2.1.3.1**). The graphs show the responses 4 hours post-dosing for all 3 experimental days. Data points are single values. Results are from study 13. Baseline recordings for this figure can be found in **Table 23**.

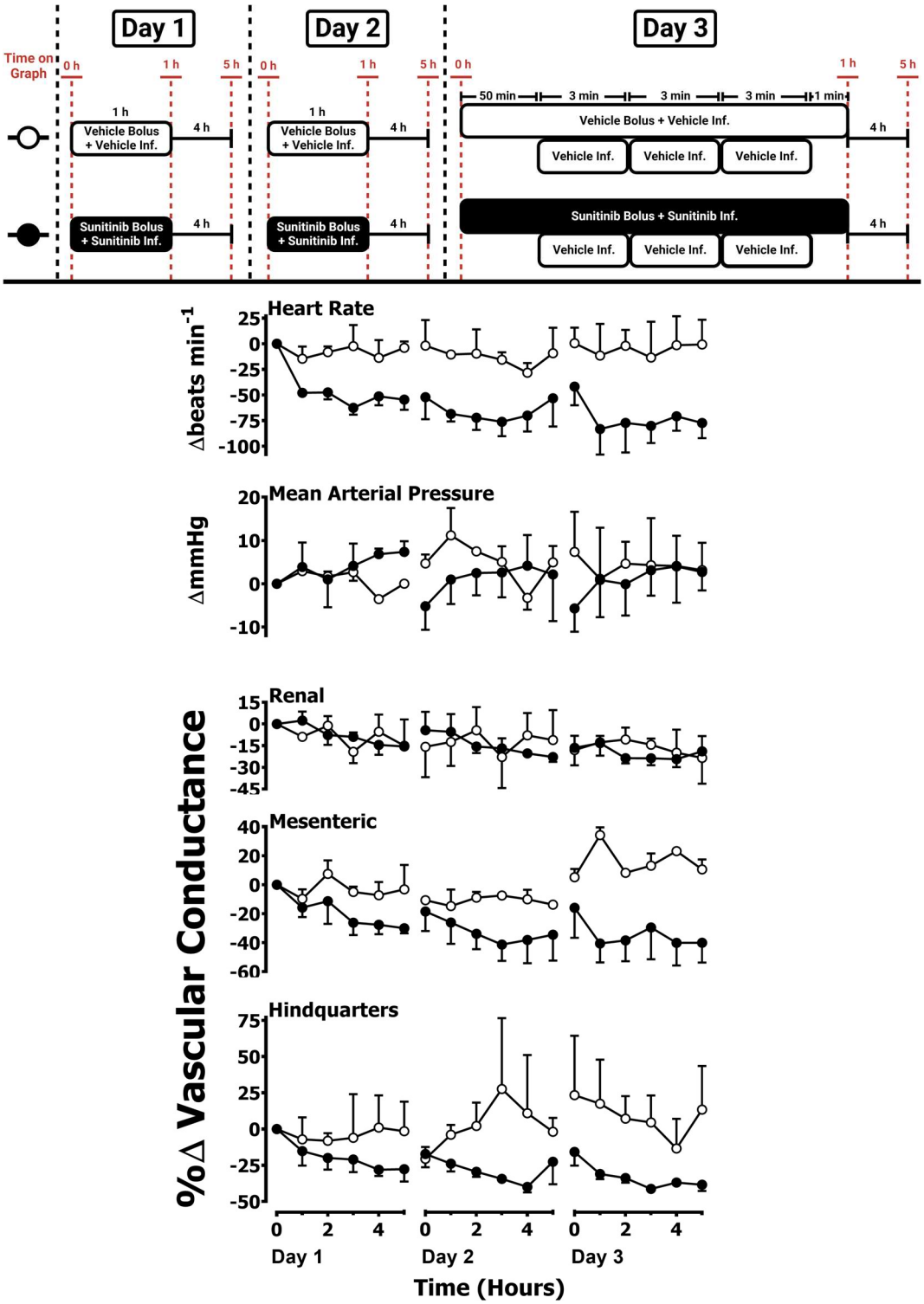


**Figure 57 Cardiovascular Responses to Sunitinib (8.0 mg/kg/day).** Conscious, freely moving rats were dosed daily for three consecutive days at time=0 each day with sunitinib (0.1 mL bolus of 4.0 mg/kg, i.v.) and an immediate subsequent infusion of sunitinib (4.0 mg/kg/hr, 0.4 mL/hr, 60 min, i.v., n=3) or vehicle (0.1 mL bolus of 5 % propylene glycol, 2 % Tween 80 in sterile saline, i.v.) and an immediate subsequent infusion of vehicle (0.4 mL/hr, 90 min, i.v., n=3). On day 3, 50 min after the start of the sunitinib or vehicle infusion, the group received an additional three infusions (0.1 mL/min, i.v.) in succession of the vehicle, with each dose infused for 3 minutes as described in the chapter 5 methodology (**5.2.1.3.1**). The graphs show the responses 4 hours post-dosing for all 3 experimental days. Data points are mean + or - SEM. Results are from study 13. Baseline recordings for this figure can be found in **Table 23**.

# References

ABI AAD, S., PIERCE, M., BARMAIMON, G., FARHAT, F. S., BENJO, A. & MOUHAYAR, E. 2015. Hypertension induced by chemotherapeutic and immunosuppresive agents: a new challenge. *Crit Rev Oncol Hematol,* 93**,** 28-35.

ABRAMS, T. J., LEE, L. B., MURRAY, L. J., PRYER, N. K. & CHERRINGTON, J. M. 2003. SU11248 inhibits KIT and platelet-derived growth factor receptor beta in preclinical models of human small cell lung cancer. *Mol Cancer Ther,* 2**,** 471-8.

ACURIO, J., HERLITZ, K., TRONCOSO, F., AGUAYO, C., BERTOGLIA, P. & ESCUDERO, C. 2017. Adenosine A2A receptor regulates expression of vascular endothelial growth factor in feto-placental endothelium from normal and late-onset pre-eclamptic pregnancies. *Purinergic Signal,* 13**,** 51-60.

ADAIR, T. H. 2005. Growth regulation of the vascular system: an emerging role for adenosine. *Am J Physiol Regul Integr Comp Physiol,* 289**,** R283-R296.

AL-KHATIB, S. M. & PRITCHETT, E. L. 1999. Clinical features of Wolff-Parkinson-White syndrome. *Am Heart J,* 138**,** 403-13.

AL JAROUDI, W. & ISKANDRIAN, A. E. 2009. Regadenoson: a new myocardial stress agent. *J Am Coll Cardiol,* 54**,** 1123-30.

ALAM, A., HERAULT, J. P., BARRON, P., FAVIER, B., FONS, P., DELESQUE-TOUCHARD, N., SENEGAS, I., LABOUDIE, P., BONNIN, J., CASSAN, C., SAVI, P., RUGGERI, B., CARMELIET, P., BONO, F. & HERBERT, J. M. 2004. Heterodimerization with vascular endothelial growth factor receptor-2 (VEGFR-2) is necessary for VEGFR-3 activity. *Biochem Biophys Res Commun,* 324**,** 909-15.

ALBERTI, C., MONOPOLI, A., CASATI, C., FORLANI, A., SALA, C., NADOR, B., ONGINI, E. & MORGANTI, A. 1997. Mechanism and pressor relevance of the short-term cardiovascular and renin excitatory actions of the selective A2A-adenosine receptor agonists. *J Cardiovasc Pharmacol,* 30**,** 320-4.

ALBERTS, B., JOHNSON, A., LEWIS, J., RAFF, M., ROBERTS, K. & WALKER, P. 2002. *Molecular Biology of the Cell,* New York, Garland Science.

ALENCAR, A. K. N., MONTES, G. C., BARREIRO, E. J., SUDO, R. T. & ZAPATA-SUDO, G. 2017. Adenosine Receptors As Drug Targets for Treatment of Pulmonary Arterial Hypertension. *Front Pharmacol,* 8**,** 858.

ALI, D. C., NAVEED, M., GORDON, A., MAJEED, F., SAEED, M., OGBUKE, M. I., ATIF, M., ZUBAIR, H. M. & CHANGXING, L. 2020. β-Adrenergic receptor, an essential target in cardiovascular diseases. *Heart Fail Rev,* 25**,** 343-354.

ALNOURI, M. W., JEPARDS, S., CASARI, A., SCHIEDEL, A. C., HINZ, S. & MULLER, C. E. 2015. Selectivity is species-dependent: Characterization of standard agonists and antagonists at human, rat, and mouse adenosine receptors. *Purinergic Signal,* 11**,** 389-407.

ANDERSSON, L. O., BARROWCLIFFE, T. W., HOLMER, E., JOHNSON, E. A. & SÖDERSTRÖM, G. 1979. Molecular weight dependency of the heparin potentiated inhibition of thrombin and activated factor X. Effect of heparin neutralization in plasma. *Thrombosis Research,* 15**,** 531-541.

ANTONIOLI, L., BLANDIZZI, C., PACHER, P. & HASKO, G. 2013a. Immunity, inflammation and cancer: a leading role for adenosine. *Nat Rev Cancer,* 13**,** 842-57.

ANTONIOLI, L., COLUCCI, R., PELLEGRINI, C., GIUSTARINI, G., TUCCORI, M., BLANDIZZI, C. & FORNAI, M. 2013b. The role of purinergic pathways in the pathophysiology of gut diseases: pharmacological modulation and potential therapeutic applications. *Pharmacol Ther,* 139**,** 157-88.

ANTONIOLI, L., FORNAI, M., BLANDIZZI, C., PACHER, P. & HASKO, G. 2019. Adenosine signaling and the immune system: When a lot could be too much. *Immunol Lett,* 205**,** 9-15.

ANTONIOLI, L., PACHER, P., VIZI, E. S. & HASKO, G. 2013c. CD39 and CD73 in immunity and inflammation. *Trends Mol Med,* 19**,** 355-67.

APARICIO-GALLEGO, G., BLANCO, M., FIGUEROA, A., GARCÍA-CAMPELO, R., VALLADARES-AYERBES, M., GRANDE-PULIDO, E. & ANTÓN-APARICIO, L. 2011. New Insights into Molecular Mechanisms of Sunitinib-Associated Side Effects. *Molecular Cancer Therapeutics,* 10**,** 2215-2223.

AREND, L. J., THOMPSON, C. I. & SPIELMAN, W. S. 1985. Dipyridamole decreases glomerular filtration in the sodium-depleted dog. Evidence for mediation by intrarenal adenosine. *Circ Res,* 56**,** 242-251.

ARNALL, B., ROTAR, V., PITSILLIDES, K., SOSA, M., GARG, V. & CALLAHAN, M. F. 2017. A new biotelemetry system to monitor true volumetric blood flow, blood pressure and temperature in small animals: Preliminary test data in rats. *FASEB J,* 31**,** 836.21-836.21.

ASAKURA, M., ASANUMA, H., KIM, J., LIAO, Y., NAKAMARU, K., FUJITA, M., KOMAMURA, K., ISOMURA, T., FURUKAWA, H., TOMOIKE, H. & KITAKAZE, M. 2007. Impact of adenosine receptor signaling and metabolism on pathophysiology in patients with chronic heart failure. *Hypertens Res,* 30**,** 781-7.

AYOUB, M. A. & PFLEGER, K. D. 2010. Recent advances in bioluminescence resonance energy transfer technologies to study GPCR heteromerization. *Curr Opin Pharmacol,* 10**,** 44-52.

BAEK MOLLER, N., BUDOLFSEN, C., GRIMM, D., KRUGER, M., INFANGER, M., WEHLAND, M. & N, E. M. 2019. Drug-Induced Hypertension Caused by Multikinase Inhibitors (Sorafenib, Sunitinib, Lenvatinib and Axitinib) in Renal Cell Carcinoma Treatment. *Int J Mol Sci,* 20**,** 4712.

BAHREYNI, A., AVAN, A., SHABANI, M., RYZHIKOV, M., FIUJI, H., SOLEIMANPOUR, S., KHAZAEI, M. & HASSANIAN, S. M. 2019. Therapeutic potential of A2 adenosine receptor pharmacological regulators in the treatment of cardiovascular diseases, recent progress, and prospective. *J Cell Physiol,* 234**,** 1295-1299.

BAKER, J. G., GARDINER, S. M., WOOLARD, J., FROMONT, C., JADHAV, G. P., MISTRY, S. N., THOMPSON, K. S. J., KELLAM, B., HILL, S. J. & FISCHER, P. M. 2017. Novel selective β(1)-adrenoceptor antagonists for concomitant cardiovascular and respiratory disease. *FASEB J,* 31**,** 3150-3166.

BAKER, J. G., KEMP, P., MARCH, J., FRETWELL, L., HILL, S. J. & GARDINER, S. M. 2011. Predicting in vivo cardiovascular properties of β-blockers from cellular assays: a quantitative comparison of cellular and cardiovascular pharmacological responses. *FASEB J,* 25**,** 4486-97.

BAKER, J. G., MIDDLETON, R., ADAMS, L., MAY, L. T., BRIDDON, S. J., KELLAM, B. & HILL, S. J. 2010. Influence of fluorophore and linker composition on the pharmacology of fluorescent adenosine A1 receptor ligands. *Br J Pharmacol,* 159**,** 772-786.

BARKI-HARRINGTON, L., PERRINO, C. & ROCKMAN, H. A. 2004. Network integration of the adrenergic system in cardiac hypertrophy. *Cardiovascular Research,* 63**,** 391-402.

BARRETT, R. J., DROPPLEMAN, D. A. & WRIGHT, K. F. 1992. N-0861 selectively antagonizes adenosine A1 receptors in vivo. *Eur J Pharmacol,* 216**,** 9-16.

BARRETT, R. J., MAY, J. M., MARTIN, P. L. & MILLER, J. R. 1993. In vitro and in vivo pharmacological characterization of N6-cyclopentyl-9-methyladenine (N-0840): a selective, orally active A1 adenosine receptor antagonist. *Journal of Pharmacology and Experimental Therapeutics,* 265**,** 227-236.

BAUER, R. M., VELA, M. B., SIMON, T. & WALDROP, T. G. 1988. A GABAergic mechanism in the posterior hypothalamus modulates baroreflex bradycardia. *Brain Res Bull,* 20**,** 633-41.

BELARDINELLI, L. & ISENBERG, G. 1983. Isolated atrial myocytes: adenosine and acetylcholine increase potassium conductance. *Am J Physiol,* 244**,** H734-7.

BENNETT, R. C. & RESTITUTTI, F. 2016. Dexmedetomidine or medetomidine: which should veterinary surgeons select? *Companion Animal,* 21**,** 128-137.

BERK, A. J. 2005. Recent lessons in gene expression, cell cycle control, and cell biology from adenovirus. *Oncogene,* 24**,** 7673-7685.

BERWICK, Z. C., PAYNE, G. A., LYNCH, B., DICK, G. M., STUREK, M. & TUNE, J. D. 2010. Contribution of adenosine A(2A) and A(2B) receptors to ischemic coronary dilation: role of K(V) and K(ATP) channels. *Microcirculation,* 17**,** 600-7.

BESSMAN, N. J., BAGCHI, A., FERGUSON, K. M. & LEMMON, M. A. 2014. Complex relationship between ligand binding and dimerization in the epidermal growth factor receptor. *Cell Rep,* 9**,** 1306-17.

BHARGAVA, P. 2009. VEGF kinase inhibitors: how do they cause hypertension? *Am J Physiol Regul Integr Comp Physiol,* 297**,** R1-R5.

BIVALACQUA, T. J., CHAMPION, H. C., LAMBERT, D. G. & KADOWITZ, P. J. 2002. Vasodilator responses to adenosine and hyperemia are mediated by A(1) and A(2) receptors in the cat vascular bed. *Am J Physiol Regul Integr Comp Physiol,* 282**,** R1696-709.

BLASI, E., HEYEN, J., PATYNA, S., HEMKENS, M., RAMIREZ, D., JOHN-BAPTISTE, A., STEIDL-NICHOLS, J. & MCHARG, A. 2012. Sunitinib, a Receptor Tyrosine Kinase Inhibitor, Increases Blood Pressure in Rats without Associated Changes in Cardiac Structure and Function. *Cardiovascular Therapeutics,* 30**,** 287-294.

BLOMS-FUNKE, P., GILLEN, C., SCHUETTLER, A. J. & WNENDT, S. 2000. Agonistic effects of the opioid buprenorphine on the nociceptin/OFQ receptor. *Peptides,* 21**,** 1141-6.

BLUME-JENSEN, P. & HUNTER, T. 2001. Oncogenic kinase signalling. *Nature,* 411**,** 355-365.

BOKNIK, P., ESKANDAR, J., HOFMANN, B., ZIMMERMANN, N., NEUMANN, J. & GERGS, U. 2021. Role of Cardiac A2A Receptors Under Normal and Pathophysiological Conditions. *Frontiers in Pharmacology,* 11**,** 627838.

BOOM, M., NIESTERS, M., SARTON, E., AARTS, L., SMITH, T. W. & DAHAN, A. 2012. Non-analgesic effects of opioids: opioid-induced respiratory depression. *Curr Pharm Des,* 18**,** 5994-6004.

BOREA, P. A., GESSI, S., MERIGHI, S. & VARANI, K. 2016. Adenosine as a Multi-Signalling Guardian Angel in Human Diseases: When, Where and How Does it Exert its Protective Effects? *Trends Pharmacol Sci,* 37**,** 419-434.

BOREA, P. A., GESSI, S., MERIGHI, S., VINCENZI, F. & VARANI, K. 2018. Pharmacology of Adenosine Receptors: The State of the Art. *Physiological Reviews,* 98**,** 1591-1625.

BORRMANN, T., HINZ, S., BERTARELLI, D. C. G., LI, W., FLORIN, N. C., SCHEIFF, A. B. & MÜLLER, C. E. 2009. 1-Alkyl-8-(piperazine-1-sulfonyl)phenylxanthines: Development and Characterization of Adenosine A2B Receptor Antagonists and a New Radioligand with Subnanomolar Affinity and Subtype Specificity. *Journal of Medicinal Chemistry,* 52**,** 3994-4006.

BORROTO-ESCUELA, D. O., FLAJOLET, M., AGNATI, L. F., GREENGARD, P. & FUXE, K. 2013. Bioluminescence resonance energy transfer methods to study G protein-coupled receptor-receptor tyrosine kinase heteroreceptor complexes. *Methods Cell Biol,* 117**,** 141-64.

BORROTO-ESCUELA, D. O. & FUXE, K. 2019. Adenosine heteroreceptor complexes in the basal ganglia are implicated in Parkinson's disease and its treatment. *J Neural Transm,* 126**,** 455-471.

BOSWELL-CASTEEL, R. C. & HAYS, F. A. 2017. Equilibrative nucleoside transporters-A review. *Nucleosides Nucleotides Nucleic Acids,* 36**,** 7-30.

BOUZO-LORENZO, M., STODDART, L. A., XIA, L., AP, I. J., HEITMAN, L. H., BRIDDON, S. J. & HILL, S. J. 2019. A live cell NanoBRET binding assay allows the study of ligand-binding kinetics to the adenosine A3 receptor. *Purinergic Signal,* 15**,** 139-153.

BOVE, T., ZANGRILLO, A., GUARRACINO, F., ALVARO, G., PERSI, B., MAGLIONI, E., GALDIERI, N., COMIS, M., CARAMELLI, F. & PASERO, D. C. 2014. Effect of fenoldopam on use of renal replacement therapy among patients with acute kidney injury after cardiac surgery: a randomized clinical trial. *JAMA,* 312**,** 2244-2253.

BRIDDON, S. J., GANDÍA, J., AMARAL, O. B., FERRÉ, S., LLUÍS, C., FRANCO, R., HILL, S. J. & CIRUELA, F. 2008. Plasma membrane diffusion of g protein-coupled receptor oligomers. *Biochimica et Biophysica Acta,* 1783**,** 2262-2268.

BRIDDON, S. J., MIDDLETON, R. J., CORDEAUX, Y., FLAVIN, F. M., WEINSTEIN, J. A., GEORGE, M. W., KELLAM, B. & HILL, S. J. 2004. Quantitative analysis of the formation and diffusion of A1-adenosine receptor-antagonist complexes in single living cells. *Proc Natl Acad Sci U S A,* 101**,** 4673-8.

BRISTOW, M. R. 2011. Treatment of chronic heart failure with β-adrenergic receptor antagonists: a convergence of receptor pharmacology and clinical cardiology. *Circ Res,* 109**,** 1176-94.

BRITO, R., PEREIRA, M. R., PAES-DE-CARVALHO, R. & CALAZA KDA, C. 2012. Expression of A1 adenosine receptors in the developing avian retina: in vivo

modulation by A(2A) receptors and endogenous adenosine. *J Neurochem,* 123**,** 239-49.

BROWN, Z. W., AMIT, Z. & WEEKS, J. R. 1976. Simple flow-thru swivel for infusions into unrestrained animals. *Pharmacology Biochemistry and Behavior,* 5**,** 363-365.

BROZZO, M. S., BJELIC, S., KISKO, K., SCHLEIER, T., LEPPANEN, V. M., ALITALO, K., WINKLER, F. K. & BALLMER-HOFER, K. 2012. Thermodynamic and structural description of allosterically regulated VEGFR-2 dimerization. *Blood,* 119**,** 1781-8.

BRYAN, P. T. & MARSHALL, J. M. 1999. Adenosine receptor subtypes and vasodilatation in rat skeletal muscle during systemic hypoxia: a role for A1 receptors. *J Physiol,* 514 ( Pt 1)**,** 151-62.

BURNSTOCK, G. & MEGHJI, P. 1983. The effect of adenyl compounds on the rat heart. *Br J Pharmacol,* 79**,** 211-218.

BUSSE, H., BITZINGER, D., HOCHERL, K., SEYFRIED, T., GRUBER, M., GRAF, B. M. & ZAUSIG, Y. A. 2016. Adenosine A2A and A2B Receptor Substantially Attenuate Ischemia/Reperfusion Injury in Septic rat Hearts. *Cardiovasc Drugs Ther,* 30**,** 551-558.

CAI, M., WANG, K., MURDOCH, C. E., GU, Y. & AHMED, A. 2017. Heterodimerisation between VEGFR-1 and VEGFR-2 and not the homodimers of VEGFR-1 inhibit VEGFR-2 activity. *Vascul Pharmacol,* 88**,** 11-20.

CALAMA, E., FERNÁNDEZ, M. M., MORÁN, A., MARTÍN, M. L. & SAN ROMÁN, L. 2002. Vasodilator and vasoconstrictor responses induced by 5-hydroxytryptamine in the in situ blood autoperfused hindquarters of the anaesthetized rat. *Naunyn Schmiedebergs Arch Pharmacol,* 366**,** 110-6.

CAMELLITI, P., GREEN, C. R., LEGRICE, I. & KOHL, P. 2004. Fibroblast network in rabbit sinoatrial node: structural and functional identification of homogeneous and heterogeneous cell coupling. *Circ Res,* 94**,** 828-35.

CANALS, M., BURGUENO, J., MARCELLINO, D., CABELLO, N., CANELA, E. I., MALLOL, J., AGNATI, L., FERRE, S., BOUVIER, M., FUXE, K., CIRUELA, F., LLUIS, C. & FRANCO, R. 2004. Homodimerization of adenosine A2A receptors:

qualitative and quantitative assessment by fluorescence and bioluminescence energy transfer. *J Neurochem,* 88**,** 726-34.

CANALS, M., MARCELLINO, D., FANELLI, F., CIRUELA, F., DE BENEDETTI, P., GOLDBERG, S. R., NEVE, K., FUXE, K., AGNATI, L. F., WOODS, A. S., FERRE, S., LLUIS, C., BOUVIER, M. & FRANCO, R. 2003. Adenosine A2A-dopamine D2 receptor-receptor heteromerization: qualitative and quantitative assessment by fluorescence and bioluminescence energy transfer. *J Biol Chem,* 278**,** 46741-9.

CARIO, G. & FRANCK, J. 1922. Über Zerlegung von Wasserstoffmolekülen durch angeregte Quecksilberatome. *Zeitschrift für Physik,* 11**,** 161-166.

CARPENTER, B. & LEBON, G. 2017. Human Adenosine A2A Receptor: Molecular Mechanism of Ligand Binding and Activation. *Front Pharmacol,* 8**,** 898.

CARTER, J. J., FRETWELL, L. V. & WOOLARD, J. 2017. Effects of 4 multitargeted receptor tyrosine kinase inhibitors on regional hemodynamics in conscious, freely moving rats. *FASEB J,* 31**,** 1193-1203.

CARTER, J. J., WHEAL, A. J., HILL, S. J. & WOOLARD, J. 2015. Effects of receptor tyrosine kinase inhibitors on VEGF165 a- and VEGF165 b-stimulated gene transcription in HEK-293 cells expressing human VEGFR2. *Br J Pharmacol,* 172**,** 3141-50.

CAVALUZZI, M. J. & BORER, P. N. 2004. Revised UV extinction coefficients for nucleoside-5′-monophosphates and unpaired DNA and RNA. *Nucleic Acids Research,* 32**,** e13.

CENSOR, D. 1984. Theory of the Doppler effect: Fact, fiction and approximation. *Radio Science,* 19**,** 1027-1040.

CHADE, A. R. 2013. Renal vascular structure and rarefaction. *Compr Physiol,* 3**,** 817-31.

CHAPIN, J. C. & HAJJAR, K. A. 2015. Fibrinolysis and the control of blood coagulation. *Blood Rev,* 29**,** 17-24.

CHAYTOR, J. L., TOKAREW, J. M., WU, L. K., LECLÈRE, M., TAM, R. Y., CAPICCIOTTI, C. J., GUOLLA, L., VON MOOS, E., FINDLAY, C. S., ALLAN, D.

S. & BEN, R. N. 2011. Inhibiting ice recrystallization and optimization of cell viability after cryopreservation. *Glycobiology,* 22**,** 123-133.

CHEN, A. P., SETSER, A., ANADKAT, M. J., COTLIAR, J., OLSEN, E. A., GARDEN, B. C. & LACOUTURE, M. E. 2012. Grading dermatologic adverse events of cancer treatments: The Common Terminology Criteria for Adverse Events Version 4.0. *Journal of the American Academy of Dermatology,* 67**,** 1025-1039.

CHEN, Y., EPPERSON, S., MAKHSUDOVA, L., ITO, B., SUAREZ, J., DILLMANN, W. & VILLARREAL, F. 2004. Functional effects of enhancing or silencing adenosine A2b receptors in cardiac fibroblasts. *Am J Physiol Heart Circ Physiol,* 287**,** H2478-86.

CHRISTIANSEN, E., HUDSON, B. D., HANSEN, A. H., MILLIGAN, G. & ULVEN, T. 2016. Development and Characterization of a Potent Free Fatty Acid Receptor 1 (FFA1) Fluorescent Tracer. *J Med Chem,* 59**,** 4849-58.

CHRUSCINSKI, A., BREDE, M. E., MEINEL, L., LOHSE, M. J., KOBILKA, B. K. & HEIN, L. 2001. Differential distribution of beta-adrenergic receptor subtypes in blood vessels of knockout mice lacking beta(1)- or beta(2)-adrenergic receptors. *Mol Pharmacol,* 60**,** 955-62.

CHU, Y. Y., TU, K. H., LEE, Y. C., KUO, Z. J., LAI, H. L. & CHERN, Y. 1996. Characterization of the rat A2a adenosine receptor gene. *DNA Cell Biol,* 15**,** 329-37.

CHUO, C. H., DEVINE, S. M., SCAMMELLS, P. J., KRUM, H., CHRISTOPOULOS, A., MAY, L. T., WHITE, P. J. & WANG, B. H. 2016. VCP746, a novel A1 adenosine receptor biased agonist, reduces hypertrophy in a rat neonatal cardiac myocyte model. *Clin Exp Pharmacol Physiol,* 43**,** 976-82.

CHURCHILL, P. C. & BIDANI, A. 1987. Renal effects of selective adenosine receptor agonists in anesthetized rats. *Am J Physiol,* 252**,** F299-303.

CIRUELA, F. 2008. Fluorescence-based methods in the study of protein–protein interactions in living cells. *Current opinion in biotechnology,* 19**,** 338-343.

CIRUELA, F., CASADÓ, V., RODRIGUES, R. J., LUJÁN, R., BURGUEÑO, J., CANALS, M., BORYCZ, J., REBOLA, N., GOLDBERG, S. R., MALLOL, J.,

CORTÉS, A., CANELA, E. I., LÓPEZ-GIMÉNEZ, J. F., MILLIGAN, G., LLUIS, C., CUNHA, R. A., FERRÉ, S. & FRANCO, R. 2006. Presynaptic Control of Striatal Glutamatergic Neurotransmission by Adenosine A1–A2A Receptor Heteromers. *The Journal of Neuroscience,* 26**,** 2080-2087.

CLARK, A. N., YOUKEY, R., LIU, X., JIA, L., BLATT, R., DAY, Y. J., SULLIVAN, G. W., LINDEN, J. & TUCKER, A. L. 2007. A1 adenosine receptor activation promotes angiogenesis and release of VEGF from monocytes. *Circ Res,* 101**,** 1130-8.

COBBE, S. M. 1987. Clinical usefulness of the Vaughan Williams classification system. *Eur Heart J,* 8 Suppl A**,** 65-9.

COFFEY, J. C. & O'LEARY, D. P. 2016. The mesentery: structure, function, and role in disease. *Lancet Gastroenterol Hepatol,* 1**,** 238-247.

COMEO, E., KINDON, N. D., SOAVE, M., STODDART, L. A., KILPATRICK, L. E., SCAMMELLS, P. J., HILL, S. J. & KELLAM, B. 2019. Subtype-Selective Fluorescent Ligands as Pharmacological Research Tools for the Human Adenosine A2A Receptor. *Journal of Medicinal Chemistry,* 63**,** 2656-2672.

COOPER, S. L., MARCH, J., HILL, S. & WOOLARD, J. 2018. Regional Haemodynamic responses to Adenosine A2A-Receptor Agonists in Conscious Freely Moving Rats. *FASEB J,* 32**,** 568.10.

COOPER, S. L., MARCH, J., SABBATINI, A. R., HILL, S. J., JORG, M., SCAMMELLS, P. J. & WOOLARD, J. 2020. The effect of two selective A1 -receptor agonists and the bitopic ligand VCP746 on heart rate and regional vascular conductance in conscious rats. *Br J Pharmacol,* 177**,** 346-359.

COOPER, S. L., WRAGG, E. S., PANNUCCI, P., SOAVE, M., HILL, S. J. & WOOLARD, J. 2022. Regionally selective cardiovascular responses to adenosine A2A and A2B receptor activation. *FASEB J,* 36**,** e22214.

COTTET, M., FAKLARIS, O., ZWIER, J. M., TRINQUET, E., PIN, J.-P. & DURROUX, T. 2011. Original Fluorescent Ligand-Based Assays Open New Perspectives in G-Protein Coupled Receptor Drug Screening. *Pharmaceuticals,* 4**,** 202-214.

COX, D. A., VITA, J. A., TREASURE, C. B., FISH, R. D., SELWYN, A. P. & GANZ, P. 1989. Reflex increase in blood pressure during the intracoronary administration of adenosine in man. *J Clin Invest,* 84**,** 592-6.

DA SILVA, J. S., GABRIEL-COSTA, D., SUDO, R. T., WANG, H., GROBAN, L., FERRAZ, E. B., NASCIMENTO, J. H., FRAGA, C. A., BARREIRO, E. J. & ZAPATA-SUDO, G. 2017. Adenosine A2A receptor agonist prevents cardiac remodeling and dysfunction in spontaneously hypertensive male rats after myocardial infarction. *Drug Des Devel Ther,* 11**,** 553-562.

DACRES, H., MICHIE, M., WANG, J., PFLEGER, K. D. & TROWELL, S. C. 2012. Effect of enhanced Renilla luciferase and fluorescent protein variants on the Forster distance of Bioluminescence resonance energy transfer (BRET). *Biochem Biophys Res Commun,* 425**,** 625-9.

DALE, N. C., JOHNSTONE, E. K. M., WHITE, C. W. & PFLEGER, K. D. G. 2019. NanoBRET: The Bright Future of Proximity-Based Assays. *Front Bioeng Biotechnol,* 7**,** 56.

DAVIS, M. I., HUNT, J. P., HERRGARD, S., CICERI, P., WODICKA, L. M., PALLARES, G., HOCKER, M., TREIBER, D. K. & ZARRINKAR, P. P. 2011. Comprehensive analysis of kinase inhibitor selectivity. *Nat Biotechnol,* 29**,** 1046-51.

DE FILIPPO, E., HINZ, S., PELLIZZARI, V., DEGANUTTI, G., EL-TAYEB, A., NAVARRO, G., FRANCO, R., MORO, S., SCHIEDEL, A. C. & MULLER, C. E. 2020. A2A and A2B adenosine receptors: The extracellular loop 2 determines high (A2A) or low affinity (A2B) for adenosine. *Biochem Pharmacol,* 172**,** 113718.

DE JESUS-GONZALEZ, N., ROBINSON, E., MOSLEHI, J. & HUMPHREYS, B. D. 2012. Management of antiangiogenic therapy-induced hypertension. *Hypertension,* 60**,** 607-15.

DERYUGINA, E. I. & QUIGLEY, J. P. 2012. Cell surface remodeling by plasmin: a new function for an old enzyme. *J Biomed Biotechnol,* 2012**,** 564259.

DHALLA, A. K., WONG, M. Y., WANG, W. Q., BIAGGIONI, I. & BELARDINELLI, L. 2006. Tachycardia caused by A2A adenosine receptor agonists is mediated by direct sympathoexcitation in awake rats. *J Pharmacol Exp Ther,* 316**,** 695-702.

DHAUN, N., WEBB, D. J. & KLUTH, D. C. 2012. Endothelin-1 and the kidney--beyond BP. *Br J Pharmacol,* 167**,** 720-31.

DIJKMAN, M. A., HESLINGA, J. W., SIPKEMA, P. & WESTERHOF, N. 1997. Perfusion-induced changes in cardiac contractility and oxygen consumption are not endothelium-dependent. *Cardiovasc Res,* 33**,** 593-600.

DIXON, A. K., GUBITZ, A. K., SIRINATHSINGHJI, D. J. S., RICHARDSON, P. J. & FREEMAN, T. C. 1996. Tissue distribution of adenosine receptor mRNAs in the rat. *Br J Pharmacol,* 118**,** 1461-1468.

DIXON, A. S., SCHWINN, M. K., HALL, M. P., ZIMMERMAN, K., OTTO, P., LUBBEN, T. H., BUTLER, B. L., BINKOWSKI, B. F., MACHLEIDT, T., KIRKLAND, T. A., WOOD, M. G., EGGERS, C. T., ENCELL, L. P. & WOOD, K. V. 2016. NanoLuc Complementation Reporter Optimized for Accurate Measurement of Protein Interactions in Cells. *ACS Chem Biol,* 11**,** 400-8.

DONOSO, M. V., LOPEZ, R., MIRANDA, R., BRIONES, R. & HUIDOBRO-TORO, J. P. 2005. A2B adenosine receptor mediates human chorionic vasoconstriction and signals through arachidonic acid cascade. *Am J Physiol Heart Circ Physiol,* 288**,** H2439-49.

DOSCH, D. D. & BALLMER-HOFER, K. 2010. Transmembrane domain-mediated orientation of receptor monomers in active VEGFR-2 dimers. *FASEB J,* 24**,** 32-38.

DOWNES, G. B. & GAUTAM, N. 1999. The G Protein Subunit Gene Families. *Genomics,* 62**,** 544-552.

DRINOVEC, L., KUBALE, V., NOHR LARSEN, J. & VRECL, M. 2012. Mathematical models for quantitative assessment of bioluminescence resonance energy transfer: application to seven transmembrane receptors oligomerization. *Front Endocrinol,* 3**,** 104.

DRURY, A. N. & SZENT-GYÖRGYI, A. 1929. The physiological activity of adenine compounds with especial reference to their action upon the mammalian heart. *The Journal of physiology,* 68**,** 213-237.

DU, Z. & LOVLY, C. M. 2018. Mechanisms of receptor tyrosine kinase activation in cancer. *Molecular Cancer,* 17**,** 58.

DUBRIDGE, R. B., TANG, P., HSIA, H. C., LEONG, P. M., MILLER, J. H. & CALOS, M. P. 1987. Analysis of mutation in human cells by using an Epstein-Barr virus shuttle system. *Mol Cell Biol,* 7**,** 379-87.

EL-GOWELLI, H. M., EL-GOWILLY, S. M., ELSALAKAWY, L. K. & EL-MAS, M. M. 2013. Nitric oxide synthase/K+ channel cascade triggers the adenosine A(2B) receptor-sensitive renal vasodilation in female rats. *Eur J Pharmacol,* 702**,** 116-25.

EL-MAS, M. M., EL-GOWILLY, S. M., FOUDA, M. A. & SAAD, E. I. 2011. Role of adenosine A2A receptor signaling in the nicotine-evoked attenuation of reflex cardiac sympathetic control. *Toxicol Appl Pharmacol,* 254**,** 229-37.

EL KHAMLICHI, C., REVERCHON-ASSADI, F., HERVOUET-COSTE, N., BLOT, L., REITER, E. & MORISSET-LOPEZ, S. 2019. Bioluminescence Resonance Energy Transfer as a Method to Study Protein-Protein Interactions: Application to G Protein Coupled Receptor Biology. *Molecules,* 24**,** 537.

EL MAATOUGUI, A., AZUAJE, J., GONZALEZ-GOMEZ, M., MIGUEZ, G., CRESPO, A., CARBAJALES, C., ESCALANTE, L., GARCIA-MERA, X., GUTIERREZ-DE-TERAN, H. & SOTELO, E. 2016. Discovery of Potent and Highly Selective A2B Adenosine Receptor Antagonist Chemotypes. *J Med Chem,* 59**,** 1967-83.

ELTZSCHIG, H. K. 2013. Extracellular adenosine signaling in molecular medicine. *J Mol Med,* 91**,** 141-6.

ELTZSCHIG, H. K., BRATTON, D. L. & COLGAN, S. P. 2014. Targeting hypoxia signalling for the treatment of ischaemic and inflammatory diseases. *Nat Rev Drug Discov,* 13**,** 852-69.

ESCUDERO, C., ROBERTS, J. M., MYATT, L. & FEOKTISTOV, I. 2014. Impaired adenosine-mediated angiogenesis in preeclampsia: potential implications for fetal programming. *Front Pharmacol,* 5**,** 134.

EVONIUK, G., VON BORSTEL, R. W. & WURTMAN, R. J. 1987. Antagonism of the cardiovascular effects of adenosine by caffeine or 8-(p-sulfophenyl)theophylline. *J Pharmacol Exp Ther,* 240**,** 428-32.

FACEMIRE, C. S., NIXON, A. B., GRIFFITHS, R., HURWITZ, H. & COFFMAN, T. M. 2009. Vascular endothelial growth factor receptor 2 controls blood pressure by regulating nitric oxide synthase expression. *Hypertension,* 54**,** 652-8.

FAIVRE, S., DEMETRI, G., SARGENT, W. & RAYMOND, E. 2007. Molecular basis for sunitinib efficacy and future clinical development. *Nature reviews Drug discovery,* 6**,** 734-745.

FAN, F., BINKOWSKI, B. F., BUTLER, B. L., STECHA, P. F., LEWIS, M. K. & WOOD, K. V. 2008. Novel Genetically Encoded Biosensors Using Firefly Luciferase. *ACS Chemical Biology,* 3**,** 346-351.

FENG, M. G. & NAVAR, L. G. 2010. Afferent arteriolar vasodilator effect of adenosine predominantly involves adenosine A2B receptor activation. *Am J Physiol Renal Physiol,* 299**,** F310-5.

FEOKTISTOV, I., BIAGGIONI, I. & CRONSTEIN, B. N. 2009. Adenosine receptors in wound healing, fibrosis and angiogenesis. *Handbook of experimental pharmacology,* 193**,** 383-397.

FEOKTISTOV, I., GOLDSTEIN, A. E., RYZHOV, S., ZENG, D., BELARDINELLI, L., VOYNO-YASENETSKAYA, T. & BIAGGIONI, I. 2002. Differential expression of adenosine receptors in human endothelial cells: role of A2B receptors in angiogenic factor regulation. *Circ Res,* 90**,** 531-8.

FERRARA, N. 2010. Vascular endothelial growth factor and age-related macular degeneration: from basic science to therapy. *Nat Med,* 16**,** 1107-11.

FISCHETTI, F., FABRIS, B., CALCI, M., CANDIDO, R., ARMINI, L., BARDELLI, M., COMINOTTO, F., BIAGI, A. & CARRETTA, R. 1994. Effects of central alpha 2-adrenergic agonists on systemic haemodynamics and on baroreceptor reflex sensitivity in spontaneously hypertensive rats. *Bollettino della Societa italiana di biologia sperimentale,* 70**,** 279-286.

FLECKNELL, P. 2015. *Laboratory Animal Anaesthesia (Fourth Edition)*, Elsevier Science & Technology.

FOGAGNOLO, A., GRASSO, S., DRES, M., GESUALDO, L., MURGOLO, F., MORELLI, E., OTTAVIANI, I., MARANGONI, E., VOLTA, C. A. & SPADARO, S.

2022. Focus on renal blood flow in mechanically ventilated patients with SARS-CoV-2: a prospective pilot study. *J Clin Monit Comput,* 36**,** 161-167.

FÖRSTER, T. 1946. Energiewanderung und Fluoreszenz. *Naturwissenschaften,* 33**,** 166-175.

FÖRSTER, T. 1948. Zwischenmolekulare Energiewanderung und Fluoreszenz. *Annalen der Physik,* 437**,** 55-75.

FÖRSTERMANN, U. & SESSA, W. C. 2012. Nitric oxide synthases: regulation and function. *European heart journal,* 33**,** 829-837.

FOTIADIS, D., LIANG, Y., FILIPEK, S., SAPERSTEIN, D. A., ENGEL, A. & PALCZEWSKI, K. 2004. The G protein-coupled receptor rhodopsin in the native membrane. *FEBS Lett,* 564**,** 281-288.

FRANCIS, S., S. D., DE JESUS, N. M., LINDSEY, M. L. & RIPPLINGER, C. M. 2016. The crossroads of inflammation, fibrosis, and arrhythmia following myocardial infarction. *J Mol Cell Cardiol,* 91**,** 114-22.

FRASER, H., GAO, Z., OZECK, M. J. & BELARDINELLI, L. 2003. N-[3-(R)-tetrahydrofuranyl]-6-aminopurine riboside, an A1 adenosine receptor agonist, antagonizes catecholamine-induced lipolysis without cardiovascular effects in awake rats. *J Pharmacol Exp Ther,* 305**,** 225-31.

FREDHOLM, B. B., AP, I. J., JACOBSON, K. A., LINDEN, J. & MULLER, C. E. 2011. International Union of Basic and Clinical Pharmacology. LXXXI. Nomenclature and classification of adenosine receptors--an update. *Pharmacol Rev,* 63**,** 1-34.

FREDHOLM, B. B., ARSLAN, G., HALLDNER, L., KULL, B., SCHULTE, G. & WASSERMAN, W. 2000. Structure and function of adenosine receptors and their genes. *Naunyn Schmiedebergs Arch Pharmacol,* 362**,** 364-74.

FREDHOLM, B. B., IRENIUS, E., KULL, B. & SCHULTE, G. 2001. Comparison of the potency of adenosine as an agonist at human adenosine receptors expressed in Chinese hamster ovary cells. *Biochemical Pharmacology,* 61**,** 443-448.

FREED, D. M., ALVARADO, D. & LEMMON, M. A. 2015. Ligand regulation of a constitutively dimeric EGF receptor. *Nat Commun,* 6**,** 7380.

FRIEDRICH, J. O., ADHIKARI, N., HERRIDGE, M. S. & BEYENE, J. 2005. Meta-analysis: low-dose dopamine increases urine output but does not prevent renal dysfunction or death. *Annals of internal medicine,* 142**,** 510-524.

FUJIMURA, J., CAMILLERI, M., LOW, P. A., NOVAK, V., NOVAK, P. & OPFER-GEHRKING, T. L. 1997. Effect of perturbations and a meal on superior mesenteric artery flow in patients with orthostatic hypotension. *J Auton Nerv Syst,* 67**,** 15-23.

FUNAKOSHI, H., CHAN, T. O., GOOD, J. C., LIBONATI, J. R., PIUHOLA, J., CHEN, X., MACDONNELL, S. M., LEE, L. L., HERRMANN, D. E., ZHANG, J., MARTINI, J., PALMER, T. M., SANBE, A., ROBBINS, J., HOUSER, S. R., KOCH, W. J. & FELDMAN, A. M. 2006. Regulated overexpression of the A1-adenosine receptor in mice results in adverse but reversible changes in cardiac morphology and function. *Circulation,* 114**,** 2240-50.

GAHBAUER, S. & BOCKMANN, R. A. 2016. Membrane-Mediated Oligomerization of G Protein Coupled Receptors and Its Implications for GPCR Function. *Front Physiol,* 7**,** 494.

GAO, Z., LI, Z., BAKER, S. P., LASLEY, R. D., MEYER, S., ELZEIN, E., PALLE, V., ZABLOCKI, J. A., BLACKBURN, B. & BELARDINELLI, L. 2001. Novel short-acting A2A adenosine receptor agonists for coronary vasodilation: inverse relationship between affinity and duration of action of A2A agonists. *J Pharmacol Exp Ther,* 298**,** 209-18.

GARDINER, S., MARCH, J., KEMP, P., BENNETT, T. & BAKER, D. 2010. Possible involvement of GLP-1(9–36) in the regional haemodynamic effects of GLP-1(7–36) in conscious rats. *Br J Pharmacol,* 161**,** 92-102.

GARDINER, S. M. & BENNETT, T. 1988. Regional hemodynamic responses to adrenoceptor antagonism in conscious rats. *Am J Physiol Heart Circ Physiol,* 255**,** H813-H824.

GARDINER, S. M., BENNETT, T. & KEMP, P. A. 1980. Systemic arterial hypertension in rats exposed to short-term isolation; intra-arterial systolic and diastolic blood pressure and baroreflex sensitivity. *Med Biol,* 58**,** 232-9.

GARDINER, S. M., COMPTON, A. M., BENNETT, T. & HARTLEY, C. J. 1990. Can pulsed Doppler technique measure changes in aortic blood flow in conscious rats? *Am J Physiol,* 259**,** H448-56.

GARDINER, S. M., KEMP, P. A. & BENNETT, T. 1991. Effects of NG-nitro-L-arginine methyl ester on vasodilator responses to acetylcholine, 5'-N-ethylcarboxamidoadenosine or salbutamol in conscious rats. *Br J Pharmacol,* 103**,** 1725-32.

GARDINER, S. M., MARCH, J. E., KEMP, P. A., MAGUIRE, J. J., KUC, R. E., DAVENPORT, A. P. & BENNETT, T. 2006. Regional heterogeneity in the haemodynamic responses to urotensin II infusion in relation to UT receptor localisation. *Br J Pharmacol,* 147**,** 612-621.

GELDENHUYS, W. J., HANIF, A., YUN, J. & NAYEEM, M. A. 2017. Exploring Adenosine Receptor Ligands: Potential Role in the Treatment of Cardiovascular Diseases. *Molecules,* 22**,** 917.

GESSI, S., FOGLI, E., SACCHETTO, V., MERIGHI, S., VARANI, K., PRETI, D., LEUNG, E., MACLENNAN, S. & BOREA, P. A. 2010. Adenosine modulates HIF-1alpha, VEGF, IL-8, and foam cell formation in a human model of hypoxic foam cells. *Arterioscler Thromb Vasc Biol,* 30**,** 90-7.

GESSI, S., MERIGHI, S., VARANI, K., LEUNG, E., MAC LENNAN, S. & BOREA, P. A. 2008. The A3 adenosine receptor: an enigmatic player in cell biology. *Pharmacol Ther,* 117**,** 123-40.

GIOVANNITTI, J. A., JR., THOMS, S. M. & CRAWFORD, J. J. 2015. Alpha-2 adrenergic receptor agonists: a review of current clinical applications. *Anesth Prog,* 62**,** 31-9.

GLIKI, G., ABU-GHAZALEH, R., JEZEQUEL, S., WHEELER-JONES, C. & ZACHARY, I. 2001. Vascular endothelial growth factor-induced prostacyclin production is mediated by a protein kinase C (PKC)-dependent activation of extracellular signal-regulated protein kinases 1 and 2 involving PKC-delta and by mobilization of intracellular Ca2+. *Biochem J,* 353**,** 503-12.

GOMEZ, R. A. & SEQUEIRA LOPEZ, M. L. 2009. Who and where is the renal baroreceptor?: the connexin hypothesis. *Kidney Int,* 75**,** 460-2.

GOODMAN, V. L., ROCK, E. P., DAGHER, R., RAMCHANDANI, R. P., ABRAHAM, S., GOBBURU, J. V., BOOTH, B. P., VERBOIS, S. L., MORSE, D. E., LIANG, C. Y., CHIDAMBARAM, N., JIANG, J. X., TANG, S., MAHJOOB, K., JUSTICE, R. & PAZDUR, R. 2007. Approval summary: sunitinib for the treatment of imatinib refractory or intolerant gastrointestinal stromal tumors and advanced renal cell carcinoma. *Clin Cancer Res,* 13**,** 1367-73.

GORDI, T., FROHNA, P., SUN, H.-L., WOLFF, A., BELARDINELLI, L. & LIEU, H. 2006. A Population Pharmacokinetic/Pharmacodynamic Analysis of Regadenoson, an Adenosine A2A-Receptor Agonist, in Healthy Male Volunteers. *Clinical Pharmacokinetics,* 45**,** 1201-1212.

GOSSELIN, R. D. 2019. Guidelines on statistics for researchers using laboratory animals: the essentials. *Lab Anim,* 53**,** 28-42.

GOTINK, K. J. & VERHEUL, H. M. 2010. Anti-angiogenic tyrosine kinase inhibitors: what is their mechanism of action? *Angiogenesis,* 13**,** 1-14.

GOTO, Y., SLINKER, B. K. & LEWINTER, M. M. 1991. Effect of coronary hyperemia on Emax and oxygen consumption in blood-perfused rabbit hearts. Energetic consequences of Gregg's phenomenon. *Circ Res,* 68**,** 482-92.

GOULDING, J., MAY, L. T. & HILL, S. J. 2018. Characterisation of endogenous A(2A) and A(2B) receptor-mediated cyclic AMP responses in HEK 293 cells using the GloSensor™ biosensor: Evidence for an allosteric mechanism of action for the A(2B)-selective antagonist PSB 603. *Biochem Pharmacol,* 147**,** 55-66.

GRAHAM, F. L., SMILEY, J., RUSSELL, W. C. & NAIRN, R. 1977. Characteristics of a Human Cell Line Transformed by DNA from Human Adenovirus Type 5. *Journal of General Virology,* 36**,** 59-72.

GRANGER, H. J. & NORRIS, C. P. 1980. Role of adenosine in local control of intestinal circulation in the dog. *Circ Res,* 46**,** 764-70.

GRANT, M. B., TARNUZZER, R. W., CABALLERO, S., OZECK, M. J., DAVIS, M. I., SPOERRI, P. E., FEOKTISTOV, I., BIAGGIONI, I., SHRYOCK, J. C. & BELARDINELLI, L. 1999. Adenosine Receptor Activation Induces Vascular Endothelial Growth Factor in Human Retinal Endothelial Cells. *Circ Res,* 85**,** 699-706.

GRATZ, L., TROPMANN, K., BRESINSKY, M., MULLER, C., BERNHARDT, G. & POCKES, S. 2020. NanoBRET binding assay for histamine H2 receptor ligands using live recombinant HEK293T cells. *Sci Rep,* 10**,** 13288.

GREGG, D. E. 1963. Effect of Coronary Perfusion Pressure or Coronary Flow on Oxygen Usage of the Myocardium. *Circ Res,* 13**,** 497-500.

GRENZ, A., OSSWALD, H., ECKLE, T., YANG, D., ZHANG, H., TRAN, Z. V., KLINGEL, K., RAVID, K. & ELTZSCHIG, H. K. 2008. The Reno-Vascular A2B Adenosine Receptor Protects the Kidney from Ischemia. *PLOS Medicine,* 5**,** e137.

GUIEU, R., KIPSON, N., RUF, J., FOURNIER, N., LAINE, M., FOUCHER, M. C., FROMONOT, J., MOTTOLA, G., BRUZZESE, L., BOUSSUGES, A., FENOUILLET, E., BONELLO, L. & PAGANELLI, F. 2015. Low basal expression of A2A adenosine receptors and increase in adenosine plasma concentration are associated with positive exercise stress testing. *Int J Cardiol,* 180**,** 15-7.

GUPTA, A. & BAJAJ, N. S. 2018. Regadenoson use for stress myocardial perfusion imaging in advance chronic kidney disease and dialysis: Safe, effective, and efficient. *J Nucl Cardiol,* 25**,** 150-152.

HALL, M. P., UNCH, J., BINKOWSKI, B. F., VALLEY, M. P., BUTLER, B. L., WOOD, M. G., OTTO, P., ZIMMERMAN, K., VIDUGIRIS, G., MACHLEIDT, T., ROBERS, M. B., BENINK, H. A., EGGERS, C. T., SLATER, M. R., MEISENHEIMER, P. L., KLAUBERT, D. H., FAN, F., ENCELL, L. P. & WOOD, K. V. 2012. Engineered luciferase reporter from a deep sea shrimp utilizing a novel imidazopyrazinone substrate. *ACS Chem Biol,* 7**,** 1848-57.

HANSEN, A. H., SERGEEV, E., PANDEY, S. K., HUDSON, B. D., CHRISTIANSEN, E., MILLIGAN, G. & ULVEN, T. 2017. Development and Characterization of a Fluorescent Tracer for the Free Fatty Acid Receptor 2 (FFA2/GPR43). *J Med Chem,* 60**,** 5638-5645.

HARNETT, E. M., ALDERMAN, J. & WOOD, T. 2007. The surface energy of various biomaterials coated with adhesion molecules used in cell culture. *Colloids and Surfaces B: Biointerfaces,* 55**,** 90-97.

HARRISON-BERNARD, L. M. 2009. The renal renin-angiotensin system. *Advances in Physiology Education,* 33**,** 270-274.

HART, M. L., JACOBI, B., SCHITTENHELM, J., HENN, M. & ELTZSCHIG, H. K. 2009. Cutting Edge: A2B Adenosine receptor signaling provides potent protection during intestinal ischemia/reperfusion injury. *J Immunol,* 182**,** 3965-8.

HARTLEY, C. J. 1981. Resolution of Frequency Aliases in Ultrasonic Pulsed Doppler Velocimeters. *IEEE Transactions on Sonics and Ultrasonics,* 28**,** 69-74.

HARTLEY, C. J. & COLE, J. S. 1974. An ultrasonic pulsed Doppler system for measuring blood flow in small vessels. *Journal of Applied Physiology,* 37**,** 626-629.

HASKO, G., ANTONIOLI, L. & CRONSTEIN, B. N. 2018. Adenosine metabolism, immunity and joint health. *Biochem Pharmacol,* 151**,** 307-313.

HAYWARD, L. F., RILEY, A. P. & FELDER, R. B. 2002. alpha(2)-Adrenergic receptors in NTS facilitate baroreflex function in adult spontaneously hypertensive rats. *Am J Physiol Heart Circ Physiol,* 282**,** H2336-45.

HAYWOOD, J. R., SHAFFER, R. A., FASTENOW, C., FINK, G. D. & BRODY, M. J. 1981. Regional blood flow measurement with pulsed Doppler flowmeter in conscious rat. *Am J Physiol,* 241**,** H273-8.

HEADRICK, J. P., ASHTON, K. J., ROSE'MEYER, R. B. & PEART, J. N. 2013. Cardiovascular adenosine receptors: expression, actions and interactions. *Pharmacol Ther,* 140**,** 92-111.

HEGDE, P. S., WALLIN, J. J. & MANCAO, C. 2018. Predictive markers of anti-VEGF and emerging role of angiogenesis inhibitors as immunotherapeutics. *Seminars in Cancer Biology,* 52**,** 117-124.

HEINONEN, I. H., BOUSHEL, R. & KALLIOKOSKI, K. K. 2016. The Circulatory and Metabolic Responses to Hypoxia in Humans - With Special Reference to Adipose Tissue Physiology and Obesity. *Front Endocrinol,* 7**,** 116.

HEPOKOSKI, M. L., MALHOTRA, A., SINGH, P. & CROTTY ALEXANDER, L. E. 2018. Ventilator-Induced Kidney Injury: Are Novel Biomarkers the Key to Prevention? *Nephron,* 140**,** 90-93.

HERMANNS, H., HOLLMANN, M. W., STEVENS, M. F., LIRK, P., BRANDENBURGER, T., PIEGELER, T. & WERDEHAUSEN, R. 2019. Molecular

mechanisms of action of systemic lidocaine in acute and chronic pain: a narrative review. *British Journal of Anaesthesia,* 123**,** 335-349.

HILEY, C. R., BOTTRILL, F. E., WARNOCK, J. & RICHARDSON, P. J. 1995. Effects of pH on responses to adenosine, CGS 21680, carbachol and nitroprusside in the isolated perfused superior mesenteric arterial bed of the rat. *Br J Pharmacol,* 116**,** 2641-6.

HILL, S. J., WILLIAMS, C. & MAY, L. T. 2010. Insights into GPCR pharmacology from the measurement of changes in intracellular cyclic AMP; advantages and pitfalls of differing methodologies. *Br J Pharmacol,* 161**,** 1266-1275.

HILLION, J., CANALS, M., TORVINEN, M., CASADO, V., SCOTT, R., TERASMAA, A., HANSSON, A., WATSON, S., OLAH, M. E., MALLOL, J., CANELA, E. I., ZOLI, M., AGNATI, L. F., IBANEZ, C. F., LLUIS, C., FRANCO, R., FERRE, S. & FUXE, K. 2002. Coaggregation, cointernalization, and codesensitization of adenosine A2A receptors and dopamine D2 receptors. *J Biol Chem,* 277**,** 18091-7.

HINZ, S., LACHER, S. K., SEIBT, B. F. & MÜLLER, C. E. 2014. BAY60-6583 acts as a partial agonist at adenosine A2B receptors. *J Pharmacol Exp Ther,* 349**,** 427-36.

HINZ, S., NAVARRO, G., BORROTO-ESCUELA, D., SEIBT, B. F., AMMON, Y.-C., DE FILIPPO, E., DANISH, A., LACHER, S. K., ČERVINKOVÁ, B., RAFEHI, M., FUXE, K., SCHIEDEL, A. C., FRANCO, R. & MÜLLER, C. E. 2018. Adenosine A(2A) receptor ligand recognition and signaling is blocked by A(2B) receptors. *Oncotarget,* 9**,** 13593-13611.

HIRSH, J., RASCHKE, C. R., WARKENTIN, T. E., DALEN, J. E., DEYKIN, D. & POLLER, L. 1995. Heparin: Mechanism of Action, Pharmacokinetics, Dosing Considerations, Monitoring, Efficacy, and Safety. *CHEST,* 108**,** 258S-275S.

HISATOME, I. 2007. Adenosine and Cardioprotection in Chronic Heart Failure: Genes and Protein Expression. *Hypertension Research,* 30**,** 757-8.

HO, M. F., LOW, L. M. & ROSE'MEYER, R. B. 2016. Pharmacology of the Adenosine A3 Receptor in the Vasculature and Essential Hypertension. *PLoS One,* 11**,** e0150021.

HOLZ, F. G. & STEINHAUSEN, M. 1987. Renovascular effects of adenosine receptor agonists. *Ren Physiol,* 10**,** 272-82.

HOVE-MADSEN, L., PRAT-VIDAL, C., LLACH, A., CIRUELA, F., CASADÓ, V., LLUIS, C., BAYES-GENIS, A., CINCA, J. & FRANCO, R. 2006. Adenosine A2A receptors are expressed in human atrial myocytes and modulate spontaneous sarcoplasmic reticulum calcium release. *Cardiovasc Res,* 72**,** 292-302.

HUBBARD, S. R. 1999. Structural analysis of receptor tyrosine kinases. *Progress in Biophysics and Molecular Biology,* 71**,** 343-358.

HUTCHISON, A. J., WEBB, R. L., OEI, H. H., GHAI, G. R., ZIMMERMAN, M. B. & WILLIAMS, M. 1989. CGS 21680C, an A2 selective adenosine receptor agonist with preferential hypotensive activity. *J Pharmacol Exp Ther,* 251**,** 47-55.

ICHINOSE, T. K., O'LEARY, D. S. & SCISLO, T. J. 2009. Activation of NTS A2a adenosine receptors differentially resets baroreflex control of renal vs. adrenal sympathetic nerve activity. *Am J Physiol Heart Circ Physiol,* 296**,** H1058-68.

INOUYE, S., WATANABE, K., NAKAMURA, H. & SHIMOMURA, O. 2000. Secretional luciferase of the luminous shrimp Oplophorus gracilirostris: cDNA cloning of a novel imidazopyrazinone luciferase. *FEBS letters,* 481**,** 19-25.

ITO, N., WERNSTEDT, C., ENGSTROM, U. & CLAESSON-WELSH, L. 1998. Identification of vascular endothelial growth factor receptor-1 tyrosine phosphorylation sites and binding of SH2 domain-containing molecules. *J Biol Chem,* 273**,** 23410-8.

ITOH, S., BRAWLEY, L., WHEELER, T., ANTHONY, F. W., POSTON, L. & HANSON, M. A. 2002. Vasodilation to vascular endothelial growth factor in the uterine artery of the pregnant rat is blunted by low dietary protein intake. *Pediatr Res,* 51**,** 485-91.

IZER, J. M., WHITCOMB, T. L. & WILSON, R. P. 2014. Atipamezole reverses ketamine-dexmedetomidine anesthesia without altering the antinociceptive effects of butorphanol and buprenorphine in female C57BL/6J mice. *J Am Assoc Lab Anim Sci,* 53**,** 675-83.

JAAKOLA, V.-P., LANE, J. R., LIN, J. Y., KATRITCH, V., IJZERMAN, A. P. & STEVENS, R. C. 2010. Ligand binding and subtype selectivity of the human A(2A)

adenosine receptor: identification and characterization of essential amino acid residues. *The Journal of biological chemistry,* 285**,** 13032-13044.

JACOB, F., LABINE, B. G., ARIZA, P., KATZ, S. A. & OSBORN, J. W. 2005. Renal denervation causes chronic hypotension in rats: role of beta1-adrenoceptor activity. *Clin Exp Pharmacol Physiol,* 32**,** 255-62.

JACOBSON, K. A. & GAO, Z. G. 2006. Adenosine receptors as therapeutic targets. *Nat Rev Drug Discov,* 5**,** 247-64.

JACOBSON, K. A., TOSH, D. K., JAIN, S. & GAO, Z.-G. 2019. Historical and Current Adenosine Receptor Agonists in Preclinical and Clinical Development. *Frontiers in cellular neuroscience,* 13**,** 124-124.

JACOBSON, M. A., JOHNSON, R. G., LUNEAU, C. J. & SALVATORE, C. A. 1995. Cloning and chromosomal localization of the human A2b adenosine receptor gene (ADORA2B) and its pseudogene. *Genomics,* 27**,** 374-376.

JAIN, R. K. 2003. Molecular regulation of vessel maturation. *Nature medicine,* 9**,** 685-693.

JAMWAL, S., MITTAL, A., KUMAR, P., ALHAYANI, D. M. & AL-ABOUDI, A. 2019. Therapeutic Potential of Agonists and Antagonists of A1, A2a, A2b and A3 Adenosine Receptors. *Curr Pharm Des,* 25**,** 2892-2905.

JANSSEN, P. J., GARDINER, S. M., COMPTON, A. M. & BENNETT, T. 1991. Mechanisms contributing to the differential haemodynamic effects of bombesin and cholecystokinin in conscious, Long Evans rats. *Br J Pharmacol,* 102**,** 123-34.

JIANG, J., SEEL, C. J., TEMIRAK, A., NAMASIVAYAM, V., ARRIDU, A., SCHABIKOWSKI, J., BAQI, Y., HINZ, S., HOCKEMEYER, J. & MÜLLER, C. E. 2019. A(2B) Adenosine Receptor Antagonists with Picomolar Potency. *J Med Chem,* 62**,** 4032-4055.

JOLLY, L., MARCH, J. E., KEMP, P. A., BENNETT, T. & GARDINER, S. M. 2008. Regional haemodynamic responses to adenosine receptor activation vary across time following lipopolysaccharide treatment in conscious rats. *Br J Pharmacol,* 154**,** 1600-10.

JONES, G. A. & BRADSHAW, D. S. 2019. Resonance Energy Transfer: From Fundamental Theory to Recent Applications. *Frontiers in Physics,* 7**,** 100.

KALYANASUNDARAM, A., LI, N., HANSEN, B. J., ZHAO, J. & FEDOROV, V. V. 2019. Canine and human sinoatrial node: differences and similarities in the structure, function, molecular profiles, and arrhythmia. *J Vet Cardiol,* 22**,** 2-19.

KAPPERS, M. H., VAN ESCH, J. H., SLUITER, W., SLEIJFER, S., DANSER, A. H. & VAN DEN MEIRACKER, A. H. 2010. Hypertension induced by the tyrosine kinase inhibitor sunitinib is associated with increased circulating endothelin-1 levels. *Hypertension,* 56**,** 675-81.

KATHOLI, R. E., WHITLOW, P. L., HAGEMAN, G. R. & WOODS, W. T. 1984. Intrarenal adenosine produces hypertension by activating the sympathetic nervous system via the renal nerves in the dog. *J Hypertens,* 2**,** 349-59.

KATSI, V., ZERDES, I., MANOLAKOU, S., MAKRIS, T., NIHOYANNOPOULOS, P., TOUSOULIS, D. & KALLIKAZAROS, I. 2014. Anti-VEGF Anticancer Drugs: Mind the Hypertension. *Recent Adv Cardiovasc Drug Discov,* 9**,** 63-72.

KE, Q. & COSTA, M. 2006. Hypoxia-Inducible Factor-1 (HIF-1). *Molecular Pharmacology,* 70**,** 1469-1480.

KECSKÉS, M., KUMAR, T. S., YOO, L., GAO, Z. G. & JACOBSON, K. A. 2010. Novel Alexa Fluor-488 labeled antagonist of the A(2A) adenosine receptor: Application to a fluorescence polarization-based receptor binding assay. *Biochem Pharmacol,* 80**,** 506-11.

KEPPLER, A., GENDREIZIG, S., GRONEMEYER, T., PICK, H., VOGEL, H. & JOHNSSON, K. 2003. A general method for the covalent labeling of fusion proteins with small molecules in vivo. *Nat Biotechnol,* 21**,** 86-9.

KEPPLER, A., PICK, H., ARRIVOLI, C., VOGEL, H. & JOHNSSON, K. 2004. Labeling of fusion proteins with synthetic fluorophores in live cells. *Proceedings of the National Academy of Sciences of the United States of America,* 101**,** 9955-9959.

KHRENOVA, M., TOPOL, I., COLLINS, J. & NEMUKHIN, A. 2015. Estimating orientation factors in the FRET theory of fluorescent proteins: the TagRFP-KFP pair and beyond. *Biophys J,* 108**,** 126-32.

KILKENNY, C., BROWNE, W., CUTHILL, I. C., EMERSON, M. & ALTMAN, D. G. 2010. Animal research: Reporting in vivo experiments: The ARRIVE guidelines. *Br J Pharmacol,* 160**,** 1577-1579.

KILPATRICK, L. E., ALCOBIA, D. C., WHITE, C. W., PEACH, C. J., GLENN, J. R., ZIMMERMAN, K., KONDRASHOV, A., PFLEGER, K. D. G., OHANA, R. F., ROBERS, M. B., WOOD, K. V., SLOAN, E. K., WOOLARD, J. & HILL, S. J. 2019. Complex Formation between VEGFR2 and the beta2-Adrenoceptor. *Cell Chem Biol,* 26**,** 1-12.

KILPATRICK, L. E., FRIEDMAN-OHANA, R., ALCOBIA, D. C., RICHING, K., PEACH, C. J., WHEAL, A. J., BRIDDON, S. J., ROBERS, M. B., ZIMMERMAN, K., MACHLEIDT, T., WOOD, K. V., WOOLARD, J. & HILL, S. J. 2017. Real-time analysis of the binding of fluorescent VEGF165a to VEGFR2 in living cells: Effect of receptor tyrosine kinase inhibitors and fate of internalized agonist-receptor complexes. *Biochem Pharmacol,* 136**,** 62-75.

KING, A. E., ACKLEY, M. A., CASS, C. E., YOUNG, J. D. & BALDWIN, S. A. 2006. Nucleoside transporters: from scavengers to novel therapeutic targets. *Trends Pharmacol Sci,* 27**,** 416-25.

KING, C. & HRISTOVA, K. 2019. Direct measurements of VEGF-VEGFR2 binding affinities reveal the coupling between ligand binding and receptor dimerization. *J Biol Chem,* 294**,** 9064-9075.

KINT, L. T., SEEWOO, B. J., HYNDMAN, T. H., CLARKE, M. W., EDWARDS, S. H., RODGER, J., FEINDEL, K. W. & MUSK, G. C. 2020. The Pharmacokinetics of Medetomidine Administered Subcutaneously during Isoflurane Anaesthesia in Sprague-Dawley Rats. *Animals,* 10**,** 1050.

KLAASSE, E. C., IJZERMAN, A. P., DE GRIP, W. J. & BEUKERS, M. W. 2008. Internalization and desensitization of adenosine receptors. *Purinergic Signal,* 4**,** 21-37.

KLINGER, M., FREISSMUTH, M. & NANOFF, C. 2002. Adenosine receptors: G protein-mediated signalling and the role of accessory proteins. *Cell Signal,* 14**,** 99-108.

KO, E. A., HAN, J., JUNG, I. D. & PARK, W. S. 2008. Physiological roles of K+ channels in vascular smooth muscle cells. *J Smooth Muscle Res,* 44**,** 65-81.

KOCH, S. & CLAESSON-WELSH, L. 2012. Signal transduction by vascular endothelial growth factor receptors. *Cold Spring Harb Perspect Med,* 2**,** a006502.

KOETSIER, G. & CANTOR, E. 2019. A practical guide to analyzing nucleic acid concentration and purity with microvolume spectrophotometers. *New England Biolabs Inc***,** 1-8.

KOLIN, A., AUSTIN, S. & COX, P. 1964. Electromagnetic Observations of Carotid Blood Flow Changes in the Conscious Rat in Response to Sensory Stimuli. *Nature,* 201**,** 573-574.

KOUGIAS, P., WEAKLEY, S. M., YAO, Q., LIN, P. H. & CHEN, C. 2010. Arterial baroreceptors in the management of systemic hypertension. *Med Sci Monit,* 16**,** Ra1-8.

KOZAK, M. 1987. At least six nucleotides preceding the AUG initiator codon enhance translation in mammalian cells. *J Mol Biol,* 196**,** 947-50.

KOZMA, E., JAYASEKARA, P. S., SQUARCIALUPI, L., PAOLETTA, S., MORO, S., FEDERICO, S., SPALLUTO, G. & JACOBSON, K. A. 2013. Fluorescent ligands for adenosine receptors. *Bioorg Med Chem Lett,* 23**,** 26-36.

KRESGE, N., SIMONI, R. D. & HILL, R. L. 2005. Earl W. Sutherland's Discovery of Cyclic Adenine Monophosphate and the Second Messenger System. *Journal of Biological Chemistry,* 280**,** e39-e40.

KRIEGER, E. M. 1988. Mechanisms of complete baroreceptor resetting in hypertension. *Drugs,* 35 (Suppl 6)**,** 98-103.

KU, D. D., ZALESKI, J. K., LIU, S. & BROCK, T. A. 1993. Vascular endothelial growth factor induces EDRF-dependent relaxation in coronary arteries. *Am J Physiol,* 265**,** H586-92.

KUIPER, J. W., VERSTEILEN, A. M. G., NIESSEN, H. W. M., VASCHETTO, R. R., SIPKEMA, P., HEIJNEN, C. J., GROENEVELD, A. B. J. & PLÖTZ, F. B. 2008. Production of Endothelin-1 and Reduced Blood Flow in the Rat Kidney During Lung-Injurious Mechanical Ventilation. *Anesthesia & Analgesia,* 107**,** 1276-1283.

KUNO, A., CRITZ, S. D., CUI, L., SOLODUSHKO, V., YANG, X.-M., KRAHN, T., ALBRECHT, B., PHILIPP, S., COHEN, M. V. & DOWNEY, J. M. 2007. Protein kinase C protects preconditioned rabbit hearts by increasing sensitivity of adenosine A2b-dependent signaling during early reperfusion. *Journal of Molecular and Cellular Cardiology,* 43**,** 262-271.

LAI, E. Y., PATZAK, A., STEEGE, A., MROWKA, R., BROWN, R., SPIELMANN, N., PERSSON, P. B., FREDHOLM, B. B. & PERSSON, A. E. 2006. Contribution of adenosine receptors in the control of arteriolar tone and adenosine-angiotensin II interaction. *Kidney Int,* 70**,** 690-8.

LANE, J. R., JAAKOLA, V. P. & IJZERMAN, A. P. 2011. The structure of the adenosine receptors: implications for drug discovery. *Adv Pharmacol,* 61**,** 1-40.

LANKHORST, S., KAPPERS, M. H. W., ESCH, J. H. M. V., SMEDTS, F. M. M., SLEIJFER, S., MATHIJSSEN, R. H. J., BAELDE, H. J., DANSER, A. H. J. & MEIRACKER, A. H. V. D. 2014. Treatment of Hypertension and Renal Injury Induced by the Angiogenesis Inhibitor Sunitinib. *Hypertension,* 64**,** 1282-1289.

LASLEY, R. D. 2018. Adenosine Receptor-Mediated Cardioprotection-Current Limitations and Future Directions. *Front Pharmacol,* 9**,** 310.

LATT, S. A., CHEUNG, H. T. & BLOUT, E. R. 1965. Energy Transfer. A System with Relatively Fixed Donor-Acceptor Separation. *Journal of the American Chemical Society,* 87**,** 995-1003.

LAUGHLIN, M. H. & RIPPERGER, J. 1987. Vascular transport capacity of hindlimb muscles of exercise-trained rats. *Journal of Applied Physiology,* 62**,** 438-443.

LAUTT, W. W. 1986. Autoregulation of superior mesenteric artery is blocked by adenosine antagonism. *Canadian Journal of Physiology and Pharmacology,* 64**,** 1291-1295.

LE, F., TOWNSEND-NICHOLSON, A., BAKER, E., SUTHERLAND, G. R. & SCHOFIELD, P. R. 1996. Characterization and chromosomal localization of the human A2a adenosine receptor gene: ADORA2A. *Biochem Biophys Res Commun,* 223**,** 461-7.

LEAL, S., SA, C., GONCALVES, J., FRESCO, P. & DINIZ, C. 2008. Immunohistochemical characterization of adenosine receptors in rat aorta and tail arteries. *Microsc Res Tech,* 71**,** 703-9.

LEBON, G., EDWARDS, P. C., LESLIE, A. G. & TATE, C. G. 2015. Molecular Determinants of CGS21680 Binding to the Human Adenosine A2A Receptor. *Mol Pharmacol,* 87**,** 907-15.

LEBON, G., WARNE, T., EDWARDS, P. C., BENNETT, K., LANGMEAD, C. J., LESLIE, A. G. & TATE, C. G. 2011. Agonist-bound adenosine A2A receptor structures reveal common features of GPCR activation. *Nature,* 474**,** 521-5.

LEDENT, C., VAUGEOIS, J. M., SCHIFFMANN, S. N., PEDRAZZINI, T., EL YACOUBI, M., VANDERHAEGHEN, J. J., COSTENTIN, J., HEATH, J. K., VASSART, G. & PARMENTIER, M. 1997. Aggressiveness, hypoalgesia and high blood pressure in mice lacking the adenosine A2a receptor. *Nature,* 388**,** 674-8.

LEE, T. K. & KOH, H. C. 2009. Involvement of NO and KATP channel in adenosine A2B receptors induced cardiovascular regulation in the posterior hypothalamus of rats. *J Cardiovasc Pharmacol,* 53**,** 167-72.

LEMMON, M. A. & SCHLESSINGER, J. 2010. Cell signaling by receptor tyrosine kinases. *Cell,* 141**,** 1117-34.

LEÓN-MATEOS, L., MOSQUERA, J. & ANTÓN APARICIO, L. 2015. Treatment of sunitinib-induced hypertension in solid tumor by nitric oxide donors. *Redox Biol,* 6**,** 421-425.

LEWIS, C. D., HOURANI, S. M., LONG, C. J. & COLLIS, M. G. 1994. Characterization of adenosine receptors in the rat isolated aorta. *Gen Pharmacol,* 25**,** 1381-7.

LI, M. & KROETZ, D. L. 2018. Bevacizumab-induced hypertension: Clinical presentation and molecular understanding. *Pharmacology & Therapeutics,* 182**,** 152-160.

LI, N., HANSEN, B. J., CSEPE, T. A., ZHAO, J., IGNOZZI, A. J., SUL, L. V., ZAKHARKIN, S. O., KALYANASUNDARAM, A., DAVIS, J. P., BIESIADECKI, B. J., KILIC, A., JANSSEN, P. M. L., MOHLER, P. J., WEISS, R., HUMMEL, J. D. & FEDOROV, V. V. 2017. Redundant and diverse intranodal pacemakers and

conduction pathways protect the human sinoatrial node from failure. *Sci Transl Med,* 9**,** eaam5607.

LIANG, B. T. & HALTIWANGER, B. 1995. Adenosine A2a and A2b receptors in cultured fetal chick heart cells: high-and low-affinity coupling to stimulation of myocyte contractility and cAMP accumulation. *Circ Res,* 76**,** 242-251.

LIEBMANN, C. & BOHMER, F. D. 2000. Signal transduction pathways of G protein-coupled receptors and their cross-talk with receptor tyrosine kinases: lessons from bradykinin signaling. *Curr Med Chem,* 7**,** 911-43.

LIEU, H. D., SHRYOCK, J. C., VON MERING, G. O., GORDI, T., BLACKBURN, B., OLMSTED, A. W., BELARDINELLI, L. & KERENSKY, R. A. 2007. Regadenoson, a selective A2A adenosine receptor agonist, causes dose-dependent increases in coronary blood flow velocity in humans. *J Nucl Cardiol,* 14**,** 514-20.

LILYESTROM, W., KLEIN, M. G., ZHANG, R., JOACHIMIAK, A. & CHEN, X. S. 2006. Crystal structure of SV40 large T-antigen bound to p53: interplay between a viral oncoprotein and a cellular tumor suppressor. *Genes Dev,* 20**,** 2373-82.

LIN, Y. C., BOONE, M., MEURIS, L., LEMMENS, I., VAN ROY, N., SOETE, A., REUMERS, J., MOISSE, M., PLAISANCE, S., DRMANAC, R., CHEN, J., SPELEMAN, F., LAMBRECHTS, D., VAN DE PEER, Y., TAVERNIER, J. & CALLEWAERT, N. 2014. Genome dynamics of the human embryonic kidney 293 lineage in response to cell biology manipulations. *Nat Commun,* 5**,** 4767.

LIU, Y. & GRAY, N. S. 2006. Rational design of inhibitors that bind to inactive kinase conformations. *Nat Chem Biol,* 2**,** 358-64.

LIU, Y., YANG, X., YANG, X. M., WALKER, S., FORSTER, K., COHEN, M. V., KRIEG, T. & DOWNEY, J. M. 2010. AMP579 is revealed to be a potent A2b-adenosine receptor agonist in human 293 cells and rabbit hearts. *Basic Res Cardiol,* 105**,** 129-37.

LOU, Q., HANSEN, B. J., FEDORENKO, O., CSEPE, T. A., KALYANASUNDARAM, A., LI, N., HAGE, L. T., GLUKHOV, A. V., BILLMAN, G. E., WEISS, R., MOHLER, P. J., GYÖRKE, S., BIESIADECKI, B. J., CARNES, C. A. & FEDOROV, V. V. 2014. Upregulation of adenosine A1 receptors facilitates

sinoatrial node dysfunction in chronic canine heart failure by exacerbating nodal conduction abnormalities revealed by novel dual-sided intramural optical mapping. *Circulation,* 130**,** 315-24.

LOW, P. A. & SINGER, W. 2008. Management of neurogenic orthostatic hypotension: an update. *Lancet Neurol,* 7**,** 451-8.

LU, Z., JIANG, G., BLUME-JENSEN, P. & HUNTER, T. 2001. Epidermal growth factor-induced tumor cell invasion and metastasis initiated by dephosphorylation and downregulation of focal adhesion kinase. *Mol Cell Biol,* 21**,** 4016-31.

LYNGE, J. & HELLSTEN, Y. 2000. Distribution of adenosine A1, A2A and A2B receptors in human skeletal muscle. *Acta Physiologica Scandinavica,* 169**,** 283-290.

MAAS, J. E., WAN, T. C., FIGLER, R. A., GROSS, G. J. & AUCHAMPACH, J. A. 2010. Evidence that the acute phase of ischemic preconditioning does not require signaling by the A2B adenosine receptor. *J Mol Cell Cardiol,* 49**,** 886-93.

MAITLAND, M. L., BAKRIS, G. L., BLACK, H. R., CHEN, H. X., DURAND, J. B., ELLIOTT, W. J., IVY, S. P., LEIER, C. V., LINDENFELD, J., LIU, G., REMICK, S. C., STEINGART, R. & TANG, W. H. 2010. Initial assessment, surveillance, and management of blood pressure in patients receiving vascular endothelial growth factor signaling pathway inhibitors. *J Natl Cancer Inst,* 102**,** 596-604.

MALLET, M. L. 2004. Proarrhythmic effects of adenosine: a review of the literature. *Emergency medicine journal : EMJ,* 21**,** 408-410.

MANNING, G., WHYTE, D. B., MARTINEZ, R., HUNTER, T. & SUDARSANAM, S. 2002. The protein kinase complement of the human genome. *Science,* 298**,** 1912-34.

MARKOVIC-MUELLER, S., STUTTFELD, E., ASTHANA, M., WEINERT, T., BLIVEN, S., GOLDIE, K. N., KISKO, K., CAPITANI, G. & BALLMER-HOFER, K. 2017. Structure of the Full-length VEGFR-1 Extracellular Domain in Complex with VEGF-A. *Structure,* 25**,** 341-352.

MARTIN, P. L. & POTTS, A. A. 1994. The endothelium of the rat renal artery plays an obligatory role in A2 adenosine receptor-mediated relaxation induced by 5'-N-

ethylcarboxamidoadenosine and N6-cyclopentyladenosine. *J Pharmacol Exp Ther,* 270**,** 893-9.

MARTIN, P. L., UEEDA, M. & OLSSON, R. A. 1993. 2-Phenylethoxy-9-methyladenine: an adenosine receptor antagonist that discriminates between A2 adenosine receptors in the aorta and the coronary vessels from the guinea pig. *J Pharmacol Exp Ther,* 265**,** 248-53.

MARULLO, S. & BOUVIER, M. 2007. Resonance energy transfer approaches in molecular pharmacology and beyond. *Trends in pharmacological sciences,* 28**,** 362-365.

MATHÔT, R. A. A., CLETON, A., SOUDIJN, W., IJZERMAN, A. P. & DANHOF, M. 1995. Pharmacokinetic modelling of the haemodynamic effects of the A2a adenosine receptor agonist CGS 21680C in conscious normotensive rats. *Br J Pharmacol,* 114**,** 761-768.

MCGRATH, J. C. & LILLEY, E. 2015. Implementing guidelines on reporting research using animals (ARRIVE etc.): new requirements for publication in BJP. *Br J Pharmacol,* 172**,** 3189-93.

MCINTOSH, V. J. & LASLEY, R. D. 2012. Adenosine receptor-mediated cardioprotection: are all 4 subtypes required or redundant? *J Cardiovasc Pharmacol Ther,* 17**,** 21-33.

MENDEL, D. B., LAIRD, A. D., XIN, X., LOUIE, S. G., CHRISTENSEN, J. G., LI, G., SCHRECK, R. E., ABRAMS, T. J., NGAI, T. J., LEE, L. B., MURRAY, L. J., CARVER, J., CHAN, E., MOSS, K. G., HAZNEDAR, J. O., SUKBUNTHERNG, J., BLAKE, R. A., SUN, L., TANG, C., MILLER, T., SHIRAZIAN, S., MCMAHON, G. & CHERRINGTON, J. M. 2003. In vivo antitumor activity of SU11248, a novel tyrosine kinase inhibitor targeting vascular endothelial growth factor and platelet-derived growth factor receptors: determination of a pharmacokinetic/pharmacodynamic relationship. *Clin Cancer Res,* 9**,** 327-37.

MERCIER, J. F., SALAHPOUR, A., ANGERS, S., BREIT, A. & BOUVIER, M. 2002. Quantitative assessment of beta 1- and beta 2-adrenergic receptor homo- and heterodimerization by bioluminescence resonance energy transfer. *J Biol Chem,* 277**,** 44925-31.

MERIGHI, S., BENINI, A., MIRANDOLA, P., GESSI, S., VARANI, K., LEUNG, E., MACLENNAN, S., BARALDI, P. G. & BOREA, P. A. 2005. A3 adenosine receptors modulate hypoxia-inducible factor-1alpha expression in human A375 melanoma cells. *Neoplasia,* 7**,** 894-903.

MERIGHI, S., BOREA, P. A., STEFANELLI, A., BENCIVENNI, S., CASTILLO, C. A., VARANI, K. & GESSI, S. 2015. A2a and a2b adenosine receptors affect HIF-1alpha signaling in activated primary microglial cells. *Glia,* 63**,** 1933-1952.

MERKUS, D., SOROP, O., HOUWELING, B., BOOMSMA, F., MEIRACKER, A. H. V. D. & DUNCKER, D. J. 2006. NO and prostanoids blunt endothelin-mediated coronary vasoconstrictor influence in exercising swine. *Am J Physiol Heart Circ Physiol,* 291**,** H2075-H2081.

MINIC, Z., O'LEARY, D. S. & SCISLO, T. J. 2015. NTS adenosine A2a receptors inhibit the cardiopulmonary chemoreflex control of regional sympathetic outputs via a GABAergic mechanism. *Am J Physiol Heart Circ Physiol,* 309**,** H185-97.

MIRABITO COLAFELLA, K. M., NEVES, K. B., MONTEZANO, A. C., GARRELDS, I. M., VAN VEGHEL, R., DE VRIES, R., UIJL, E., BAELDE, H. J., VAN DEN MEIRACKER, A. H., TOUYZ, R. M., DANSER, A. H. J. & VERSMISSEN, J. 2020. Selective ETA vs. dual ETA/B receptor blockade for the prevention of sunitinib-induced hypertension and albuminuria in WKY rats. *Cardiovasc Res,* 116**,** 1779-1790.

MITCHELL, G. F., PFEFFER, M. A., WESTERHOF, N. & PFEFFER, J. M. 1994. Measurement of aortic input impedance in rats. *Am J Physiol Heart Circ Physiol,* 267**,** H1907-H1915.

MOCKING, T. A. M., VERWEIJ, E. W. E., VISCHER, H. F. & LEURS, R. 2018. Homogeneous, Real-Time NanoBRET Binding Assays for the Histamine H(3) and H(4) Receptors on Living Cells. *Mol Pharmacol,* 94**,** 1371-1381.

MOSER, G. H., SCHRADER, J. & DEUSSEN, A. 1989. Turnover of adenosine in plasma of human and dog blood. *Am J Physiol,* 256**,** C799-806.

MOTZER, R. J., ESCUDIER, B., GANNON, A. & FIGLIN, R. A. 2017. Sunitinib: Ten Years of Successful Clinical Use and Study in Advanced Renal Cell Carcinoma. *Oncologist,* 22**,** 41-52.

MOTZER, R. J., HUTSON, T. E., TOMCZAK, P., MICHAELSON, M. D., BUKOWSKI, R. M., OUDARD, S., NEGRIER, S., SZCZYLIK, C., PILI, R., BJARNASON, G. A., GARCIA-DEL-MURO, X., SOSMAN, J. A., SOLSKA, E., WILDING, G., THOMPSON, J. A., KIM, S. T., CHEN, I., HUANG, X. & FIGLIN, R. A. 2009. Overall survival and updated results for sunitinib compared with interferon alfa in patients with metastatic renal cell carcinoma. *J Clin Oncol,* 27**,** 3584-90.

MOURAD, J. J., DES GUETZ, G., DEBBABI, H. & LEVY, B. I. 2008. Blood pressure rise following angiogenesis inhibition by bevacizumab. A crucial role for microcirculation. *Ann Oncol,* 19**,** 927-34.

MÜLLER, C. E. & JACOBSON, K. A. 2011. Recent developments in adenosine receptor ligands and their potential as novel drugs. *Biochim Biophys Acta,* 1808**,** 1290-308.

MUROI, Y., THEUSCH, C. M., CZAJKOWSKI, C. & JACKSON, M. B. 2009. Distinct Structural Changes in the GABAA Receptor Elicited by Pentobarbital and GABA. *Biophysical Journal,* 96**,** 499-509.

MURRISON, E. M., GOODSON, S. J., EDBROOKE, M. R. & HARRIS, C. A. 1996. Cloning and characterisation of the human adenosine A3 receptor gene. *FEBS Lett,* 384**,** 243-6.

MUSTAFA, S. J., MORRISON, R. R., TENG, B. & PELLEG, A. 2009. Adenosine receptors and the heart: role in regulation of coronary blood flow and cardiac electrophysiology. *Handb Exp Pharmacol,* 193**,** 161-88.

NAGY, J. A., CHANG, S. H., DVORAK, A. M. & DVORAK, H. F. 2009. Why are tumour blood vessels abnormal and why is it important to know? *Br J Cancer,* 100**,** 865-9.

NATARAJAN, K. & BERK, B. C. 2006. Crosstalk Coregulation Mechanisms of G Protein- Coupled Receptors and Receptor Tyrosine Kinases. *Methods Cell Biol,* 332**,** 51-77.

NEKOOEIAN, A. A. & TABRIZCHI, R. 1996. Effects of adenosine a2a receptor agonist, cgs 21680, on blood pressure, cardiac index and arterial conductance in anaesthetized rats. *European Journal of Pharmacology,* 307**,** 163-169.

NEKOOEIAN, A. A. & TABRIZCHI, R. 1998. Haemodynamic effects of a selective adenosine A2A receptor agonist, CGS 21680, in chronic heart failure in anaesthetized rats. *Br J Pharmacol,* 125**,** 651-8.

NEUMAR, R. W., OTTO, C. W., LINK, M. S., KRONICK, S. L., SHUSTER, M., CALLAWAY, C. W., KUDENCHUK, P. J., ORNATO, J. P., MCNALLY, B., SILVERS, S. M., PASSMAN, R. S., WHITE, R. D., HESS, E. P., TANG, W., DAVIS, D., SINZ, E. & MORRISON, L. J. 2010. Part 8: adult advanced cardiovascular life support: 2010 American Heart Association Guidelines for Cardiopulmonary Resuscitation and Emergency Cardiovascular Care. *Circulation,* 122**,** S729-67.

NI, Y., LIANG, D., TIAN, Y., KRON, I. L., FRENCH, B. A. & YANG, Z. 2018. Infarct-Sparing Effect of Adenosine A2B Receptor Agonist Is Primarily Due to Its Action on Splenic Leukocytes Via a PI3K/Akt/IL-10 Pathway. *The Journal of surgical research,* 232**,** 442-449.

NILSSON, I., BAHRAM, F., LI, X., GUALANDI, L., KOCH, S., JARVIUS, M., SODERBERG, O., ANISIMOV, A., KHOLOVA, I., PYTOWSKI, B., BALDWIN, M., YLA-HERTTUALA, S., ALITALO, K., KREUGER, J. & CLAESSON-WELSH, L. 2010. VEGF receptor 2/-3 heterodimers detected in situ by proximity ligation on angiogenic sprouts. *Embo j,* 29**,** 1377-88.

NYQUIST, H. 1928. Certain Topics in Telegraph Transmission Theory. *Transactions of the American Institute of Electrical Engineers,* 47**,** 617-644.

OGINO, K., HATANAKA, K., KAWAMURA, M., KATORI, M. & HARADA, Y. 1997. Evaluation of pharmacological profile of meloxicam as an anti-inflammatory agent, with particular reference to its relative selectivity for cyclooxygenase-2 over cyclooxygenase-1. *Pharmacology,* 55**,** 44-53.

OLAH, M. E., JACOBSON, K. A. & STILES, G. L. 1994. Role of the second extracellular loop of adenosine receptors in agonist and antagonist binding. Analysis of chimeric A1/A3 adenosine receptors. *J Biol Chem,* 269**,** 24692-8.

OLDHAM, W. M. & HAMM, H. E. 2006. Structural basis of function in heterotrimeric G proteins. *Quarterly Reviews of Biophysics,* 39**,** 117-166.

OLDHAM, W. M. & HAMM, H. E. 2008. Heterotrimeric G protein activation by G-protein-coupled receptors. *Nature Reviews Molecular Cell Biology,* 9**,** 60-71.

OLLERO, M. & SAHALI, D. 2014. Inhibition of the VEGF signalling pathway and glomerular disorders. *Nephrology Dialysis Transplantation,* 30**,** 1449-1455.

ORTIZ-CAPISANO, M. C., ATCHISON, D. K., HARDING, P., LASLEY, R. D. & BEIERWALTES, W. H. 2013. Adenosine inhibits renin release from juxtaglomerular cells via an A1 receptor-TRPC-mediated pathway. *Am J Physiol Renal Physiol,* 305**,** F1209-19.

OSBORN, J. L., DIBONA, G. F. & THAMES, M. D. 1981. Beta-1 receptor mediation of renin secretion elicited by low-frequency renal nerve stimulation. *Journal of Pharmacology and Experimental Therapeutics,* 216**,** 265-269.

PAGANELLI, F., GAUDRY, M., RUF, J. & GUIEU, R. 2021. Recent advances in the role of the adenosinergic system in coronary artery disease. *Cardiovasc Res,* 117**,** 1284-1294.

PAGANELLI, F., RESSEGUIER, N., MARLINGE, M., LAINE, M., MALERGUE, F., KIPSON, N., ARMANGAU, P., PEZZOLI, N., KERBAUL, F., BONELLO, L., MOTTOLA, G., FENOUILLET, E., GUIEU, R. & RUF, J. 2018. Specific Pharmacological Profile of A2A Adenosine Receptor Predicts Reduced Fractional Flow Reserve in Patients With Suspected Coronary Artery Disease. *J Am Heart Assoc,* 7**,** e008290.

PALCZEWSKI, K., KUMASAKA, T., HORI, T., BEHNKE, C. A., MOTOSHIMA, H., FOX, B. A., LE TRONG, I., TELLER, D. C., OKADA, T., STENKAMP, R. E., YAMAMOTO, M. & MIYANO, M. 2000. Crystal structure of rhodopsin: A G protein-coupled receptor. *Science,* 289**,** 739-45.

PARAMONOV, V. M., MAMAEVA, V., SAHLGREN, C. & RIVERO-MULLER, A. 2015. Genetically-encoded tools for cAMP probing and modulation in living systems. *Front Pharmacol,* 6**,** 196.

PATHAN, H. & WILLIAMS, J. 2012. Basic opioid pharmacology: an update. *Br J Pain,* 6**,** 11-6.

PAUL, M. D. & HRISTOVA, K. 2019. The transition model of RTK activation: A quantitative framework for understanding RTK signaling and RTK modulator activity. *Cytokine Growth Factor Rev,* 49**,** 23-31.

PAUWELS, P. J. & PALMIER, C. 1994. Inhibition by 5-HT of forskolin-induced cAMP Formation in the renal opossum Epithelial cell line OK: Mediation by a 5-HT1B like receptor and antagonism by methiothepin. *Neuropharmacology,* 33**,** 67-75.

PEACH, C., MIGNONE, V., ARRUDA, M., ALCOBIA, D., HILL, S., KILPATRICK, L. & WOOLARD, J. 2018. Molecular pharmacology of VEGF-A isoforms: binding and signalling at VEGFR2. *Int J Mol Sci,* 19**,** 1264.

PEACH, C. J., KILPATRICK, L. E., WOOLARD, J. & HILL, S. J. 2019. Comparison of the ligand-binding properties of fluorescent VEGF-A isoforms to VEGF receptor 2 in living cells and membrane preparations using NanoBRET. *Br J Pharmacol,* 176**,** 3220-3235.

PEACH, C. J., KILPATRICK, L. E., WOOLARD, J. & HILL, S. J. 2021. Use of NanoBiT and NanoBRET to monitor fluorescent VEGF-A binding kinetics to VEGFR2/NRP1 heteromeric complexes in living cells. *Br J Pharmacol,* 178**,** 2393-2411.

PEART, J. N. & HEADRICK, J. P. 2007. Adenosinergic cardioprotection: multiple receptors, multiple pathways. *Pharmacol Ther,* 114**,** 208-21.

PEETERS, M. C., VAN WESTEN, G. J., LI, Q. & AP, I. J. 2011. Importance of the extracellular loops in G protein-coupled receptors for ligand recognition and receptor activation. *Trends Pharmacol Sci,* 32**,** 35-42.

PEGG, D. E. 2007. Principles of Cryopreservation. *In:* DAY, J. G. & STACEY, G. N. (eds.) *Cryopreservation and Freeze-Drying Protocols.* Totowa, NJ: Humana Press.

PERCIE DU SERT, N., BAMSEY, I., BATE, S. T., BERDOY, M., CLARK, R. A., CUTHILL, I., FRY, D., KARP, N. A., MACLEOD, M., MOON, L., STANFORD, S. C. & LINGS, B. 2017. The Experimental Design Assistant. *PLOS Biology,* 15**,** e2003779.

PERNOW, J., FRANCO-CERECEDA, A., MATRAN, R. & LUNDBERG, J. M. 1989. Effect of endothelin-1 on regional vascular resistances in the pig. *J Cardiovasc Pharmacol,* 13 (Suppl 5)**,** S205-6.

PETERFREUND, R. A., MACCOLLIN, M., GUSELLA, J. & FINK, J. S. 1996. Characterization and Expression of the Human A2a Adenosine Receptor Gene. *Journal of Neurochemistry,* 66**,** 362-368.

PETERSEN, M., ANDERSEN, J. T., JIMENEZ-SOLEM, E., BROEDBAEK, K., HJELVANG, B. R., HENRIKSEN, T., FRANDSEN, E., FORMAN, J. L., TORP-PEDERSEN, C., KØBER, L. & POULSEN, H. E. 2012. Effect of the Arg389Gly β1-adrenoceptor polymorphism on plasma renin activity and heart rate, and the genotype-dependent response to metoprolol treatment. *Clinical and Experimental Pharmacology and Physiology,* 39**,** 779-785.

PFLEGER, K. D. & EIDNE, K. A. 2006. Illuminating insights into protein-protein interactions using bioluminescence resonance energy transfer (BRET). *Nat Methods,* 3**,** 165-74.

PFLEGER, K. D., SEEBER, R. M. & EIDNE, K. A. 2006. Bioluminescence resonance energy transfer (BRET) for the real-time detection of protein-protein interactions. *Nature protocols,* 1**,** 337-45.

PIERCE, K. D., FURLONG, T. J., SELBIE, L. A. & SHINE, J. 1992. Molecular cloning and expression of an adenosine A2b receptor from human brain. *Biochem Biophys Res Commun,* 187**,** 86-93.

PIIRAINEN, H., ASHOK, Y., NANEKAR, R. T. & JAAKOLA, V. P. 2011. Structural features of adenosine receptors: from crystal to function. *Biochim Biophys Acta,* 1808**,** 1233-44.

POLGÁR, L. 2005. The catalytic triad of serine peptidases. *Cellular and Molecular Life Sciences CMLS,* 62**,** 2161-2172.

PONNOTH, D. S., SANJANI, M. S., LEDENT, C., ROUSH, K., KRAHN, T. & MUSTAFA, S. J. 2009. Absence of adenosine-mediated aortic relaxation in A(2A) adenosine receptor knockout mice. *Am J Physiol Heart Circ Physiol,* 297**,** H1655-60.

POTTIER, C., FRESNAIS, M., GILON, M., JÉRUSALEM, G., LONGUESPÉE, R. & SOUNNI, N. E. 2020. Tyrosine Kinase Inhibitors in Cancer: Breakthrough and Challenges of Targeted Therapy. *Cancers,* 12**,** 731.

PRIETO-DÍAZ, R., GONZÁLEZ-GÓMEZ, M., FOJO-CARBALLO, H., AZUAJE, J., EL MAATOUGUI, A., MAJELLARO, M., LOZA, M. I., BREA, J., FERNÁNDEZ-DUEÑAS, V., PALEO, M. R., DÍAZ-HOLGUÍN, A., GARCIA-PINEL, B., MALLO-ABREU, A., ESTÉVEZ, J. C., ANDÚJAR-ARIAS, A., GARCÍA-MERA, X., GOMEZ-TOURINO, I., CIRUELA, F., SALAS, C. O., GUTIÉRREZ-DE-TERÁN, H. & SOTELO, E. 2023. Exploring the Effect of Halogenation in a Series of Potent and Selective A(2B) Adenosine Receptor Antagonists. *J Med Chem,* 66**,** 890-912.

PROMEGA 2010. Promega Technical Bulletin: GloResponse™ NFAT-RE-luc2P KEK293 Cell Line, Instructions for use of Product. (Old). *Accessed 25 Jan 2021*.

PROMEGA 2019. Technical Manual: Promega Glosensor™ cAMP Assay. *Accessed 25 Jan 2021*.

PYNE, N. J. & PYNE, S. 2011. Receptor tyrosine kinase-G-protein-coupled receptor signalling platforms: out of the shadow? *Trends Pharmacol Sci,* 32**,** 443-50.

RABADI, M. M. & LEE, H. T. 2015. Adenosine receptors and renal ischaemia reperfusion injury. *Acta Physiol,* 213**,** 222-31.

RANPURA, V., PULIPATI, B., CHU, D., ZHU, X. & WU, S. 2010. Increased risk of high-grade hypertension with bevacizumab in cancer patients: a meta-analysis. *Am J Hypertens,* 23**,** 460-8.

RASHID, A. J., SO, C. H., KONG, M. M., FURTAK, T., EL-GHUNDI, M., CHENG, R., O'DOWD, B. F. & GEORGE, S. R. 2007. D1-D2 dopamine receptor heterooligomers with unique pharmacology are coupled to rapid activation of Gq/11 in the striatum. *Proc Natl Acad Sci U S A,* 104**,** 654-9.

RAY, C. J. & MARSHALL, J. M. 2006. The cellular mechanisms by which adenosine evokes release of nitric oxide from rat aortic endothelium. *J Physiol,* 570**,** 85-96.

REDFORS, B., BRAGADOTTIR, G., SELLGREN, J., SWÄRD, K. & RICKSTEN, S.-E. 2011. Effects of norepinephrine on renal perfusion, filtration and oxygenation in vasodilatory shock and acute kidney injury. *Intensive care medicine,* 37**,** 60-67.

REEDER, G. S., CURRIE, P. J., HAGLER, D. J., TAJIK, A. J. & SEWARD, J. B. 1986. Use of Doppler techniques (continuous-wave, pulsed-wave, and color flow

imaging) in the noninvasive hemodynamic assessment of congenital heart disease. *Mayo Clin Proc,* 61**,** 725-44.

REMINGTON, S. J. 2011. Green fluorescent protein: a perspective. *Protein Sci,* 20**,** 1509-19.

REN, H. & STILES, G. L. 1994. Characterization of the human A1 adenosine receptor gene. Evidence for alternative splicing. *J Biol Chem,* 269**,** 3104-10.

RIXE, O., BILLEMONT, B. & IZZEDINE, H. 2007. Hypertension as a predictive factor of Sunitinib activity. *Ann Oncol,* 18**,** 1117.

ROBBA, C., BONATTI, G., BATTAGLINI, D., ROCCO, P. R. M. & PELOSI, P. 2019. Mechanical ventilation in patients with acute ischaemic stroke: from pathophysiology to clinical practice. *Critical Care,* 23**,** 388.

ROBINSON, D. R., WU, Y.-M. & LIN, S.-F. 2000. The protein tyrosine kinase family of the human genome. *Oncogene,* 19**,** 5548-5557.

ROBINSON, E. S., KHANKIN, E. V., CHOUEIRI, T. K., DHAWAN, M. S., ROGERS, M. J., KARUMANCHI, S. A. & HUMPHREYS, B. D. 2010a. Suppression of the nitric oxide pathway in metastatic renal cell carcinoma patients receiving vascular endothelial growth factor-signaling inhibitors. *Hypertension,* 56**,** 1131-6.

ROBINSON, E. S., KHANKIN, E. V., KARUMANCHI, S. A. & HUMPHREYS, B. D. 2010b. Hypertension induced by vascular endothelial growth factor signaling pathway inhibition: mechanisms and potential use as a biomarker. *Semin Nephrol,* 30**,** 591-601.

ROSENBERG, R. D. & ROSENBERG, J. S. 1984. Natural anticoagulant mechanisms. *J Clin Invest,* 74**,** 1-6.

ROSKOSKI, R., JR. 2008. VEGF receptor protein-tyrosine kinases: structure and regulation. *Biochem Biophys Res Commun,* 375**,** 287-91.

ROUQUETTE, M., LEPETRE-MOUELHI, S. & COUVREUR, P. 2019. Adenosine and lipids: A forced marriage or a love match? *Adv Drug Deliv Rev,* 151-152**,** 233-244.

ROUTH, H. F. 1996. Doppler ultrasound. *IEEE Engineering in Medicine and Biology Magazine,* 15**,** 31-40.

ROZENFELD, R. & DEVI, L. A. 2010. Receptor heteromerization and drug discovery. *Trends Pharmacol Sci,* 31**,** 124-30.

RUBINO, A., RALEVIC, V. & BURNSTOCK, G. 1995. Contribution of P1-(A2b subtype) and P2-purinoceptors to the control of vascular tone in the rat isolated mesenteric arterial bed. *Br J Pharmacol,* 115**,** 648-52.

RUDICH, N., DEKEL, O. & SAGI-EISENBERG, R. 2015. Down-regulation of the A3 adenosine receptor in human mast cells upregulates mediators of angiogenesis and remodeling. *Mol Immunol,* 65**,** 25-33.

RYZHOV, S., GOLDSTEIN, A. E., NOVITSKIY, S. V., BLACKBURN, M. R., BIAGGIONI, I. & FEOKTISTOV, I. 2012. Role of A2B adenosine receptors in regulation of paracrine functions of stem cell antigen 1-positive cardiac stromal cells. *J Pharmacol Exp Ther,* 341**,** 764-74.

RYZHOV, S., NOVITSKIY, S. V., CARBONE, D. P., BIAGGIONI, I., ZAYNAGETDINOV, R., GOLDSTEIN, A. E., DIKOV, M. M. & FEOKTISTOV, I. 2008. Host A2B Adenosine Receptors Promote Carcinoma Growth. *Neoplasia,* 10**,** 987-995.

SAHOO, H. 2011. Förster resonance energy transfer – A spectroscopic nanoruler: Principle and applications. *Journal of Photochemistry and Photobiology C: Photochemistry Reviews,* 12**,** 20-30.

SANJANI, M. S., TENG, B., KRAHN, T., TILLEY, S., LEDENT, C. & MUSTAFA, S. J. 2011. Contributions of A2A and A2B adenosine receptors in coronary flow responses in relation to the KATP channel using A2B and A2A/2B double-knockout mice. *Am J Physiol Heart Circ Physiol,* 301**,** H2322-33.

SARABIPOUR, S., BALLMER-HOFER, K. & HRISTOVA, K. 2016. VEGFR-2 conformational switch in response to ligand binding. *Elife,* 5**,** e13876.

SASSONE-CORSI, P. 2012. The cyclic AMP pathway. *Cold Spring Harb Perspect Biol,* 4**,** a011148.

SAWMILLER, D. R. & CHOU, C. C. 1988. Adenosine plays a role in food-induced jejunal hyperemia. *Am J Physiol,* 255**,** G168-74.

SAWMILLER, D. R. & CHOU, C. C. 1992. Role of adenosine in postprandial and reactive hyperemia in canine jejunum. *Am J Physiol Gastrointest Liver Physiol,* 263**,** G487-G493.

SAXENA, P. R. 1992. Interaction between the renin-angiotensin-aldosterone and sympathetic nervous systems. *Journal of cardiovascular pharmacology,* 19 (Suppl 6)**,** S80-8.

SCHÄFERS, R. F., ADLER, S., DAUL, A., ZEITLER, G., VOGELSANG, M., ZERKOWSKI, H. R. & BRODDE, O. E. 1994. Positive inotropic effects of the beta 2-adrenoceptor agonist terbutaline in the human heart: effects of long-term beta 1-adrenoceptor antagonist treatment. *J Am Coll Cardiol,* 23**,** 1224-33.

SCHENK, J., HEBDEN, A. & MCNEILL, J. H. 1992. Measurement of cardiac left ventricular pressure in conscious rats using a fluid-filled catheter. *J Pharmacol Toxicol Methods,* 27**,** 171-5.

SCHIEDEL, A. C., HINZ, S., THIMM, D., SHERBINY, F., BORRMANN, T., MAASS, A. & MULLER, C. E. 2011. The four cysteine residues in the second extracellular loop of the human adenosine A2B receptor: role in ligand binding and receptor function. *Biochem Pharmacol,* 82**,** 389-99.

SCHMIDT, M., HAJAGE, D., ALEXANDRE, D., TÀI, P., COMBES, A., MARTIN, D., SAID, L., ANTOINE, K., ALAIN, M. & GAËTAN, B. 2021. Clinical characteristics and day-90 outcomes of 4244 critically ill adults with COVID-19: a prospective cohort study. *Intensive Care Medicine,* 47**,** 60-73.

SCHONENBACH, N. S., RIETH, M. D., HAN, S. & O'MALLEY, M. A. 2016. Adenosine A2a receptors form distinct oligomers in protein detergent complexes. *FEBS Lett,* 590**,** 3295-306.

SCHULTE, G. & FREDHOLM, B. B. 2000. Human Adenosine $A_1$, $A_{2A}$, $A_{2B}$, and $A_3$ Receptors Expressed in Chinese Hamster Ovary Cells All Mediate the Phosphorylation of Extracellular-Regulated Kinase 1/2. *Molecular Pharmacology,* 58**,** 477-482.

SCHULTE, G. & FREDHOLM, B. B. 2003. Signalling from adenosine receptors to mitogen-activated protein kinases. *Cell Signal,* 15**,** 813-27.

SCHWEDA, F., SEGERER, F., CASTROP, H., SCHNERMANN, J. & KURTZ, A. 2005. Blood pressure-dependent inhibition of Renin secretion requires A1 adenosine receptors. *Hypertension,* 46**,** 780-6.

SCISLO, T. J., ICHINOSE, T. K. & O'LEARY, D. S. 2008. Stimulation of NTS A1 adenosine receptors differentially resets baroreflex control of regional sympathetic outputs. *Am J Physiol Heart Circ Physiol,* 294**,** H172-82.

SEIBT, B. F., SCHIEDEL, A. C., THIMM, D., HINZ, S., SHERBINY, F. F. & MULLER, C. E. 2013. The second extracellular loop of GPCRs determines subtype-selectivity and controls efficacy as evidenced by loop exchange study at A2 adenosine receptors. *Biochem Pharmacol,* 85**,** 1317-29.

SHALABY, F., ROSSANT, J., YAMAGUCHI, T. P., GERTSENSTEIN, M., WU, X. F., BREITMAN, M. L. & SCHUH, A. C. 1995. Failure of blood-island formation and vasculogenesis in Flk-1-deficient mice. *Nature,* 376**,** 62-6.

SHAO, Y. M., MA, X., PAIRA, P., TAN, A., HERR, D. R., LIM, K. L., NG, C. H., VENKATESAN, G., KLOTZ, K. N., FEDERICO, S., SPALLUTO, G., CHEONG, S. L., CHEN, Y. Z. & PASTORIN, G. 2018. Discovery of indolylpiperazinylpyrimidines with dual-target profiles at adenosine A2A and dopamine D2 receptors for Parkinson's disease treatment. *PLoS One,* 13**,** e0188212.

SHETH, S., BRITO, R., MUKHERJEA, D., RYBAK, L. P. & RAMKUMAR, V. 2014. Adenosine receptors: expression, function and regulation. *International journal of molecular sciences,* 15**,** 2024-2052.

SHRYOCK, J. C., SNOWDY, S., BARALDI, P. G., CACCIARI, B., SPALLUTO, G., MONOPOLI, A., ONGINI, E., BAKER, S. P. & BELARDINELLI, L. 1998. A2A-adenosine receptor reserve for coronary vasodilation. *Circulation,* 98**,** 711-718.

SINCLAIR, M. D. 2003. A review of the physiological effects of alpha2-agonists related to the clinical use of medetomidine in small animal practice. *Can Vet J,* 44**,** 885-97.

SOAVE, M., STODDART, L. A., BROWN, A., WOOLARD, J. & HILL, S. J. 2016. Use of a new proximity assay (NanoBRET) to investigate the ligand-binding

characteristics of three fluorescent ligands to the human beta1-adrenoceptor expressed in HEK-293 cells. *Pharmacol Res Perspect,* 4**,** e00250.

SORRENTINO, C. & MORELLO, S. 2017. Role of adenosine in tumor progression: focus on A2B receptor as potential therapeutic target. *Journal of Cancer Metastasis and Treatment,* 3**,** 127-38.

SOUDERS, C. A., BOWERS, S. L. & BAUDINO, T. A. 2009. Cardiac fibroblast: the renaissance cell. *Circ Res,* 105**,** 1164-76.

SPIELMAN, W. S. & AREND, L. J. 1991. Adenosine receptors and signaling in the kidney. *Hypertension,* 17**,** 117-130.

ST HILAIRE, C., KOUPENOVA, M., CARROLL, S. H., SMITH, B. D. & RAVID, K. 2008. TNF-alpha upregulates the A2B adenosine receptor gene: The role of NAD(P)H oxidase 4. *Biochemical and biophysical research communications,* 375**,** 292-296.

STANLEY, T. H. 2014. The Fentanyl Story. *The Journal of Pain,* 15**,** 1215-1226.

STEHLE, J. H., RIVKEES, S. A., LEE, J. J., WEAVER, D. R., DEEDS, J. D. & REPPERT, S. M. 1992. Molecular cloning and expression of the cDNA for a novel A2-adenosine receptor subtype. *Mol Endocrinol,* 6**,** 384-93.

STEINER, A. L., PARKER, C. W. & KIPNIS, D. M. 1972. Radioimmunoassay for Cyclic Nucleotides: I. PREPARATION OF ANTIBODIES AND IODINATED CYCLIC NUCLEOTIDES. *Journal of Biological Chemistry,* 247**,** 1106-1113.

STODDART, L. A., JOHNSTONE, E. K. M., WHEAL, A. J., GOULDING, J., ROBERS, M. B., MACHLEIDT, T., WOOD, K. V., HILL, S. J. & PFLEGER, K. D. G. 2015. Application of BRET to monitor ligand binding to GPCRs. *Nat Methods,* 12**,** 661-663.

STODDART, L. A., KILPATRICK, L. E. & HILL, S. J. 2018a. NanoBRET Approaches to Study Ligand Binding to GPCRs and RTKs. *Trends Pharmacol Sci,* 39**,** 136-147.

STODDART, L. A., VERNALL, A. J., BOUZO-LORENZO, M., BOSMA, R., KOOISTRA, A. J., DE GRAAF, C., VISCHER, H. F., LEURS, R., BRIDDON, S. J., KELLAM, B. & HILL, S. J. 2018b. Development of novel fluorescent histamine H1-

receptor antagonists to study ligand-binding kinetics in living cells. *Sci Rep,* 8**,** 1572.

STODDART, L. A., VERNALL, A. J., DENMAN, J. L., BRIDDON, S. J., KELLAM, B. & HILL, S. J. 2012. Fragment screening at adenosine-A(3) receptors in living cells using a fluorescence-based binding assay. *Chem Biol,* 19**,** 1105-15.

STODDART, L. A., WHITE, C. W., NGUYEN, K., HILL, S. J. & PFLEGER, K. D. 2016. Fluorescence- and bioluminescence-based approaches to study GPCR ligand binding. *Br J Pharmacol,* 173**,** 3028-37.

STRYER, L. & HAUGLAND, R. P. 1967. Energy transfer: a spectroscopic ruler. *Proceedings of the National Academy of Sciences,* 58**,** 719-726.

STUART, S. D. F., DE JESUS, N. M., LINDSEY, M. L. & RIPPLINGER, C. M. 2016. The crossroads of inflammation, fibrosis, and arrhythmia following myocardial infarction. *Journal of molecular and cellular cardiology,* 91**,** 114-122.

SUAREZ-ROCA, H., MAMOUN, N., SIGURDSON, M. I. & MAIXNER, W. 2021. Baroreceptor Modulation of the Cardiovascular System, Pain, Consciousness, and Cognition. *Compr Physiol,* 11**,** 1373-1423.

SUEHIRO, J.-I., KANKI, Y., MAKIHARA, C., SCHADLER, K., MIURA, M., MANABE, Y., ABURATANI, H., KODAMA, T. & MINAMI, T. 2014. Genome-wide approaches reveal functional vascular endothelial growth factor (VEGF)-inducible nuclear factor of activated T cells (NFAT) c1 binding to angiogenesis-related genes in the endothelium. *The Journal of biological chemistry,* 289**,** 29044-29059.

SUTHERLAND, E. W. & RALL, T. W. 1958. Fractionation and characterization of a cyclic adenine ribonucleotide formed by tissue particles. *J Biol Chem,* 232**,** 1077-91.

TABRIZCHI, R. & LUPICHUK, S. M. 1995. Vasodilatation produced by adenosine in isolated rat perfused mesenteric artery: a role for endothelium. *Naunyn Schmiedebergs Arch Pharmacol,* 352**,** 412-8.

TANG, L., PARKER, M., FEI, Q. & LOUTZENHISER, R. 1999. Afferent arteriolar adenosine A2a receptors are coupled to KATP in in vitro perfused hydronephrotic rat kidney. *Am J Physiol,* 277**,** F926-33.

TANK, J., DIEDRICH, A., SZCZECH, E., LUFT, F. C. & JORDAN, J. 2004. Alpha-2 adrenergic transmission and human baroreflex regulation. *Hypertension,* 43**,** 1035-41.

TARASEVICIENE-STEWART, L., KASAHARA, Y., ALGER, L., HIRTH, P., MC MAHON, G., WALTENBERGER, J., VOELKEL, N. F. & TUDER, R. M. 2001. Inhibition of the VEGF receptor 2 combined with chronic hypoxia causes cell death-dependent pulmonary endothelial cell proliferation and severe pulmonary hypertension. *FASEB J,* 15**,** 427-38.

TARDIEU, J.-L. 2008. Selecting a cyclic AMP kit for assaying GPCR target activation. *Nature Methods,* 5**,** iii-iv.

TAURA, J., VALLE-LEON, M., SAHLHOLM, K., WATANABE, M., VAN CRAENENBROECK, K., FERNANDEZ-DUENAS, V., FERRE, S. & CIRUELA, F. 2018. Behavioral control by striatal adenosine A2A -dopamine D2 receptor heteromers. *Genes Brain Behav,* 17**,** e12432.

TENG, B., FIL, D., TILLEY, S. L., LEDENT, C., KRAHN, T. & MUSTAFA, S. J. 2013. Functional and RNA Expression Profile of Adenosine Receptor Subtypes in Mouse Mesenteric Arteries. *Journal of Cardiovascular Pharmacology,* 61**,** 70-76.

TERMAN, B. I., DOUGHER-VERMAZEN, M., CARRION, M. E., DIMITROV, D., ARMELLINO, D. C., GOSPODAROWICZ, D. & BOHLEN, P. 1992. Identification of the KDR tyrosine kinase as a receptor for vascular endothelial cell growth factor. *Biochem Biophys Res Commun,* 187**,** 1579-86.

THOMAS, P. & SMART, T. G. 2005. HEK293 cell line: A vehicle for the expression of recombinant proteins. *Journal of Pharmacological and Toxicological Methods,* 51**,** 187-200.

TIAN, Y., PIRAS, B. A., KRON, I. L., FRENCH, B. A. & YANG, Z. 2015. Adenosine 2B Receptor Activation Reduces Myocardial Reperfusion Injury by Promoting Anti-Inflammatory Macrophages Differentiation via PI3K/Akt Pathway. *Oxid Med Cell Longev,* 2015**,** 585297.

TOLDO, S., ZHONG, H., MEZZAROMA, E., VAN TASSELL, B. W., KANNAN, H., ZENG, D., BELARDINELLI, L., VOELKEL, N. F. & ABBATE, A. 2012. GS-6201, a selective blocker of the A2B adenosine receptor, attenuates cardiac remodeling

after acute myocardial infarction in the mouse. *J Pharmacol Exp Ther,* 343**,** 587-95.

VALLON, V. & OSSWALD, H. 2009. Adenosine receptors and the kidney. *Handb Exp Pharmacol***,** 443-70.

VAN DAELE, M., COOPER, S. L., PANNUCCI, P., WRAGG, E. S., MARCH, J., DE JONG, I. & WOOLARD, J. 2022. Monitoring haemodynamic changes in rodent models to better inform safety pharmacology: Novel insights from in vivo studies and waveform analysis. *JRSM Cardiovascular Disease,* 11**,** 20480040221092893.

VAN DEN HOFF, M., LABRUYERE, W. T., MOORMAN, A. & LAMERS, W. H. 1993. Mammalian gene expression is improved by use of a longer SV40 early polyadenylation cassette. *Nucleic acids research,* 21**,** 4987-4988.

VAN VLIET, B. N., CHAFE, L. L., ANTIC, V., SCHNYDER-CANDRIAN, S. & MONTANI, J. P. 2000. Direct and indirect methods used to study arterial blood pressure. *J Pharmacol Toxicol Methods,* 44**,** 361-73.

VEMURI, S. V., ROLFSEN, M. L., SYKES, A. V., TAKIAR, P. G., LEONARD, A. J., MALHOTRA, A., SPRAGG, R. G., MACEDO, E. & HEPOKOSKI, M. L. 2022. Association Between Acute Kidney Injury During Invasive Mechanical Ventilation and ICU Outcomes and Respiratory System Mechanics. *Critical Care Explorations,* 4**,** e0720.

VERHEUL, H. M., VOEST, E. E. & SCHLINGEMANN, R. O. 2004. Are tumours angiogenesis-dependent? *J Pathol,* 202**,** 5-13.

VERNALL, A. J., STODDART, L. A., BRIDDON, S. J., HILL, S. J. & KELLAM, B. 2012. Highly Potent and Selective Fluorescent Antagonists of the Human Adenosine A3 Receptor Based on the 1,2,4-Triazolo[4,3-a]quinoxalin-1-one Scaffold. *Journal of Medicinal Chemistry,* 55**,** 1771-1782.

VERONESE, M. L., MOSENKIS, A., FLAHERTY, K. T., GALLAGHER, M., STEVENSON, J. P., TOWNSEND, R. R. & O'DWYER, P. J. 2006. Mechanisms of hypertension associated with BAY 43-9006. *J Clin Oncol,* 24**,** 1363-9.

VIDI, P. A., CHEN, J., IRUDAYARAJ, J. M. & WATTS, V. J. 2008. Adenosine A(2A) receptors assemble into higher-order oligomers at the plasma membrane. *FEBS Lett,* 582**,** 3985-90.

VIRK, M. S., ARTTAMANGKUL, S., BIRDSONG, W. T. & WILLIAMS, J. T. 2009. Buprenorphine Is a Weak Partial Agonist That Inhibits Opioid Receptor Desensitization. *The Journal of Neuroscience,* 29**,** 7341-7348.

VIRTANEN, R. 1989. Pharmacological profiles of medetomidine and its antagonist, atipamezole. *Acta veterinaria Scandinavica. Supplementum,* 85**,** 29-37.

VIVANET, G., GERVASO, L., LAFFI, A., RUBINO, M., SPADA, F. & FAZIO, N. 2022. Ten years-experience of sunitinib in the treatment of advanced pan-NETs: an update on safety profile. *Expert Opinion on Drug Safety,* 21**,** 303-310.

WAKENO, M., MINAMINO, T., SEGUCHI, O., OKAZAKI, H., TSUKAMOTO, O., OKADA, K., HIRATA, A., FUJITA, M., ASANUMA, H., KIM, J., KOMAMURA, K., TAKASHIMA, S., MOCHIZUKI, N. & KITAKAZE, M. 2006. Long-term stimulation of adenosine A2b receptors begun after myocardial infarction prevents cardiac remodeling in rats. *Circulation,* 114**,** 1923-32.

WALLACE, J. L. 2013. Mechanisms, prevention and clinical implications of nonsteroidal anti-inflammatory drug-enteropathy. *World J Gastroenterol,* 19**,** 1861-76.

WANG, T., LI, Z., CVIJIC, M. E., ZHANG, L. & SUM, C. S. 2017. Measurement of cAMP for Galphas- and Galphai Protein-Coupled Receptors (GPCRs). *Assay Guidance Manual.* Bethesda (MD): Eli Lilly & Company and the National Center for Advancing Translational Sciences . *Accessed 25 Jan 2021*.

WELSH, C. & VALADEZ-MELTZER, A. 2005. Buprenorphine: a (relatively) new treatment for opioid dependence. *Psychiatry (Edgmont),* 2**,** 29-39.

WHITE, C. W., JOHNSTONE, E. K. M., SEE, H. B. & PFLEGER, K. D. G. 2019. NanoBRET ligand binding at a GPCR under endogenous promotion facilitated by CRISPR/Cas9 genome editing. *Cell Signal,* 54**,** 27-34.

WHITE, J. F., GRODNITZKY, J., LOUIS, J. M., TRINH, L. B., SHILOACH, J., GUTIERREZ, J., NORTHUP, J. K. & GRISSHAMMER, R. 2007. Dimerization of the class A G protein-coupled neurotensin receptor NTS1 alters G protein interaction. *Proceedings of the National Academy of Sciences of the United States of America,* 104**,** 12199-12204.

WHORTON, M. R., BOKOCH, M. P., RASMUSSEN, S. G. F., HUANG, B., ZARE, R. N., KOBILKA, B. & SUNAHARA, R. K. 2007. A monomeric G protein-coupled receptor isolated in a high-density lipoprotein particle efficiently activates its G protein. *Proceedings of the National Academy of Sciences of the United States of America,* 104**,** 7682-7687.

WIEDENMANN, J., OSWALD, F. & NIENHAUS, G. U. 2009. Fluorescent proteins for live cell imaging: opportunities, limitations, and challenges. *IUBMB Life,* 61**,** 1029-42.

WILEY, K. E. & DAVENPORT, A. P. 2001. Physiological antagonism of endothelin-1 in human conductance and resistance coronary artery. *Br J Pharmacol,* 133**,** 568-574.

WILLOUGHBY, D. & COOPER, D. M. F. 2007. Organization and Ca2+ Regulation of Adenylyl Cyclases in cAMP Microdomains. *Physiological Reviews,* 87**,** 965-1010.

WOOLARD, J., BENNETT, T., DUNN, W. R., HEAL, D. J., ASPLEY, S. & GARDINER, S. M. 2004. Acute cardiovascular effects of sibutramine in conscious rats. *J Pharmacol Exp Ther,* 308**,** 1102-10.

WOUTERS, J., HÄMING, L. & SHELDRICK, G. 1996. HEPES. *Acta Crystallographica Section C: Crystal Structure Communications,* 52**,** 1687-1688.

XIA, Y., JAVADOV, S., GAN, T. X., PANG, T., COOK, M. A. & KARMAZYN, M. 2007. Distinct KATP channels mediate the antihypertrophic effects of adenosine receptor activation in neonatal rat ventricular myocytes. *J Pharmacol Exp Ther,* 320**,** 14-21.

XU, Y., PISTON, D. W. & JOHNSON, C. H. 1999. A bioluminescence resonance energy transfer (BRET) system: application to interacting circadian clock proteins. *Proceedings of the National Academy of Sciences,* 96**,** 151-156.

YAMADA, K. A., MOERSCHBAECHER, J. M., HAMOSH, P. & GILLIS, R. A. 1983. Pentobarbital causes cardiorespiratory depression by interacting with a GABAergic system at the ventral surface of the medulla. *Journal of Pharmacology and Experimental Therapeutics,* 226**,** 349-355.

YANG, D., ZHANG, Y., NGUYEN, H. G., KOUPENOVA, M., CHAUHAN, A. K., MAKITALO, M., JONES, M. R., HILAIRE, C. S., SELDIN, D. C., TOSELLI, P., LAMPERTI, E., SCHREIBER, B. M., GAVRAS, H., WAGNER, D. D. & RAVID, K. 2006. The A2B adenosine receptor protects against inflammation and excessive vascular adhesion. *The Journal of Clinical Investigation,* 116**,** 1913-1923.

YANG, R., THOMAS, G. R., BUNTING, S., KO, A., FERRARA, N., KEYT, B., ROSS, J. & JIN, H. 1996. Effects of vascular endothelial growth factor on hemodynamics and cardiac performance. *J Cardiovasc Pharmacol,* 27**,** 838-44.

YAP, S. C. & LEE, H. T. 2012. Adenosine and protection from acute kidney injury. *Curr Opin Nephrol Hypertens,* 21**,** 24-32.

YU, M., GUO, G., HUANG, L., DENG, L., CHANG, C. S., ACHYUT, B. R., CANNING, M., XU, N., ARBAB, A. S., BOLLAG, R. J., RODRIGUEZ, P. C., MELLOR, A. L., SHI, H., MUNN, D. H. & CUI, Y. 2020. CD73 on cancer-associated fibroblasts enhanced by the A2B-mediated feedforward circuit enforces an immune checkpoint. *Nat Commun,* 11**,** 515.

YUAN, J., XU, W., JIANG, S., YU, H. & POON, F. 2018. The scattered twelve tribes of HEK293. *Biomedical and Pharmacology Journal,* 11**,** 621-623.

ZABLOCKI, J. A., WU, L., SHRYOCK, J. & BELARDINELLI, L. 2004. Partial A(1) adenosine receptor agonists from a molecular perspective and their potential use as chronic ventricular rate control agents during atrial fibrillation (AF). *Curr Top Med Chem,* 4**,** 839-54.

ZACHARY, I. & GLIKI, G. 2001. Signaling transduction mechanisms mediating biological actions of the vascular endothelial growth factor family. *Cardiovasc Res,* 49**,** 568-81.

ZADRAN, S., STANDLEY, S., WONG, K., OTINIANO, E., AMIGHI, A. & BAUDRY, M. 2012. Fluorescence resonance energy transfer (FRET)-based biosensors: visualizing cellular dynamics and bioenergetics. *Appl Microbiol Biotechnol,* 96**,** 895-902.

ZEHENDER, M., JERON, A., FABER, T., BRUNNER, M. & JUST, H. 1996. Adenosine in treating cardiac arrhythmias. *J Auton Pharmacol,* 16**,** 329-31.

ZHANG, H., ZHONG, H., EVERETT, T. H. T., WILSON, E., CHANG, R., ZENG, D., BELARDINELLI, L. & OLGIN, J. E. 2014. Blockade of A2B adenosine receptor reduces left ventricular dysfunction and ventricular arrhythmias 1 week after myocardial infarction in the rat model. *Heart Rhythm,* 11**,** 101-9.

ZHANG, J., YANG, P. L. & GRAY, N. S. 2009. Targeting cancer with small molecule kinase inhibitors. *Nat Rev Cancer,* 9**,** 28-39.

ZHANG, Y., GEIGER, J. D., LÉGARÉ, D. J. & WAYNE LAUTT, W. 1991. Dilazep-induced vasodilation is mediated through adenosine receptors. *Life Sciences,* 49**,** PL129-PL133.

ZHU, X., WU, S., DAHUT, W. L. & PARIKH, C. R. 2007. Risks of proteinuria and hypertension with bevacizumab, an antibody against vascular endothelial growth factor: systematic review and meta-analysis. *Am J Kidney Dis,* 49**,** 186-93.

ZOCCHI, C., ONGINI, E., FERRARA, S., BARALDI, P. G. & DIONISOTTI, S. 1996. Binding of the radioligand [3H]-SCH 58261, a new non-xanthine A2A adenosine receptor antagonist, to rat striatal membranes. *Br J Pharmacol,* 117**,** 1381-1386.

ZWIER, J. M., ROUX, T., COTTET, M., DURROUX, T., DOUZON, S., BDIOUI, S., GREGOR, N., BOURRIER, E., OUESLATI, N. & NICOLAS, L. 2010. A fluorescent ligand-binding alternative using Tag-lite® technology. *Journal of biomolecular screening,* 15**,** 1248-1259.